



Durham E-Theses

Fundamentals of Heterogeneous Selective Ethylene Oligomerisation

LAMB, MICHAEL,JAMES

How to cite:

LAMB, MICHAEL,JAMES (2018) *Fundamentals of Heterogeneous Selective Ethylene Oligomerisation*, Durham theses, Durham University. Available at Durham E-Theses Online:
<http://etheses.dur.ac.uk/12613/>

Use policy

The full-text may be used and/or reproduced, and given to third parties in any format or medium, without prior permission or charge, for personal research or study, educational, or not-for-profit purposes provided that:

- a full bibliographic reference is made to the original source
- a [link](#) is made to the metadata record in Durham E-Theses
- the full-text is not changed in any way

The full-text must not be sold in any format or medium without the formal permission of the copyright holders.

Please consult the [full Durham E-Theses policy](#) for further details.

Academic Support Office, Durham University, University Office, Old Elvet, Durham DH1 3HP
e-mail: e-theses.admin@dur.ac.uk Tel: +44 0191 334 6107
<http://etheses.dur.ac.uk>

Fundamentals of Heterogeneous Selective Ethylene Oligomerisation



Thesis submitted for the degree of Doctor of Philosophy

By

Michael James Lamb MChem

Department of Chemistry
Durham University

Confidential – FOR EXAMINERS ONLY

January 2018

Statement of Originality

This thesis is based on work conducted in the department of Chemistry at Durham University between October 2013 and December 2017. All work was carried out by the author, unless otherwise stated, and has not been submitted for another degree at this, or any other university.

The copyright of this thesis rests with the author. No quotation from it should be published without the author's prior written consent and information derived from it should be acknowledged.

Signed: _____

Date: _____

Michael James Lamb

Memorandum

Part of this work has been the subject of the following article, which is currently in the press:

➤ M. J. Lamb, D. C. Apperley, M. J. Watson, P. W. Dyer, *Top. Catal.*, **2018**.

Article Title: The Role of Catalyst Support, Diluent and Co-catalyst in

Chromium-mediated Heterogeneous Ethylene Trimerisation.

DOI: 10.1007/s11244-018-0891-8

Abstract

Title: Fundamentals of Heterogeneous Selective Ethylene Oligomerisation

Sequential treatment of a partially dehydroxylated oxide (*i.e.* SiO_2 , $\gamma\text{-Al}_2\text{O}_3$, or mixed $\text{SiO}_2\text{-Al}_2\text{O}_3$) with solutions of $\text{Cr}\{\text{N}(\text{SiMe}_3)_2\}_3$ (0.71 wt% Cr) and a Lewis acidic alkyl aluminium-based co-catalyst ($\text{Al}/\text{Cr} = 15$) affords initiator systems active for the oligo- and poly-merisation of ethylene. The influence of the oxide support, calcination temperature, co-catalyst, and reaction diluent on the catalytic performance of such oxide-supported chromium initiators have been investigated in Chapter 2. The best performing combination { $\text{SiO}_2\text{-600}$, modified methyl aluminoxane (MMAO-12), heptane} generates a mixture of hexenes (61 wt%; 79% 1-hexene), and polyethylene (PE; 16 wt%) with an overall activity of $2403 \text{ g g}_{\text{Cr}}^{-1} \text{ h}^{-1}$. The observed product distribution is rationalised by two competing processes: trimerisation *via* a supported metallocycle-based mechanism and polymerisation through a classical Cossee-Arlman-type chain growth pathway. This is supported by the indirect observation of two distinct chromium environments at the surface of silica by a solid-state ^{29}Si direct excitation (DE) magic-angle spinning (MAS) nuclear magnetic resonance (NMR) spectroscopic study of the $\text{Cr}\{\text{N}(\text{SiMe}_3)_2\}_x/\text{SiO}_2\text{-600}$ pro-initiator.

Chapter 3 describes the development of the $\text{Cr}\{\text{N}(\text{SiMe}_3)_2\}_x/\text{SiO}_2\text{-600}/\text{MMAO-12}$ ethylene trimerisation batch reaction at a constant ethylene concentration in the slurry-phase using heptane as a diluent. A series of experimental parameters were tested to evidence their impact on catalytic performance. These include varying chromium concentration, Al/Cr loadings, reaction temperature, ethylene working pressure, stirrer speed, reaction time, diluent volume, and the impact of potential promoters, namely 1,2-dimethoxyethane (1,2-DME) and Et_2Zn . It has been shown that $\text{Cr}\{\text{N}(\text{SiMe}_3)_2\}_x/\text{SiO}_2\text{-600}$ activated with 15 molar equivalents of MMAO-12 at $120 \text{ }^\circ\text{C}$, and at a fixed ethylene pressure of 30 barg for 30 minutes yields a highly active heterogeneous ethylene trimerisation catalyst. In addition to the aforementioned ethylene trimerisation and polymerisation processes, compelling evidence supporting a 2,1-insertion mechanism for the step-wise isomerisation of 1-hexene, as well as its reincorporation into the metallocyclic trimerisation manifold has been reported. These claims are substantiated by the characterisation of internal hexenes and seven internal and/or branched decenes afforded by the silica-supported chromium initiator using solution-phase NMR spectroscopy. Both 1,2-DME and Et_2Zn had a negative impact on catalytic performance.

Acknowledgements

Firstly, I'd like to whole-heartedly thank my supervisor Dr Phil Dyer for all of his support and guidance throughout my time here at Durham University. Before arriving in Durham, I was told by one of my previous academic co-supervisors having known Phil for over 20 years that he is a very good supervisor, and I would do well under his tutelage. Indeed his fundamental knowledge, passion for chemistry, his kind-heartedness and, perhaps, most of all patience has set the foundations for this work. Without him none of this work would have been possible.

I'd like to express thanks to Dr Mike Watson for our many useful discussions both in Billingham and at the annual Johnson Matthey academic conferences. My first experience of the so-called "chicken parmo" at Café Jardin was a particular highlight.

Johnson Matthey and the Engineering and Physical Sciences Research Council (EPSRC) are thanked for their funding allowing me to undertake this project.

Being a member of the Dyer group has granted me the privilege of meeting so many talented and enthusiastic chemists – post-docs, PhD and Masters' students alike. Li Li, Luke, Flora, Jas, Ben, Anna, Josie, Hilary, Billy, Sarah, Jamie, Cherry, Kate and Leo to name but a few. A special mention goes to James, who essentially taught Jas, Anna and I all in our first year at the time the fundamentals of air-sensitive chemistry. It was a steep learning curve, but (somehow) we made it! I'd like to thank Jack for his generosity of spirit (pardon the pun) as well as time, making me feel welcome in the department, but, most importantly for putting me up on occasion after a few coca colas. Thank you Michael (New), Stephen, Claire, Dominikus, Eder, Kevin, and Alana for keeping my spirits high with playful banter. This was crucial in maintaining at least an element of my sanity, especially during the writing up of this thesis. This has been the single most stressful period of my life. I've even got the grey hairs now to prove it!

The solid- and solution-state NMR services (Dr David Apperley, Dr Alan Kenright, Dr Juan Aguilar and Mrs Catherine Heffernan), the thermal analysis service (Mr Douglas Carswell), the Glassblowers (Mr Malcolm Richardson and Mr Aaron Brown) as well as the engineers and electricians (Mr Neil Holmes, Mr Kelvin Appleby and Mr Omer Ekinoglu) in the mechanical and electrical workshops are also warmly acknowledged.

My heartfelt thanks go to my Mum, Dad and my brother Johnathan.

Finally, thank you Hayley for being my rock. Sticking by me and supporting me through the good times and the bad. Words simply cannot express enough gratitude.

Contents

1.	Introduction	
1.1	Linear Alpha Olefins	1
1.1.1	Uses of Linear Alpha Olefins.....	1
1.1.2	Synthesis of Linear Alpha Olefins	2
1.2	Non-selective Ethylene Oligomerisation Catalysis.....	4
1.2.1	Selected Examples of Non-selective Ethylene Oligomerisation.....	5
1.2.1.1	The Aufbau Reaction	5
1.2.1.1.1	Chevron-Phillips Ziegler Process.....	5
1.2.1.1.2	INEOS Ethyl Process.....	6
1.2.1.2	Shell Higher Olefins Process	6
1.2.2	Summary of Non-selective Ethylene Oligomerisation Catalysis	7
1.3	Selective Ethylene Oligomerisation Catalysis	9
1.3.1	Selected Examples of Homogeneous Ethylene Tri-/Tetra-merisation	9
1.3.1.1	Case Study 1: Cr(2-EH) ₃ /PIBAO Ethylene Trimerisation Initiator	9
1.3.1.2	Case Study 2: Cr(2,5-DMP) ₃ /Et ₃ Al Ethylene Trimerisation Process.....	14
1.3.1.3	Case Study 3: Cr PNP ^{OCH₃} /MAO Ethylene Trimerisation Catalyst	18
1.3.1.4	Case Study 4: Cr PNP/MAO Ethylene Tetramerisation System	21
1.3.1.5	Mechanistic Studies: Selective Ethylene Oligomerisation Catalysis	25
1.3.1.5.1	Metallacyclic Ethylene Tri-/Tetra-merisation Reaction Manifold	25
1.3.1.5.2	Metallacycle-based Ethylene Co-oligomerisation	28
1.3.1.5.3	Formation of Methylcyclopentane and Methylenecyclopentane.....	29
1.3.1.5.4	Role of Co-catalysts in Selective Ethylene Oligomerisation	30
1.3.1.6	Summary of Homogeneous Selective Ethylene Oligomerisation.....	35
1.3.2	An Overview of Heterogeneous Catalytic Ethylene Oligomerisation	36
1.3.2.1	Phillips Heterogeneous Cr/SiO ₂ Ethylene Polymerisation Process	36
1.3.2.2	Modified Phillips CrCl(TAC)/SiO ₂ Ethylene Trimerisation System	38
1.3.2.3	Heterogenisation of the Cr PNP/MMAO-3A Ethylene Tetramerisation Catalyst	39
1.3.2.4	Supported Cr PNPNH/Et ₃ Al Ethylene Trimerisation Initiator	41
1.3.2.5	Cr{N(SiMe ₃) ₂ } ₂ /SiO ₂ /IBAO Ethylene Trimerisation Process	42
1.3.2.6	Non-chromium-based Heterogeneous Olefin Oligomerisation	45
1.3.2.6.1	Heterogeneous s(FI)Ti Ethylene Trimerisation Initiator	45
1.3.2.6.2	{η ⁵ -C ₅ H ₄ (CMe ₂ Ph)}Ti(O ⁱ Pr) ₂ /SiO ₂ /MAO Ethylene Trimerisation Catalyst	47
1.3.2.6.3	Me ₂ TaCl ₂ /SiO ₂ Ethylene Trimerisation System.....	48
1.4	Thesis Aims and Objectives.....	50
1.5	References.....	51

2.	Role of Catalyst Support, Co-catalyst and Diluent in Chromium-mediated Heterogeneous Ethylene Trimerisation	
2.1	Introduction	55
2.2	Results and Discussion	56
2.2.1	Role of the Oxide Support in the $\text{Cr}\{\text{N}(\text{SiMe}_3)_2\}_x/\text{Oxide}_{-600}/\text{MMAO-12}$ Ethylene Trimerisation System	56
2.2.2	Influence of the Lewis Acidic Co-catalyst on the Performance of the $\text{Cr}\{\text{N}(\text{SiMe}_3)_2\}_x/\text{SiO}_{2-600}$ Ethylene Trimerisation Pro-initiator.....	58
2.2.3	Effect of Diluent on $\text{Cr}\{\text{N}(\text{SiMe}_3)_2\}_x/\text{SiO}_{2-600}/\text{MMAO-12}$ -mediated Ethylene Trimerisation.....	60
2.2.4	Understanding the Nature and Catalytic Behaviour of the $\text{Cr}\{\text{N}(\text{SiMe}_3)_2\}_x/\text{SiO}_{2-600}/\text{MMAO-12}$ Initiator System.....	62
2.2.4.1	Solid-state Raman Spectroscopic Analysis.....	62
2.2.4.2	Solid-state ^{29}Si DE MAS NMR Spectroscopic Study.....	66
2.2.4.2.1	Solid-state ^{29}Si DE MAS NMR Spectroscopic Analysis of SiO_{2-600}	66
2.2.4.2.2	Solid-state ^{29}Si DE MAS NMR Spectroscopic Analysis of $\text{Cr}\{\text{N}(\text{SiMe}_3)_2\}_x/\text{SiO}_{2-600}$	66
2.2.4.2.3	Solid-state ^{29}Si DE MAS Saturation-Recovery T_1 NMR Spectroscopic Study	70
2.2.4.3	X-Ray Photoelectron Spectroscopic Analysis of $\text{Cr}\{\text{N}(\text{SiMe}_3)_2\}_x/\text{SiO}_{2-600}$	72
2.2.4.4	Titration of SiO_{2-600} with $\text{Cr}\{\text{N}(\text{SiMe}_3)_2\}_3$	73
2.2.4.5	Rutherford Backscattering Spectrometric Analysis of $\text{Cr}\{\text{N}(\text{SiMe}_3)_2\}_x/\text{SiO}_{2-600}$	74
2.2.5	Impact of Support Calcination Temperature on the Selectivity of the $\text{Cr}\{\text{N}(\text{SiMe}_3)_2\}_x/\text{SiO}_2/\text{MMAO-12}$ Initiator System	76
2.2.5.1	Electron Paramagnetic Resonance Spectroscopic Analyses of the SiO_{2-200} - and SiO_{2-600} -supported Chromium Pro-initiators	82
2.2.6	Activation of the $\text{Cr}\{\text{N}(\text{SiMe}_3)_2\}_x/\text{SiO}_{2-600}$ Pro-initiator	84
2.3	Conclusions	86
2.4	References	87

3.	Influence of Experimental Process Parameters on Chromium-mediated Heterogeneous Ethylene Trimerisation	
3.1	Introduction	91
3.2	Results	92
3.2.1	Catalyst Test Reproducibility	92
3.2.2	Influence of Catalyst Support Dehydroxylation upon the Selectivity of the Cr{N(SiMe ₃) ₂ } _x /SiO ₂ /MMAO-12 Initiator	94
3.2.3	Effect of Molecular Precursor on Catalytic Performance: Cr{N(SiMe ₃) ₂ } ₃ vs. Cr(acac) ₃ vs. CrCl ₃ (thf) ₃	98
3.2.4	Impact of Process Parameters upon Chromium-mediated Heterogeneous Ethylene Trimerisation	100
3.2.4.1	Influence of Chromium Concentration upon the Heterogeneous Cr{N(SiMe ₃) ₂ } _x /SiO ₂₋₆₀₀ /MMAO-12 Ethylene Trimerisation System	101
3.2.4.2	Effect of Al/Cr Mole Ratio on Catalytic Performance	102
3.2.4.3	Temperature Dependence of the Cr{N(SiMe ₃) ₂ } _x /SiO ₂₋₆₀₀ /MMAO-12 Ethylene Trimerisation System	103
3.2.4.4	Effect of the Stirrer Speed Regime on the Catalytic Performance of Cr{N(SiMe ₃) ₂ } _x /SiO ₂₋₆₀₀ /MMAO-12	104
3.2.4.5	Pressure Dependency of the Cr{N(SiMe ₃) ₂ } _x /SiO ₂₋₆₀₀ /MMAO-12 Initiator System	105
3.2.4.6	Influence of Reaction Time upon the Cr{N(SiMe ₃) ₂ } _x /SiO ₂₋₆₀₀ /MMAO-12 Initiator System	106
3.2.4.7	Effect of Potential Promoters (1,2-DME or Et ₂ Zn) on the Catalytic Performance of Cr{N(SiMe ₃) ₂ } _x /SiO ₂₋₆₀₀ /MMAO-12	107
3.2.4.8	Influence of 1-Hexene Concentration on the Product Selectivity of the Cr{N(SiMe ₃) ₂ } _x /SiO ₂₋₆₀₀ /MMAO-12 Ethylene Trimerisation Process	108
3.3	Discussion: Effects of Varying Reaction Test Parameters on the Performance of Cr{N(SiMe ₃) ₂ } _x /SiO ₂₋₆₀₀ /MMAO-12	110
3.3.1	Effect of Chromium Metal Loading	110
3.3.2	Effect of Reaction Temperature	112
3.3.3	Effect of Stirrer Speed	113
3.3.4	Effect of Ethylene Concentration	114
3.3.5	Catalyst Lifetime	116
3.3.6	Evaluation of Catalyst Poisoning Effects	118
3.3.7	Exploring the Dependence of Decene Formation upon Hexene Concentration ..	120
3.4	Solution-phase NMR and DSC analyses of Organic Product Fractions Afforded by Cr{N(SiMe ₃) ₂ } _x /SiO ₂₋₆₀₀ /MMAO-12	121
3.4.1	Pureshift ¹ H– ¹³ C HSQC NMR Spectroscopic Analysis of the Hexene-containing Distillate	122
3.4.2	¹³ C{ ¹ H} NMR Spectroscopic Analysis of the Decene-containing Distillate	124
3.4.3	Analysis of Polyethylene By-product of Ethylene Oligomerisation Testing Mediated by Cr{N(SiMe ₃) ₂ } _x /SiO ₂₋₆₀₀ /MMAO-12	126
3.5	Conclusions	128
3.6	References	129

4.	Experimental	
4.1	General Experimental Considerations	133
4.2	Characterisation of Oxide-based Catalyst Supports	136
4.2.1	ICP-OES Trace Elemental Analyses.....	136
4.2.2	BET Specific Surface Area and BJH Pore Volume/Size Analyses	137
4.1.1	Solid-state NMR Spectroscopy.....	137
4.2.2.1	Evonik Aeroperl 300/30 Fumed Silica	137
4.2.2.2	Sigma Aldrich Silica-alumina Grade 135 Catalyst Support.....	137
4.2.2.3	Alfa Aesar γ -Alumina.....	137
4.2.3	Thermogravimetric Analyses of Catalyst Supports.....	138
4.3	General Procedures for the Calcination of Oxide Supports.....	139
4.3.1	Thermal Pre-treatment of Oxide Supports under a Flow of N_2	139
4.3.1.1	NMR Spectroscopic Analysis of SiO_{2-200}	139
4.3.1.2	NMR Spectroscopic Analysis of SiO_{2-400}	139
4.3.1.3	Analysis of SiO_{2-600}	140
4.3.1.3.1	Silanol Quantification: Titration of SiO_{2-600} with <i>para</i> -Tolyl Magnesium Bromide	140
4.3.1.3.2	Titration of SiO_{2-600} with $Cr\{N(SiMe_3)_2\}_3$	141
4.1.2	Thermal Pre-treatment of Silica <i>in vacuo</i>	142
4.1.2.1	BET Specific Surface Area and BJH Pore Volume/Size Analyses	142
4.2	Attempted Preparation of $Cr(NPh_2)_3$ and $Cr(N^iPr_2)_3$	143
4.2.1	Lithium Diphenylamide.....	143
4.2.2	Chromium(III) Diphenylamide.....	143
4.2.3	Chromium(III) Diisopropylamide.....	144
4.3	General Protocol for the Preparation of Oxide-supported Chromium Pro-initiators	145
4.3.1	General Protocol for the Determination of Chromium Metal Loading in Oxide-supported Pro-initiators by ICP-OES	146
4.3.2	Analysis of $Cr\{N(SiMe_3)_2\}_x/SiO_{2-600}$	148
4.4	Preparation of Isobutyl Aluminoxane.....	148
4.5	Typical “Closed” Ethylene Oligomerisation Test Procedure	149
4.6	Typical “Open” Ethylene Oligomerisation Test Procedure.....	152
4.6.1	Isolation/Separation of Hexene- and Decene-containing Product Fractions by Distillation	158
4.7	References	160

5.	Appendix	
5.1	GC-FID Analysis of the Liquid Fraction Obtained from Chromium-mediated Ethylene Trimerisation	161
5.2	Quantifying the Mass of Analytes using GC-FID Analysis.....	162
5.2.1	Validating the Assumption that $RF_i = FW_i$	166
5.2.1.1	Using the Formula Weight of the Analyte as its Response Factor	166
5.2.1.2	Determination of the Relative Response Factor with a Calibration Curve	168
5.2.2	Quantifying the Mass of Liquid-phase Oligomers afforded from Chromium-mediated Ethylene Oligomerisation using GC-FID Analysis.....	170
5.3	References.....	172
6.	Thesis Summary, Outlook and Future Work	
6.1	Summary	173
6.2	Outlook.....	175
6.3	Future Work	176
6.4	References.....	178

List of Abbreviations

1,2-DME = 1,2-Dimethoxyethane

2,3,4,5-TMP = 2,3,4,5-Tetramethylpyrrole

2,5-DMP = 2,5-Dimethylpyrrolide

2-EH = 2-Ethylhexanoate

acac = 2,4-Pentanedionate

aq = Aqueous

Al₂O₃ = Alumina

BET = Brunauer Emmett Teller

SSA = Specific surface area

BJH = Barrett Joyner Halenda

Cat = Catalyst

CHN = Elemental analysis

COSHH = Control of substances hazardous to health

Concentration

at% = Atomic percentage

wt% = Weight percentage

w/w = Weight per weight

ppm = Parts per million

% w/w = Percentage weight per weight

Cr/SiO₂ = Phillips heterogeneous ethylene polymerisation catalyst

DSC = Differential scanning calorimetry

T_m = Melting point

H_m = Enthalpy of melting

H_m^o = Enthalpy of melting for 100% crystalline polyethylene

χ_c = Percentage crystallinity

DFT = Density functional theory

DTG = Differential thermogravimetry

E_a = Activation energy

Energy

eV = Electron volt

keV = Kiloelectron volt

MeV = Megaelectron volt

EPR = Electron paramagnetic resonance

CW = Continuous-wave

HYSCORE = Hyperfine sublevel correlation spectroscopy

Et = Ethyl

EXAFS = Extended X-ray absorption spectroscopy fine-structure

FI = Phenoxyimine

Frequency

Hz = Hertz

kHz = Kilohertz

MHz = Megahertz

GHz = Gigahertz

ν_{\max} = Maximum of the energy distribution plotted in terms of frequency

G = Gibbs free energy

GC = Gas chromatography

FID = Flame ionisation detection

MS = Mass spectrometry

PONA = Paraffins, olefins, naphthalenes and aromatics

GPC = Gel permeation chromatography

M_n = Number average molecular mass

M_w = Weight average molecular mass

D_M = Dispersity index

IBAO = Isobutyl aluminoxane

ⁱBu = Isobutyl

ICP-OES = Inductively coupled plasma-optical emission spectroscopy

ⁱPr = Isopropyl

IR = Infrared

I.D. = Inner diameter

LAO = Linear alpha olefin

1-C₄ = 1-Butene

1-C₆ = 1-Hexene

1-C₈ = 1-Octene

1-C₁₀ = 1-Decene

1-C₁₂ = 1-Dodecene

1-C₁₄ = 1-Tetradecene

Length

Å = Angstrom

nm = Nanometre

mm = Millimetre

cm = Centimetre

dm = Decimetre

m = Metre

LX = Generic three-electron donor ligand

Mass

Da = Dalton

mg = Milligram

g = gram

MAO = Methyl aluminoxane

Me = Methyl

MMAO = Modified methyl aluminoxane

MMAO-3A = Modified methyl aluminoxane, type 3A

MMAO-12 = Modified methyl aluminoxane, type 12

Moles

M = Molar

μmol = Micromoles

mmol = Millimoles

mol = Moles

xs = Molar excess

NMR = Nuclear magnetic resonance

B_0 = Applied magnetic field

DE = Direct excitation

HSQC = Heteronuclear single quantum correlation

INEPT = Insensitive nuclei enhanced by polarisation transfer

MAS = Magic-angle spinning

m = Magnetisation

r = Radius

s = Singlet

T_1 = Longitudinal relaxation time

T_1^{-1} = Longitudinal relaxation rate

t = Triplet

ω_r = Magic-angle spin rate

NPNP = *bis*-(Aminophosphine)

o- = *ortho*

O.D. = Outer diameter

P = Pressure

bar = bar absolute

barg = bar gauge

mbar = millibar

p- = *para*

PE = Polyethylene

- HDPE** = High density polyethylene
- HMWPE** = High molecular weight polyethylene
- LLDPE** = Linear low density polyethylene
- UHMWPE** = Ultra-high molecular weight polyethylene

Ph = Phenyl

PIBAO = *poly*-(Isobutyl) aluminium oxide

PNP = Diphosphinoamine

- PNP^{OC_{D3}}** = Diphosphinoamine with an *ortho*-methoxy-*d*₃ aryl substituent
- PNP^{OCH₃}** = Diphosphinoamine with an *ortho*-methoxy aryl substituent

PNPN = *bis*-(Phosphinoamine)

Q₂ = Geminal silanol

Q₃ = Isolated silanol

Q₄ = Siloxane bridge

RBF = Round-bottomed flask

RBS = Rutherford backscattering

RDS = Rate-determining step

R = Alkyl

S = Stirrer speed regime

- rpm** = Revolutions per minute

s(FI) = Supported phenoxyimine

SHOP = Shell higher olefins process

SiO₂ = Silica

SiO₂-Al₂O₃ = Silica-alumina

SOMC = Surface organometallic chemistry

T = Temperature

- °C** = degrees Celsius
- K** = Kelvin
- RT** = Room temperature

t = Time

- s** = Seconds
- mins** = Minutes
- h** = Hours

TAC = 1,3,5-Tribenzylhexahydro-1,3,5-triazine

TGA = Thermogravimetric analysis

thf = Tetrahydrofuran

TM = Transition metal

Productivity

TOF = Turnover frequency ($\text{g g}_{\text{Cr}}^{-1} \text{h}^{-1}$)

TON = Turnover number ($\text{g g}_{\text{Cr}}^{-1}$)

UHV = Ultra-high vacuum

Volume

μL = Microlitre

mL = Millilitre

L = Litre

x = Isotopic ratio

XAS = X-Ray absorption spectroscopy

XPS = X-Ray photoelectron spectroscopy

XRD = X-Ray diffraction

$\gamma\text{-Al}_2\text{O}_3$ = Alumina, gamma phase

σ = Sigma bonding mode

Δ = Change

δ = Chemical shift

η = Hapticity

Nomenclature Used In This Thesis

- Catalyst supports are classified by the conditions under which they were calcined, *e.g.*
 - **SiO₂₋₆₀₀** denotes Evonik Aeroperl 300/30 fumed silica thermally pre-treated at 600 °C for 24 hours under a flow of dry N₂.
 - **SiO_{2-600v}** denotes Evonik Aeroperl 300/30 fumed silica thermally pre-treated at 600 °C for 24 hours under dynamic vacuum (~0.1 mbar).
- Pro-initiators are referred to by their molecular precursor and the oxide support, *e.g.*
 - **Cr{N(SiMe₃)₂}_x/SiO₂₋₆₀₀** denotes SiO₂₋₆₀₀ impregnated with Cr{N(SiMe₃)₂}₃.
 - **Cr{N(SiMe₃)₂}_x/SiO_{2-600v}** denotes SiO_{2-600v} impregnated with Cr{N(SiMe₃)₂}₃.
- Initiators are referred to simply by their catalyst precursor and the Lewis acidic alkyl aluminium co-catalyst employed, *e.g.*
 - **Cr{N(SiMe₃)₂}_x/SiO₂₋₆₀₀/MMAO-12** denotes Cr{N(SiMe₃)₂}_x/SiO₂₋₆₀₀ activated with MMAO-12.
 - **Cr{N(SiMe₃)₂}_x/SiO_{2-600v}/MMAO-12** denotes Cr{N(SiMe₃)₂}_x/SiO_{2-600v} activated with MMAO-12.
- Silica-supported chromium species may be referred to as:
 - **=SiO₂CrN(SiMe₃)₂** denotes chromium(III) *mono*-(hexamethylsilazide) species derived from Cr{N(SiMe₃)₂}₃ reacting with both **Q₂** and vicinal silanols.
 - **=SiO₂CrR** denotes *mono*-alkylated chromium(III) species arising from the reaction between =SiO₂CrN(SiMe₃)₂ and MMAO-12.
 - **≡SiOCr{N(SiMe₃)₂}₂** denotes chromium(III) *bis*-(hexamethylsilazide) species derived from Cr{N(SiMe₃)₂}₃ reacting with **Q₃** silanols.
 - **≡SiOCrR₂** denotes *bis*-alkylated chromium(III) species arising from the reaction between ≡SiOCr{N(SiMe₃)₂}₂ and MMAO-12.

This page has been intentionally left blank.

Chapter 1:
Introduction

1.1 Linear Alpha Olefins

This PhD thesis aims to develop fundamental understanding and critical insight into the field of *heterogeneous* ethylene oligomerisation for the selective production of linear alpha olefins (LAOs). This class of hydrocarbon comprise a linear carbon chain, typically in the range of C₂-C₃₈, and a terminal unsaturated C=C bond (Figure 1).

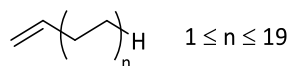


Figure 1: Skeletal structure of a linear alpha olefin

1.1.1 Uses of Linear Alpha Olefins

LAOs are valuable commodity chemicals that are used in the production of polymers (C₄-C₈), plasticisers (C₆-C₁₀), synthetic lubricants (C₁₀), and detergents (C₁₂-C₂₀);¹ Figure 2 shows the breakdown of worldwide LAO consumption in terms of their many industrial applications.² Indeed, the importance of LAOs in the petrochemical industry is reflected in their total annual consumption, which exceeded 5000 metric kilotons in 2016,² and is expected to increase on average by 3.7% *per annum* between 2016 and 2021.³

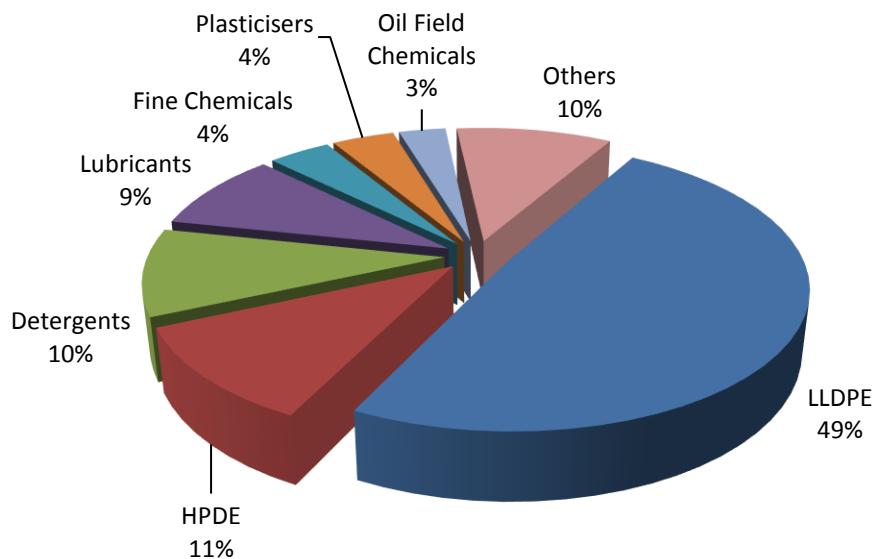
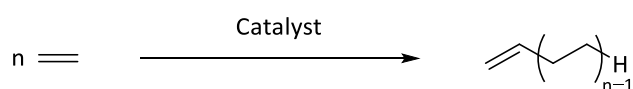


Figure 2: Global linear alpha olefin consumption, adapted from Thammanayakatip *et al.*, 2017²

Approximately 60% of worldwide LAO consumption in 2016 was attributed to the manufacture of linear low density polyethylene (LLDPE) and high density polyethylene (HDPE),² both of which are prepared *via* the co-polymerisation of ethylene with 1-butene, 1-hexene and/or 1-octene co-monomers.⁴ Indeed, the demand for LLDPE and HDPE is increasing at a higher rate than that for lubricants and detergents (derived from heavier C₁₀₊ LAO fractions), which has led to a greater demand for lighter LAOs (C₄-C₈).⁵ Hence, the selective production of C₄-C₈ LAOs has become an area of significant importance in both academic and industrial research.⁶

1.1.2 Synthesis of Linear Alpha Olefins

LAOs have traditionally been prepared through four separate routes: cracking or dehydrogenation of paraffinic oil fractions, dehydration of alcohols, and olefin oligomerisation.^{1,7} The latter route is currently the main source of LAO production, because it provides an efficient means of upgrading residual (light) crude oil-derived fractions into lucrative commodity chemicals.¹ Ethylene oligomerisation, in particular, is an attractive process since it utilises a relatively cheap, abundant and potentially sustainable resource.⁷ Furthermore, ethylene is readily available from established catalytic processes, such as steam cracking (of natural/shale gas or of petroleum distillates),⁸ or through the dehydration of ethanol (which in turn may be derived from biomass fermentation).⁹ In 2016, the annual global production of ethylene had reached 150 million metric tons.¹⁰ Together, these features make ethylene the preferred feedstock for the manufacture of LAOs (Scheme 1).¹¹



Scheme 1: Generalised reaction scheme for ethylene oligomerisation catalysis

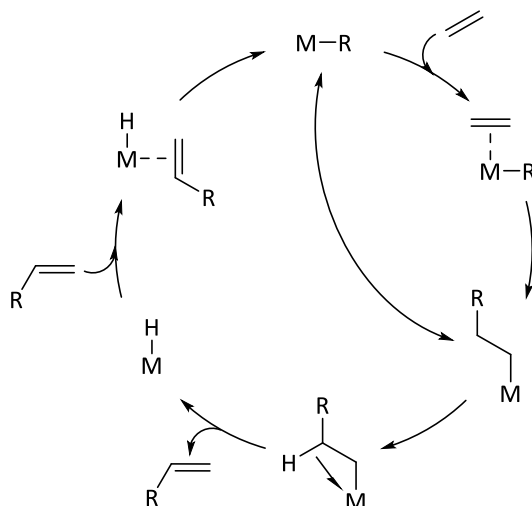
The first example of ethylene oligomerisation was reported by Ziegler in 1952.¹² Here, a soluble, molecular alkyl aluminium reagent was used as an initiator to generate a statistical “Poisson” distribution of LAOs, a process that is now known as the Aufbau reaction (See Page 5). Since then, there has been significant progress made in this field of *homogeneous* ethylene oligomerisation catalysis.^{1,6,7,8,11,13,14,15,16,17} In fact, there are now several commercialised processes that employ soluble, well-defined initiators, such as those currently operated by INEOS, Shell, Sabic/Linde, Chevron-Phillips and Sasol Technology, that produce LAOs.¹⁸ The underpinning work that has led to the development of such systems has come about principally as a result of extensive design and optimisation of organic ligand frameworks, which control not only solubility, but also the steric and electronic demands of the metal centre to which they are bound, coupled with in-depth mechanistic and kinetic investigations.

However, in contrast to these homogeneous ethylene oligomerisation initiator systems, there are relatively few examples of *heterogeneous* olefin oligomerisation initiators reported in the literature, despite heterogeneous catalysts generally being the industrial standard for commodity chemical manufacture.¹¹ In part, this can be attributed to the difficulty in the optimisation of solid-phase catalysts and the establishment of the crucial structure-reactivity relationships, not least because the desired chemical reactions typically occur at highly dispersed active sites that make up a small proportion of its surface area, which makes structural definition at a molecular level much more challenging.¹⁹ Hence, progress in the field of heterogeneous ethylene oligomerisation has relied primarily on empirical methodologies.

Surface organometallic chemistry (SOMC) provides an alternative synthetic approach,²⁰ in which a well-defined molecular organometallic olefin oligomerisation catalyst precursor can be grafted onto a solid support to prepare a related heterogeneous pro-initiator. In theory, SOMC provides greater control over the coordination number, geometry and oxidation state of the supported transition metal (TM) complex resulting in a relatively high proportion of well-defined active sites.²¹ However, in practice, the heterogenisation of several molecular olefin oligomerisation initiator systems has yielded mixed results in terms of their productivity and selectivity towards specific LAO product fractions.^{22,23,24,25,26,27,28,29,30} Consequently, work in this area continues, coupled with the development of alternative strategies to mediate the selective transformation of ethylene to LAOs with the desired C₄-C₈ chain lengths. Thus, it is important to highlight that although this PhD thesis is a fundamental study into the field of heterogeneous olefin oligomerisation, an overview of a few prominent examples of *homogeneous* ethylene oligomerisation will be given (in addition to the prerequisite solid-phase catalysts) in order to put the work in context. Particular emphasis will be placed on mechanistic implications and insights from soluble initiator systems that are relevant to *heterogeneous* selective olefin oligomerisation.

1.2 Non-selective Ethylene Oligomerisation Catalysis

The vast majority of ethylene oligomerisation initiator systems reported in the literature lack selectivity towards a single product, instead producing a broad range of liquid-phase oligomers as well as solid polyethylene (PE).^{7,8,14} In spite of the increased market for C₄-C₈ LAOs, three commercialised homogeneous non-selective ethylene oligomerisation processes, namely the Chevron-Phillips Ziegler process, the INEOS Ethyl process, and the Shell higher olefins process (SHOP), still dominate global LAO supply.⁸ Broadly speaking, non-selective ethylene oligomerisation processes are thought to proceed *via* the so-called “Cossee-Arlman” chain growth mechanism (Scheme 2),^{31,32,33} which involves consecutive ethylene coordination and migratory insertion steps resulting in the propagation of an alkyl chain. Here, chain termination is a competing β -hydride elimination reaction that liberates the oligo-/poly-meric product. The distribution of LAOs afforded by the Cossee-Arlman mechanism typically follows a statistical “Schulz-Flory” exponential decay function that is based on the relative probability of chain propagation *versus* chain termination.³⁴

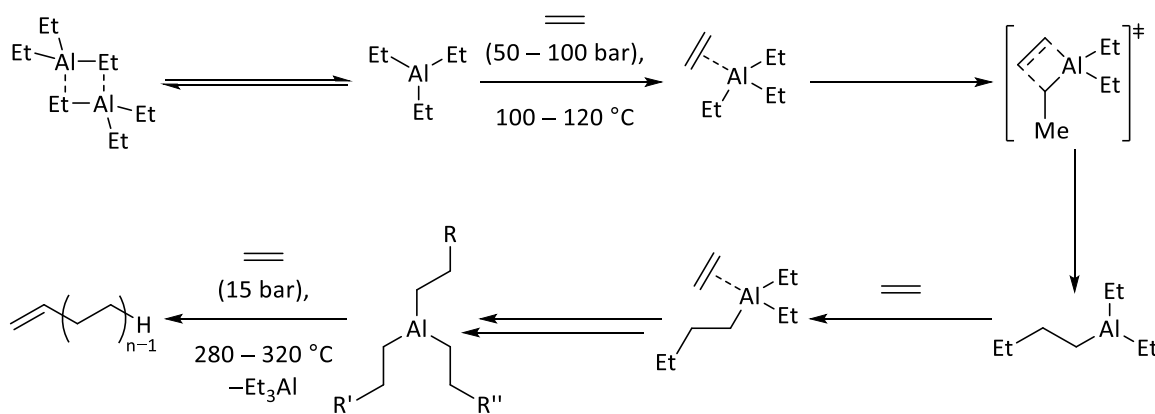


Scheme 2: Non-selective ethylene oligomerisation *via* a Cossee-Arlman-type reaction mechanism^{31,32,33}

1.2.1 Selected Examples of Non-selective Ethylene Oligomerisation

1.2.1.1 The Aufbau Reaction

Originally discovered by Ziegler in 1952,¹² the Aufbau reaction involves the step-wise propagation of an alkyl chain initiated by Et_3Al through successive ethylene coordination and migratory insertion reactions.³⁵ The ensuing n -alkyl aluminium species is thought to undergo β -hydride elimination in the presence of ethylene to produce a broad Poisson distribution of LAOs and regenerate Et_3Al (Scheme 3).³⁵ The Aufbau reaction has provided the basis for two Ziegler-type ethylene oligomerisation processes currently being operated by Chevron-Phillips and INEOS, which will be explored in greater detail below.



Scheme 3: The Aufbau reaction, adapted from Budzelaar *et al.*, 2003³⁵

1.2.1.1.1 Chevron-Phillips Ziegler Process

The Aufbau reaction was initially developed and commercialised by the Gulf Oil Chemicals Company, before being transferred to the Phillips Chemical Company in 1985 (prior to a merger with the Chevron Chemical Company in 2000).¹⁸ This one-pot, so-called “Ziegler” process generates LAOs through the propagation and displacement of Et_3Al at high reaction temperatures (175 – 290 °C) and high ethylene pressures (138 – 276 bar).¹⁸ At the end of the reaction the alkyl aluminium reagent is quenched to limit olefin isomerisation, and thus maximise LAO purity. The resulting product stream comprises a mixture of LAOs, including both branched and internal isomers, which can, to an extent, be separated by fractional distillation (Figure 3).¹⁸

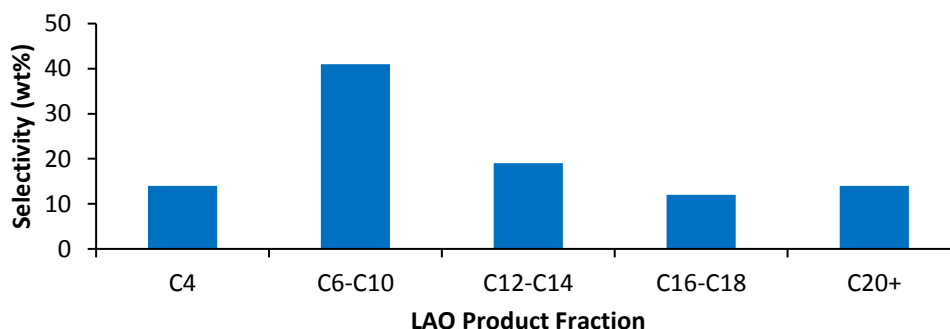


Figure 3: Chevron-Phillips Ziegler process LAO selectivity as reported by Camara Greiner *et al.*, 2010¹⁸

1.2.1.1.2 INEOS Ethyl Process

The Aufbau reaction was further developed by the Ethyl Corporation to include separate batch reactions for chain propagation and chain termination, which provides greater flexibility in terms of the resulting LAO product distribution.¹⁸ This modified Ziegler-type process was commercialised before being purchased by INEOS in 2005, and more recently became known as the Ethyl process.¹⁸ Here, in this modified process, chain propagation of R_3Al typically occurs at high temperatures (116 – 132 °C) and high ethylene pressures (186 – 207 bar), whereas the chain termination step is conducted at higher temperatures (260 – 316 °C) and lower ethylene working pressures (16 – 17 bar), which together gives rise to a Poisson distribution of oligomers.¹⁸ Additionally, INEOS have incorporated an ethylene and a butene recycle loop into the Ethyl process, which allows the resulting product distribution to be skewed towards the more desirable C_6 - C_{14} LAO fractions (Figure 4).¹⁸

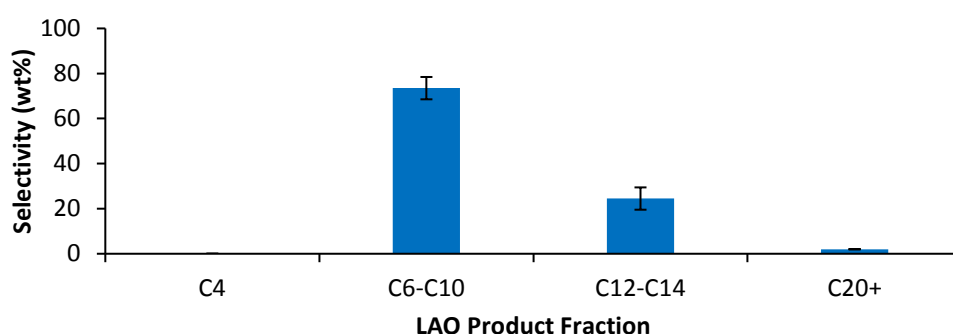


Figure 4: INEOS Ethyl process LAO selectivity, modified from Camara Greiner *et al.*, 2010¹⁸

1.2.1.2 Shell Higher Olefins Process

In contrast to these alkyl aluminium-based Ziegler-type processes, Shell Chemicals have developed a nickel(II)-catalysed non-selective ethylene oligomerisation reaction that has been integrated into a package generally known as the Shell higher olefins process (SHOP). This is operated as a continuous flow system that upgrades ethylene into primary C_{11} - C_{15} oxo-alcohols that are principally used in the production of detergents (Figure 5).³⁶ This is achieved through coupling a series of sequential reactions into a single process sheet, namely ethylene oligomerisation, olefin isomerisation, and metathesis that together maximises the yield of their desired LAO product range (C_{10} - C_{14}), prior to the hydroformylation step.

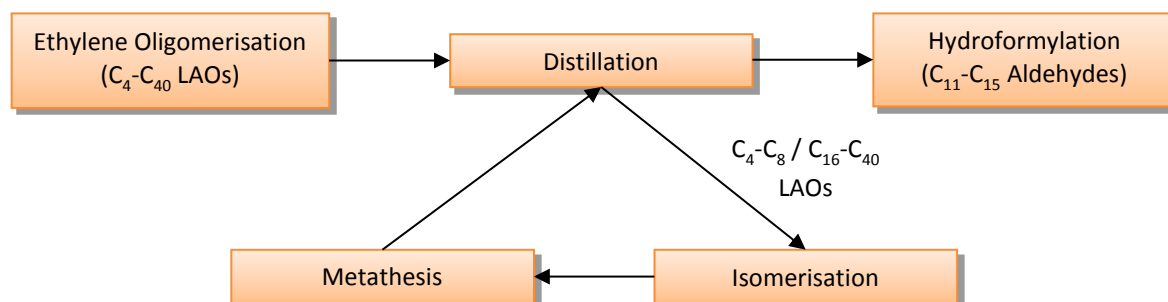
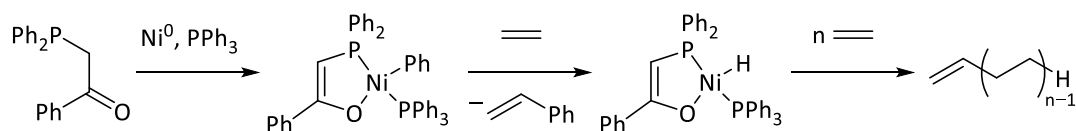


Figure 5: Flow diagram of the Shell higher olefins process, adapted from Reuben *et al.*, 1988³⁶

The first stage of the SHOP process is non-selective ethylene oligomerisation, in which Shell employ a molecular Ni^{II}-based catalyst to facilitate the production of a broad range of LAOs (Scheme 4).³⁷ Workers at Shell have designed a bidentate chelating anionic P–O ligand that enforces the square planar geometry of the Ni^{II} centre, which is critical for ethylene oligomerisation activity,³⁷ ensuring a *cis* relationship between ethylene and the propagating alkyl chain, a prerequisite of migratory insertion.³⁸ The product distribution of LAOs generated by such Ni^{II}-based P–O ethylene oligomerisation initiator systems is consistent with a Schulz-Flory mathematical function (Figure 6),¹⁸ something that is typically associated with a Cossee-Arlman chain growth mechanism.^{31,32,33}



Scheme 4: SHOP-type non-selective ethylene oligomerisation reaction as reported by Kuhn *et al.*, 2007³⁷

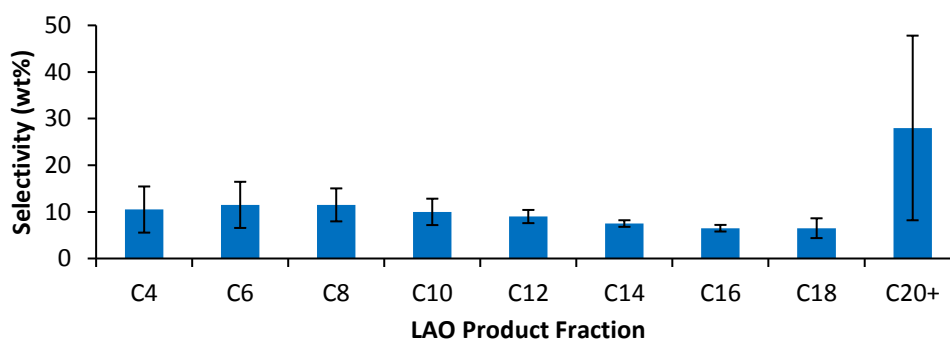


Figure 6: Schulz-Flory LAO distribution produced by the SHOP process, modified from Camara Greiner *et al.*, 2010¹⁸

1.2.2 Summary of Non-selective Ethylene Oligomerisation Catalysis

The Chevron-Phillips Ziegler process, the INEOS Ethyl process, and the Shell higher olefins process (SHOP) were responsible for the manufacture of over 70% of the world's supply of LAOs in 2010.¹⁸ However, it is clear that the (broad) distribution of LAOs afforded by these non-selective ethylene oligomerisation initiator systems differ quite significantly from today's commercial demand for pure 1-butene, 1-hexene and 1-octene (as co-monomers in the manufacture of HDPE and LLDPE).⁶ Consequently, in order to satisfy such high market-driven demand for these light LAO fractions, efforts have been made to develop highly selective ethylene oligomerisation processes that efficiently generate C₄-C₈ LAOs.¹¹ Hence, the field of ethylene tri-/tetra-merisation catalysis, in particular, has become the focus of intense research in both industry and academia.³⁹

This page has been intentionally left blank.

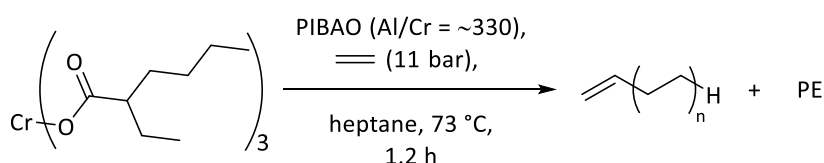
1.3 Selective Ethylene Oligomerisation Catalysis

Over the last 50 years, significant progress has been made in the field of *homogeneous* selective ethylene oligomerisation.⁶ Indeed, the Chevron-Phillips Chemical Company and Sasol Technology have successfully commercialised highly active and selective chromium-based ethylene oligomerisation processes that facilitate the production of 1-hexene and 1-octene, respectively.⁸ Moreover, there has been an explosion of publications, both in the patent and open literature regarding selective, molecular TM-catalysed ethylene tri-/tetra-merisation. As a result, there have been a number of review articles that have been published including those by Dixon (2004),¹¹ Hessen (2004),¹³ Wass (2007),¹⁵ McGuinness (2011),⁶ Bryliakov (2012),¹⁶ Breuil (2015),⁸ and Alferov (2017),¹⁷ which survey these areas. By comparison, there are very few examples of heterogeneous selective ethylene oligomerisation catalysts.²² Hence, this section of the thesis will initially discuss four prominent examples of homogeneous selective ethylene tri-/tetra-merisation catalysis, focusing predominantly on mechanistic insight that is relevant to the future development of heterogeneous selective olefin oligomerisation systems, before critically evaluating several such solid initiators that have previously been reported in the literature.

1.3.1 Selected Examples of Homogeneous Ethylene Tri-/Tetra-merisation

1.3.1.1 Case Study 1: Cr(2-EH)₃/PIBAO Ethylene Trimerisation Initiator

In 1967 Manyik *et al.* filed multiple patents on behalf of the Union Carbide Corporation that described an ethylene polymerisation process, in which chromium(III) *tris*-(2-ethylhexanoate) {Cr(2-EH)₃} activated by *poly*-(isobutyl) aluminium oxide (PIBAO), a hydrolysed derivative of ^tBu₃Al, mediated the production of a PE material that contained both ethyl and butyl side chains.^{40,41} It was proposed that the origin of these ethyl and butyl branches arose from the co-polymerisation of ethylene with 1-butene and 1-hexene co-monomers, respectively. It was postulated that these two LAOs were generated *in situ* by competing ethylene di-/tri-merisation processes.^{40,41} Manyik and co-workers later disclosed details of the Union Carbide Cr(2-EH)₃/PIBAO ethylene polymerisation initiator system in the open literature.⁴² In this report, a solution of ^tBu₃Al in heptane was reacted with 1.2 molar equivalents of water to form the PIBAO co-catalyst prior to the addition of the molecular Cr(2-EH)₃ pro-initiator, which generated the active species responsible for ethylene oligo-/poly-merisation (Scheme 5).⁴² Under the reaction conditions employed, the Cr(2-EH)₃/PIBAO initiator operated as a slurry in heptane predominantly generated PE (86 wt%) as well as 1-hexene (13 wt%).⁴²



Scheme 5: Ethylene oligo-/poly-merisation catalysed by Cr(2-EH)₃/PIBAO, adapted from Manyik *et al.*, 1977⁴²

Gas chromatographic (GC) analysis of the liquid-phase organic products afforded by the Union Carbide $\text{Cr}(2\text{-EH})_3/\text{PIBAO}$ initiator not only demonstrated high selectivity towards 1-hexene (93 wt%; Figure 7), but a disproportionately high selectivity towards branched decenes (1.9 wt%) when compared with 1-octene (1 wt%) and 1-decene (0.1 wt%).⁴² Together, these observations are not consistent with either a Poisson or a Schulz-Flory statistical distribution of LAOs, and therefore cannot be attributed to a classical Cossee-Arlman-type chain growth process.^{31,32,33} Furthermore, Manyik and co-workers reported here that selective ethylene trimerisation is a second order process with respect to ethylene concentration (Figure 8),⁴² something that also cannot be explained by the Cossee-Arlman mechanism, which is known to have a first order kinetic dependence on ethylene concentration.^{31,32,33} Consequently, in order to rationalise these observations, it was postulated that competing ethylene tri- and poly-merisation reaction mechanisms must be operative.⁴² In fact, Manyik and co-workers even suggested that 1-hexene may co-trimerise with two further molecules of ethylene to generate the branched decene isomers observed by GC.⁴²

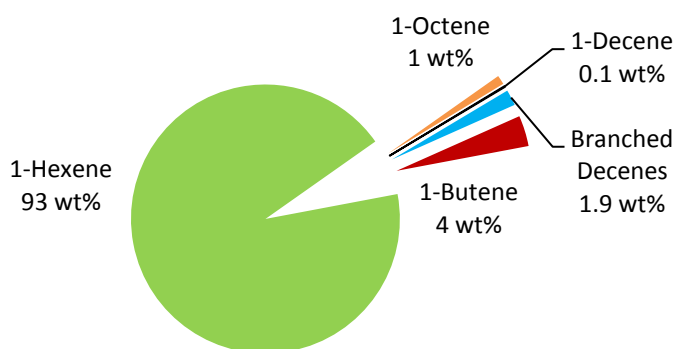


Figure 7: GC analysis of the liquid-phase oligomers afforded by the $\text{Cr}(2\text{-EH})_3/\text{PIBAO}$ ethylene polymerisation system, modified from Manyik *et al.*, 1977⁴²

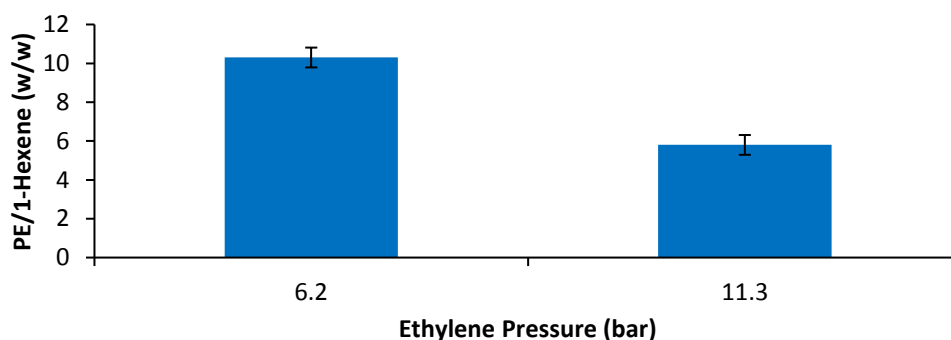
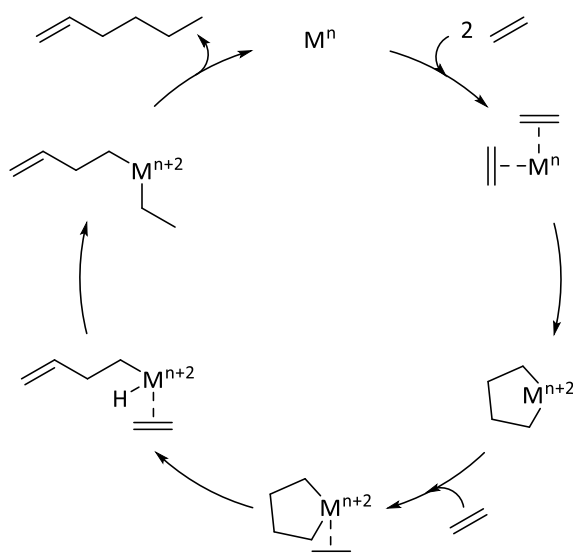


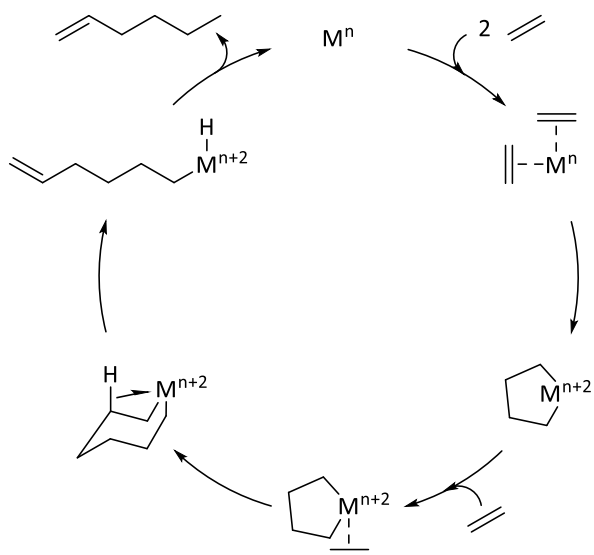
Figure 8: Kinetic dependence of the Union Carbide $\text{Cr}(2\text{-EH})_3/\text{PIBAO}$ initiator system on ethylene concentration, adapted from Manyik *et al.*, 1977⁴²

To account for these observations, Manyik *et al.* proposed a new metallacycle-based ethylene trimerisation reaction manifold, which provides a rationale for the high selectivity towards 1-hexene (and branched decenes) afforded by the Union Carbide Cr(2-EH)₃/PIBAO system (Scheme 6).⁴² This new mechanism involves the chromium-mediated oxidative coupling of two ethylene molecules resulting in the formation of a metallacyclopentane species. Subsequent, successive ethylene association and β-hydride elimination steps then produce a TM hydride complex that may, in turn, undergo migratory insertion generating a chromium butenyl ethyl species, prior to reductive elimination of 1-hexene.⁴² Crucially, it was inferred that the oxidative coupling of two ethylene molecules was the rate-determining step (RDS) within this reaction manifold (dubbed the metallacycle mechanism), something that explains the observed second order kinetic dependence of the Cr(2-EH)₃/PIBAO ethylene trimerisation initiator with respect to ethylene concentration.⁴²



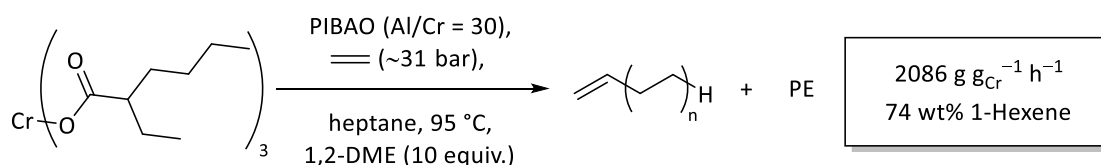
Scheme 6: Metallacycle-based ethylene trimerisation reaction mechanism proposed by Manyik *et al.*, 1977⁴²

In 1989 Briggs proposed a modification to the original metallacycle mechanism, which involved the expansion of the chromacyclopentane intermediate to a chromacycloheptane species, prior to β -hydride elimination and reductive elimination of 1-hexene (Scheme 7).⁴³ The inherent selectivity of the metallacyclic reaction manifold was attributed to the relative stability of the metallacyclopentane intermediate *versus* the metallacycloheptane species,^{44,45} as well as the respective activation energy (E_a) barriers for β -hydride elimination and reductive elimination from the metallacycloheptane ring, and that for further metallacycle expansion.⁴⁶ Briggs assumed that the rate of ethylene insertion into the chromacyclopentane intermediate was greater than that for the reductive elimination of 1-butene, and that β -hydride elimination and reductive elimination of 1-hexene from the chromacycloheptane species was more favourable than further insertion reactions to yield larger chromacycles.⁴³ This so-called metallacycle mechanism developed by Briggs has since become ubiquitous in the field of selective ethylene oligomerisation.^{1,6,8,11,13,15,16,17}



Scheme 7: Briggs' proposed modification to the metallacyclic ethylene trimerisation reaction manifold, 1989⁴³

Additionally, Briggs disclosed that the product selectivity of the $\text{Cr}(\text{2-EH})_3/\text{PIBAO}$ ethylene trimerisation catalyst could be improved either by reducing the Al/Cr loading (by a factor of 10), and/or through the inclusion of an electron-donating “additive” such as 1,2-dimethoxyethane (1,2-DME), as shown in Scheme 8.⁴³ It was later demonstrated using density functional theory (DFT) that the coordination of 1,2-DME to a cationic $\text{Cr}^{\text{I/III}}$ model ethylene trimerisation initiator could potentially increase the E_a barrier for the expansion of the chromacycloheptane intermediate, and thus favour β -hydride elimination and, hence, the subsequent reductive elimination of 1-hexene (Figure 9).⁴⁷



Scheme 8: Selective $\text{Cr}(\text{2-EH})_3/\text{PIBAO}/1,2\text{-DME}$ ethylene trimerisation system, modified from Briggs, 1989⁴³

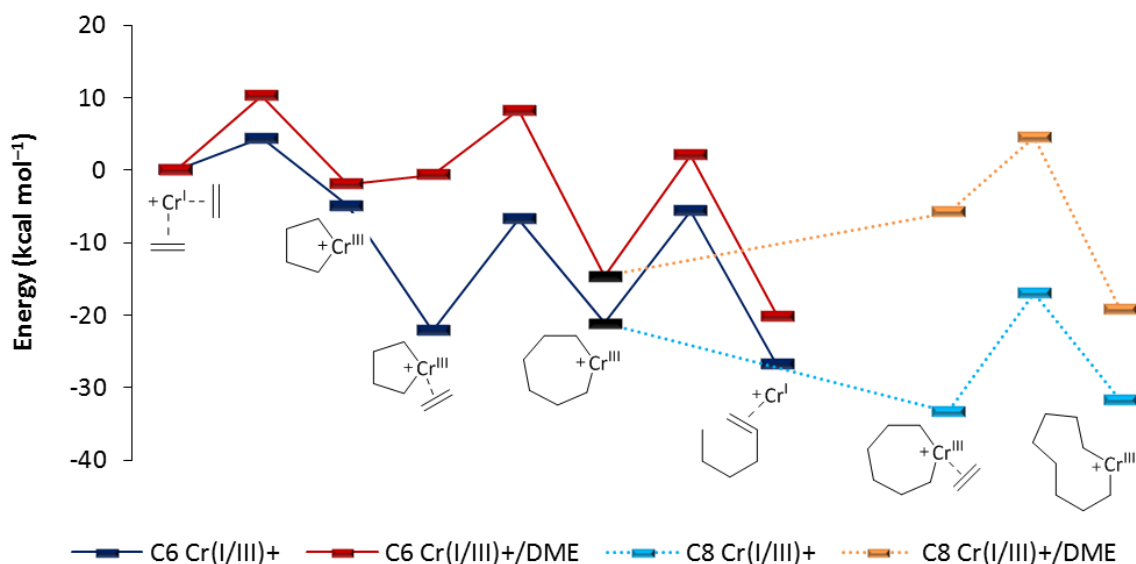
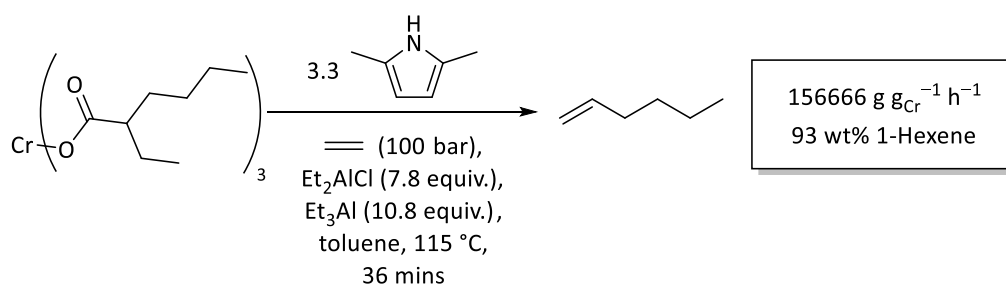


Figure 9: Effect of 1,2-DME coordination on the metallacyclic ethylene trimerisation reaction profile of a $[\text{Cr}^{\text{I/III}}]^+$ model initiator at the B3LYP level using the LANL2DZ and 6-31G(d,p) basis sets, adapted from Qi *et al.*, 2010⁴⁷

In summary, the pioneering work carried out by Manyik, Briggs *et al.* on the Union Carbide $\text{Cr}(\text{2-EH})_3/\text{PIBAO}$ ethylene trimerisation process, and the metallacyclic reaction manifold in particular,^{42,43,48} has become the foundation for many of the ensuing selective ethylene oligomerisation systems developed to date.^{1,6,8,11,13,15,16,17} Although not deemed suitable for industrial application, the molecular $\text{Cr}(\text{2-EH})_3/\text{PIBAO}$ initiator directly preceded a related, highly active and selective ethylene trimerisation catalyst derived from $\text{Cr}(\text{EH})_3$, 2,5-dimethylpyrrole and Et_3Al , a system that has since been commercialised by the Chevron-Phillips Chemical Company.^{49,50}

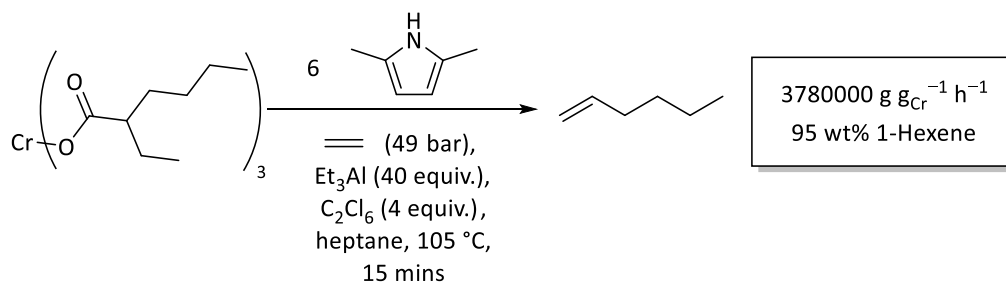
1.3.1.2 Case Study 2: Cr(2,5-DMP)₃/Et₃Al Ethylene Trimerisation Process

In the late 1980s Reagen discovered that a chromium(III) pyrrolide complex activated with a Lewis acidic alkyl aluminium reagent catalysed the production of 1-hexene.⁵¹ Consequently, workers at the Phillips Petroleum Company filed multiple patents in the 1990s relating to novel chromium pyrrolide ethylene trimerisation pro-initiators, which in turn could be used in tandem with ethylene polymerisation catalysts to generate HDPE and/or LLDPE.^{52,53} In 1994 Reagan and Conroy disclosed details of their highly active and selective ethylene trimerisation initiator system, which comprised specifically of Cr(2-EH)₃, 2,5-dimethylpyrrole and Et₃Al,⁵⁴ a system that was later patented as an ethylene trimerisation catalyst package by the Phillips Petroleum Company (Scheme 9).^{49,50}



Scheme 9: Phillips ethylene trimerisation process as reported by Freeman *et al.*, 1999⁵⁰

In response to the Phillips ethylene trimerisation system, rival companies developed their own ethylene oligomerisation processes, albeit based on the already well-established chromium(III) 2,5-dimethylpyrrolide (2,5-DMP) pro-initiator.¹¹ For example, the Mitsubishi Chemical Corporation patented an extremely active variant of the Phillips ethylene trimerisation system that consisted of Cr(2-EH)₃, 2,5-dimethylpyrrole, Et₃Al and C₂Cl₆ (Scheme 10).⁵⁵ The enhanced productivity of this Mitsubishi-Phillips initiator system was attributed to weak interactions between chlorinated promoters such as C₂Cl₆ and dimeric Et₃Al that results in the formation of monomeric Et₃Al, which is a stronger reducing agent than its parent dimer, and thus generates ethylene trimerisation-active chromium species more efficiently.⁵⁶ In this context, it is clear that for all selective homogeneous ethylene oligomerisation systems reported to date, the nature and mode of action of co-catalysts is critical to the success of many systems, and hence, this topic is surveyed in more detail in Section 1.3.1.5.4.



Scheme 10: Mitsubishi-Phillips ethylene trimerisation system, adapted from Araki *et al.*, 1999⁵⁵

After the merger of the Chevron Chemical Company and the Phillips Petroleum Company in 2000, the newly-formed Chevron-Phillips Chemical Company successfully commercialised a homogeneous ethylene trimerisation process, which was derived from $\text{Cr}(2,5\text{-DMP})_3$ and Et_3Al .¹¹ Utilising this technology Chevron-Phillips have since collaborated with the Qatar Chemical Company, as well as the Saudi Industrial Investment Group, to develop a process that can produce over 400000 metric tons of 1-hexene *per annum*.¹⁸

Numerous research groups have investigated the Chevron-Phillips ethylene trimerisation system in great detail with a view to optimising the process and understanding its mode of operation.¹¹ For example, Tang *et al.* studied the effect of chromium concentration, ethylene working pressure and reaction temperature on the Chevron-Phillips ethylene trimerisation initiator.⁵⁷ Here it was shown that the optimal ethylene pressure and reaction temperature for the Chevron-Phillips $\text{Cr}(2,5\text{-DMP})_3/\text{Et}_3\text{Al}$ ethylene trimerisation catalyst in terms of 1-hexene production were 25 bar and 95 °C, respectively (Figure 10).⁵⁷

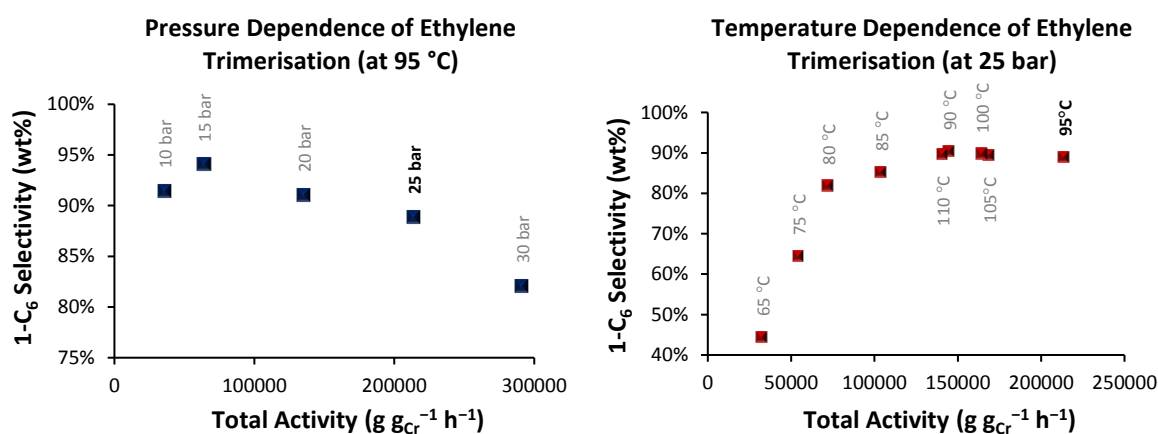


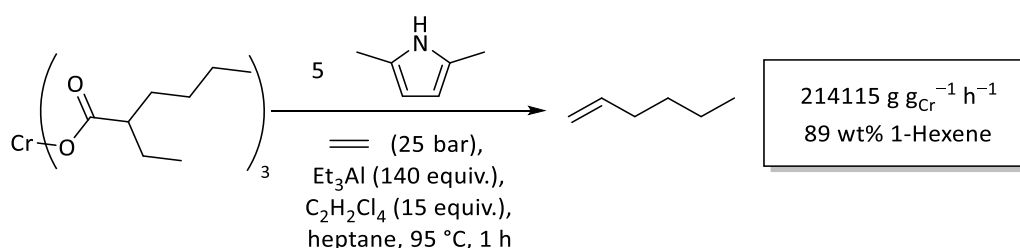
Figure 10: Kinetic dependence of the Chevron-Phillips $\text{Cr}(2,5\text{-DMP})_3/\text{Et}_3\text{Al}$ ethylene trimerisation initiator system, modified from Tang *et al.*, 2014⁵⁷

Tang and co-workers calculated a rate equation for the Chevron-Phillips ethylene trimerisation reaction (Equation 1), which is believed to be first order with respect to chromium, and second order with respect to ethylene concentration.⁵⁷ These observations were consistent with previous work on the Union Carbide $\text{Cr}(\text{EH})_3/\text{PIBAO}$ ethylene trimerisation initiator, as well as with a metallacyclic reaction manifold.^{42,43} Hence, it is now generally accepted that the high selectivity towards 1-hexene achieved by the Chevron-Phillips $\text{Cr}(2,5\text{-DMP})_3/\text{Et}_3\text{Al}$ ethylene trimerisation process, and perhaps other related systems, can also be attributed to a metallacycle-based reaction mechanism.^{6,8,11,13,15,16,17}

$$R = 5.23 \times 10^{18} \times e^{-\frac{99.1}{RT}} \times [\text{Cr}]^{1.12} \times [\text{C}_2\text{H}_4]^{1.95}$$

Equation 1: Rate equation for the Chevron-Phillips ethylene trimerisation process as reported by Tang *et al.*, 2014⁵⁷

Additionally, Tang *et al.* explored a number of experimental parameters, including the Lewis acidic co-catalyst and the Al/Cr mole ratio in order to optimise the activity and selectivity of the Chevron-Phillips ethylene trimerisation initiator (Scheme 11).⁵⁷ Here it was noted that the nature of the co-catalyst and the Al/Cr molar ratio are indeed critical parameters that can be used to tune the productivity and selectivity of the Chevron-Phillips ethylene trimerisation system towards 1-hexene.⁵⁷ Although a range of different co-catalysts including Et₃Al, ⁱBu₃Al, (C₂H₅)₃Al₂Cl₃ and Et₂Zn were screened in combination with Cr(2,5-DMP)₃, Et₃Al proved to be the optimal activator for the Chevron-Phillips ethylene trimerisation process in terms of both overall activity and selectivity towards 1-hexene.⁵⁷ Tang and co-workers also reported that the productivity of the Chevron-Phillips ethylene trimerisation system could be further enhanced by increasing the molar ratio of Et₃Al to Cr(2-EH)₃ from 20 to 180.⁵⁷ However, the optimal Al/Cr loading for the Chevron-Phillips ethylene trimerisation process in terms of 1-hexene selectivity was reported to be 140 molar equivalents; increasing the Al/Cr mole ratio to 180 led to a reduction in 1-hexene selectivity in favour of decene formation, presumably a result of a secondary metallacycle-based ethylene/1-hexene co-trimerisation reaction.⁵⁷



Scheme 11: Chevron-Phillips ethylene trimerisation system optimised by Tang *et al.*, 2014⁵⁷

At this juncture it is important to emphasise that one of the most important components in the Chevron-Phillips ethylene trimerisation system is 2,5-dimethylpyrrole. Indeed in the absence of the 2,5-dimethylpyrrolide (2,5-DMP) ligand, the performance of the highly active and selective Chevron-Phillips ethylene trimerisation initiator would be comparable to that of the moderately active and selective Union Carbide Cr(2-EH)₃/PIBAO system (see Section 1.3.1.1). In terms of the role of 2,5-DMP, it has been suggested that it may behave as a hemilabile ligand that can “flip” between σ - and η^5 -coordination modes at various points within the metallacycle mechanism compensating for electronic and/or steric changes at the chromium metal centre during ethylene trimerisation catalysis (Figure 11).⁴⁶

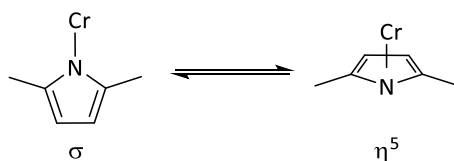


Figure 11: σ - and η^5 -bonding modes of the 2,5-dimethylpyrrolide ligand

In order to establish the coordination mode of the 2,5-DMP ligand in the Chevron-Phillips ethylene trimerisation system during catalysis, van Rensburg *et al.* used DFT to plot a Gibbs free energy (ΔG) profile of a metallacyclic reaction manifold mediated by σ - and η^5 -pyrrolide derivatives of a $\text{Cr}^{\text{II/IV}}$ redox couple (Figure 12).⁴⁶ According to this DFT study, it was proposed that 2,5-DMP would preferentially adopt the η^5 -coordination mode prior to the formation of, and after the expansion of the chromacyclopentane intermediate.⁴⁶ Conversely, during metallacycle expansion, *i.e.* coordination and insertion of the third molecule of ethylene into the metallacyclopentane species, the σ -bonding mode of 2,5-DMP is computed to be thermodynamically favoured.⁴⁶ Most interestingly, based on transition state geometry calculations within the proposed metallacycle mechanism, it was concluded that ring slippage of 2,5-DMP between σ - and η^5 -bonding modes could facilitate selective ethylene trimerisation.⁴⁶ Not only is the ring slippage of 2,5-DMP in the Chevron-Phillips ethylene trimerisation system favoured thermodynamically, it is kinetically feasible due to the small associated E_a barriers (*i.e.* 2.6 and 5.9 kcal mol⁻¹; Figure 12).⁴⁶ Hence, ligand hemilability has become a key feature of subsequent ethylene trimerisation initiators (see Page 18).^{6,15}

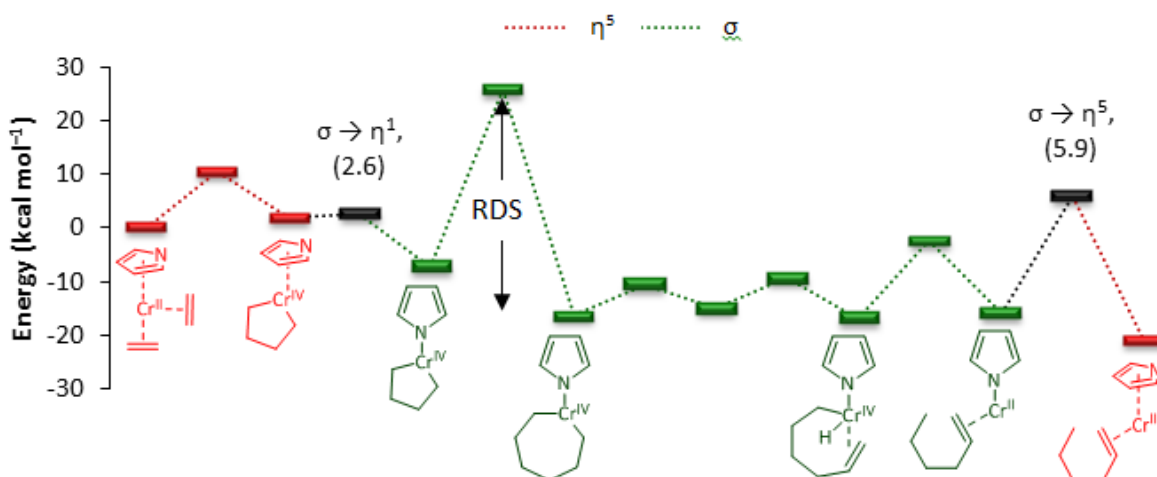
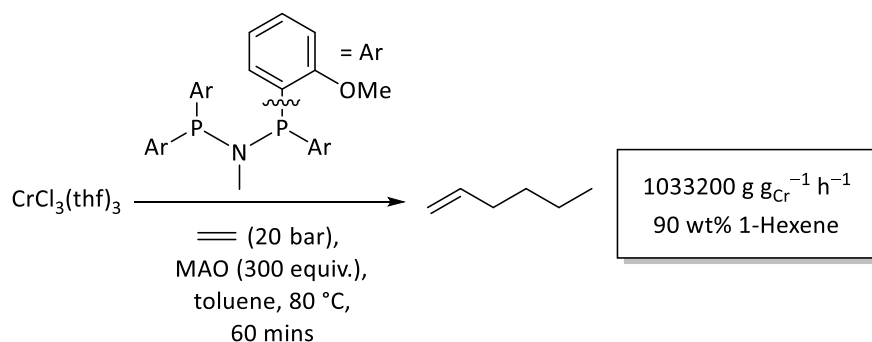


Figure 12: DFT-derived Gibbs free energy profile of the metallacycle-based ethylene trimerisation reaction mechanism facilitated by a σ -/ η^5 -pyrrolide $\text{Cr}^{\text{II/IV}}$ model initiator system at the PW91 level using the DNP basis sets, adapted from van Rensburg *et al.*, 2004⁴⁶

1.3.1.3 Case Study 3: Cr PNP^{OCH₃}/MAO Ethylene Trimerisation Catalyst

Since the discovery of the Chevron-Phillips Cr(2,5-DMP)₃ ethylene trimerisation pro-initiator, the nature of the coordination sphere around the chromium metal centre has become the subject of intense research.¹¹ Although very few reported systems can match the performance of the Chevron-Phillips ethylene trimerisation process, Wass (BP) patented a chromium(III) diphosphinoamine (PNP^{OCH₃}) pro-initiator in 2002,⁵⁸ which when activated with methyl aluminoxane (MAO), a partially hydrolysed derivative of Me₃Al, exhibited unprecedented ethylene trimerisation activity (Scheme 12).⁵⁹



Scheme 12: Highly active Cr PNP^{OCH₃}/MAO ethylene trimerisation initiator as reported by Carter *et al.*, 2002⁵⁹

Carter *et al.* conducted a comprehensive study of the BP Cr PNP^{OCH₃} ethylene trimerisation system, in which a range of *bis*-(diaryldiphosphine) ligands (Figure 13) were evaluated in combination with chromium(III) chloride *tris*-(tetrahydrofuran) {CrCl₃(thf)₃} and modified methyl aluminoxane (MMAO) for their catalytic activity.⁵⁹ Crucially, it was shown that the substitution of the nitrogen heteroatom on the PNP^{OCH₃} ligand with a hydrocarbon, or the *ortho*-methoxy aryl substituents with *para*-methoxy groups (Figure 13) resulted in the complete loss of ethylene trimerisation activity.⁵⁹ Hence, it was deemed that the diphosphinoamine (PNP) backbone and the *o*-OCH₃ aryl substituents are both critical to the high productivity and selectivity achieved by the BP Cr PNP^{OCH₃}/MAO ethylene trimerisation initiator.⁵⁹ Carter and co-workers even suggested that the *o*-CH₃ aryl group on the PNP^{OCH₃} ligand could behave as a labile pendant donor that can stabilise coordinatively unsaturated intermediates formed during ethylene trimerisation catalysis,⁵⁹ akin to 2,5-DMP in the related Chevron-Phillips process (see Figure 12).⁴⁶

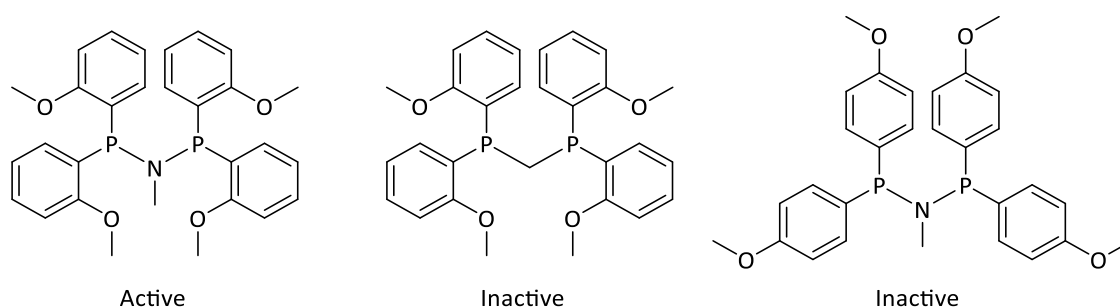
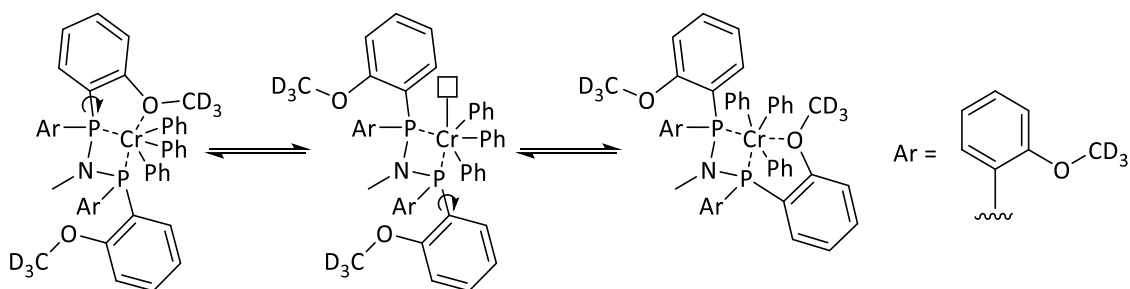


Figure 13: *bis*-(Diaryldiphosphines) evaluated by Carter *et al.* in the BP ethylene trimerisation process, 2002⁵⁹

In order to demonstrate the variable coordination of the $\text{PNP}^{\text{OCH}_3}$ ligand in such selective ethylene oligomerisation processes, Schofer *et al.* analysed a deuterated analogue of the BP catalyst precursor, namely $\text{CrPh}_3 \text{PNP}^{\text{OCD}_3}$, using X-ray crystallography and ^2H nuclear magnetic resonance (NMR) spectroscopy.⁶⁰ On the one hand, single crystal X-ray diffraction showed that the $\text{PNP}^{\text{OCD}_3}$ ligand coordinates to the chromium(III) metal centre *via* two phosphorus atoms and a single *ortho*-methoxy- d_3 donor on the aryl ring.⁶⁰ Conversely, solution-phase ^2H NMR spectroscopy indicated that all four *o*- OCD_3 substituents are equivalent at room temperature (RT), and therefore must all be involved in a dynamic exchange process (Scheme 13).⁶⁰



Scheme 13: Fluxional exchange of *o*- CD_3 donor ligands in $\text{CrPh}_3 \text{PNP}^{\text{OCD}_3}$, modified from Schofer *et al.*, 2006⁶⁰

Subsequently, Schofer and co-workers used variable temperature ^2H NMR spectroscopy to probe the dynamic exchange of the pendant *o*- OCD_3 aryl groups present in the $\text{CrPh}_3 \text{PNP}^{\text{OCD}_3}$ ethylene trimerisation pro-initiator.⁶⁰ At $-95\text{ }^\circ\text{C}$, a broad resonance at 50 ppm and a sharp resonance at 4 ppm in a 1:3 ratio were observed in the ^2H NMR spectrum of $\text{CrPh}_3 \text{PNP}^{\text{OCD}_3}$, which have been assigned to a single pendant *o*- OCD_3 donor ligand and three non-coordinated *o*- OCD_3 aryl groups, respectively.⁶⁰ As the NMR sample of $\text{CrPh}_3 \text{PNP}^{\text{OCD}_3}$ was warmed from -95 to $-75\text{ }^\circ\text{C}$, these signals were found to coalesce, which is indicative of a fluxional process that involves the dissociation of one *o*- OCD_3 ligand followed by the association of another.⁶⁰ Moreover, two resonances are present in a 1:1 ratio in the ^2H NMR spectrum of $\text{CrPh}_3 \text{PNP}^{\text{OCD}_3}$ at $-50\text{ }^\circ\text{C}$, whereas only one peak is observed above $-41\text{ }^\circ\text{C}$, and thus proves beyond doubt that all four *o*- OCD_3 aryl substituents are involved in the dynamic exchange process.⁶⁰ Since Schofer *et al.* have aptly demonstrated the variable coordination of the $\text{PNP}^{\text{OCD}_3}$ ligand,⁶⁰ it could be argued that the pendant *o*- CH_3 aryl substituents could potentially moderate the steric and/or electronic demands of the BP $\text{Cr PNP}^{\text{OCH}_3}$ /MAO ethylene trimerisation reaction.¹⁵

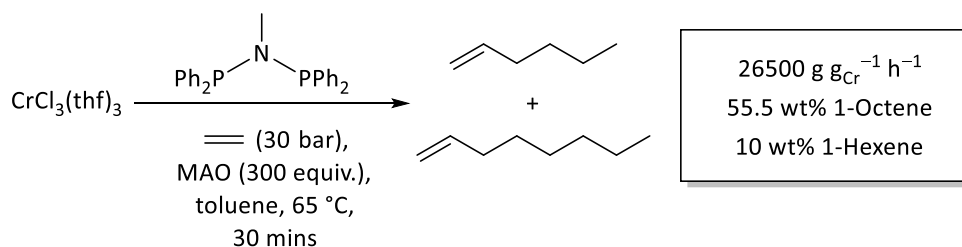
Parallels were inevitably drawn between the BP $\text{Cr PNP}^{\text{OCH}_3}$ /MAO ethylene trimerisation initiator and the related Union Carbide $\text{Cr}(2\text{-EH})_3/\text{PIBAO}$ and Chevron-Phillips $\text{Cr}(2,5\text{-DMP})_3/\text{Et}_3\text{Al}$ systems.¹⁵ Indeed, the BP $\text{Cr PNP}^{\text{OCH}_3}$ /MAO ethylene trimerisation catalyst exhibited second order kinetics with respect to ethylene, and achieved high selectivity towards 1-hexene (90 wt%) and decenes (8.5 wt%).⁵⁹ These observations were deemed to be consistent with Briggs' metallacycle mechanism (see Page 12).^{42,43,59} However, it was Agapie *et al.* who confirmed that the metallacyclic reaction manifold was indeed operative *via* an innovative deuterium-labelling

investigation of the BP Cr PNP^{OCH₃}/MAO ethylene trimerisation reaction.^{61,62} The same research group have even elucidated a plausible mechanism for the activation of the BP Cr PNP^{OCH₃} ethylene trimerisation catalyst precursor.⁶² These pioneering mechanistic investigations will be described in more detail in Section 1.3.1.5.

In summary, the BP Cr PNP^{OCH₃}/MAO ethylene trimerisation initiator, albeit impressive in terms of its catalytic activity, suffers with a lower selectivity compared with that of the established Chevron-Phillips process, and therefore was not considered suitable for industrial application.⁶ However, the discovery of the diphosphinoamine (PNP) class of ligand employed in the BP ethylene trimerisation system has since opened up an alternative approach of research in the field. More specifically, Sasol Technology have since tuned the BP ethylene trimerisation initiator, through a series of modifications to the patented PNP^{OCH₃} ligand to produce a selective chromium-mediated ethylene tetramerisation system.¹⁵

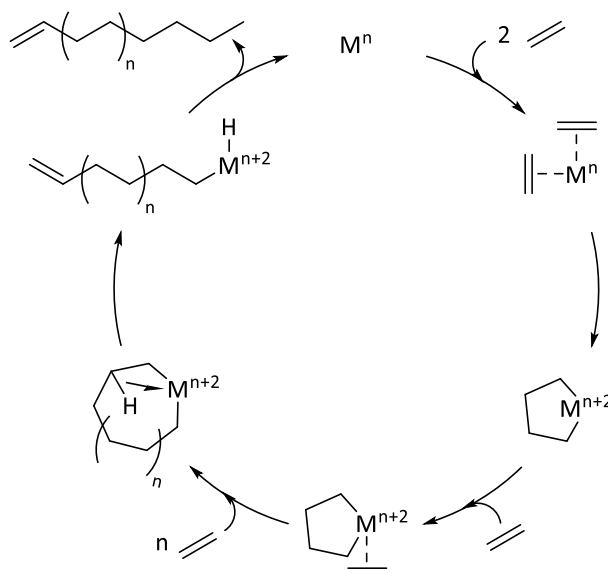
1.3.1.4 Case Study 4: Cr PNP/MAO Ethylene Tetramerisation System

Researchers at Sasol Technology have prepared and evaluated a related series of diphosphinoamine (PNP) ligands, in combination with a chromium(III) molecular precursor [*i.e.* CrCl₃(thf)₃ or chromium(III) 2,4-pentanedionate {Cr(acac)₃}] and MAO for their ethylene trimerisation behaviour.^{63,64,65} It was discovered that the removal of the pendant *o*-OCH₃ aryl substituents used in the BP Cr PNP^{OCH₃} ethylene trimerisation pro-initiator resulted in a switch in the product selectivity from 1-hexene in favour of 1-octene formation (Scheme 14).⁶³ Consequently, this technology was patented in a homogeneous chromium-mediated ethylene tetramerisation process in 2004.⁶⁶



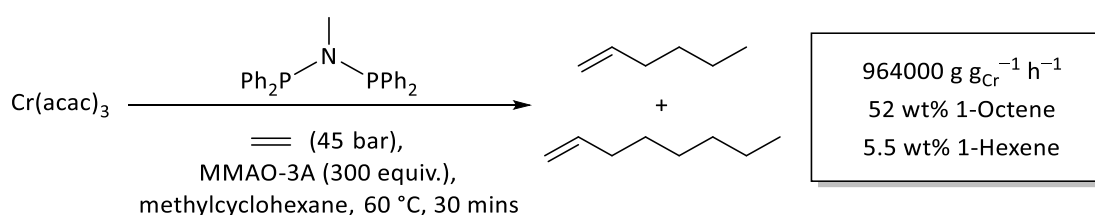
Scheme 14: Novel Cr PNP/MAO ethylene tetramerisation catalyst, adapted from Bollmann *et al.*, 2004⁶³

Overett *et al.* suggested that the high selectivity exhibited by the Sasol Cr PNP/MMAO-3A initiator towards 1-octene *via* ethylene tetramerisation could be explained by an extension of Briggs' metallacycle mechanism (Scheme 15).^{43,67} It was postulated that ethylene could insert into the chromacycloheptane intermediate resulting in the formation of a chromacyclononane species prior to β -hydride elimination, and the reductive elimination of 1-octene.⁶⁷



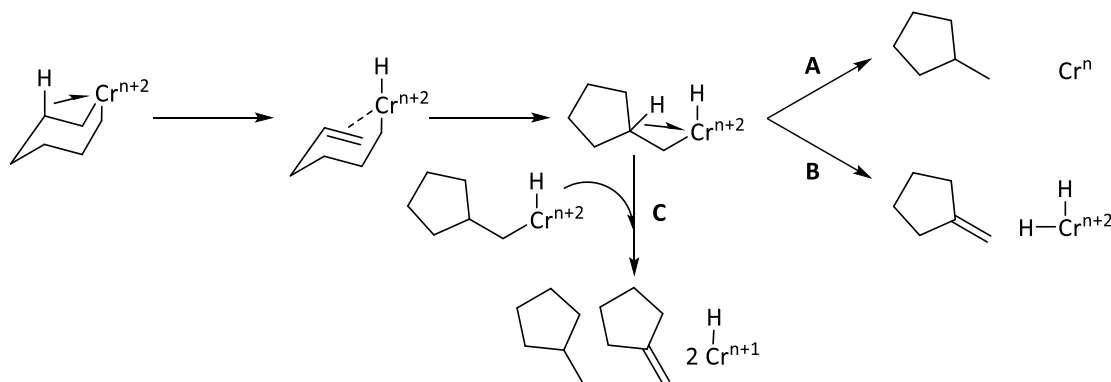
Scheme 15: Ethylene tetramerisation *via* an extended metallacycle mechanism, modified from Overett *et al.*, 2005⁶⁷

Blann and co-workers later reported that the productivity of the Sasol Cr PNP/MMAO-3A ethylene tetramerisation process could be enhanced by employing methylcyclohexane as the reaction diluent rather than toluene (Scheme 16).⁶⁸ It was reasoned that, despite ethylene solubility in methylcyclohexane being marginally higher than in toluene, the improved catalytic activity achieved by the Cr PNP/MMAO-3A ethylene tetramerisation initiator system in methylcyclohexane could not be wholly attributed to the increased concentration of ethylene in the liquid-phase.⁶⁸ Instead it was argued that toluene may coordinate to the active species resulting in the deactivation of the ethylene tetramerisation catalyst.⁶⁸ It has previously been reported that treatment of molecular chromium(III) complexes with alkyl aluminium reagents in aromatic diluents, for example Cr(acac)₃/Me₃Al in toluene,⁶⁹ will generate reduced chromium(I) sandwich complexes of the type [Cr(η⁶-arene)₂]⁺.⁷⁰ Hence, a similar reaction pathway for the deactivation of the Sasol Cr PNP/MMAO-3A ethylene tetramerisation initiator could be proposed.



Scheme 16: Enhanced productivity of the Sasol Cr PNP/MMAO-3A ethylene tetramerisation initiator in methylcyclohexane as reported by Blann *et al.*, 2007⁶⁸

In addition to 1-octene and 1-hexene, Overett *et al.* reported that the third most abundant product fraction generated by the Sasol Cr PNP/MMAO-3A ethylene tetramerisation process was consistently a 1:1 ratio of methylcyclopentane and methylenecyclopentane.⁶⁷ Here it was postulated that the chromacycloheptane intermediate may rearrange and cyclise to produce a methylcyclopentyl chromium species, which may then undergo either reductive elimination (**A**) to produce methylcyclopentane, β-hydride elimination (**B**) to form methylenecyclopentane or liberate both *via* disproportionation (**C**), as shown in Scheme 17.⁶⁷ However, the origin of these cyclic side products of ethylene tetramerisation has been the subject of considerable debate in the literature, and will be discussed later in Section 1.3.1.5.3.^{39,67,71,72}



Scheme 17: Proposed formation of methylcyclopentane and methylenecyclopentane *via* reductive elimination (A), β-hydride elimination (B) or disproportionation (C), modified from Overett *et al.*, 2005⁶⁷

Sasol Technology commissioned a comprehensive structure-reactivity investigation in an attempt to optimise the diphosphinoamine (PNP) ligand employed in their ethylene tetramerisation process.^{68,73,74,75} Consequently, it was discovered that the formation of the methylcyclopentane and methylenecyclopentane by-products of the Sasol Cr PNP/MMAO-3A ethylene tetramerisation reaction could be limited by increasing the steric bulk surrounding the nitrogen heteroatom in the ligand backbone (Table 1; Entries 1 – 3).^{68,73} Moreover, it has been shown that the catalytic behaviour of the Sasol Cr PNP ethylene tetramerisation pro-initiator may also be tuned through the variation in the steric and electronic properties of the *bis*-(phosphine) donor motifs and the P–P ligand backbone (*e.g.* N versus C, P–P bite angle; Table 1).^{68,75}

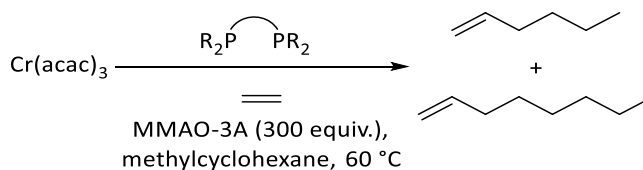


Table 1: Effect of ligand structural variation in the Sasol Cr PNP/MMAO-3A ethylene tetramerisation initiator, adapted from ^aBlann *et al.*, 2007⁶⁸, ^bKillian *et al.*, 2007⁷³ and ^cOverett *et al.*, 2008⁷⁵

Entry	Pressure (bar)	Al/Cr Ratio	Ligand 	C ₆ = {wt%} (%1-C ₆ =)	C ₈ = {wt%} (%1-C ₈ =)	Activity (g g _{Cr} ⁻¹ h ⁻¹)
1 ^a	45	300		16 (33)	54 (96)	964000
2 ^a	45	300		19 (75)	68 (99)	2150000
3 ^a	45	300		25 (86)	66 (99)	3200000
4 ^b	50	480		19 (47)	64 (97)	1070000
5 ^c	50	500		Schulz-Flory Distribution		21000
6 ^c	50	500		25 (55)	60 (100)	174000
7 ^c	50	500		88 (99)	6 (100)	11000

Researchers at Sasol Technology have also compiled extensive kinetic data regarding their Cr PNP/MMAO-3A ethylene tetramerisation process.^{71,76,77} Most interestingly, Kuhlmann *et al.* demonstrated that both the productivity and selectivity of the Sasol Cr PNP/MMAO-3A ethylene tetramerisation initiator can be significantly increased by lowering the reaction temperature from 80 to 40 °C (Figure 14a).⁷¹ For reference, Carter and co-workers found that the ethylene trimerisation behaviour of the closely-related BP Cr PNP^{OCH₃}/MAO system hardly changed as the reaction temperature was decreased from 110 to 80 °C.⁵⁹ In an attempt to rationalise the improved catalytic performance of the Sasol Cr PNP/MMAO-3A ethylene tetramerisation system at lower temperatures, Kuhlmann *et al.* determined the individual reaction orders for 1-hexene and 1-octene formation, which were found to be 1.3 and 2.1, respectively, in terms of ethylene concentration.⁷⁷ Since the rate of 1-octene production was reportedly more sensitive to ethylene concentration than that of 1-hexene,⁷⁷ it was postulated that the enhanced activity and selectivity achieved by the Sasol Cr PNP/MMAO-3A ethylene tetramerisation catalyst at lower temperatures can, in part, be attributed to the increased solubility of ethylene in the liquid-phase.⁷¹ It is perhaps unsurprising then that increasing the ethylene working pressure led to an increased productivity, as well as a slight increase in selectivity towards 1-octene, as shown in Figure 14b.⁷¹ Following the rational design and development of the molecular (homogeneous) Cr PNP pro-initiator, Sasol Technology have commissioned the world's first selective ethylene tetramerisation plant with a capacity of 100000 metric tons of 1-octene *per annum*.^{8,18}

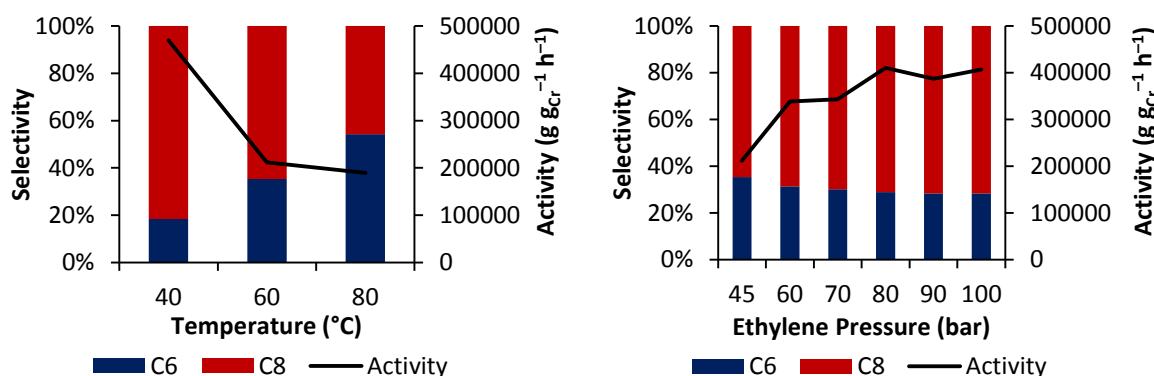


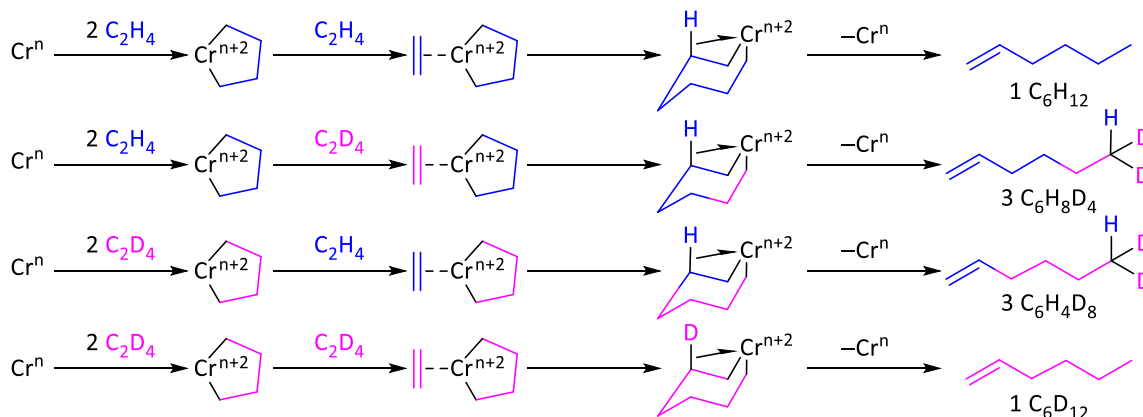
Figure 14: Influence of (a) reaction temperature (Left; at 45 bar) and (b) working ethylene pressure (Right; at 60 °C) on the Sasol Cr PNP/MMAO-3A ethylene tetramerisation process as reported by Kuhlmann *et al.*, 2006⁷¹

The next section of this thesis will discuss a series of mechanistic studies that probe the reaction mechanism(s) that are operative in selective homogeneous ethylene tri-/tetra-merisation catalysis. This will provide crucial insight into the activation and the mode of operation of related heterogeneous selective olefin oligomerisation systems.

1.3.1.5 Mechanistic Studies: Selective Ethylene Oligomerisation Catalysis

1.3.1.5.1 Metallocyclic Ethylene Tri-/Tetra-merisation Reaction Manifold

As alluded to earlier in Section 1.3.1.3, it was Agapie *et al.* who provided the clearest evidence yet that selective ethylene trimerisation is mediated by a metallocyclic reaction manifold.⁶² Indeed, a metallocyclopentane derivative of the BP Cr PNP^{OCH₃} ethylene trimerisation pro-initiator was activated using MAO, and reacted with a 1:1 ratio of C₂H₄ and C₂D₄ to produce 1-hexene.^{62,78} Gas chromatographic-mass spectrometric (GC-MS) analysis of the resulting liquid-phase oligomers revealed that 1-hexene contained only an even number of deuterons, with an isotopomer distribution of 1:3:3:1 that is consistent with a metallocycle-based reaction mechanism, as illustrated in Scheme 18.^{61,62} Further ethylene trimerisation experiments were completed using *cis*-, *gem*- and *trans*-ethylene-*d*₂, which afforded 1-hexene isotopomers with terminal CDH groups.⁶² Together, these product distributions infer that the BP Cr PNP^{OCH₃}/MAO ethylene trimerisation reaction involves β-hydride elimination and reductive elimination steps, something that is indicative of a metallocyclic pathway, rather than a Cossee-Arman chain growth process.⁶²



Scheme 18: Isotopomer distribution of 1-hexene production via a metallocycle-based ethylene trimerisation reaction mechanism, adapted from Agapie *et al.*, 2007⁶²

As previously stated in Section 1.3.1.1, the inherent selectivity of Briggs' metallocycle mechanism towards 1-hexene is considered to be regulated by the relative stability of the chromacyclopentane intermediate *versus* the chromacycloheptane species,^{43,45} as well as the E_a barriers for β-hydride elimination and the reductive elimination of 1-hexene, and that for further metallocycle expansion.⁴⁶ In fact, the insertion of a fourth ethylene molecule into the chromacycloheptane intermediate was not initially considered to be energetically feasible.⁴⁶ In spite of this, Overett and co-workers reacted the Sasol Cr PNP/MMAO-12 ethylene tetramerisation catalyst with a 1:1 ratio of C₂H₄ and C₂D₄ in an attempt to validate their hypothesis that 1-octene formation could be mediated by an extension of Briggs' metallocycle mechanism.⁶⁷ The ensuing liquid fraction was analysed by GC-MS to determine the isotopomer distribution for 1-hexene and 1-octene.⁶⁷ In theory, if the metallocycle-based reaction mechanism is in operation, the resulting isotopomer distributions for 1-hexene and 1-octene should both be

consistent with Pascal's triangle. Indeed, if the isotopic ratio of C_2H_4 to C_2D_4 (x) incorporated into 1-hexene and 1-octene were both equal to 1, their respective isotopomer distributions would be 1:3:3:1 and 1:4:6:4:1 (Figure 15).⁶⁷

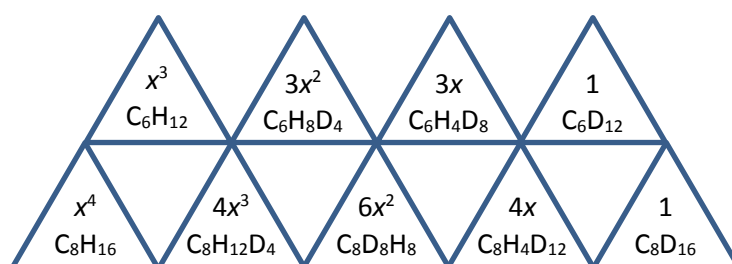


Figure 15: Ideal isotopomer distribution of 1-hexene and 1-octene as reported by Overett *et al.*, 2005⁶⁷

Most interestingly, Overett *et al.* determined the isotopic ratio of C_2H_4 to C_2D_4 (x) incorporated into 1-hexene and 1-octene generated by the Sasol Cr PNP/MMAO-12 ethylene tetramerisation catalyst to be 2.5 and 1.9, respectively.⁶⁷ Taking these ratios into account, it was reasoned that the relative isotopic distributions for both 1-hexene ($x = 2.5$) and 1-octene ($x = 1.9$) are consistent with Pascal's triangle, and thus is indicative of a metallacyclic reaction manifold (Figure 16).⁶⁷

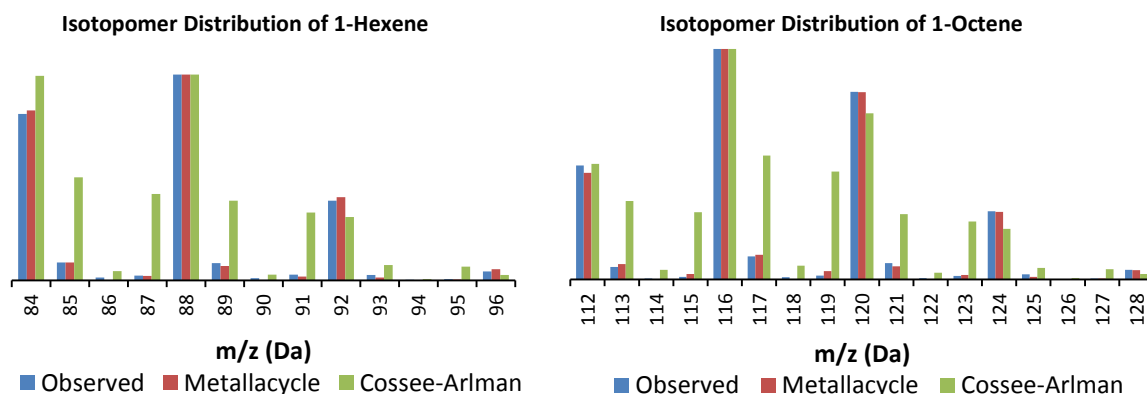
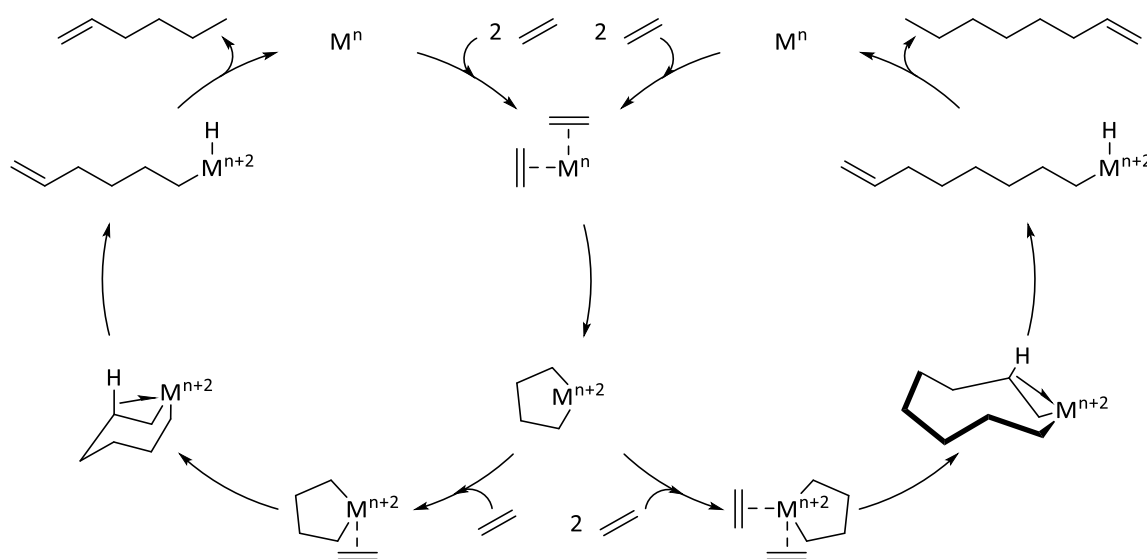


Figure 16: Isotopic labelling investigation of the Sasol Cr PNP/MMAO-12 ethylene tetramerisation process, modified from Overett *et al.*, 2005⁶⁷

Now that the basis of the metallacyclic reaction manifold has been established for the selective tri- and tetra-merisation of ethylene, it was important to qualify the kinetic dependence of 1-hexene and 1-octene formation with respect to ethylene concentration. It has been widely reported in the literature that ethylene trimerisation is a second order process and that the oxidative coupling of two ethylene molecules is the RDS in the metallacycle mechanism.^{42,57,59,67,79} Conversely, 1-hexene formation has also been described as a *pseudo*-first order process, and that the RDS in the metallacycle-based ethylene trimerisation reaction mechanism is the expansion of the chromacyclopentane intermediate.^{39,46,72,77,80,81,82} Selective ethylene tetramerisation, on the other hand, displays a second order kinetic dependence on ethylene concentration.⁷⁷ Here it was postulated that the RDS in the metallacyclic tetramerisation reaction manifold is the insertion of

two further ethylene molecules into the chromacyclopentane species. In order to rationalise these observations, Britovsek and co-workers proposed a modification to the metallacycle mechanism, in which there is a single-/double-coordination of ethylene to the chromacyclopentane species, prior to β -hydride elimination and the reductive elimination of either 1-hexene or 1-octene (Scheme 19).^{39,83} Based on ΔG values derived from DFT calculations, it was proposed that the double-coordination of ethylene to a cationic chromium(III) diphosphinoamine (PNP) metallacycle is favoured thermodynamically (Figure 17).³⁹ It was even suggested that an equilibrium exists between the positively-charged *mono-/bis*-(ethylene) chromacyclopentane intermediates, which dictates the selectivity of the Cr PNP/MAO catalyst towards either 1-hexene or 1-octene.^{39,72}



Scheme 19: Metallacycle-based single-/double-insertion selective ethylene oligomerisation reaction mechanism proposed by Britovsek *et al.*, 2015³⁹

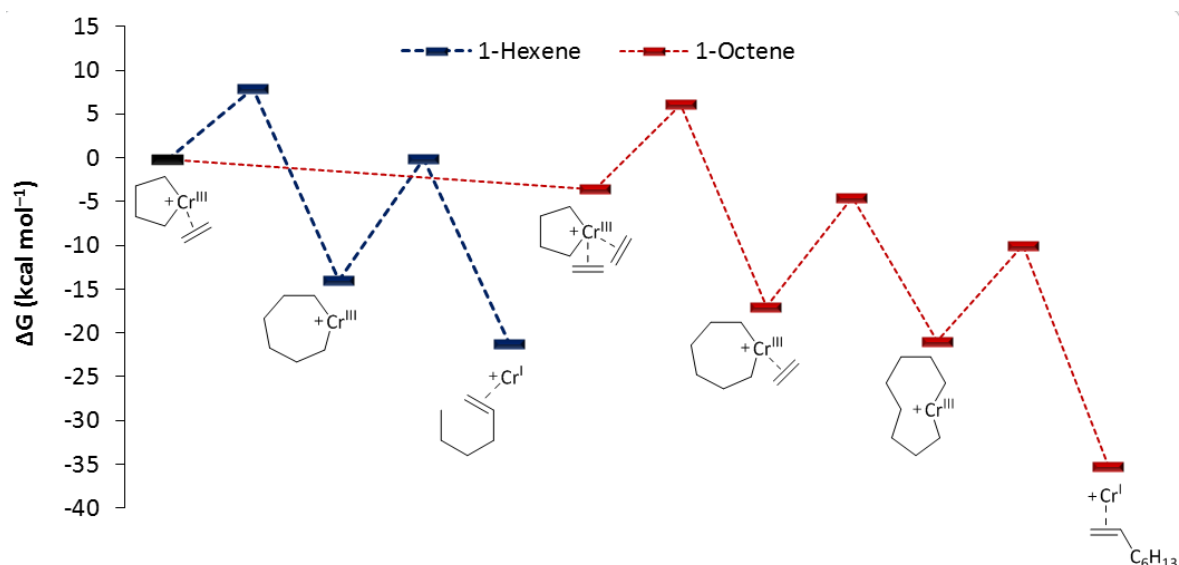
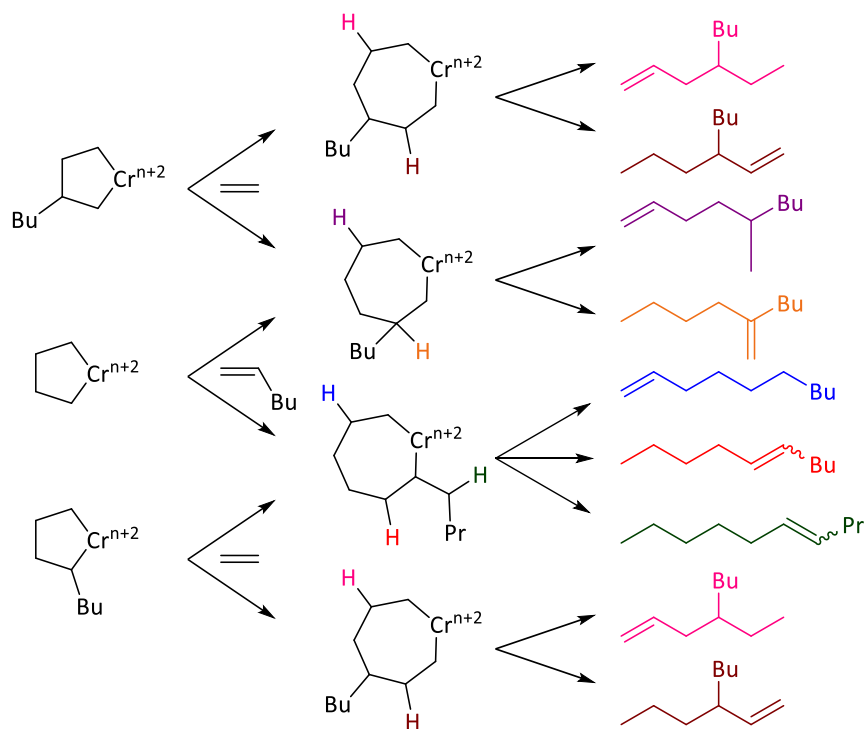


Figure 17: Theoretical Gibbs free energy profile for the metallacyclic single-/double-insertion manifold from $[(\text{PNP})\text{Cr}(\text{C}_4\text{H}_8)(\text{ethylene})]^+$ at the M06L level using the BS1 and BS2 basis sets, modified from Britovsek *et al.*, 2015³⁹

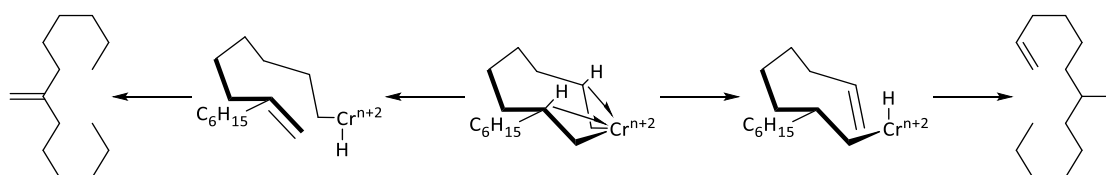
1.3.1.5.2 Metallacycle-based Ethylene Co-oligomerisation

Another characteristic of the metallacycle-based ethylene trimerisation reaction mechanism is the reincorporation of 1-hexene, which may undergo co-trimerisation with two further molecules of ethylene to liberate 1-decene and/or a mixture of branched decenes.^{42,49} Overett, Do, Zilbershtein and co-workers have since characterised several decenes, including both branched and internal isomers, whose formation can be rationalised by an extension of the metallacycle mechanism (Scheme 20).^{67,84,85}



Scheme 20: Proposed secondary metallacyclic ethylene/1-hexene co-trimerisation reaction manifold, adapted from Overett *et al.*, 2005,⁶⁷ Do *et al.*, 2012⁸⁴ and Zilbershtein *et al.*, 2014⁸⁵

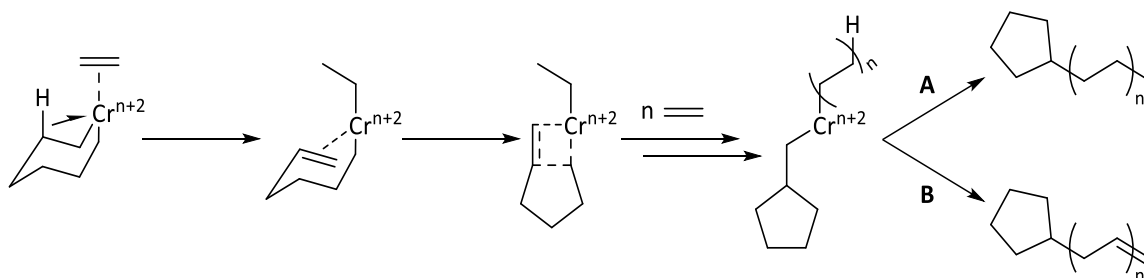
Workers at BP and Sasol Technology also observed C_{12} , C_{14} and/or C_{16+} olefinic by-products of their respective ethylene tri-/tetra-merisation processes, presumably originating from the reincorporation of either 1-hexene and/or 1-octene into the metallacycle mechanism.^{59,67,84} Notably, Overett *et al.* identified two components that made up ~ 70 wt% of the C_{14} oligomeric product fraction afforded by the Sasol Cr PNP/MMAO-3A ethylene tetramerisation initiator, namely 7-methylenetridecane and 7-methyltridecene whose formation has been attributed to a secondary ethylene/1-octene co-tetramerisation reaction (Scheme 21).⁶⁷



Scheme 21: Metallacycle-based co-tetramerisation of ethylene/1-octene as reported by Overett *et al.*, 2005⁶⁷

1.3.1.5.3 Formation of Methylcyclopentane and Methylene-cyclopentane

As previously stated (see Section 1.3.1.4), the third most abundant product fraction afforded by the homogeneous Sasol Cr PNP/MMAO-3A ethylene tetramerisation process was a mixture of methylcyclopentane and methylenecyclopentane.⁶⁷ It was originally claimed that the formation of these cyclic products, specifically in a 1:1 ratio could not easily be rationalised by competing reductive elimination and β -hydride elimination reactions from a methylcyclopentyl chromium species (see Scheme 17).⁶⁷ Hence, it was reasoned that these cyclic compounds must be the products of disproportionation.⁶⁷ In support of this proposed disproportionation pathway, Kuhlmann *et al.* reported that the rate of methylcyclopentane and methylenecyclopentane formation are both independent of ethylene concentration.⁷¹ In direct contrast, however, Britovsek and co-workers more recently reported that the formation of methylcyclopentane and methylenecyclopentane exhibit a *pseudo*-first order dependence on ethylene concentration.³⁹ Together with the fact that these cyclic by-products of the Sasol Cr PNP/MMAO-3A ethylene tetramerisation process are not observed during ethylene trimerisation catalysis, the aforementioned disproportionation route was therefore discounted.³⁹ Instead, an alternative reaction mechanism was postulated in which the chromacycloheptane intermediate undergoes ethylene coordination, migratory insertion and cyclisation to produce a methylcyclopentyl ethyl chromium species, prior to chain propagation and either reductive elimination (**A**; Scheme 22) or β -hydride elimination (**B**).³⁹ Crucially, it was demonstrated computationally that the respective E_a barriers for these two reaction pathways are similar, which may explain the 1:1 ratio of methylcyclopentane and methylenecyclopentane formed during ethylene tetramerisation catalysis.^{39,72}



Scheme 22: Formation of longer chain cyclopentane derivatives *via* chromium-mediated reductive elimination (**A**) or β -hydride elimination (**B**) proposed by Britovsek *et al.*, 2015³⁹

1.3.1.5.4 Role of Co-catalysts in Selective Ethylene Oligomerisation

At this point, it is important to emphasise that the exact structure of the active species for any known selective ethylene oligomerisation initiator system remains a matter of considerable debate.⁶ Unfortunately, elucidation of their composition/structure is complicated by the paramagnetic nature of the chromium species involved, and further convoluted by the ill-defined nature of some Lewis acidic aluminium-based co-catalysts (*i.e.* PIBAO, MAO, MMAO), which often lead to conflicting hypotheses in the literature.⁸⁶ For example, although methyl aluminoxane (MAO) can be defined as a partially hydrolysed derivative of Me_3Al , its structure has been reported as a 1-D linear chain, cyclic ring, 3-D cluster and a cage (Figure 18).⁸⁶ Moreover, solutions of MAO typically contain interconverting “free” and “associated” Me_3Al that participate in equilibria with MAO-based oligomers.⁸⁶ Furthermore, MAO is neither considered to be very soluble in aliphatic solvents, or indeed thermally stable.^{68,86} Conversely, modified methyl aluminoxanes (MMAO), which are typically prepared by the partial hydrolysis of a mixture of Me_3Al and $t\text{Bu}_3\text{Al}$, are known for their increased solubility in aliphatic diluents and stability at elevated temperatures.^{68,86} Hence, commercially-available solutions of MMAO are commonly employed as activators in selective ethylene oligomerisation.^{59,68,84} However, since the structure of MMAO is also ill-defined, mechanistic studies of ethylene tri-/tetra-merisation systems often employ more well-defined co-catalysts, such as $\text{Na}[\text{B}\{\text{C}_6\text{H}_3(\text{CF}_3)_2\}_4]$.⁶²

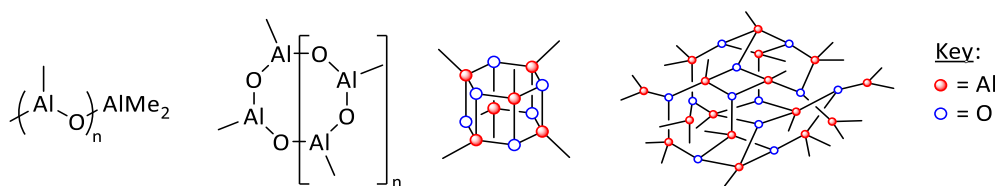
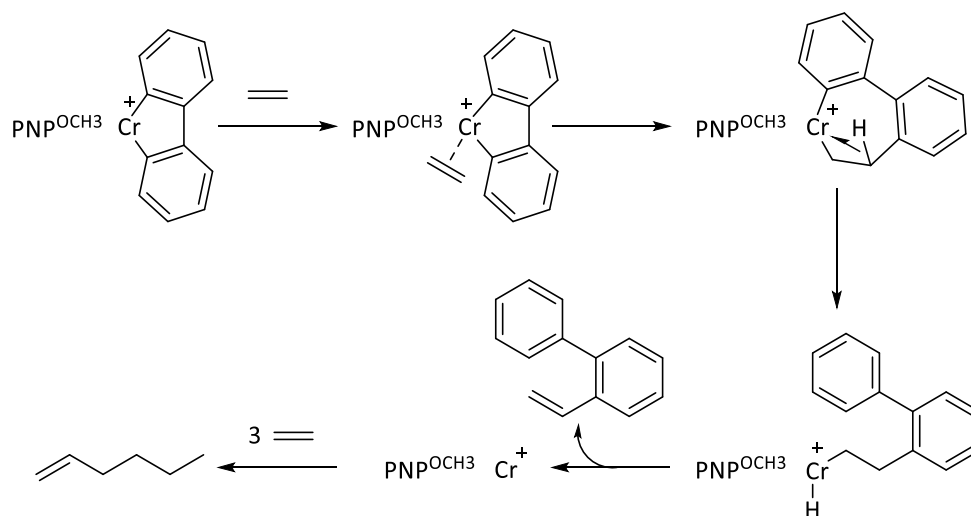


Figure 18: Proposed structures of MAO, adapted from Chen *et al.*, 2000⁸⁶

In order to probe the activation of the BP Cr PNP^{OCH₃} ethylene trimerisation pro-initiator, Agapie and co-workers studied the reaction between a model chromium(III) metallacyclopentane bromide complex and $\text{Na}[\text{B}\{\text{C}_6\text{H}_3(\text{CF}_3)_2\}_4]$ under an atmosphere of ethylene.⁶² Here the authors observed the formation of both 4-phenylstyrene and 1-hexene by ¹H NMR spectroscopy, whereas in the absence of $\text{Na}[\text{B}\{\text{C}_6\text{H}_3(\text{CF}_3)_2\}_4]$, ethylene trimerisation does not occur. Hence, it was postulated that the co-catalyst may abstract the bromide ligand from the Cr PNP^{OCH₃} biphenyldiyl bromide ethylene trimerisation catalyst precursor generating a coordinatively-unsaturated cationic metallacyclic species.⁶² Sequential ethylene association, migratory insertion, β -hydride elimination and reductive elimination reactions are thought to liberate 4-phenylstyrene, and yield the $[\text{Cr PNP}^{\text{OCH}_3}]^+$ species that is responsible for 1-hexene production (Scheme 23).⁶² Not only does the positively-charged chromium metal centre possess an additional vacant coordination site, but its inherent electrophilicity may be necessary for the ethylene coordination and oxidative addition steps involved in the metallacyclic reaction manifold.⁶² Although Agapie and co-workers did not

specifically mention the oxidation state of the active catalyst, it has been suggested that these findings support the hypothesis that a Cr^I/Cr^{III} redox couple mediates ethylene trimerisation *via* a metallacycle-based reaction mechanism.¹⁵

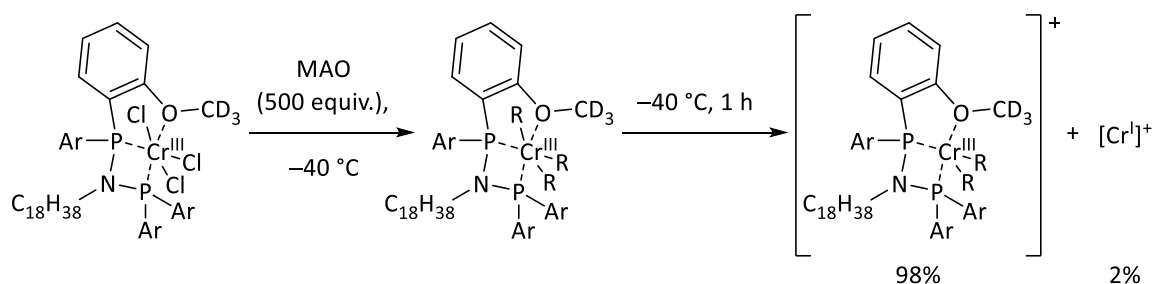


Scheme 23: Activation of a model Cr^{III} PNP^{OCH₃}₃ biphenyldiyl bromide ethylene trimerisation pro-initiator using Na[B(C₆H₃(CF₃)₂)₄], modified from Agapie *et al.*, 2007⁶²

Now, it should be highlighted that there are conflicting reports in the literature that describe selective ethylene oligomerisation processes being facilitated by a Cr^I/Cr^{III}-, Cr^{II}/Cr^{IV}- or Cr^{III}/V-based metallacyclic reaction manifold.^{39,46,72,81,83,87} That being said, several experimental approaches have provided compelling evidence that supports the notion that the Cr^I/Cr^{III} redox couple mediates ethylene tri-/tetra-merisation catalysis. For example, Skobelev and co-workers used electron paramagnetic resonance (EPR) spectroscopy to monitor the relationship between the concentration of a Cr^I and Cr^{III} species in solution and ethylene trimerisation activity.⁸⁸ *In situ* EPR measurements of a series of ethylene trimerisation initiators in cyclohexane, analogous to the Chevron-Phillips Cr(2,5-DMP)₃/Et₃Al catalyst, established a correlation between 1-hexene formation and the concentration of a Cr^I species.⁸⁸ However, based on this evidence alone, it could be inferred that the EPR-silent Cr^{II}/Cr^{IV} redox couple may instead be responsible for the ethylene trimerisation behaviour observed.

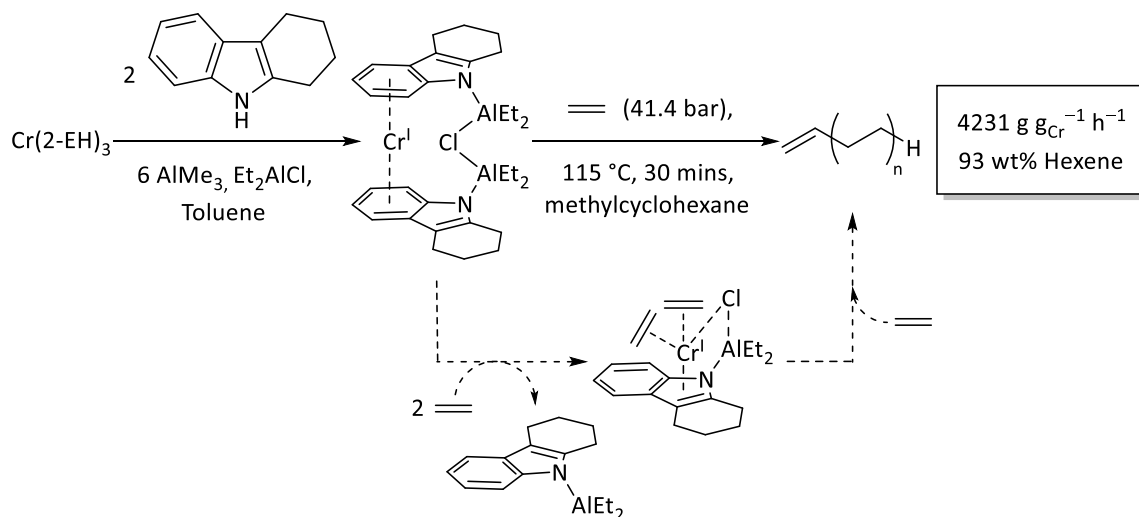
Fang *et al.* activated the Chevron-Phillips Cr(2,5-DMP)₃ ethylene trimerisation catalyst precursor with Et₃Al, and “preserved” the reaction mixture by encapsulating it in solid paraffin.⁸⁹ The resulting paraffin-coated chromium(III) species was exposed to air for over 24 hours, and yet was still found to trimerise ethylene with very high selectivity (94 wt% 1-hexene).⁸⁹ X-Ray photoelectron spectroscopic (XPS) analysis of the paraffin-coated reaction mixture revealed that only Cr^{III} and Cr^{VI} species were present in the sample. Hence, the authors concluded that a chromium(III) species must play an active role in the Chevron-Phillips ethylene trimerisation process,⁸⁹ presumably as part of the Cr^I/Cr^{III} redox couple.

Do and co-workers monitored the activation of a $\text{CrCl}_3 \text{PNP}^{\text{OCD}_3}$ ethylene trimerisation catalyst precursor using *in situ* EPR spectroscopy in an attempt to elucidate the oxidation state of the active species.⁹⁰ In order to overcome solubility problems at low temperatures, the *N*-methyl group on the $\text{PNP}^{\text{OCD}_3}$ ligand was substituted with an octadecyl chain (*i.e.* $\text{CrCl}_3 \text{PN}^{\text{C}_{18}\text{P}^{\text{OCD}_3}}$).⁹⁰ Treatment of $\text{CrCl}_3 \text{PN}^{\text{C}_{18}\text{P}^{\text{OCD}_3}}$ with MAO in chlorobenzene at -40°C quickly generated another octahedral Cr^{III} species in nearly quantitative yield, whose EPR spectrum closely resembles that of $\text{Cr}(\text{2-EH})_3$.⁹⁰ Over the course of an hour, two new sets of resonances were observed in the resulting EPR spectrum, consistent with a high spin Cr^{III} (98%) and a Cr^{I} species (2%).⁹⁰ It was reasoned that MAO alkylates the $\text{CrCl}_3 \text{PN}^{\text{C}_{18}\text{P}^{\text{OCD}_3}}$ complex, and abstracts an alkyl group to produce a high spin cationic Cr^{III} species, which may then undergo reductive elimination to yield a positively-charged Cr^{I} -based ethylene trimerisation initiator (Scheme 24).⁹⁰ Although this may be true, neither of the aforementioned Cr^{I} or Cr^{III} species were observed by EPR spectroscopy when $\text{CrCl}_3 \text{PN}^{\text{C}_{18}\text{P}^{\text{OCD}_3}}$ was reacted with MAO in chlorobenzene at RT. Instead, the EPR spectrum of the resulting reaction mixture presents signals consistent with $[\text{Cr}(\eta^6\text{-arene})_2]^+$, presumably originating from a reaction between the $[\text{Cr}^{\text{I}}]^+$ species and chlorobenzene (See Page 22),^{69,70} and accounts for 6% of the total chromium concentration.⁹⁰ Again, based on this evidence alone, the EPR-silent chromium components (94%) represent an equally viable candidate for the active catalyst responsible for chromium-mediated ethylene trimerisation.



Scheme 24: EPR study of the reaction between $\text{Cr} \text{PN}^{\text{C}_{18}\text{P}^{\text{OCD}_3}}$ and MAO at -40°C , adapted from Do *et al.*, 2013⁹⁰

Jabri *et al.* provided further evidence that the metallacyclic ethylene trimerisation manifold is indeed catalysed by a Cr^I/Cr^{III} redox couple.⁹¹ Here the authors reacted Cr(2-EH)₃ with tetrahydrocarbazole in the presence of Et₃Al and Et₂AlCl. The resulting *pseudo*-octahedral chromium(I) sandwich complex was isolated and then employed as a so-called “self-activating” ethylene trimerisation initiator.⁹¹ It was assumed that the active catalyst is generated *via* ring slippage to the η⁵-pyrrolide moiety prior to ligand dissociation, thus vacating the coordination sites required for ethylene trimerisation (Scheme 25).⁹¹



Scheme 25: “Self-activating” Cr^I ethylene trimerisation catalyst as reported by Jabri *et al.*, 2008⁹¹

Moreover, Jabri and co-workers proposed that the oxidation state of the chromium-based ethylene oligo-/poly-merisation initiator system determines its product selectivity.⁹¹ In addition to the aforementioned “self-activating” Cr^I ethylene trimerisation initiator, the authors prepared and evaluated the corresponding Cr^{II} and Cr^{III} analogues for their catalytic behaviour (Figure 19).⁹¹ In the absence of any further co-catalyst, the Cr^{II} derivative of the activated Chevron-Phillips ethylene trimerisation initiator polymerised ethylene, whereas the Cr^{III}-based catalyst produced a statistical distribution of oligomers as well as PE.⁹¹

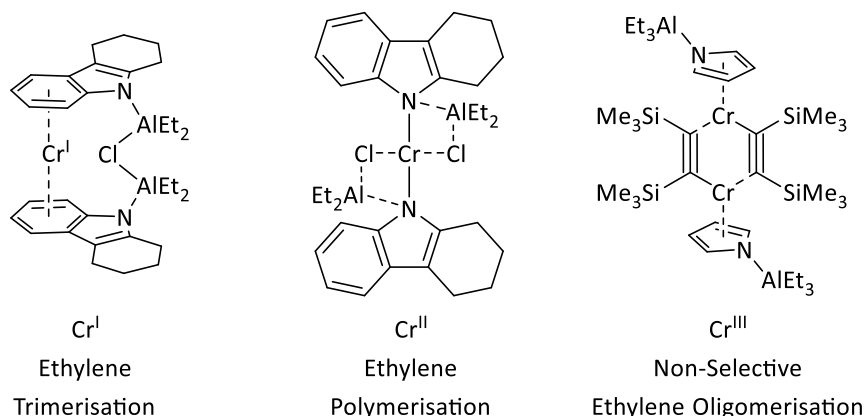
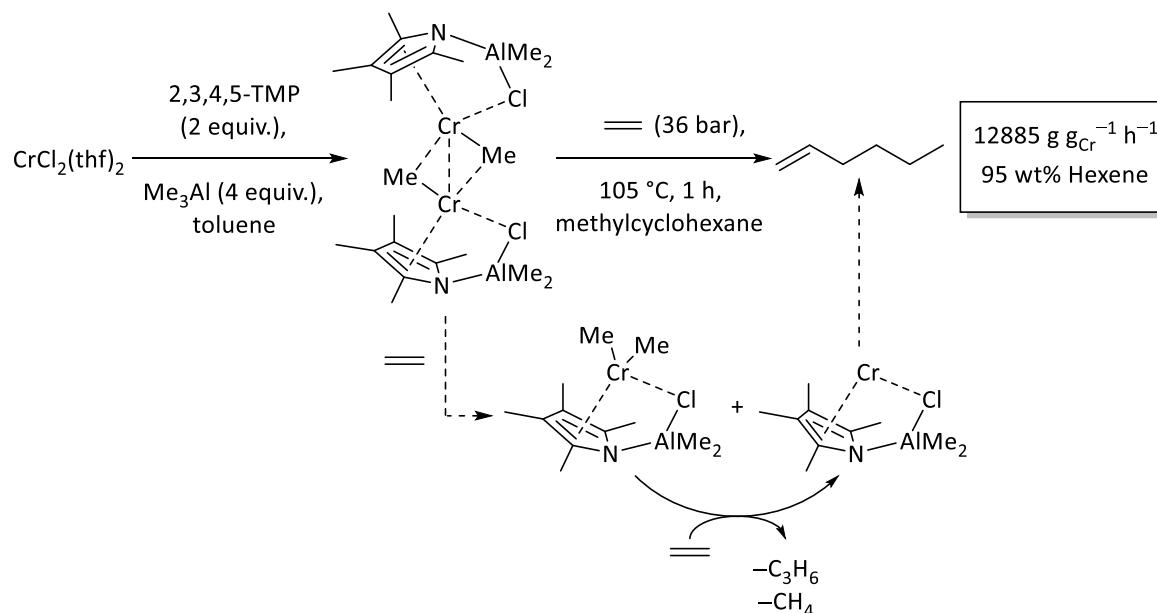


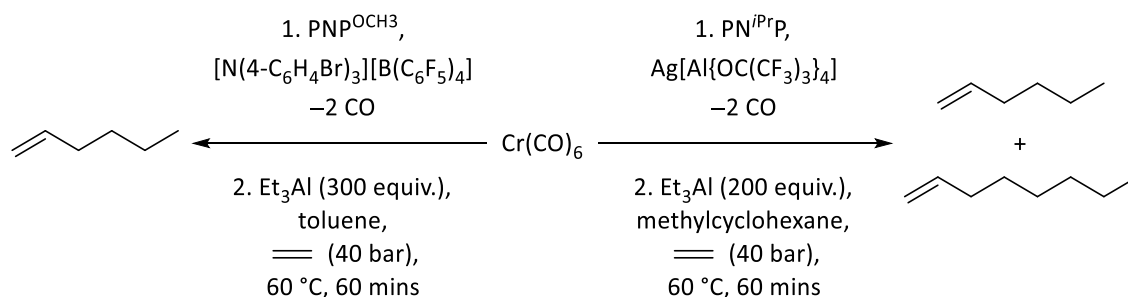
Figure 19: Impact of oxidation state on ethylene oligo-/poly-merisation catalysis, modified from Jabri *et al.*, 2008⁹¹

Vidyaratne *et al.* reacted $\text{CrCl}_2(\text{thf})_2$ with 2,3,4,5-tetramethylpyrrole (2,3,4,5-TMP) and Me_3Al resulting in the formation of a dimeric chromium species, which was subsequently employed as a “self-activating” ethylene trimerisation initiator (Scheme 26).⁹² In this case, the authors suggested that this dimeric complex disproportionates in the presence of ethylene to form an active chromium(I)-based catalyst that is responsible for 1-hexene production.⁹²



Scheme 26: Isolation of a “self-activating” trimerisation catalyst, adapted from Vidyaratne *et al.*, 2009⁹²

Since the metallacyclic reaction manifold has now been attributed to a $\text{Cr}^{\text{I/III}}$ redox couple,⁹¹ Bowen, Rucklidge *et al.* have attempted to activate respective chromium(0) derivatives of the BP Cr $\text{PNP}^{\text{OCH}_3}$ and Sasol Cr PNP selective ethylene oligomerisation pro-initiator electrochemically (*via* a one-electron oxidation).^{93,94} Unfortunately, in both cases, an excess of Et_3Al (~300 equivalents) was required as a scavenger to abstract CO ligands from the relatively stable chromium(0) carbonyl pro-initiator to generate the active species responsible for 1-hexene and/or 1-octene formation (Scheme 27).^{93,94} Nevertheless, the one-electron electrochemical oxidation of more labile chromium(0) ethylene tri-/tetra-merisation catalyst precursors may yet provide a safer and more economical alternative to the conventional reduction of a chromium(III) pro-initiator mediated by an alkyl aluminium-based co-catalyst (*e.g.* Et_3Al , MAO, MMAO).



Scheme 27: One-electron electrochemical oxidation of respective Cr^0 derivatives of the BP and Sasol selective ethylene oligomerisation catalyst precursor, modified from Bowen *et al.*, 2007⁹³ and Rucklidge *et al.* 2007⁹⁴

1.3.1.6 Summary of Homogeneous Selective Ethylene Oligomerisation

In spite of the paramagnetic nature of the chromium species involved and the ill-defined nature of aluminoxane-based co-catalysts often employed, significant mechanistic insight has been made in the field of selective ethylene oligomerisation catalysis by studying a series of soluble molecular pro-initiators.^{6,15,16} Generally, the Lewis acidic co-catalyst is widely believed to react with a, typically, chromium(III)-based ethylene tri-/tetra-merisation pro-initiator to yield a coordinatively unsaturated $[\text{Cr}^{\text{III}}]^+$ species, which may then undergo reductive elimination to generate a $[\text{Cr}^{\text{I}}]^+$ species that facilitates the production of 1-hexene and/or 1-octene *via* a $\text{Cr}^{\text{I}}/\text{Cr}^{\text{III}}$ -based metallacyclic reaction manifold.^{62,91} Subsequent reincorporation of 1-hexene and/or 1-octene into the metallacycle mechanism may lead to co-oligomerisation with further molecules of ethylene to liberate a mixture of higher LAOs (*e.g.* C_{10} , C_{12} , C_{14} and C_{16+}), including both internal and branched isomers.^{67,84,85}

It is clear that the oxidation state of the chromium metal centre, nature of the ligand sphere, alkyl aluminium-based co-catalyst, Al/Cr mole ratio, diluent and reaction conditions all play an intimate role in dictating the activity and selectivity of *homogeneous* selective ethylene oligomerisation catalysts.¹¹ Such fundamental understanding will be crucial when developing *heterogeneous* selective ethylene oligomerisation systems in this PhD project. The final section of this introduction will aim to describe and critically evaluate several examples of already established solid-phase olefin oligomerisation initiators.

1.3.2 An Overview of Heterogeneous Catalytic Ethylene Oligomerisation

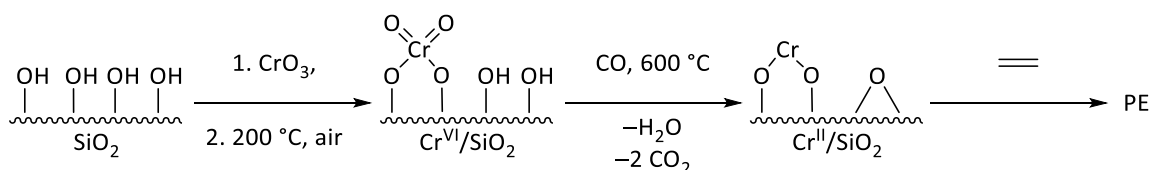
Notwithstanding the successful commercialisation of the respective molecular (*homogeneous*) Chevron-Phillips and Sasol Technology ethylene tri-/tetra-merisation processes, there is still a drive to develop *heterogeneous* selective olefin oligomerisation systems.^{29,95} Indeed, solid ethylene oligomerisation catalysts offer numerous advantages over their soluble molecular counterparts, including:

- more efficient separation of liquid-phase oligomers from the solid catalyst;^{29,95}
- increased stability of the initiator;^{23,28}
- potential catalyst recyclability;^{23,29}
- possibility of a solvent-free reaction.^{28,95}

To date, progress in the field of heterogeneous selective olefin oligomerisation has been limited. Recent attempts at immobilising existing molecular ethylene tri-/tetra-merisation initiators onto solid support materials have often led to a reduced selectivity towards LAOs, typically in favour of PE formation, coupled with a lower catalytic activity.^{22,23,24,25,26,27,28} In order to rationalise the former, it is necessary to describe the closely-related long-standing commercialised Phillips heterogeneous so-called “Cr/SiO₂” ethylene polymerisation catalyst, which is responsible for approximately 40 – 50% of the world’s supply of HDPE.^{4,96} Although the Phillips Cr/SiO₂ ethylene polymerisation system is not strictly relevant to olefin oligomerisation catalysis, there is significant overlap between the two processes, particularly in terms of the potential involvement of a supported variant of the metallacycle mechanism (often invoked to account for ethylene oligomerisation selectivity in TM-mediated processes) in addition to the more conventional Cossee-Arlman-type chain growth process.^{4,97}

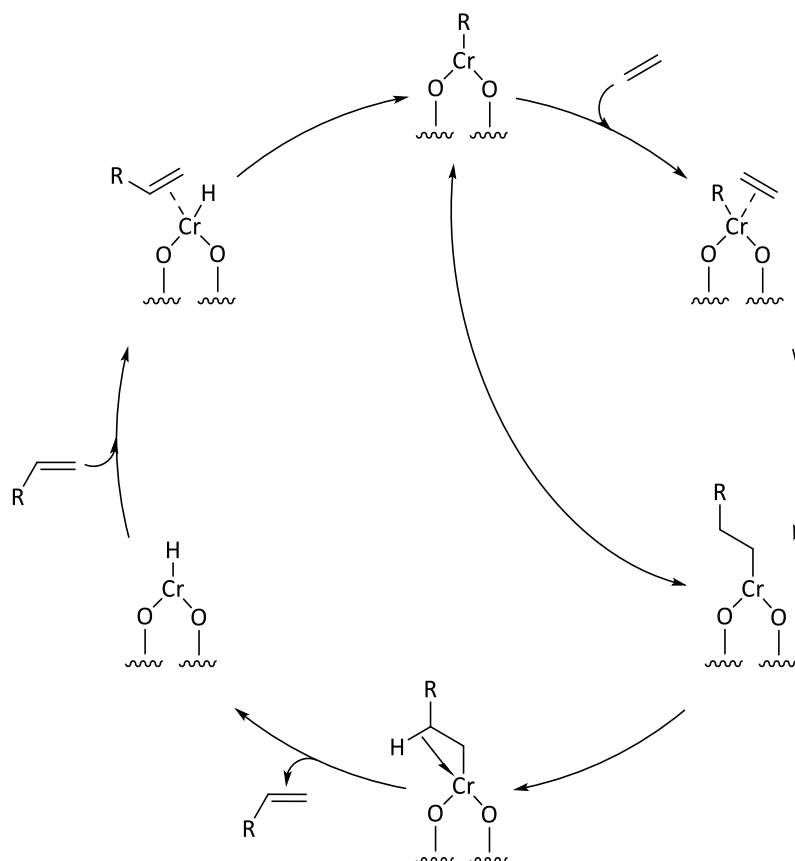
1.3.2.1 Phillips Heterogeneous Cr/SiO₂ Ethylene Polymerisation Process

The Phillips heterogeneous Cr^{II}/SiO₂ ethylene polymerisation pro-initiator can be prepared by impregnating silica with CrO₃, prior to consecutive calcinations at 200 °C in air, and at 600 °C under an atmosphere of either CO or H₂.⁹⁸ The chromium(VI) oxide molecular precursor is believed to react with surface-bound silanol groups at elevated temperatures *via* an esterification mechanism, before being reduced to a Cr^{II} species.⁹⁸ The resulting solid pro-initiator may then be activated *in situ* under an atmosphere of ethylene to generate a highly active catalyst that facilitates ethylene polymerisation (Scheme 28).⁹⁸



Scheme 28: Preparation of the Phillips Cr/SiO₂ ethylene polymerisation catalyst as reported by McDaniel, 1988⁹⁸

Unfortunately, despite the efforts of a number of research groups, the mechanism for the initiation of the Phillips heterogeneous Cr^{II}/SiO₂ ethylene polymerisation pro-initiator is not known.^{4,97,99,100,101,102,103,104,105} This said, based on *in situ* ultraviolet-visible (UV-Vis) and X-ray absorption spectroscopic (XAS) measurements, Brown *et al.* proposed that the activated Phillips Cr/SiO₂ ethylene polymerisation catalyst is in fact a silica-supported Cr^{III} organometallic species.¹⁰⁴ Here, the authors observed the reduction of the Cr^{VI} molecular precursor to a Cr^{II} species under a reducing atmosphere of CO, prior to the formation of a Cr^{III} species in the presence of ethylene.¹⁰⁴ Moreover, it has been suggested that this Cr^{III}-based active site mediates ethylene polymerisation *via* a supported variant of the Cossee-Arlman chain growth mechanism (Scheme 29).^{4,97}



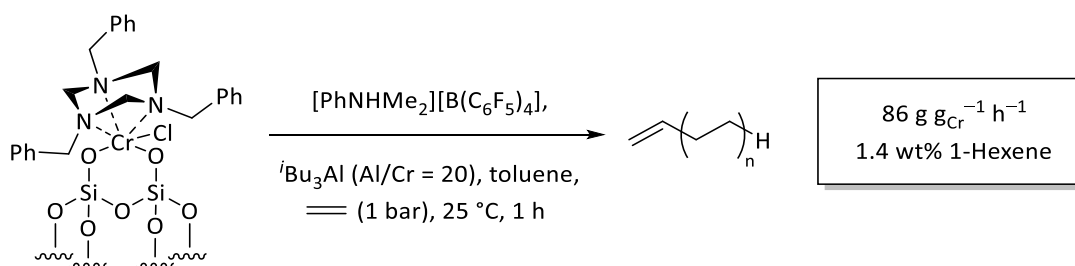
Scheme 29: Ethylene polymerisation mediated by a supported Cossee-Arlman-type reaction mechanism^{31,32,33}

Most significantly, in the presence of a metal alkyl co-catalyst (*e.g.* Et₃Al), the Phillips Cr/SiO₂ ethylene polymerisation initiator also facilitates the production of 1-hexene,^{4,106,107} presumably *via* a competing metallacyclic reaction manifold, a co-monomer that is consumed during the formation of HDPE.¹⁰⁷ Hence, parallels have been drawn between the Phillips heterogeneous Cr/SiO₂ ethylene polymerisation initiator and the related *homogeneous* Union Carbide Cr(2-EH)₃/PIBAO process. Considering that the product selectivity of the soluble (molecular) Cr(2-EH)₃/PIBAO ethylene polymerisation system was switched in favour of ethylene trimerisation {by replacing 2-ethylhexanoate (2-EH) with 2,5-dimethylpyrrolide (2,5-DMP) and *poly*-(isobutyl) aluminium oxide (PIBAO) with Et₃Al}, it may be reasoned that the Phillips

heterogeneous Cr/SiO₂ ethylene polymerisation catalyst could be tuned to promote 1-hexene production. Indeed, Nenu *et al.* claimed to have reported the first successful silica-supported chromium initiator for the selective production of 1-hexene, which comprised a pre-reduced Phillips Cr^{II}/SiO₂ pro-initiator, 1,3,5-tribenzylhexahydro-1,3,5-triazine (TAC), [PhNHMe₂][B(C₆F₅)₄] and ⁱBu₃Al.²²

1.3.2.2 Modified Phillips CrCl(TAC)/SiO₂ Ethylene Trimerisation System

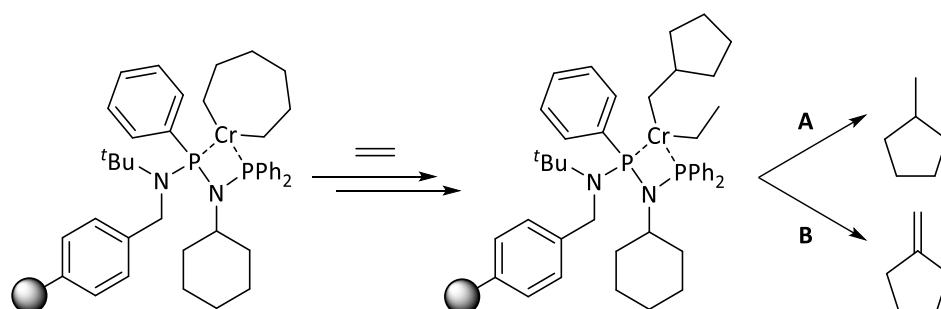
Nenu and co-workers reacted a pre-reduced Phillips-type heterogeneous Cr^{II}/SiO₂ ethylene polymerisation pro-initiator with a charge-neutral 1,3,5-tribenzylhexahydro-1,3,5-triazine (TAC) ligand in dichlorobenzene, which generated a *pseudo*-octahedral Cr^{III} complex, according to XAS at the Cr K- and L_{2,3}-edge.²² Here, it was proposed that a chloride must have been abstracted from the dichlorobenzene diluent resulting in the formation of a Cr^{III} species, something that was later validated by extended X-ray absorption spectroscopy fine-structure (EXAFS).¹⁰⁸ The ensuing catalyst precursor was subsequently activated with a mixture of [PhNHMe₂][B(C₆F₅)₄] and ⁱBu₃Al, and evaluated for its ethylene trimerisation behaviour (Scheme 30).²² For the sake of clarity, this initiator system will be referred to hereafter as CrCl(TAC)/SiO₂.



Scheme 30: Modified Phillips CrCl(TAC)/SiO₂ ethylene trimerisation initiator, adapted from Nenu *et al.*, 2005²²

Under the mild reaction conditions employed, the CrCl(TAC)/SiO₂ initiator system achieved very high selectivity towards 1-hexene (91 wt%) in the liquid fraction, which prompted Nenu *et al.* to speculate that a supported variant of the metallacyclic reaction manifold must be in operation.²² However, in truth, the resulting solid hydrocarbon accounted for 98.5 wt% of the overall product fraction.²² Based on weight ($M_w = 324$ Da) and number ($M_n = 173$ Da) average molecular masses of all the polymer chains in the sample, derived from gel permeation chromatography (GPC), coupled with a continuous melting transition, as inferred by differential scanning calorimetry (DSC), the solid by-product afforded by the CrCl(TAC)/SiO₂ ethylene trimerisation system was classified as oligomer rather than polyethylene (PE).²² Most interestingly, the relatively low dispersity index (M_w/M_n) of this solid oligomer (1.87),²² which is in direct contrast to the polydisperse nature of PE typically afforded by the Phillips Cr/SiO₂ ethylene polymerisation catalyst ($M_w/M_n = 6 - 15$),¹⁰⁸ is indicative of “single-site” catalytic behaviour, albeit at low temperatures and ethylene pressures. In this context, “single-site” character can be defined as a homogeneous distribution of active sites on the surface of a solid support material,

It was suggested that the high product selectivity exhibited by these polymer-supported Cr NPNP initiator systems for methylcyclopentane and methylenecyclopentane, in particular, can be explained primarily by steric arguments.²⁵ Indeed Shoji and Friedrich speculated that the steric hindrance imposed by the Merrifield Resin-type polymeric support may inhibit the expansion of the supported chromacycloheptane intermediate, instead favouring the rearrangement and cyclisation of the metallacycloheptane species, prior to a disproportionation step that liberated both methylcyclopentane and methylenecyclopentane (See Page 29).²⁵ Alternatively, the polymer-supported chromacycloheptane intermediate may undergo sequential ethylene coordination, migratory insertion and cyclisation reactions, prior to the formation of methylcyclopentane (**A**) and methylenecyclopentane (**B**), as shown in Scheme 32.³⁹

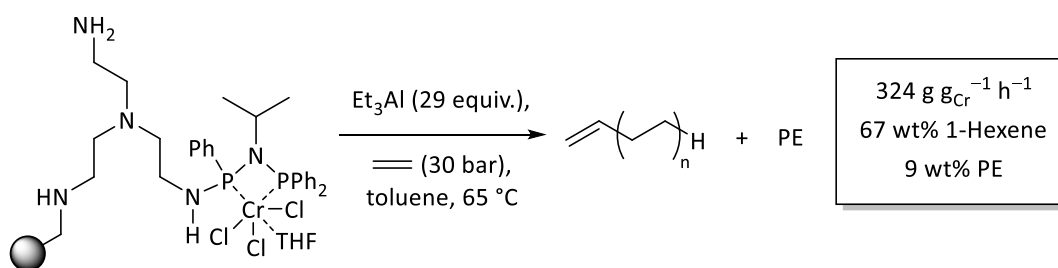


Scheme 32: Rearrangement of a supported NPNP chromacycloheptane intermediate followed by either reductive elimination of methylcyclopentane (A) or β -hydride elimination of methylenecyclopentane (B), modified from Shoji *et al.*, 2012²⁵ and Britovsek *et al.*, 2015³⁹

The loss of selectivity towards LAOs, coupled with a significant reduction in productivity upon immobilising these highly active and selective molecular Cr PNP ethylene tetramerisation pro-initiators onto a solid support, aptly demonstrates some of the challenges involved in the field of heterogeneous selective ethylene oligomerisation.²⁵ That being said, based on topics covered in previous sections of this introduction (See Pages 18 and 23),^{59,68,73,75} one could conceivably design a supported chromium *bis*-(aminophosphine) initiator system that restricts the formation of both methylcyclopentane and methylenecyclopentane, and thus improve its selectivity towards 1-hexene and/or 1-octene.

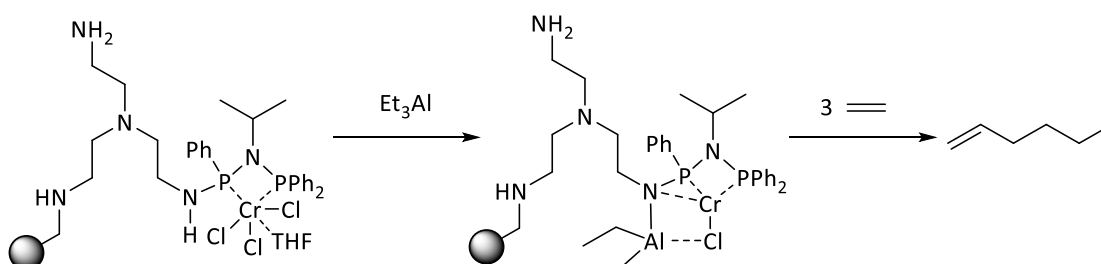
1.3.2.4 Supported Cr PNPNH/Et₃Al Ethylene Trimerisation Initiator

In 2009 researchers at Sabic and Linde patented a recyclable heterogeneous polymer-supported chromium *bis*-(phosphinoamine) ethylene trimerisation pro-initiator that, upon activation with Et₃Al, consistently produced 85 wt% 1-hexene, albeit at a relatively low rate.¹¹¹ However, the following year, Peulecke *et al.* disclosed details of a closely-related poorly active, yet moderately selective solid ethylene trimerisation initiator that comprised an amino-functionalised polystyrene resin, Ph₂PN(*i*Pr)P(Ph)Cl, CrCl₃(thf)₃ and Et₃Al (Scheme 33).²³ It was suggested that the moderately high selectivity towards 1-hexene achieved by such initiator systems could be attributed to a supported metallacyclic reaction manifold. Moreover, the disproportionately high selectivity towards decenes²³ is consistent with prior work involving the operation of a metallacycle-based ethylene/1-hexene co-trimerisation reaction mechanism.^{67,84,85} Most notably, however, the solid Cr PNPNH/Et₃Al ethylene trimerisation catalyst was recycled seven times without significant loss of activity.²³



Scheme 33: Heterogeneous Cr PNPNH/Et₃Al ethylene trimerisation initiator as reported by Peulecke *et al.*, 2010²³

It has been reported that the secondary amine functional group is a critical feature of this supported Cr PNPNH/Et₃Al ethylene trimerisation system.^{23,112} In fact, it has even been suggested that Et₃Al will deprotonate the secondary amine functionality on the PNPNH ligand resulting in the formation of a coordinatively unsaturated bimetallic amidophosphine species that may be responsible for 1-hexene production (Scheme 34).^{23,112}

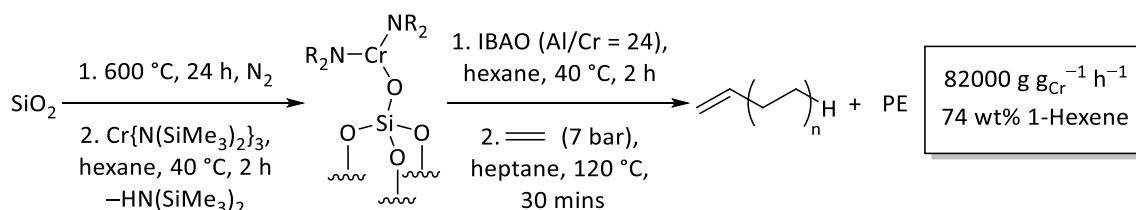


Scheme 34: Proposed activation of the supported Cr PNPNH ethylene trimerisation catalyst precursor with Et₃Al, adapted from Peulecke *et al.*, 2010²³ and Peitz *et al.*, 2010¹¹³

Despite the poor activity and moderate selectivity achieved by the polymer-supported Cr PNPNH/Et₃Al ethylene trimerisation initiator, Peulecke *et al.* insisted that the high purity of the 1-hexene produced, consistent productivity over an extended timeframe, and proven catalyst recyclability make for an “interesting candidate” for commercialisation.²³ The heterogeneous Cr PNPNH/Et₃Al ethylene trimerisation system is presently unsuitable for industrial application because the extent of polymer formation is too high, and will result in reactor fouling.

1.3.2.5 Cr{N(SiMe₃)₂}₂/SiO₂/IBAO Ethylene Trimerisation Process

In 1997 workers at the Showa Denko Chemical Company patented a highly selective supported ethylene trimerisation initiator derived from Cr{N(SiMe₃)₂}₃, partially dehydroxylated silica, isobutyl aluminoxane (IBAO), a partially hydrolysed derivative of ⁱBu₃Al, and 1,2-DME that catalysed the production of 1-hexene (98 wt%), albeit at a rate of 224 g g_{Cr}⁻¹ h⁻¹.^{114,115} More recently, however, an analogous system was developed by Monoi and Sasaki that is currently the most active heterogeneous ethylene trimerisation catalyst reported in the open literature.¹¹⁶ Here, Cr{N(SiMe₃)₂}₃ was assumed to have reacted with isolated silanols at the surface of silica to liberate HN(SiMe₃)₂ and generate the so-called “Cr{N(SiMe₃)₂}₂/SiO₂” pro-initiator that, upon activation with IBAO predominantly afforded 1-hexene (Scheme 35).¹¹⁶ Despite its promise, the rate of polymer formation is still too great to be viable for industrial application.



Scheme 35: Supported Cr{N(SiMe₃)₂}₂/SiO₂/IBAO ethylene trimerisation initiator as reported by Monoi *et al.*, 2002¹¹⁶

Based on the experimental catalytic data obtained (Table 3), it was proposed that the distribution of liquid-phase oligomers afforded by the solid Cr{N(SiMe₃)₂}₂/SiO₂/IBAO ethylene trimerisation catalyst may be rationalised by a supported metallacyclic reaction manifold.¹¹⁶ Moreover, it was reported that the relative proportion of decenes generated by the Cr{N(SiMe₃)₂}₂/SiO₂/IBAO ethylene trimerisation initiator increased over extended reaction times, which is indicative of a secondary metallacycle-based ethylene/1-hexene co-trimerisation process.¹¹⁶

Table 3: Product distribution afforded by the heterogeneous Cr{N(SiMe₃)₂}₂/SiO₂/IBAO ethylene trimerisation initiator system, adapted from Monoi *et al.*, 2002¹¹⁶

1-Butene	1-Hexene	1-Octene	Decenes	Polymer
0.5 wt%	74 wt%	3.5 wt%	15 wt%	7 wt%

Monoï and Sasaki also investigated the influence of the reaction temperature and ethylene pressure on the heterogeneous $\text{Cr}\{\text{N}(\text{SiMe}_3)_2\}_2/\text{SiO}_2/\text{IBAO}$ ethylene trimerisation system.¹¹⁶ Here, the authors reported that the rate of ethylene trimerisation was significantly reduced at lower temperatures, *i.e.* $4800 \text{ g}_{1-\text{C}_6} \text{ g}_{\text{Cr}}^{-1} \text{ h}^{-1}$ at $110 \text{ }^\circ\text{C}$, that they were not able to quantify the resulting product distribution under these conditions. Furthermore, the supported $\text{Cr}\{\text{N}(\text{SiMe}_3)_2\}_2/\text{SiO}_2/\text{IBAO}$ ethylene trimerisation initiator reportedly exhibited a first order kinetic dependence on ethylene concentration, which suggests that the expansion of the supported chromacyclopentane species is the RDS in the metallacycle mechanism.¹¹⁶ That being said, not enough data points have been reported to draw any valid conclusions from these batch reactions (Figure 20).

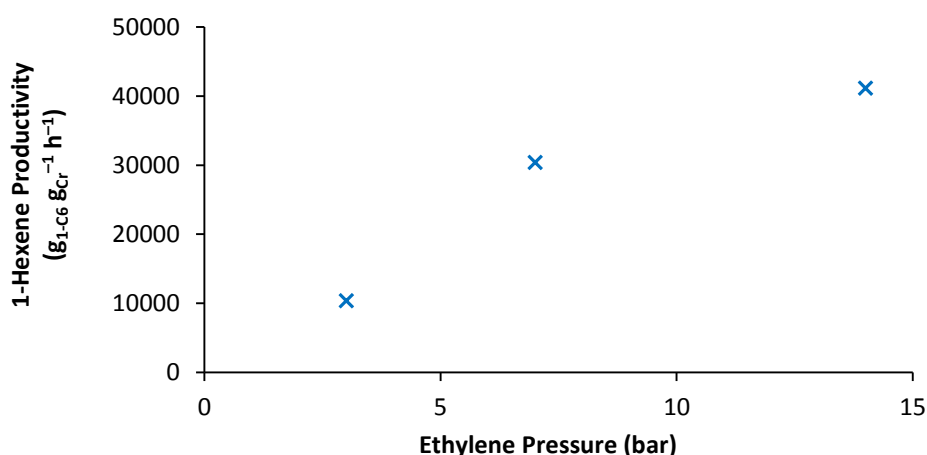


Figure 20: Pressure dependence of the heterogeneous $\text{Cr}\{\text{N}(\text{SiMe}_3)_2\}_2/\text{SiO}_2/\text{IBAO}$ ethylene trimerisation initiator, modified from Monoï *et al.*, 2002¹¹⁶

Monoï and Sasaki explored the effect of various ethereal additives (*e.g.* 1,2-DME) on the performance of their heterogeneous $\text{Cr}\{\text{N}(\text{SiMe}_3)_2\}_2/\text{SiO}_2/\text{IBAO}$ ethylene trimerisation system.¹¹⁶ Here it was found that the selectivity of the silica-supported chromium initiator could be improved with the addition of 0.15 molar equivalents of 1,2-DME, albeit at the expense of catalytic activity. As stated previously, coordination of 1,2-DME to the chromium metal centre may increase the E_a barrier for the expansion of the chromacycloheptane intermediate, and thus favour β -hydride elimination and the reductive elimination of 1-hexene (See Page 13).⁴⁷

Notably, the siliceous catalyst support was found to play a crucial role in *heterogeneous* selective ethylene trimerisation.¹¹⁶ This was achieved by comparing the solid $\text{Cr}\{\text{N}(\text{SiMe}_3)_2\}_2/\text{SiO}_2/\text{IBAO}$ ethylene trimerisation catalyst with its molecular counterpart.¹¹⁶ The activity of the *homogeneous* $\text{Cr}\{\text{N}(\text{SiMe}_3)_2\}_3/\text{IBAO}$ initiator was reported to be $77 \text{ g}_{1-\text{C}_6} \text{ g}_{\text{Cr}}^{-1} \text{ h}^{-1}$, which is significantly less than that of the analogous supported system (*i.e.* $61000 \text{ g}_{1-\text{C}_6} \text{ g}_{\text{Cr}}^{-1} \text{ h}^{-1}$). Hence, Monoï and Sasaki concluded that the active component within their solid $\text{Cr}\{\text{N}(\text{SiMe}_3)_2\}_2/\text{SiO}_2/\text{IBAO}$ ethylene trimerisation catalyst is present at the surface of silica.¹¹⁶

Additionally, Monoi and Sasaki reported that the performance of their solid $\text{Cr}\{\text{N}(\text{SiMe}_3)_2\}_2/\text{SiO}_2/\text{IBAO}$ ethylene trimerisation initiator was heavily dependent on the thermal pre-treatment of the siliceous catalyst support.¹¹⁶ Indeed, the authors demonstrated that by lowering the temperature at which silica is calcined from 600 to 300 °C, the resulting supported chromium initiator favoured PE (87 wt%) over 1-hexene production.¹¹⁶ Conversely, the selectivity of the $\text{Cr}\{\text{N}(\text{SiMe}_3)_2\}_2/\text{SiO}_2/\text{IBAO}$ ethylene trimerisation process could be further enhanced by increasing the catalyst support calcination temperature to 780 °C, albeit at the expense of catalytic activity.¹¹⁶ Consequently, Monoi and Sasaki inferred that ethylene trimerisation sites are formed at high calcination temperatures (600 °C), and that polymerisation sites are generated at lower calcination temperatures (300 °C).¹¹⁶ In fact, since nearly all of the residual silanol functionality present at the surface of silica >500 °C are isolated,¹¹⁷ it was reasoned that the active species responsible for 1-hexene production must be grafted to the catalyst support through a single Si–O–Cr bond (see Scheme 35).¹¹⁶

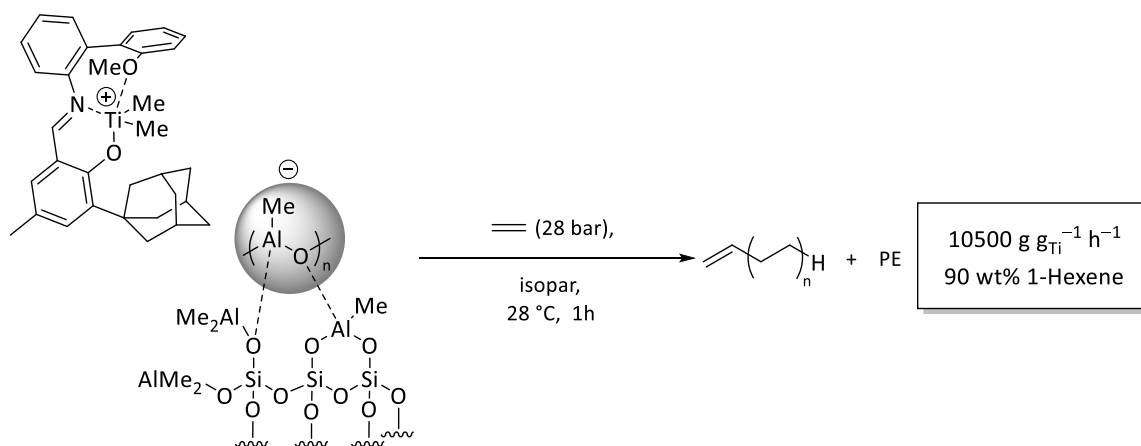
Although the $\text{Cr}\{\text{N}(\text{SiMe}_3)_2\}_2/\text{SiO}_2/\text{IBAO}$ ethylene trimerisation initiator is an interesting prospect in terms of its high catalytic activity and moderately high selectivity towards 1-hexene, there is still room, and indeed a necessity, to develop the process further in order to limit PE formation, and thus reduce the potential for reactor fouling. In fact, the highly active $\text{Cr}\{\text{N}(\text{SiMe}_3)_2\}_2/\text{SiO}_2$ pro-initiator provides a convenient starting point for developing future understanding in the field of heterogeneous selective olefin oligomerisation.

1.3.2.6 Non-chromium-based Heterogeneous Olefin Oligomerisation

Although the majority of selective ethylene tri-/tetra-merisation systems reported in the literature are chromium-based,¹¹⁸ there are several heterogeneous olefin oligomerisation initiators that utilise other TMs, namely titanium,^{26,27,28} nickel,⁹⁵ tantalum²⁴ and tungsten.^{29,30} For completeness, this section will now discuss three notable examples of non-chromium-based heterogeneous ethylene tri-/tetra-merisation catalysts.

1.3.2.6.1 Heterogeneous s(FI)Ti Ethylene Trimerisation Initiator

The Duchateau and Bercaw research groups have both developed a supported selective olefin trimerisation system,^{26,28} based on an existing molecular (*homogeneous*) phenoxyimine (FI) titanium pro-initiator.⁷⁹ Partially dehydroxylated silica that had been calcined at 600 °C was treated with MAO at 90 °C resulting in the quantitative loss of silanols, according to infrared (IR) spectroscopic analysis.²⁶ Subsequently, the ensuing MAO-modified catalyst support was reacted with (FI)TiCl₃ to generate a moderately active, yet highly selective solid-phase ethylene trimerisation catalyst (Scheme 36), which will be referred to hereafter as s(FI)Ti.²⁶

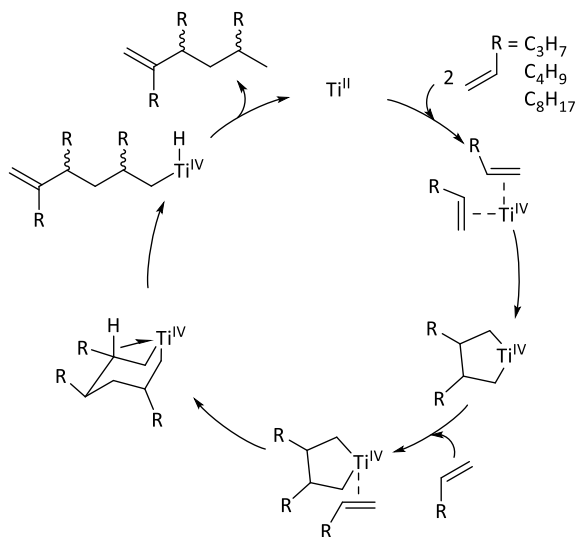


Scheme 36: Highly selective s(FI)Ti ethylene trimerisation catalyst, adapted from Karbach *et al.*, 2015²⁶

Based on previous work on the related *homogeneous* (FI)TiCl₃/MAO ethylene trimerisation catalyst,⁷⁹ it was reasoned that the high selectivity towards 1-hexene, decenes, and tetradecenes achieved by the *heterogeneous* s(FI)Ti catalyst could be attributed to a Ti^{II/IV}-based metallacyclic reaction manifold.²⁸ In fact, Sattler and co-workers identified three major decene isomers, namely 5-methyl-1-nonene, 5-methylene-nonane and 4-ethylene-octane, afforded by the s(FI)Ti ethylene trimerisation initiator,²⁸ which have previously been rationalised by a secondary metallacycle-based ethylene/1-hexene co-trimerisation process.^{67,84,85}

Sattler *et al.* presented a number of key advantages of the heterogeneous s(FI)Ti ethylene trimerisation system over its molecular analogue.²⁸ Firstly, the s(FI)Ti catalyst is pre-activated, and therefore could be employed in a solvent-free process.²⁸ Secondly, the authors demonstrated that the s(FI)Ti ethylene trimerisation initiator is more stable than its *homogeneous* counterpart in terms of its prolonged catalyst lifetime (22 hours on stream as opposed to only 4 hours).²⁸ Finally,

Sattler and co-workers expanded the scope of the heterogeneous s(FI)Ti olefin trimerisation process by changing the monomer feedstock from ethylene to 1-pentene, 1-hexene and 1-decene in order to synthesise high value products, *e.g.* jet fuel, diesel and lubricants.²⁸ Most notably, the high *regio*-selectivity (85%) achieved by the s(FI)Ti olefin trimerisation initiator package with respect to C₁₅, C₁₈ and C₃₀ olefins is consistent with a metallacyclic trimerisation reaction manifold (Scheme 37).²⁸

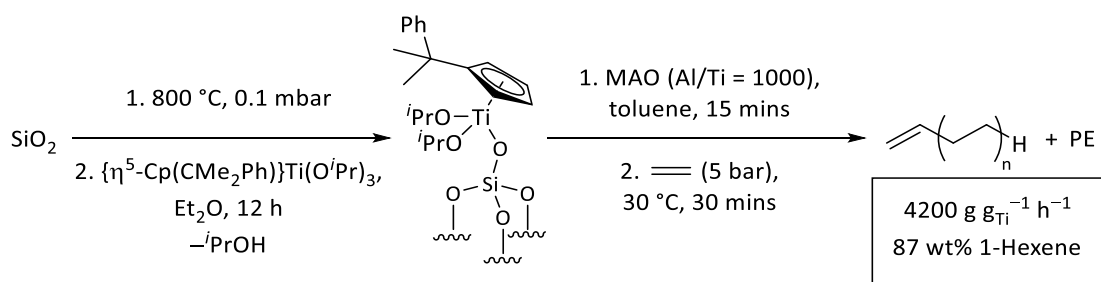


Scheme 37: Selective olefin trimerisation mediated by a $Ti^{II/IV}$ -based metallacycle-based reaction mechanism, adapted from Sattler *et al.*, 2016²⁸

Even though the heterogeneous s(FI)Ti ethylene trimerisation system offers several advantages over its parent molecular (FI)TiCl₃ pro-initiator, Suzuki's original *homogeneous* analogue would be a more viable candidate for commercialisation due to its vastly superior activity and selectivity towards 1-hexene (*i.e.* 7140000 g g_{Ti}⁻¹ h⁻¹; 92 wt% 1-hexene).⁷⁹ That being said, successfully increasing the scope of the solid s(FI)Ti catalyst to longer chain LAOs makes for an interesting prospect in the field of heterogeneous selective olefin oligomerisation.

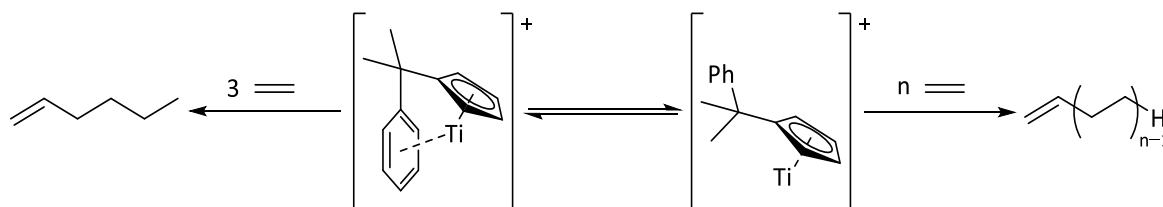
1.3.2.6.2 $\{\eta^5\text{-C}_5\text{H}_4(\text{CMe}_2\text{Ph})\}\text{Ti}(\text{O}^i\text{Pr})_2/\text{SiO}_2/\text{MAO}$ Ethylene Trimerisation Catalyst

Varga *et al.* impregnated a partially dehydroxylated siliceous catalyst support with a derivative of an already-established titanium-based molecular ethylene trimerisation catalyst precursor, namely $\{\eta^5\text{-C}_5\text{H}_4(\text{CMe}_2\text{Ph})\}\text{Ti}(\text{O}^i\text{Pr})_3$, to prepare a related heterogeneous pro-initiator.^{27,119} It was reasoned that the molecular precursor would react with an isolated silanol to liberate one equivalent of the corresponding alcohol.²⁷ The resulting $\{\eta^5\text{-C}_5\text{H}_4(\text{CMe}_2\text{Ph})\}\text{Ti}(\text{O}^i\text{Pr})_2/\text{SiO}_2$ catalyst precursor was subsequently activated with MAO, and evaluated for its ethylene trimerisation behaviour (Scheme 38).²⁷ For reference, Deckers and co-workers had previously reported an analogous, highly active and selective *homogeneous* ethylene trimerisation catalyst that comprised $\{\eta^5\text{-C}_5\text{H}_4(\text{CMe}_2\text{Ph})\}\text{TiCl}_3$ and MAO (*i.e.* 83 wt% 1-hexene; $70150 \text{ g g}_{\text{Ti}}^{-1} \text{ h}^{-1}$).¹¹⁹



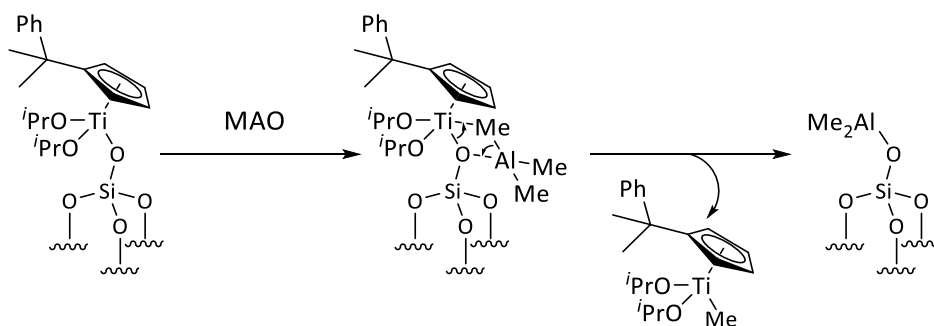
Scheme 38: Highly selective, supported $\{\eta^5\text{-C}_5\text{H}_4(\text{CMe}_2\text{Ph})\}\text{Ti}(\text{O}^i\text{Pr})_2/\text{SiO}_2/\text{MAO}$ ethylene trimerisation system, modified from Varga *et al.*, 2015²⁷

Notably, Deckers and co-workers highlighted the importance of the phenyl substituent on the cyclopentadienyl ligand, in that the selectivity of the molecular $\{\eta^5\text{-C}_5\text{H}_4(\text{CMe}_2\text{Ph})\}\text{TiCl}_3/\text{MAO}$ ethylene trimerisation initiator towards 1-hexene was completely lost when the dimethyl benzyl group was replaced with a *tertiary*-butyl substituent.¹¹⁹ Consequently, the authors speculated that the phenyl group could act as a hemilabile η^6 -arene moiety that could switch the selectivity of the $\{\eta^5\text{-C}_5\text{H}_4(\text{CMe}_2\text{Ph})\}\text{TiCl}_3/\text{MAO}$ catalyst from ethylene polymerisation *via* a Cossee-Arlman chain growth process to a $\text{Ti}^{\text{II/IV}}$ -based metallacycle mechanism (Scheme 39).^{119,120} By extension, the ancillary η^6 -arene donor present also in the *heterogeneous* $\{\eta^5\text{-C}_5\text{H}_4(\text{CMe}_2\text{Ph})\}\text{Ti}(\text{O}^i\text{Pr})_2/\text{SiO}_2/\text{MAO}$ ethylene trimerisation system may stabilise coordinatively unsaturated intermediates within a supported $\text{Ti}^{\text{II/IV}}$ metallacyclic reaction manifold.



Scheme 39: Proposed variable coordination of the $\eta^5\text{-C}_5\text{H}_4(\text{CMe}_2\text{Ph})$ ligand, modified from Hessen *et al.*, 2001¹¹⁹

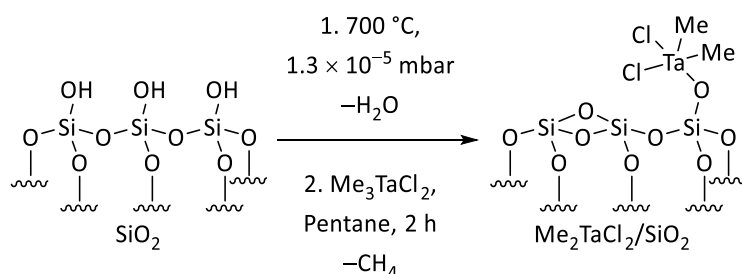
The ostensibly “high” productivity achieved by the $\{\eta^5\text{-C}_5\text{H}_4(\text{CMe}_2\text{Ph})\}\text{Ti}(\text{O}^i\text{Pr})_2/\text{SiO}_2/\text{MAO}$ ethylene trimerisation initiator aroused suspicion that MAO could potentially leach a catalytically active Ti-based molecular species from the support, and that the active component was in fact *homogeneous* in nature.²⁷ To this end, Varga *et al.* treated the $\{\eta^5\text{-C}_5\text{H}_4(\text{CMe}_2\text{Ph})\}\text{Ti}(\text{O}^i\text{Pr})_2/\text{SiO}_2$ pro-initiator with 1000 equivalents of MAO, and filtered the resulting solution into an autoclave before the system was heated and pressurised with ethylene. This filtrate reportedly produced approximately 20 wt% of the 1-hexene afforded by the $\{\eta^5\text{-C}_5\text{H}_4(\text{CMe}_2\text{Ph})\}\text{Ti}(\text{O}^i\text{Pr})_2/\text{SiO}_2/\text{MAO}$ initiator. Consequently, the authors proposed that MAO cleaves the Ti–O–Si bond *via* a methylation reaction pathway generating an active molecular Ti-based ethylene trimerisation catalyst *in situ* (Scheme 40).²⁷ This case study highlights another significant challenge involved in *heterogeneous* ethylene trimerisation catalysis, in that an alkyl aluminium reagent could leach a catalytically active molecular species from the solid support.



Scheme 40: Cleavage of the Ti–O–Si bond *via* methylation as reported by Varga *et al.*, 2015²⁷

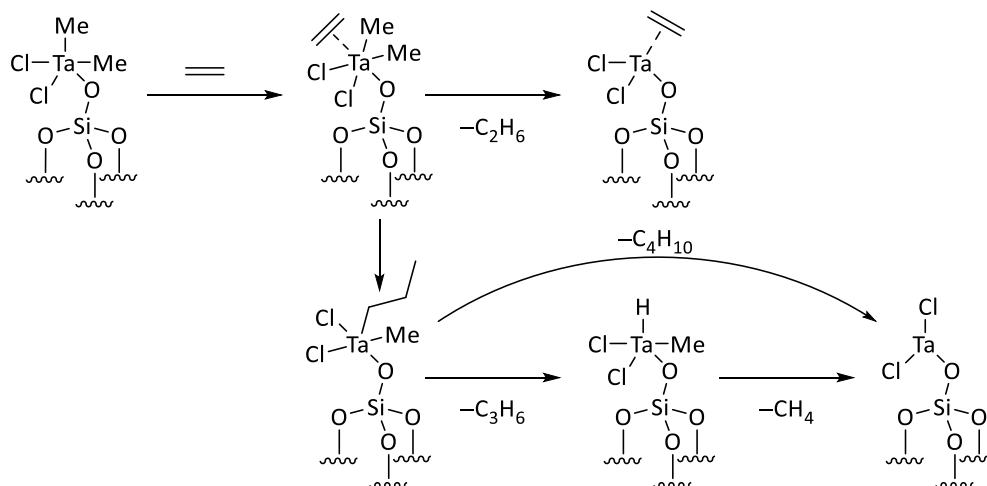
1.3.2.6.3 $\text{Me}_2\text{TaCl}_2/\text{SiO}_2$ Ethylene Trimerisation System

Chen *et al.* impregnated a partially dehydroxylated *meso*-porous silica with an alkylated derivative of an existing molecular tantalum-based ethylene trimerisation catalyst precursor, namely Me_3TaCl_2 , in order to prepare a related “single-site” heterogeneous pro-initiator.^{24,121} Based on extensive solid-state ^1H NMR and IR spectroscopic analyses, the authors reasoned that Me_3TaCl_2 reacts with isolated silanols at the surface of silica to liberate one molar equivalent of methane (Scheme 41).²⁴



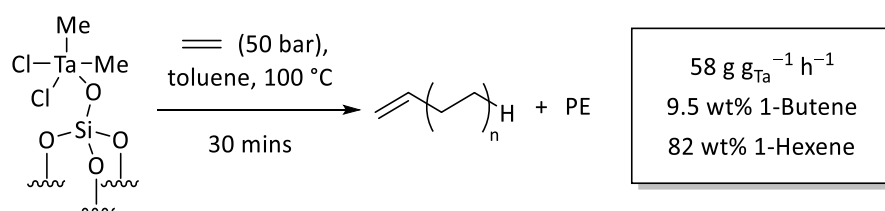
Scheme 41: Preparation of $\text{Me}_2\text{TaCl}_2/\text{SiO}_2$ ethylene trimerisation pro-initiator as reported by Chen *et al.*, 2012²⁴

The initiation process undergone by the $\text{Me}_2\text{TaCl}_2/\text{SiO}_2$ ethylene trimerisation catalyst precursor was monitored by GC under a flow of ethylene (in the absence of a Lewis acidic alkyl aluminium-based co-catalyst).²⁴ Most interestingly, the reaction between $\text{Me}_2\text{TaCl}_2/\text{SiO}_2$ and ethylene produced a mixture of methane, ethane, propylene and butane, as well as 1-butene and 1-hexene. In order to rationalise these observations, Chen and co-workers proposed a plausible reaction mechanism for the activation of the $\text{Me}_2\text{TaCl}_2/\text{SiO}_2$ ethylene trimerisation pro-initiator (Scheme 42).²⁴ It was postulated that the silica-supported catalyst precursor may undergo successive ethylene association, migratory insertion, and reductive elimination steps to generate a Ta^{III} -based active species responsible for 1-butene and 1-hexene production.



Scheme 42: Initiation of $\text{Me}_2\text{TaCl}_2/\text{SiO}_2$ ethylene trimerisation pro-initiator proposed by Chen *et al.*, 2012²⁴

The so-called “ $\text{TaCl}_2/\text{SiO}_2$ ” ethylene trimerisation initiator exhibited high selectivity towards 1-hexene and 1-butene, something that is proposed to be indicative of a $\text{Ta}^{\text{III/V}}$ -based metallacycle mechanism,^{24,121} albeit with a relatively low activity (Scheme 43).²⁴ Perhaps the poor productivity of the $\text{TaCl}_2/\text{SiO}_2$ ethylene trimerisation catalyst may be due in part to its inefficient initiation. Indeed, the $\text{Me}_2\text{TaCl}_2/\text{SiO}_2$ ethylene trimerisation pro-initiator required approximately 120 minutes under a flow of ethylene to commence ethylene oligomerisation, and despite being on stream for 1000 minutes only managed to activate 90% of supported Ta^{V} species; the remaining 10% were assumed to have decomposed *via* the elimination of methane.²⁴ Nevertheless, this system provides crucial insight into the activation of a *heterogeneous* ethylene trimerisation pro-initiator. In fact, $\text{Me}_2\text{TaCl}_2/\text{SiO}_2$ has now set a precedent that selective ethylene oligomerisation can be achieved in the absence of a co-catalyst.²⁴



Scheme 43: Ethylene oligomerisation mediated by $\text{Me}_2\text{TaCl}_2/\text{SiO}_2$, modified from Chen *et al.*, 2012²⁴

1.4 Thesis Aims and Objectives

This thesis aims to deliver mechanistic insight into the mode of operation in heterogeneous selective olefin oligomerisation. Owing to its high activity, moderate selectivity towards 1-hexene and relative ease of access, the so-called “Cr{N(SiMe₃)₂}₂/SiO₂” catalyst precursor, previously reported by Monoi and Sasaki (see Section 1.3.2.5),¹¹⁶ was chosen as a starting point for our fundamental study into the field of heterogeneous selective ethylene oligomerisation.

Chapter 2 will recount a preliminary catalytic screening investigation to assess the impact of the nature of the oxide support and its pre-treatment, the nature of the alkyl aluminium-based co-catalyst and reaction diluent upon the productivity and selectivity of the previously-reported Cr{N(SiMe₃)₂}₂/SiO₂ ethylene trimerisation system. This chapter will attempt to establish a correlation between isolated and geminal silanol sites at the surface of silica, and the respective tri-/poly-merisation activity afforded by the ensuing initiator system as a function of calcination temperature using solid-state ²⁹Si NMR spectroscopic and thermogravimetric analyses (TGA).

Chapter 3 will probe the influence of experimental processing parameters, including chromium concentration, Al/Cr loading, reaction temperature, ethylene pressure, stirrer speed, reaction time, and diluent volume as well as the impact of potential promoters upon the catalytic activity and selectivity of the best-performing silica-supported chromium initiator. From these data, it is hoped that the underpinning knowledge of this supported ethylene trimerisation system can be utilised in the future development of heterogeneous selective olefin oligomerisation processes.

1.5 References

- (1) F. Speiser, P. Braunstein, W. Saussine, *Acc. Chem. Res.*, **2005**, *38*, 784-793.
- (2) C. Thammanayakatip, "Linear Alpha Olefins", http://apic2017.jp/pdf/0519_cm2_04.pdf, 26/7/17.
- (3) Anonymous, "Chemical Economics Handbook: Linear Alpha Olefins", IHS Chemical, 2017.
- (4) M. P. McDaniel, *Adv. Catal.*, **2010**, *53*, 123-606.
- (5) A. Boudier, P.-A. R. Breuil, L. Magna, C. Rangheard, J. Ponthus, H. Olivier-Bourbigou, P. Braunstein, *Organometallics*, **2011**, *30*, 2640-2642.
- (6) D. S. McGuinness, *Chem. Rev.*, **2011**, *111*, 2321-2341.
- (7) J. Skupinska, *Chem. Rev.*, **1991**, *91*, 613-648.
- (8) P.-A. R. Breuil, L. Magna, H. Olivier-Bourbigou, *Catal. Lett.*, **2015**, *145*, 173-192.
- (9) B. Harvey, H. Meylemans, *Green Chem.*, **2013**, *16*, 770-776.
- (10) Anonymous, "Global Supply and Demand of Petrochemical Products Relied on LPG as Feedstock", http://www.lpgc.or.jp/corporate/information/program5_Japan2.pdf, 25/7/17.
- (11) J. T. Dixon, M. J. Green, F. M. Hess, D. H. Morgan, *J. Organomet. Chem.*, **2004**, *689*, 3641-3668.
- (12) K. Ziegler, *Angew. Chem.*, **1952**, *64*, 323-329.
- (13) B. Hessen, *J. Mol. Catal. A: Chem.*, **2004**, *213*, 129-135.
- (14) V. C. Gibson, C. Redshaw, G. A. Solan, *Chem. Rev.*, **2007**, *107*, 1745-1776.
- (15) D. F. Wass, *Dalton Trans.*, **2007**, 816-819.
- (16) K. P. Bryliakov, E. P. Talsi, *Coord. Chem. Rev.*, **2012**, *256*, 2994-3007.
- (17) K. A. Alferov, G. P. Belov, Y. Meng, *Appl. Catal. A: Gen.*, **2017**, *542*, 71-124.
- (18) E. O. Camara Greiner, Y. Inoguchi, "Chemical Economics Handbook: Linear Alpha Olefins", IHS Chemical, 2010.
- (19) M. P. Conley, C. Copéret, C. Thieuleux, *ACS Catal.*, **2014**, *4*, 1458-1469.
- (20) F. Lefebvre, J. Thivolle-Cazat, V. Dufaud, G. P. Niccolai, J.-M. Basset, *Appl. Catal. A: Gen.*, **1999**, *182*, 1-8.
- (21) M. Jezequel, V. Dufaud, M. J. Ruiz-Garcia, F. Carrillo-Hermosilla, U. Neugebauer, G. P. Niccolai, F. Lefebvre, F. Bayard, J. Corker, S. Fiddy, J. Evans, J.-P. Broyer, J. Malinge, J.-M. Basset, *J. Am. Chem. Soc.*, **2001**, *123*, 3520-3540.
- (22) C. N. Nenu, B. M. Weckhuysen, *J. Chem. Soc., Chem. Commun.*, **2005**, 1865-1867.
- (23) N. Peulecke, B. H. Müller, S. E. Peitz, B. R. Aluri, U. Rosenthal, A. I. Wohl, W. Müller, M. H. Al-Hazmi, F. M. Mosa, *Chem. Cat. Chem.*, **2010**, *2*, 1079-1081.
- (24) Y. Chen, E. Callens, E. Abou-Hamad, N. Merle, A. J. P. White, M. Taoufik, C. Copéret, E. Le Roux, J.-M. Basset, *Angew. Chem. Int. Ed.*, **2012**, *51*, 11886-11889.
- (25) M. L. Shoji, H. B. Friedrich, *S. Afr. J. Chem.*, **2012**, *65*, 214-222.
- (26) F. F. Karbach, J. R. Severn, R. Duchateau, *ACS Catal.*, **2015**, *5*, 5068-5076.
- (27) V. Varga, T. Hodik, M. Lamac, M. Horacek, A. Zikal, N. Zilkova, W. O. Parker Jr., J. Pinkas, *J. Org. Chem.*, **2015**, *777*, 57-66.
- (28) A. Sattler, D. C. Aluthge, J. R. Winkler, J. A. Labinger, J. E. Bercaw, *ACS Catal.*, **2016**, *6*, 19-22.
- (29) C. M. R. Wright, Z. R. Turner, J.-C. Buffet, D. O'Hare, *Chem. Commun.*, **2016**, *52*, 2850-2853.
- (30) C. M. R. Wright, T. J. Williams, Z. R. Turner, J.-C. Buffet, D. O'Hare, *Inorg. Chem. Front.*, **2017**, *4*, 1048-1060.
- (31) P. Cossee, *J. Catal.*, **1964**, *3*, 80-88.
- (32) E. J. Arlman, *J. Catal.*, **1964**, *3*, 89-98.
- (33) E. J. Arlman, P. Cossee, *J. Catal.*, **1964**, *3*, 99-104.
- (34) G. J. P. Britovsek, R. Malinowski, D. S. McGuinness, J. D. Nobbs, A. K. Tomov, A. W. Wadswley, C. T. Young, *ACS Catal.*, **2015**, *5*, 6922-6925.

- (35) P. H. M. Budzelaar, G. Talarico, In *Group 13 Chemistry III: Industrial Applications*; H. W. Roesky, D. A. Atwood, Eds.; Springer-Verlag Berlin Heidelberg: Berlin, Heidelberg, 2003; Vol. 105, p 141-165.
- (36) B. Reuben, H. Wittcoff, *J. Chem. Educ.*, **1988**, *65*, 605-607.
- (37) P. Kuhn, D. Semeril, D. Matt, M. J. Chetcuti, P. Lutz, *Dalton Trans.*, **2007**, 515-528.
- (38) W. Keim, *Angew. Chem. Int. Ed.*, **2013**, *52*, 12492-12496.
- (39) G. J. P. Britovsek, D. S. McGuinness, T. S. Wierenga, C. T. Young, *ACS Catal.*, **2015**, *5*, 4152-4166.
- (40) R. M. Manyik, W. E. Walker, T. P. Wilson, **1967**, *US3300458*, Union Carbide Corporation.
- (41) R. M. Manyik, W. E. Walker, T. P. Wilson, **1967**, *US3347840*, Union Carbide Corporation.
- (42) R. M. Manyik, W. E. Walker, T. P. Wilson, *J. Catal.*, **1977**, *47*, 197-209.
- (43) J. R. Briggs, *J. Chem. Soc., Chem. Commun.*, **1989**, *11*, 674-675.
- (44) J. X. McDermott, J. F. White, G. M. Whitesides, *J. Am. Chem. Soc.*, **1973**, *95*, 4451-4452.
- (45) R. Emrich, O. Heinemann, P. W. Jolly, C. Kru, G. P. J. Verhovnik, *Organometallics*, **1997**, *16*, 1511-1513.
- (46) W. J. van Rensburg, C. Grové, J. P. Steynberg, K. B. Stark, J. J. Huyser, P. J. Steynberg, *Organometallics*, **2004**, *23*, 1207-1222.
- (47) Y. Qi, Q. Dong, L. Zhong, Z. Liu, P. Qiu, R. Cheng, X. He, J. Vanderbilt, B. Liu, *Organometallics*, **2010**, *29*, 1588-1602.
- (48) J. R. Briggs, **1987**, *US4668838*, Union Carbide Corporation.
- (49) M. E. Lashier, J. W. Freeman, R. D. Knudsen, **1996**, *US5543375*, Phillips Petroleum Company.
- (50) J. W. Freeman, J. L. Buster, R. D. Knudsen, **1999**, *US005856257*, Phillips Petroleum Company.
- (51) W. K. Reagen, *Am. Chem. Soc. Symp., Div. Pet. Chem.*, **1989**, *34*, 583-588.
- (52) W. K. Reagen, **1991**, *EP0417477A2*, Phillips Petroleum Company.
- (53) T. M. Pettijohn, W. K. Reagen, S. J. Martin, **1994**, *US5331070*, Phillips Petroleum Company.
- (54) W. K. Reagen, B. K. Conroy, **1994**, *US5198563A*, Phillips Petroleum Company.
- (55) Y. Araki, H. Nakamura, Y. Nanba, T. Okanu, **1999**, *US5856612*, Mitsubishi Chemical Corporation.
- (56) Y. Yang, H. Kim, J. Lee, H. Paik, H. G. Jang, *Appl. Catal. A: Gen.*, **2000**, *193*, 29-38.
- (57) S. Tang, Z. Liu, X. Yan, N. Li, R. Cheng, X. He, B. Liu, *Appl. Catal. A: Gen.*, **2014**, *481*, 39-48.
- (58) D. F. Wass, **2002**, *US6800702B2*, BP Chemicals Ltd.
- (59) A. Carter, S. A. Cohen, N. A. Cooley, A. Murphy, J. Scutt, D. F. Wass, *Chem. Commun.*, **2002**, 858-859.
- (60) S. J. Schofer, M. W. Day, L. M. Henling, J. A. Labinger, J. E. Bercaw, *Organometallics*, **2006**, *25*, 2743-2749.
- (61) T. Agapie, S. J. Schofer, J. A. Labinger, J. E. Bercaw, *J. Am. Chem. Soc.*, **2004**, *126*, 1304-1305.
- (62) T. Agapie, J. A. Labinger, J. E. Bercaw, *J. Am. Chem. Soc.*, **2007**, 14281-14295.
- (63) A. Bollmann, K. Blann, J. T. Dixon, F. M. Hess, E. Killian, H. Maumela, D. S. McGuinness, D. H. Morgan, A. Neveling, S. Otto, M. Overett, A. M. Z. Slawin, P. Wasserscheid, S. Kuhlmann, *J. Am. Chem. Soc.*, **2004**, *126*, 14712-14713.
- (64) K. Blann, A. Bollmann, J. T. Dixon, F. M. Hess, E. Killian, H. Maumela, D. H. Morgan, A. Neveling, S. Otto, M. J. Overett, *Chem. Commun.*, **2005**, 620-621.
- (65) M. J. Overett, K. Blann, A. Bollmann, J. T. Dixon, F. Hess, E. Killian, H. Maumela, D. H. Morgan, A. Neveling, S. Otto, *Chem. Commun.*, **2005**, 622-624.
- (66) K. Blann, A. Bollmann, J. T. Dixon, A. Neveling, D. H. Morgan, H. Maumela, E. Killian, F. M. Hess, S. Otto, M. J. Overett, **2004**, *WO2004056478A1*, Sasol Technology Ltd.

- (67) M. J. Overett, K. Blann, A. Bollmann, J. T. Dixon, D. Haasbroek, E. Killian, H. Maumela, D. S. McGuinness, D. H. Morgan, *J. Am. Chem. Soc.*, **2005**, *127*, 10723-10730.
- (68) K. Blann, A. Bollmann, H. de Bod, J. T. Dixon, E. Killian, P. Nongodlwana, M. C. Maumela, H. Maumela, A. E. McConnell, D. H. Morgan, M. J. Overett, M. Pr torius, S. Kuhlmann, P. Wasserscheid, *J. Catal.*, **2007**, *249*, 244-249.
- (69) E. Angelescu, C. Nicolau, Z. Simon, *J. Am. Chem. Soc.*, **1966**, *88*, 3910-3912.
- (70) L. McDyre, E. Carter, K. J. Cavell, D. M. Murphy, J. A. Platts, K. Sampford, B. D. Ward, W. F. Gabrielli, M. J. Hanton, D. M. Smith, *Organometallics*, **2011**, *30*, 4505-4508.
- (71) S. Kuhlmann, J. T. Dixon, M. Haumann, D. H. Morgan, J. Ofili, O. Spuhl, N. Taccardi, P. Wasserscheid, *Adv. Synth. Catal.*, **2006**, *348*, 1200-1206.
- (72) G. J. Britovsek, D. S. McGuinness, *Chem. Eur. J.*, **2016**, *22*, 16891-16896.
- (73) E. Killian, K. Blann, A. Bollmann, J. T. Dixon, S. Kuhlmann, M. C. Maumela, H. Maumela, D. H. Morgan, P. Nongodlwana, M. J. Overett, M. Pretorius, K. H fener, P. Wasserscheid, *J. Mol. Catal. A: Chem.*, **2007**, *270*, 214-218.
- (74) S. Kuhlmann, K. Blann, A. Bollmann, J. T. Dixon, E. Killian, M. C. Maumela, H. Maumela, D. H. Morgan, M. Pr torius, N. Taccardi, P. Wasserscheid, *J. Catal.*, **2007**, *245*, 279-284.
- (75) M. J. Overett, K. Blann, A. Bollmann, R. de Villiers, J. T. Dixon, E. Killian, M. C. Maumela, H. Maumela, D. S. McGuinness, D. H. Morgan, A. Rucklidge, A. M. Z. Slawin, *J. Mol. Catal. A: Chem.*, **2008**, *283*, 114-119.
- (76) R. Walsh, D. H. Morgan, A. Bollmann, J. T. Dixon, *Appl. Catal. A: Gen.*, **2006**, *306*, 184-191.
- (77) S. Kuhlmann, C. Paetz, C. H gele, K. Blann, R. Walsh, J. T. Dixon, J. Scholz, M. Haumann, P. Wasserscheid, *J. Catal.*, **2009**, *262*, 83-91.
- (78) T. Agapie, M. W. Day, L. M. Henling, J. A. Labinger, J. E. Bercaw, *Organometallics*, **2006**, *25*, 2733-2742.
- (79) Y. Suzuki, S. Kinoshita, A. Shibahara, S. Ishii, K. Kawamura, Y. Inoue, T. Fujita, *Organometallics*, **2010**, *29*, 2394-2396.
- (80) P. J. W. Deckers, B. Hessen, J. H. Teuben, *Organometallics*, **2002**, *21*, 5122-5135.
- (81) P. H. M. Budzelaar, *Can. J. Chem.*, **2009**, *87*, 832-837.
- (82) A. W hl, W. M ller, S. Peitz, N. Peulecke, B. R. Aluri, B. H. M ller, D. Heller, U. Rosenthal, M. H. Al-Hazmi, F. M. Mosa, *Chem. Eur. J.*, **2010**, *16*, 7833-7842.
- (83) D. S. McGuinness, B. Chan, G. J. P. Britovsek, B. F. Yates, *Aust. J. Chem.*, **2014**, *67*, 1481-1490.
- (84) L. H. Do, J. A. Labinger, J. E. Bercaw, *Organometallics*, **2012**, *31*, 5143-5149.
- (85) T. M. Zilbershtein, V. A. Kardash, V. V. Suvorova, A. K. Golovko, *Appl. Catal. A: Gen.*, **2014**, *475*, 371-378.
- (86) E. Y.-X. Chen, T. J. Marks, *Chem. Rev.*, **2000**, *100*, 1391-1434.
- (87) N. Meijboom, C. J. Schaverien, A. G. Orpen, *Organometallics*, **1990**, *9*, 774-782.
- (88) I. Y. Skobelev, V. N. Panchenko, O. Y. Lyakin, K. P. Bryliakov, V. A. Zakharov, E. P. Talsi, *Organometallics*, **2010**, *29*, 2943-2950.
- (89) Y. Fang, Y. Liu, Y. Ke, C. Guo, N. Zhua, X. Mi, Z. Ma, Y. Hu, *Appl. Catal. A: Gen.*, **2002**, *235*, 33-38.
- (90) L. H. Do, J. A. Labinger, J. E. Bercaw, *ACS Catal.*, **2013**, *3*, 2582-2585.
- (91) A. Jabri, C. B. Mason, Y. Sim, S. Gambarotta, T. J. Burchell, R. Duchateau, *Angew. Chem. Int. Ed.*, **2008**, *47*, 9717-9721.
- (92) I. Vidyaratne, G. B. Nikiforov, S. I. Gorelsky, S. Gambarotta, R. Duchateau, I. Korobkov, *Angew. Chem. Int. Ed.*, **2009**, *48*, 6552 -6556.
- (93) L. E. Bowen, M. F. Haddow, A. G. Orpen, D. F. Wass, *Dalton Trans.*, **2007**, 1160-1168.
- (94) A. J. Rucklidge, D. S. McGuinness, R. P. Tooze, A. M. Z. Slawin, J. D. A. Pelletier, M. J. Hanton, P. B. Webb, *Organometallics*, **2007**, *26*, 2782-2787.
- (95) A. Finiels, F. Fajula, V. Hulea, *Catal. Sci. Technol.*, **2014**, *4*, 2412-2426.

- (96) J. P. Hogan, R. L. Banks, **1958**, US22825721, Phillips Petroleum Company.
- (97) D. S. McGuinness, N. W. Davies, J. Horne, I. Ivanov, *Organometallics*, **2010**, *29*, 6111-6116.
- (98) M. P. McDaniel, *Ind. Eng. Chem. Res.*, **1988**, *27*, 1559-1564.
- (99) V. J. Ruddick, P. W. Dyer, G. Bell, V. C. Gibson, J. P. S. Badyal, *J. Phys. Chem.*, **1996**, *100*, 11062-11066.
- (100) Y. V. Kissin, A. J. Brandolini, *J. Polym. Sci. A Polym. Chem.*, **2008**, *46*, 5330-5347.
- (101) C. A. Demmelmaier, R. E. White, J. A. van Bokhoven, S. L. Scott, *J. Catal.*, **2009**, *262*, 44-56.
- (102) M. P. Conley, M. F. Delley, G. Siddiqi, G. Lapadula, S. Norsic, V. Monteil, O. V. Safonova, C. Copéret, *Angew. Chem. Int. Ed.*, **2014**, *53*, 1872-1876.
- (103) M. F. Delley, F. Núñez-Zarur, M. P. Conley, A. Comas-Vives, G. Siddiqi, S. Norsic, V. Monteil, O. V. Safonova, C. Copéret, *Proc. Natl. Acad. Sci. U.S.A.*, **2014**, *111*, 11624-11629.
- (104) C. Brown, J. Krzystek, R. Achey, A. Lita, R. Fu, R. W. Meulenberg, M. Polinski, N. Peek, Y. Wang, L. J. van de Burgt, S. Profeta Jr., A. E. Stiegman, S. L. Scott, *ACS Catal.*, **2015**, *5*, 5574-5583.
- (105) A. Fong, B. Peters, S. L. Scott, *ACS Catal.*, **2016**, *6*, 6073-6085.
- (106) R. D. Köhn, M. Haufe, S. Mihan, D. Lilge, *Chem. Commun.*, **2000**, 1927-1928.
- (107) R. D. Köhn, D. Smith, D. Lilge, S. Mihan, F. Molnar, M. Prinz, In *Beyond Metallocenes*; ACS Symposium Series: Washington DC, 2003; Vol. 857, p 88-100.
- (108) C. N. Nenu, J. N. J. van Lingen, F. M. de Groot, D. C. Koningsberger, B. M. Weckhuysen, *Chem. Eur. J.*, **2006**, *12*, 4756-4763.
- (109) C. P. Nicholas, H. Ahn, T. J. Marks, *J. Am. Chem. Soc.*, **2003**, *125*, 4325-4331.
- (110) C. N. Nenu, P. Bodart, B. M. Weckhuysen, *J. Mol. Catal. A: Chem.*, **2007**, *269*, 5-11.
- (111) V. O. Aliyev, M. Al-Hazmi, F. Mosa, U. Rosenthal, B. H. Müller, M. Hapke, N. Peulecke, A. Wöhl, P. M. Fritz, H. Bölt, **2009**, WO2009121456A1, Linde Ag, Saudi Basic Industries Corporation.
- (112) S. Peitz, N. Peulecke, B. R. Aluri, B. H. Müller, A. Spannenberg, U. Rosenthal, M. H. Al-Hazmi, F. M. Mosa, A. Wöhl, W. Müller, *Chem. Eur. J.*, **2010**, *16*, 12127-12132.
- (113) S. Peitz, N. Peulecke, B. R. Aluri, S. Hansen, B. H. Müller, A. Spannenberg, U. Rosenthal, M. H. Al-Hazmi, F. M. Mosa, A. Wöhl, W. Müller, *Eur. J. Inorg. Chem.*, **2010**, *2010*, 1167-1171.
- (114) H. Monoi, H. Torigoe, M. Fushimi, M. Yamamoto, **1997**, JPH0920692 (A), Showa Denko.
- (115) H. Monoi, H. Torigoe, M. Fushimi, M. Yamamoto, **1997**, JPH0920693 (A), Showa Denko.
- (116) T. Monoi, Y. Sasaki, *J. Mol. Catal. A: Chem.*, **2002**, *187*, 135-141.
- (117) L. T. Zhuravlev, *Colloids Surf. A*, **2000**, *173*, 1-38.
- (118) J. E. Radcliffe, A. S. Batsanov, D. M. Smith, J. A. Scott, P. W. Dyer, M. J. Hanton, *ACS Catal.*, **2015**, *5*, 7095-7098.
- (119) P. J. W. Deckers, B. Hessen, J. H. Teuben, *Angew. Chem. Int. Ed.*, **2001**, *40*, 2516-2519.
- (120) E. Otten, A. A. Batinas, A. Meetsma, B. Hessen, *J. Am. Chem. Soc.*, **2009**, *131*, 5298-5312.
- (121) C. Andes, S. B. Harkins, S. Murtuza, K. Oyler, A. Sen, *J. Am. Chem. Soc.*, **2001**, *123*, 7423-7424.

Chapter 2:
Role of Catalyst Support, Co-catalyst and Diluent in
Chromium-mediated Heterogeneous Ethylene
Trimerisation

2.1 Introduction

Owing to its high productivity, moderate selectivity towards 1-hexene, and relative ease of access, the “Cr{N(SiMe₃)₂}₂/SiO₂” pro-initiator (see Section 1.3.2.5), previously described by Monoi and Sasaki,¹ provides a convenient starting point for developing understanding of heterogeneous selective olefin oligomerisation. This chapter reports our findings from a survey of the fundamental factors that influence the catalytic behaviour of a solid-phase Cr{N(SiMe₃)₂}₂/oxide/Al-activator ethylene trimerisation initiator system.¹ In particular, an assessment is made here of the impact of the nature of the oxide support and its pre-treatment, the nature of the alkyl aluminium-based co-catalyst, and the reaction diluent upon the system’s performance.

Solid-state Raman and ²⁹Si direct excitation (DE) magic-angle spinning (MAS) nuclear magnetic resonance (NMR) spectroscopic studies of the most effective oxide-supported chromium pro-initiator are described. Based on these analyses, it is proposed that the “Cr{N(SiMe₃)₂}₂/SiO₂” catalyst precursor comprises at least two supported chromium(III) amide species derived from isolated (Q₃) and geminal (Q₂) silanols at the surface of silica that, upon activation with an aluminium-based co-catalyst, mediate two competing tri- and poly-merisation processes, respectively.

Previous studies have shown that the temperature at which silica is calcined greatly influences the product selectivity of the “Cr{N(SiMe₃)₂}₂/SiO₂” pro-initiator either in favour of ethylene trimerisation or indeed polymerisation (see Section 1.3.2.5).^{1,2} Following on from this preliminary observation, solid-state ²⁹Si DE MAS NMR spectroscopic analysis is used to establish a correlation between the relative population of isolated (Q₃) and geminal (Q₂) silanol sites at the silica surface as a function of calcination temperature, and the product selectivity of the resulting silica-supported chromium initiator.

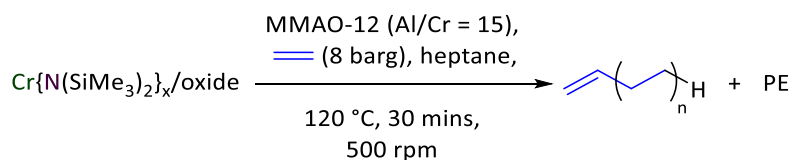
2.2 Results and Discussion

2.2.1 Role of the Oxide Support in the Cr{N(SiMe₃)₂}_x/Oxide-600/MMAO-12 Ethylene Trimerisation System

Evonik Aeroperl 300/30 fumed silica (described herein as SiO₂), Alfa Aesar γ -alumina (1/8" pellets ground and sieved to <250 μ m; described herein as γ -Al₂O₃), and Sigma Aldrich silica-alumina grade 135 catalyst support (13 wt% Al₂O₃;³ described herein as SiO₂-Al₂O₃) were screened as potential catalyst supports for chromium-mediated ethylene oligomerisation. To enable comparisons with the prior work of Monoi and Sasaki of a related system (see Section 1.3.2.5),¹ each of these three oxide materials was calcined at 600 °C for 24 hours under a flow of dry N₂. The resulting catalyst supports are classified by the temperature at which they were calcined, *e.g.* SiO₂₋₆₀₀ denotes silica pre-treated at 600 °C for 24 hours under a flow of dry N₂. Sequential treatment of these partially dehydroxylated oxide supports with a heptane solution of Cr{N(SiMe₃)₂}₃, and modified methyl aluminoxane (MMAO-12; 7 wt% solution in toluene) affords initiator systems active for ethylene oligo-/poly-merisation. These resulting initiator systems are referred to simply by their molecular precursor, oxide support and the Lewis acidic alkyl aluminium-based co-catalyst employed, *e.g.* Cr{N(SiMe₃)₂}_x/SiO₂₋₆₀₀/MMAO-12 denotes SiO₂₋₆₀₀ impregnated with Cr{N(SiMe₃)₂}₃, and subsequently activated with MMAO-12. Note that in all cases the chromium-functionalised oxide materials produced are extremely sensitive to both moisture and oxygen, something that dictates rigorous manipulation under dry, anaerobic conditions at all times, using either glove box or Schlenk line techniques.

The selective ethylene oligomerisation catalytic performance of SiO₂₋₆₀₀, γ -Al₂O₃₋₆₀₀ and SiO₂-Al₂O₃₋₆₀₀-supported chromium initiators were assessed in the slurry phase in heptane under identical test conditions (Scheme 1). In each case, the contents of the reactor (*i.e.* pro-initiator, co-catalyst, diluent and internal standard) were heated to 120 °C, whilst being stirred at 500 revolutions per minute (rpm), before the autoclave was pressurised with ethylene to 8 barg, and then sealed for the duration of the reaction. Consequently, the catalytic activities achieved in the following investigations are limited by the concentration of the monomer feedstock, which in some cases was wholly consumed over the course of the ethylene trimerisation reaction. Additionally, such tests do not take into account the pressure dependency of ethylene solubility in the organic diluent.

The results of these ethylene trimerisation runs are summarised in Table 1. Unless otherwise stated, the total catalytic activities quoted hereafter correspond to the total mass of all products per gram of chromium per hour (*i.e.* g g_{Cr}⁻¹ h⁻¹). For completeness, a homogeneous solution of Cr{N(SiMe₃)₂}₃ was activated with MMAO-12, and tested in an analogous fashion.



Scheme 1: General reaction scheme used for screening oxide-supported chromium ethylene trimerisation initiators

Table 1: Comparison of ethylene oligomerisation runs mediated by $\text{Cr}\{\text{N}(\text{SiMe}_3)_2\}_3$ or $\text{Cr}\{\text{N}(\text{SiMe}_3)_2\}_x/\text{oxide}$ (i.e. $\text{SiO}_2\text{-600}$, $\text{SiO}_2\text{-Al}_2\text{O}_3\text{-600}$ or $\gamma\text{-Al}_2\text{O}_3\text{-600}$) with MMAO-12 as activator in heptane.

Entry	Catalyst Support	C ₄ ^a {wt%}	C ₆ ^a {wt%}	C ₈ ^a {wt%}	C ₁₀ ^a {wt%}	C ₁₂₊ ^a {wt%}	PE ^b {wt%}	Total Activity {g Cr ⁻¹ h ⁻¹ }
			(%1-C ₆ =)					
1	No Support	12	26 (81)	6	7	9	41	80
2	SiO ₂ -600	1	61 (79)	2	16	6	13	2403
3	SiO ₂ -Al ₂ O ₃ -600	1	71 (94)	3	10	3	12	1401
4	γ-Al ₂ O ₃ -600	2	3 (71)	3	3	4	85	237

Reaction conditions: 27 μmol Cr (mass of $\text{Cr}\{\text{N}(\text{SiMe}_3)_2\}_x/\text{oxide}$ = 0.2 g); 410 μmol MMAO-12 (Al:Cr = 15:1); 60 mL heptane; 120 °C; 500 rpm; 8 barg ethylene pressure; 0.5 h.

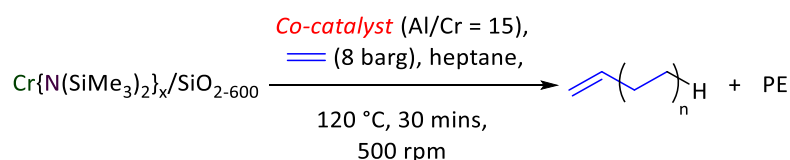
^a Determined by gas chromatographic-flame ionisation detection (GC-FID) relative to the internal standard (1 mL nonane).

^b Polymer isolated by filtration, dried to constant mass and weighed.

The preliminary test results (Table 1) show that the SiO₂-600- and SiO₂-Al₂O₃-600-supported chromium initiators afford hexenes as the principle products, with moderate selectivity towards 1-hexene in both cases (Entries 2 and 3). These observations are broadly in agreement with those made previously by Monoi and Sasaki using a related ethylene trimerisation system.¹ In contrast, $\text{Cr}\{\text{N}(\text{SiMe}_3)_2\}_x/\gamma\text{-Al}_2\text{O}_3\text{-600}/\text{MMAO-12}$ demonstrates a complete switch in product selectivity, favouring polyethylene (PE) formation over oligomerisation; this difference is accompanied by a significantly lower catalytic activity (Entry 4). Both the SiO₂-600- and SiO₂-Al₂O₃-600-supported chromium initiator systems exhibit selectivity towards C₆ and C₁₀ olefins, which is indicative of a metallacycle-based trimerisation reaction manifold being operative (see Section 1.3.1.5),^{4,5,6,7,8} rather than giving rise to broad statistical product distributions, something typically associated with a Cossee-Arlman-type chain growth mechanism (see Section 1.2).^{9,10,11} In contrast, catalytic tests using the soluble (molecular) $\text{Cr}\{\text{N}(\text{SiMe}_3)_2\}_3$ complex in combination with MMAO-12 as activator (Table 1; Entry 1) resulted in an extremely low productivity, along with a preference towards PE formation. Together these observations are consistent with the oxide support playing an intimate role in the stabilisation of the active chromium species, as well as determining the nature of the catalytically active chromium functionalities.

2.2.2 Influence of the Lewis Acidic Co-catalyst on the Performance of the $\text{Cr}\{\text{N}(\text{SiMe}_3)_2\}_x/\text{SiO}_{2-600}$ Ethylene Trimerisation Pro-initiator

Previous studies have shown that Lewis acidic co-catalysts, typically alkyl aluminium reagents, are necessary to activate homogeneous selective ethylene oligomerisation pro-initiators.^{12,13} Furthermore, it is well established that the nature of the aluminium activator has a profound impact on the performance of early transition metal (TM)-mediated olefin oligomerisation processes, both in terms of activity as well as in selectivity (See Section 1.3.1.5.4).^{13,14,15,16,17} Such effects result from a complex interplay between the reducing capability, steric hindrance, stability, and the potential coordinating strength of the anionic component generated by the reaction between the TM molecular precursor and the alkyl aluminium-based co-catalyst.^{14,16} Therefore, it is essential to evaluate a range of activators, namely $i\text{Bu}_3\text{Al}$, isobutyl aluminoxane (IBAO), Me_3Al , methyl aluminoxane (MAO), MMAO-12 and Et_2AlCl , in combination with the best performing $\text{Cr}\{\text{N}(\text{SiMe}_3)_2\}_x/\text{SiO}_{2-600}$ pro-initiator to establish the most effective heterogeneous ethylene trimerisation catalytic system (Scheme 2).



Scheme 2: General reaction scheme used for screening co-catalysts in the $\text{Cr}\{\text{N}(\text{SiMe}_3)_2\}_x/\text{SiO}_{2-600}$ ethylene trimerisation system

Table 2: Comparison of ethylene oligomerisation tests mediated by $\text{Cr}\{\text{N}(\text{SiMe}_3)_2\}_x/\text{SiO}_{2-600}$ with varying co-catalysts (i.e. none, $i\text{Bu}_3\text{Al}$, IBAO, Me_3Al , MAO, MMAO-12 or Et_2AlCl) as activator in heptane.

Entry	Activator	$\text{C}_4=^a$ {wt%}	$\text{C}_6=^a$ {wt%}	$\text{C}_8=^a$ {wt%}	$\text{C}_{10}=^a$ {wt%}	$\text{C}_{12+}=^a$ {wt%}	PE^b {wt%}	Total Activity { $\text{g g}_{\text{Cr}}^{-1} \text{h}^{-1}$ }
1	No Activator	0	0 (0)	0	0	0	0	0
2	$i\text{Bu}_3\text{Al}$	3	33 (29)	0	0	7	56	1125
3	IBAO	12	19 (41)	0	1	62	6	358
4	Me_3Al	5	44 (68)	4	3	9	35	243
5	MAO	0	9 (52)	0	0	14	76	969
6	MMAO-12	1	61 (79)	2	16	6	13	2403
7	Et_2AlCl	2	4 (89)	3	2	16	74	114

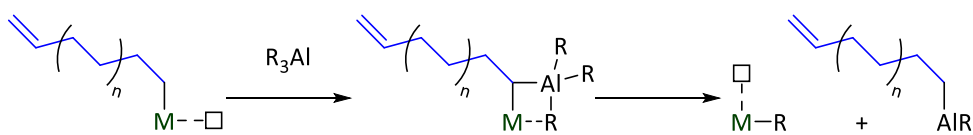
Reaction conditions: 27 μmol Cr (mass of $\text{Cr}\{\text{N}(\text{SiMe}_3)_2\}_x/\text{SiO}_{2-600}$ = 0.2 g); 410 μmol co-catalyst (Al:Cr = 15:1); 60 mL heptane; 120 $^\circ\text{C}$; 500 rpm; 8 barg ethylene pressure; 0.5 h.

^a Determined by GC-FID relative to the internal standard (1 mL nonane).

^b Polymer isolated by filtration, dried to constant mass and weighed.

In line with the established trends for homogeneous chromium-mediated ethylene oligomerisation initiators,^{13,14,15,16,17} the performance of the heterogeneous $\text{Cr}\{\text{N}(\text{SiMe}_3)_2\}_x/\text{SiO}_{2-600}$ pro-initiator described in this thesis is also found to exhibit a dependency on the nature of the co-catalyst (Table 2). Under the reaction conditions employed herein, MMAO-12 proved to be the optimal activator in terms of both the resulting activity and selectivity towards 1-hexene (Entry 6). Notably, in our hands, activation using IBAO afforded a system that was an order of magnitude less active (Entry 3) and produced comparatively high levels of heavier (C_{12+}) oligomers compared to the results previously described by Monoi and Sasaki.¹ While the origins of the enhanced performance of MMAO-12 as activator in the $\text{Cr}\{\text{N}(\text{SiMe}_3)_2\}_x/\text{SiO}_{2-600}$ -mediated process remain obscure, it is likely that the greater thermal stability, and better solubility of MMAO-12 in heptane compared with that of the other aluminium-based co-catalysts screened here, including MAO (Entry 6), is a significant factor under the reaction conditions employed.^{18,19}

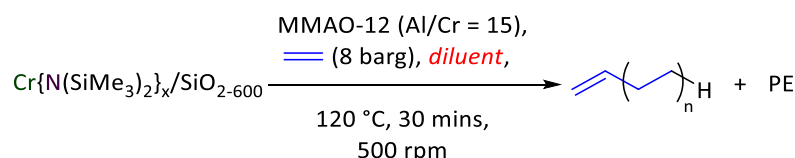
At this point, it must be stated that the precise roles and modes of action of alkyl aluminium activators in both olefin oligo- and poly-merisation are complex, and generally remain rather poorly understood.¹⁸ Consequently, it is possible that other factors will also contribute to differences observed between the performances of the various co-catalysts screened herein. These include potential coordination of alkyl aluminium species to the active chromium metal centre, either directly or through ligation of the pendant amide groups,^{20,21} which can impede olefin coordination,^{14,22} and in turn provide a pathway for alkyl chain transfer (Scheme 3).^{23,24,25,26} Furthermore, since calcined oxides such as silica and alumina are established supports for alkyl aluminium reagents themselves in both olefin oligo-/poly-merisation catalysis, binding of the co-catalyst to SiO_{2-600} cannot be ruled out, something that may also lead to a modification of the aluminoxanes (*e.g.* IBAO, MAO, MMAO-12) through sequestration of residual trialkyl aluminium species inherently present.^{27,28,29} For example, preferential depletion of $i\text{Bu}_3\text{Al}$ from modified methyl aluminoxane (MMAO) by way of reaction with partially dehydroxylated silica has previously been ascribed to account for the promotion of titanium-mediated propylene polymerisation through the suppression of chain transfer processes.²⁹



Scheme 3: Chain transfer mediated by an alkyl aluminium reagent, modified from Tanaka *et al.*, 2017²⁹

2.2.3 Effect of Diluent on Cr{N(SiMe₃)₂}_x/SiO₂₋₆₀₀/MMAO-12-mediated Ethylene Trimerisation

Previous studies have shown that homogeneous selective olefin oligomerisation processes are subject to substantial solvent effects.^{17,19,20,30} Accordingly, a series of batch ethylene oligomerisation runs using the heterogeneous Cr{N(SiMe₃)₂}_x/SiO₂₋₆₀₀/MMAO-12 ethylene trimerisation system were conducted to explore the impact of the liquid organic diluent phase on catalytic performance (Scheme 4).



Scheme 4: General reaction scheme used for screening reaction diluents in the Cr{N(SiMe₃)₂}_x/SiO₂₋₆₀₀/MMAO-12 ethylene trimerisation process

Table 3: Comparison of ethylene oligomerisation tests using Cr{N(SiMe₃)₂}_x/SiO₂₋₆₀₀ with MMAO-12 as activator employing various diluents (*i.e.* heptane, methylcyclohexane, toluene or chlorobenzene).

Entry	Activator	C ₄ ^a {wt%}	C ₆ ^a {wt%}	C ₈ ^a {wt%}	C ₁₀ ^a {wt%}	C ₁₂₊ ^a {wt%}	PE ^b {wt%}	Total Activity {g Cr ⁻¹ h ⁻¹ }
1	Heptane	1	61 (79)	2	16	6	13	2403
2	Methylcyclohexane	1	61 (72)	4	12	6	16	2132
3	Toluene	2	51 (96)	3	3	5	36	449
4	Chlorobenzene	1	1 (85)	1	1	2	94	792

Reaction conditions: 27 μmol Cr (mass of Cr{N(SiMe₃)₂}_x/SiO₂₋₆₀₀ = 0.2 g); 410 μmol MMAO-12 (Al:Cr = 15:1); 60 mL diluent; 120 °C; 500 rpm; 8 barg ethylene pressure; 0.5 h.

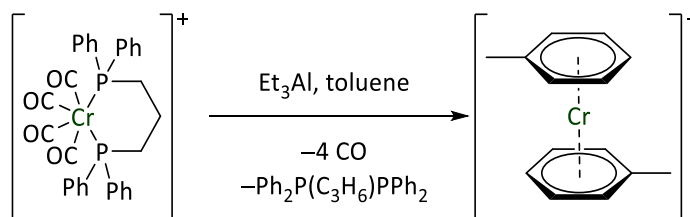
^a Determined by GC-FID relative to the internal standard (1 mL nonane).

^b Polymer isolated by filtration, dried to constant mass and weighed.

Based on our experimental catalytic data obtained (Table 3), it is clear that the Cr{N(SiMe₃)₂}_x/SiO₂₋₆₀₀/MMAO-12 initiator system performs best in aliphatic, non-polar diluents such as heptane and methylcyclohexane (Entries 1 and 2). Conversely, use of aromatic diluents such as toluene and chlorobenzene (Entries 3 and 4) leads to a considerable drop in catalytic activity and an associated switch in product selectivity from oligomerisation to PE formation.

It has been reported previously that treatment of molecular chromium(III) complexes with alkyl aluminium reagents in aromatic diluents, *e.g.* chromium(III) *tris*-(2,4-pentanedionate) {Cr(acac)₃} and Me₃Al in toluene,³¹ can generate reduced chromium(I) sandwich complexes of the type [Cr(η⁶-arene)₂]⁺ (Scheme 5),³² something that has been invoked to account for the deactivation of *homogeneous* selective ethylene oligomerisation systems.^{19,20} Hence, it is reasonable to propose that analogous Cr^I *bis*-(arene) species may also be formed during the

activation of the *heterogeneous* $\text{Cr}\{\text{N}(\text{SiMe}_3)_2\}_x/\text{SiO}_{2-600}$ ethylene trimerisation pro-initiator with MMAO-12 in either toluene or chlorobenzene, which may rationalise the low activity observed in these two diluents.

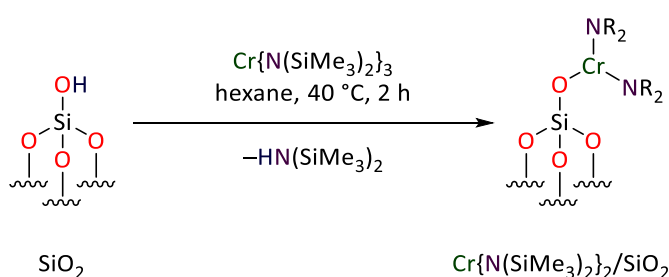


Scheme 5: Deactivation of $[\text{Cr}^I \text{PNP}]^+$ ethylene tetramerisation initiator proposed by McDyre *et al.*, 2011³²

2.2.4 Understanding the Nature and Catalytic Behaviour of the $\text{Cr}\{\text{N}(\text{SiMe}_3)_2\}_x/\text{SiO}_2\text{-600}/\text{MMAO-12}$ Initiator System

2.2.4.1 Solid-state Raman Spectroscopic Analysis

In order to understand the mode of action of the $\text{Cr}\{\text{N}(\text{SiMe}_3)_2\}_x/\text{SiO}_2\text{-600}/\text{MMAO-12}$ ethylene trimerisation system presented in the preceding sections, it is essential to develop insight into the nature of the supported chromium species. Based on previous work,¹ it is assumed that the $\text{Cr}\{\text{N}(\text{SiMe}_3)_2\}_3$ molecular precursor will react with residual isolated (Q_3) silanols at the surface of $\text{SiO}_2\text{-600}$ eliminating the corresponding amine, $\text{HN}(\text{SiMe}_3)_2$ (Scheme 6). Raman spectroscopy is ideally suited to validating this hypothesis, because it can be used to detect the Cr–O–Si linkage(s) that would form between the chromium(III) amide and the partially dehydroxylated $\text{SiO}_2\text{-600}$ catalyst support.



Scheme 6: Reaction between $\text{Cr}\{\text{N}(\text{SiMe}_3)_2\}_3$ and a residual isolated silanol functionality at the surface of silica previously calcined at $600\text{ }^\circ\text{C}$ for 24 hours as reported by Monoi *et al.*, 2002¹

Before this investigation was undertaken, an extensive literature search for vibrational spectroscopic analyses of Cr–O–Si bonding modes yielded data largely limited to the Phillips heterogeneous $\text{CrO}_3/\text{SiO}_2$ ethylene polymerisation pro-initiator.^{33,34,35} For example, Guesmi *et al.* conducted a density functional theory (DFT) study to predict the Raman spectrum of several model supported chromium(VI) species that may be present at the surface of $\text{CrO}_3/\text{SiO}_2$, which indicated that the frequency range for the Cr–O–Si stretches were between $820 - 980\text{ cm}^{-1}$ (Figure 1).³³ For reference, Moisii, Chakrabarti and co-workers have assigned bands to Cr–O–Si in the experimentally-derived infrared (IR) and Raman spectra of $\text{CrO}_3/\text{SiO}_2$ at 906 and 919 cm^{-1} , respectively.^{34,35} Since vibrational bonding modes associated with silica in the $200 - 1300\text{ cm}^{-1}$ window barely contribute to the inelastic scattering of light, they are scarcely observed in Raman spectra.³⁶ Raman spectroscopy should therefore be able to identify the Cr–O–Si linkage(s) as well as the respective Cr–N, N–Si, Si–C and C–H vibrational bonding modes present in $\text{Cr}\{\text{N}(\text{SiMe}_3)_2\}_x/\text{SiO}_2\text{-600}$.

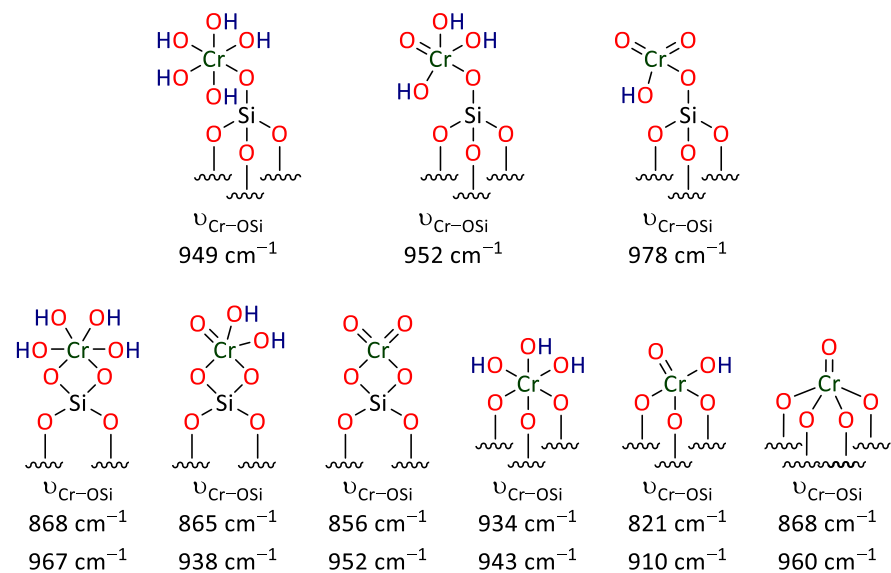


Figure 1: DFT-derived Raman-active Cr–O–Si bands present in $\text{CrO}_3/\text{SiO}_2$, adapted from Guesmi *et al.*, 2012³³

With this prior literature information in hand, a sample of the solid $\text{Cr}\{\text{N}(\text{SiMe}_3)_2\}_x/\text{SiO}_{2-600}$ pro-initiator was loaded into a standard glass J. Young valve NMR tube inside a nitrogen-filled glove box, and sealed under an inert atmosphere. Subsequently, the 532 nm Raman spectrum of $\text{Cr}\{\text{N}(\text{SiMe}_3)_2\}_x/\text{SiO}_{2-600}$ was measured and compared to that of its molecular precursor, and its parent catalyst support (Figure 2). In spite of a relatively low signal to noise ratio, several characteristic bands present in the Raman spectrum of $\text{Cr}\{\text{N}(\text{SiMe}_3)_2\}_x/\text{SiO}_{2-600}$ were found to be consistent with those observed in a sample of bulk $\text{Cr}\{\text{N}(\text{SiMe}_3)_2\}_3$. These vibrational bonding modes were assigned based on a previously reported IR spectrum of the molecular precursor (Table 4).³⁷ The Raman spectrum of the $\text{Cr}\{\text{N}(\text{SiMe}_3)_2\}_x/\text{SiO}_{2-600}$ pro-initiator exhibits bands in accordance with the retention of amide ligand(s), as well as an additional broad peak between $\sim 1000 - 1100 \text{ cm}^{-1}$ that is not present in either $\text{Cr}\{\text{N}(\text{SiMe}_3)_2\}_3$ or SiO_{2-600} , which has provisionally been attributed to a Cr–O–Si vibrational stretching mode. It is therefore postulated that a chromium(III) amide species is covalently grafted to the partially dehydroxylated SiO_{2-600} catalyst support (see Scheme 6).

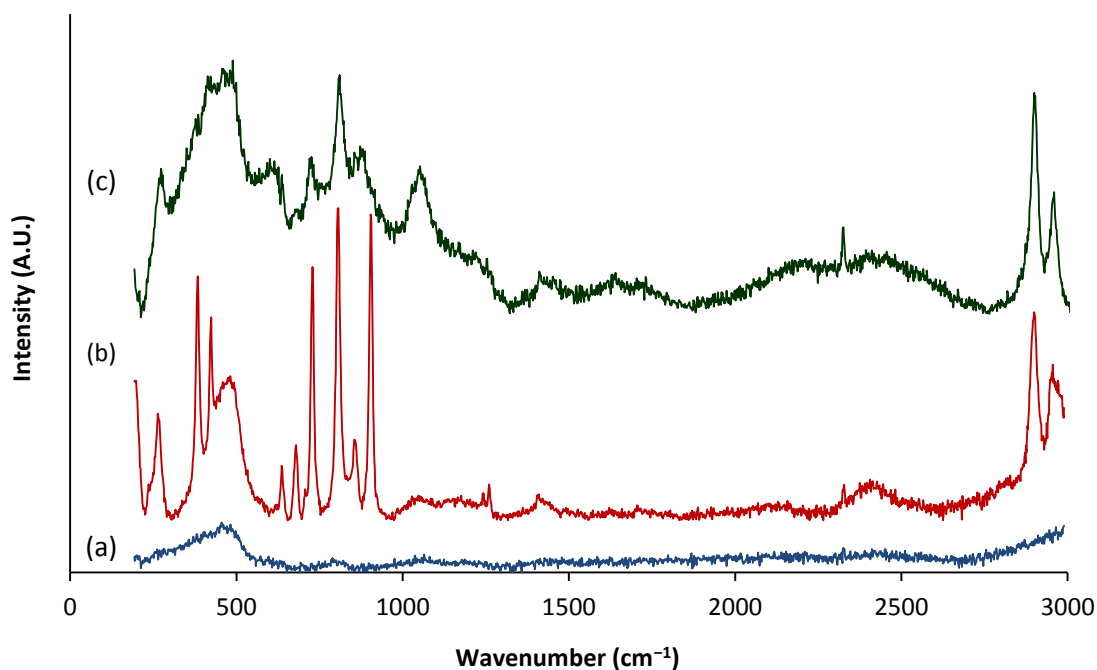


Figure 2: Solid-state 532 nm Raman spectra: (a) SiO_{2-600} ; (b) $\text{Cr}\{\text{N}(\text{SiMe}_3)_2\}_3$; (c) $\text{Cr}\{\text{N}(\text{SiMe}_3)_2\}_x/\text{SiO}_{2-600}$.

Table 4: Solid-state 532 nm Raman-active bands present in Cr{N(SiMe₃)₂}₃ and Cr{N(SiMe₃)₂}_x/SiO₂₋₆₀₀, compared to IR spectroscopic data corresponding to Cr{N(SiMe₃)₂}₃ previously reported by Alyea *et al.*, 1972³⁷

Vibrational Bonding Modes	Cr{N(SiMe₃)₂}₃ IR (cm⁻¹)³⁷	Cr{N(SiMe₃)₂}₃ Raman (cm⁻¹)	Cr{N(SiMe₃)₂}_x/SiO₂₋₆₀₀ Raman (cm⁻¹)
CH	-	2956	2960
	-	2898	2899
CH₃	1260	1260	1252
	1250	1240	
CrOSi	-	-	~1052
CrNSi₂ (A₂, E)	902	904	-
CH₃	865	855	854
	840		
CrNSi₂ (A₁, E)	820	805	807
	790		
CH₃	758	728	726
SiC₃ (A₁)	708	707	726
SiC₃ (E)	676	679	637
	620	636	
CrN₃ (A₁)	420	424	423
CrN₃ (E)	376	382	385

2.2.4.2 Solid-state ^{29}Si DE MAS NMR Spectroscopic Study

Since it has been established using Raman spectroscopy that the $\text{Cr}\{\text{N}(\text{SiMe}_3)_2\}_3$ molecular precursor is covalently grafted to the surface of SiO_{2-600} , it was necessary to explore the nature of the Cr–O–Si linkage(s). To this end, solid-state ^{29}Si DE MAS NMR spectroscopic analyses of the partially dehydroxylated siliceous catalyst support and the resulting $\text{Cr}\{\text{N}(\text{SiMe}_3)_2\}_x/\text{SiO}_{2-600}$ catalyst precursor were undertaken.

2.2.4.2.1 Solid-state ^{29}Si DE MAS NMR Spectroscopic Analysis of SiO_{2-600}

Solid-state ^{29}Si DE MAS NMR spectroscopy was used to quantify the change in the relative proportion of geminal (Q_2) {–91 ppm} and isolated (Q_3) {–99 ppm} silanols at the surface of Evonik Aeroperl 300/30 fumed silica as a function of calcination temperature (Figure 3), with spectral assignments made in accordance with a previously reported, but related NMR spectroscopic study.³⁸ Both Evonik Aeroperl 300/30 fumed silica and SiO_{2-600} samples exhibit three resonances in their ^{29}Si DE MAS NMR spectra, although it is impossible to discriminate between Q_3 and vicinal silanols as their characteristic resonance frequencies overlap at –99 ppm.³⁸ However, since it is widely accepted that vicinal silanols fully condense at calcination temperatures of 400 °C and above,^{39,40,41} it is proposed that the SiO_{2-600} material comprises both Q_2 and Q_3 silanol functionalities, according to ^{29}Si DE MAS NMR spectroscopy, in a 1:29 ratio by deconvolution using a Gaussian distribution curve fit. Comparison of the deconvoluted ^{29}Si DE MAS NMR spectra of untreated Evonik Aeroperl 300/30 fumed silica with that of SiO_{2-600} highlight that the calcined oxide support has a significantly lower concentration of Q_2 , Q_3 and vicinal silanol groups.

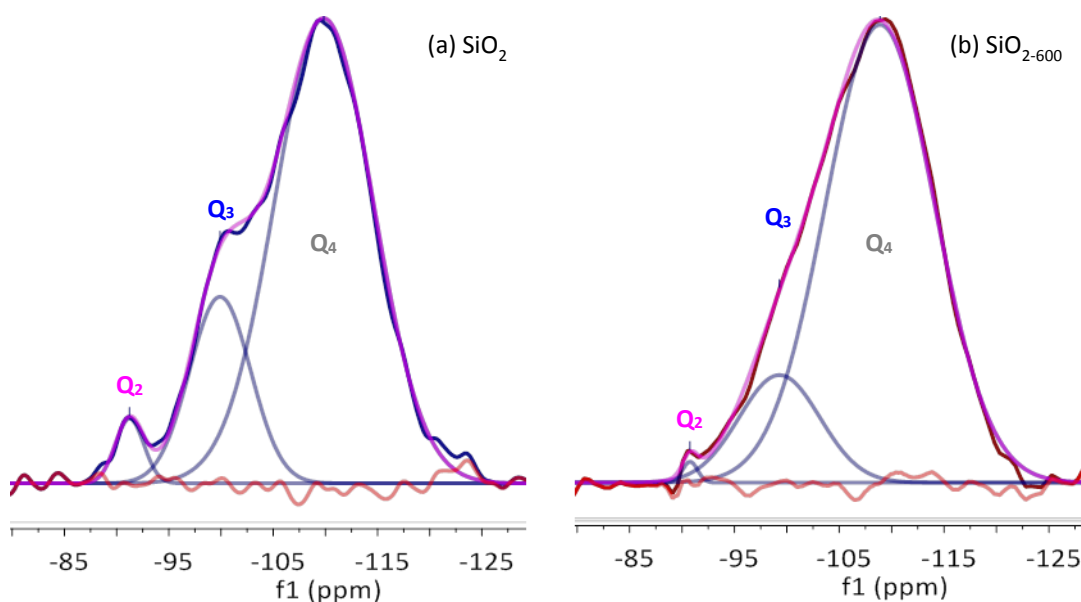
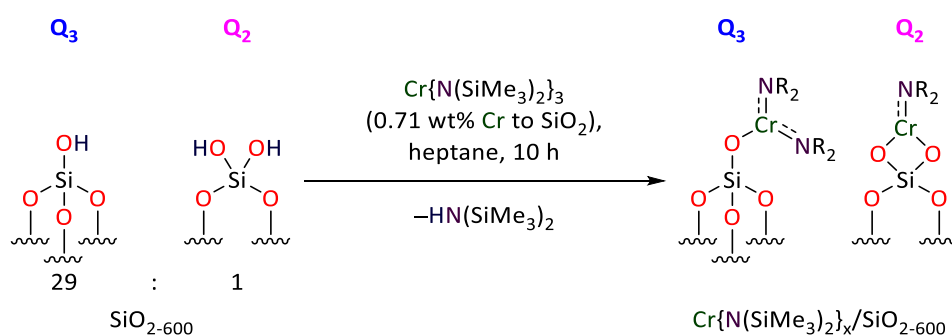


Figure 3: Comparison of solid-state ^{29}Si DE MAS NMR spectra (79 MHz frequency, 6 kHz rotation) deconvoluted using a Gaussian distribution: (a) Evonik Aeroperl 300/30 fumed silica (as received); (b) SiO_{2-600} .

2.2.4.2.2 Solid-state ^{29}Si DE MAS NMR Spectroscopic Analysis of $\text{Cr}\{\text{N}(\text{SiMe}_3)_2\}_x/\text{SiO}_{2-600}$

Up until now, it has been assumed that $\text{Cr}\{\text{N}(\text{SiMe}_3)_2\}_3$ will react with residual Q_3 silanols at the surface of SiO_{2-600} , liberating one molar equivalent of the corresponding amine to afford a supported chromium *bis*-(hexamethyldisilazide) complex.^{1,40} However, considering that Q_3 silanols outnumber Q_2 sites by 29:1 (see Section 2.2.4.2.1), we propose that the chromium(III) amide complex will react with both Q_3 and Q_2 silanol functionalities, resulting in the formation of one and two Si–O–Cr bonds, respectively, as demonstrated in Scheme 7, and hence two types of surface-bound chromium species. Consequently, upon treatment of this material with an alkyl aluminium-based activator (*e.g.* MMAO-12) it is proposed that two distinct active species will be formed, something that is attributed here to be the origin of the simultaneous ethylene tri- and poly-merisation catalytic behaviour described in the preceding catalyst test sections.



Scheme 7: Impregnation of SiO_{2-600} with $\text{Cr}\{\text{N}(\text{SiMe}_3)_2\}_3$ eliminating $\text{HN}(\text{SiMe}_3)_2$

In order to investigate the nature of the supported chromium(III) *mono*- and *bis*-(hexamethyldisilazide) species bound at the surface of silica, the intrinsic paramagnetic character of $\text{Cr}\{\text{N}(\text{SiMe}_3)_2\}_x/\text{SiO}_{2-600}$ has been exploited in a ^{29}Si DE MAS NMR spectroscopic study. In particular, it was desired to probe how the ^{29}Si resonances for each of the various silanol moieties were affected by the presence of the paramagnetic chromium. This builds upon a previous study that has shown that this type of approach provided useful insight into the nature of the catalytically-relevant paramagnetic chromium species present in the Phillips heterogeneous so-called “Cr/SiO₂” ethylene polymerisation system.⁴² These experiments exploit the fact that the time constant for dipolar coupling relaxation increases with distance as r^6 , so the recovered magnetisation of an NMR sample at time t after saturation, $m(t)$, will be that of the spins contained in a sphere of radius r corresponding to $t^{1/6}$.^{42,43} Since dipolar coupling is typically transmitted over long distances by nuclear spin-spin diffusion, magic-angle spinning (MAS) about an axis at 54.74° to the applied magnetic field, B_0 , at a rate of ω_r averages the secular component of the dipolar coupling between spin- $1/2$ nuclei (*i.e.* $3\cos^2\theta - 1 = 0$),^{44,45} which effectively quenches nuclear-spin diffusion between neighbouring ^{29}Si nuclei.^{43,46} Conversely, the magnitude of the ^{29}Si nuclear longitudinal relaxation rate T_1^{-1} induced by a dipolar coupling with a fixed paramagnetic impurity is inversely proportional to the distance between the unpaired electron(s) and the nucleus being observed by NMR (r^6).^{42,43} Together, this provides a cut-off above which nuclear-spin relaxation occurs. In turn, this affords a measure of proximity between the immobilised paramagnetic chromium(III) amide species and the ^{29}Si nuclei present in the $\text{Cr}\{\text{N}(\text{SiMe}_3)_2\}_x/\text{SiO}_{2-600}$ NMR sample (Figure 4).^{42,43,47}

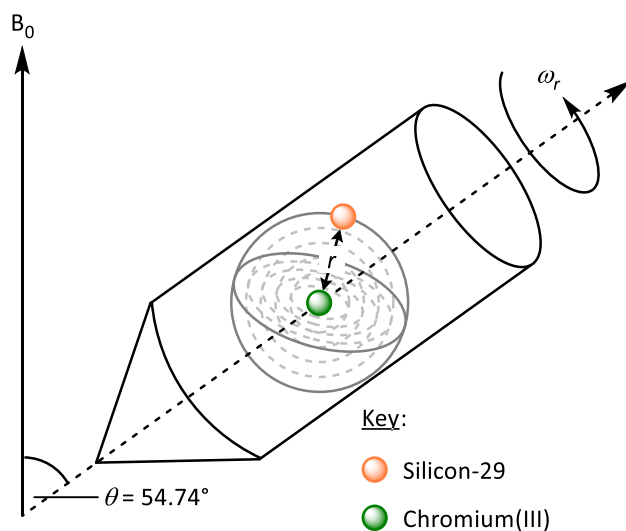


Figure 4: Coordinate system for a ^{29}Si -Cr^{III} inter-nuclear vector under magic-angle spinning conditions, modified from Bertini *et al.*, 2017⁴⁷

To this end, a sample of the paramagnetic $\text{Cr}\{\text{N}(\text{SiMe}_3)_2\}_x/\text{SiO}_{2-600}$ pro-initiator was packed into an airtight rotor inside a nitrogen-filled glove box, and sealed under an inert atmosphere prior to solid-state ^{29}Si DE MAS NMR spectroscopic analysis (Figure 5). The paramagnetic chromium(III) amide species behaves as a relaxation agent in that it decreased the T_1^{-1} of ^{29}Si nuclei resulting in line broadening of the resonances associated with both Q_3 and Q_2 environments. Notably, the resonance associated with Q_2 ^{29}Si nuclei in $\text{Cr}\{\text{N}(\text{SiMe}_3)_2\}_x/\text{SiO}_{2-600}$ is broadened to such an extent that it is proposed to be lost in the baseline. Since T_1 is directly proportional to the distance between the unpaired electron(s) and the nucleus being observed by NMR spectroscopy (r^6),^{42,43} it is inferred that the ^{29}Si nuclei corresponding to both Q_2 and Q_3 sites are in close proximity to the paramagnetic chromium(III) metal centre. In addition, the chromium(III) complex acts as a paramagnetic NMR shift reagent, such that the signal associated with Q_3 ^{29}Si nuclei is shifted to a lower frequency ($\Delta\delta = -5$ ppm) than that for the Q_4 environment ($\Delta\delta = -1$ ppm). Since these changes in resonance frequency brought about by a through-space dipolar interaction are inversely proportional to the distance between the unpaired electron(s) and the nucleus being observed by NMR spectroscopy (r^3),⁴³ the paramagnetic chromium(III) amide species must be in closer proximity to Q_3 ^{29}Si nuclei than those in Q_4 sites. Together, these observations can be rationalised by chromium(III) species being covalently bound to SiO_{2-600} at both Q_2 and Q_3 sites (see Scheme 7). This is consistent with the notion that both chromium(III) *mono-/bis*-(hexamethyldisilazide) species are present at the surface of SiO_{2-600} , which will be referred to hereinafter as $=\text{SiO}_2\text{CrN}(\text{SiMe}_3)_2$ and $\equiv\text{SiOCr}\{\text{N}(\text{SiMe}_3)_2\}_2$ respectively. This is further substantiated by an additional broad resonance in the ^{29}Si DE MAS NMR spectrum of the $\text{Cr}\{\text{N}(\text{SiMe}_3)_2\}_x/\text{SiO}_{2-600}$ pro-initiator centred at approximately 10 ppm, which is indicative of the hexamethyldisilazide functionality also coordinated to the paramagnetic chromium metal centre.

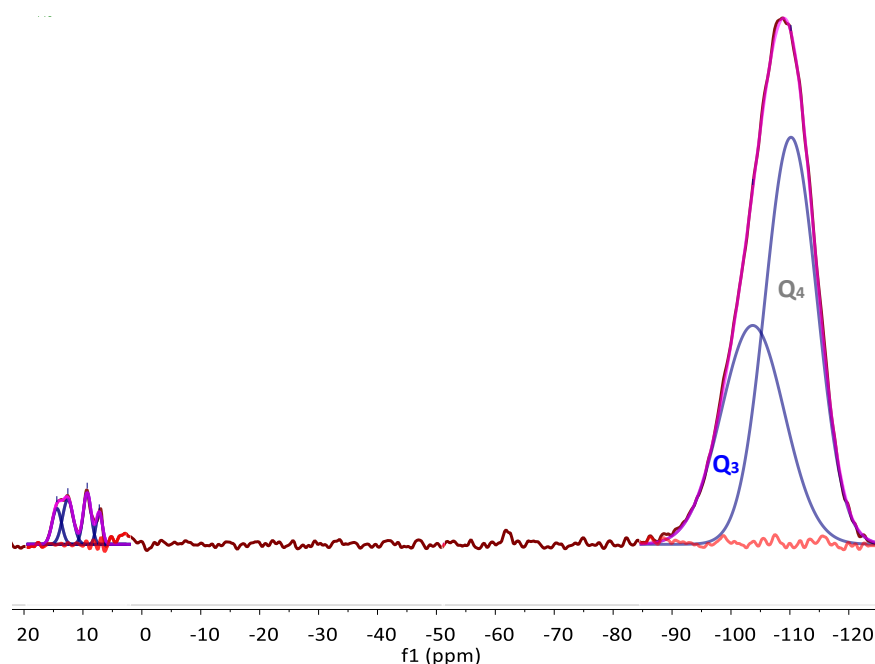


Figure 5: Solid-state ^{29}Si DE MAS NMR spectrum of $\text{Cr}\{\text{N}(\text{SiMe}_3)_2\}_x/\text{SiO}_{2-600}$ deconvoluted using a Gaussian distribution; 79 MHz frequency, 8 kHz rotation.

2.2.4.2.3 Solid-state ^{29}Si DE MAS Saturation-Recovery T_1 NMR Spectroscopic Study

In Section 2.2.4.2.2, it was shown that the paramagnetic chromium(III) amide species present in $\text{Cr}\{\text{N}(\text{SiMe}_3)_2\}_x/\text{SiO}_{2-600}$ increases the longitudinal relaxation rate (T_1^{-1}) of ^{29}Si nuclei, as evidenced by solid-state ^{29}Si DE MAS NMR spectroscopy, something that resulted in line broadening of the resonances associated with Q_2 and Q_3 silanols. To determine the respective T_1^{-1} values for SiO_{2-600} and $\text{Cr}\{\text{N}(\text{SiMe}_3)_2\}_x/\text{SiO}_{2-600}$, a set of ^{29}Si DE MAS saturation-recovery NMR spectroscopic experiments were undertaken. In line with previous work,^{42,43} non-exponential relaxation behaviour of ^{29}Si nuclei was observed (Figure 6), and thus multiple longitudinal relaxation times (T_1) were reported for both $\text{Cr}\{\text{N}(\text{SiMe}_3)_2\}_x/\text{SiO}_{2-600}$ and SiO_{2-600} (Table 5). One possible explanation for this could be that ^{29}Si nuclei corresponding to Q_2 , Q_3 and/or Q_4 sites relax with different recovery times. In fact, ^{29}Si - ^1H dipolar relaxation *via* hydroxyl groups present in SiO_{2-600} may lessen the T_1 values of Q_2 and Q_3 ^{29}Si nuclei relative to that of Q_4 environments, especially of those in the bulk of the oxide support.⁴⁸ Hence, it is reasonable to assume that the comparatively low $T_1(1)$ associated with SiO_{2-600} (25 s; Table 5) corresponds to Q_2 and Q_3 silanols, and equally $T_1(2)$, which is an order of magnitude greater than $T_1(1)$ at 360 s, be assigned to Q_4 sites. In truth, however, $T_1(1)$ accounts for 35% of ^{29}Si nuclei in the NMR sample of SiO_{2-600} , which is greater than the combined relative population of Q_2 and Q_3 silanols ($\sim 15\%$), as determined by deconvolution using a Gaussian distribution curve fit. Therefore, $T_1(1)$ must encompass a proportion of Q_4 sites as well as Q_2 and Q_3 silanol functionalities at the surface of SiO_{2-600} whose T_1 is also reduced, because of ^{29}Si - ^1H dipolar interactions.

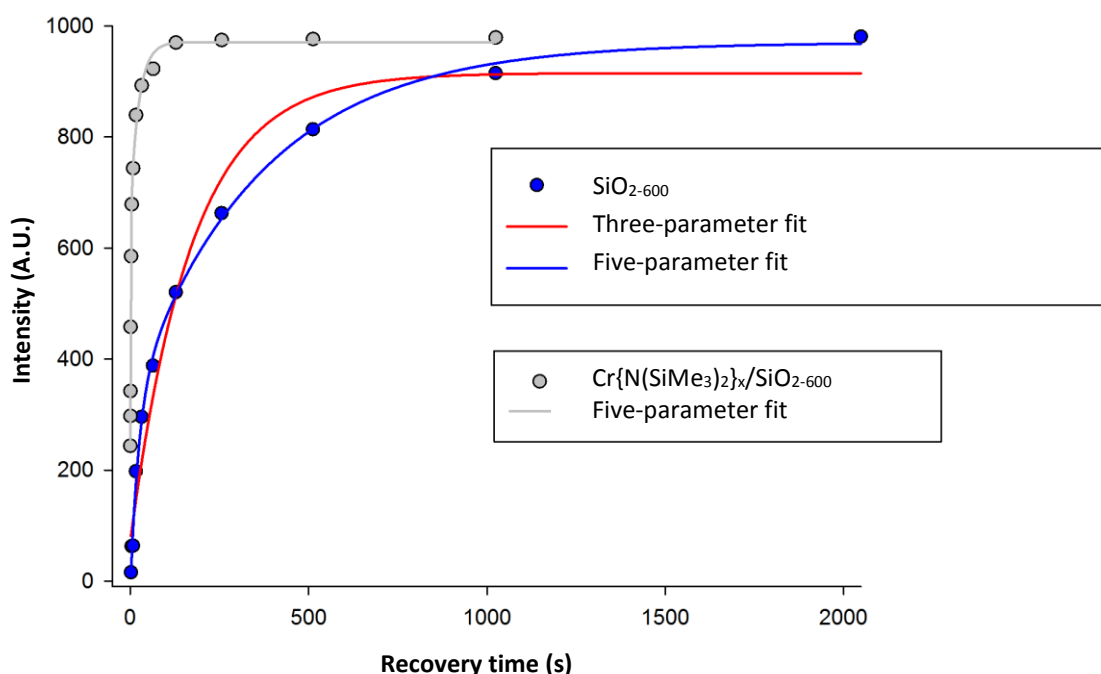


Figure 6: Solid-state ^{29}Si DE MAS saturation-recovery T_1 NMR spectroscopic analyses of SiO_{2-600} and $\text{Cr}\{\text{N}(\text{SiMe}_3)_2\}_x/\text{SiO}_{2-600}$; 79 MHz frequency, 6 – 8 kHz rotation.

Table 5: Experimentally-derived ^{29}Si T_1 values for SiO_{2-600} and $\text{Cr}\{\text{N}(\text{SiMe}_3)_2\}_x/\text{SiO}_{2-600}$ using a five-parameter fit of solid-state DE MAS saturation-recovery NMR experiments; 79 MHz frequency, 6 – 8 kHz rotation.

	Calcined Support	Pro-initiator
	SiO_{2-600}	$\text{Cr}\{\text{N}(\text{SiMe}_3)_2\}_x/\text{SiO}_{2-600}$
$T_1(1)$	25 s (35%)	14 s (47%)
$T_1(2)$	360 s (67%)	24 s (31%)
Baseline	-1%	22%
R^2	0.9979	0.9981

It must be stated that the two-component model for the solid-state ^{29}Si DE MAS saturation-recovery T_1 NMR spectroscopic study of $\text{Cr}\{\text{N}(\text{SiMe}_3)_2\}_x/\text{SiO}_{2-600}$ (Table 5) is also oversimplified, because there is at least one other fast-relaxing (<50 ms) ^{29}Si species present in the sample, which is ascribed to account for the relatively high baseline (~22%). Together with the fact that T_1 is directly proportional to r^6 ,⁴³ it is suggested that such fast-relaxing component(s) correspond to ^{29}Si nuclei either within, or in close proximity to the coordination sphere of the immobilised paramagnetic chromium(III) metal centre (*i.e.* Q_2 and/or Q_3 sites). Moreover, the comparatively high $T_1(1)$ and $T_1(2)$ values derived from the ^{29}Si DE MAS NMR saturation-recovery of $\text{Cr}\{\text{N}(\text{SiMe}_3)_2\}_x/\text{SiO}_{2-600}$ (Table 5), which equate to 78% of ^{29}Si nuclei in the sample, have provisionally been assigned to unreacted, potentially inaccessible silanols, as well as Q_4 sites in the bulk of the catalyst support.

2.2.4.3 X-Ray Photoelectron Spectroscopic Analysis of $\text{Cr}\{\text{N}(\text{SiMe}_3)_2\}_x/\text{SiO}_{2-600}$

Since it has been proposed that $\text{Cr}\{\text{N}(\text{SiMe}_3)_2\}_3$ reacts with both Q_2 and Q_3 silanols at the surface of SiO_{2-600} to form two distinct supported chromium(III) amide species, as inferred from ^{29}Si NMR spectroscopic analysis, it was important to qualify the ratio of Cr : N, as well as the oxidation state of chromium using X-ray photoelectron spectroscopy (XPS). However, despite several attempts to analyse $\text{Cr}\{\text{N}(\text{SiMe}_3)_2\}_x/\text{SiO}_{2-600}$ by XPS under an inert atmosphere using a purpose-built sample transfer cell, each time the air- and moisture-sensitive pro-initiator changed colour from green to brown during the introduction of the sample into the instrument. As a result, only this degraded brown-coloured material could be subject to XPS analysis (work undertaken by Dr W. Murdoch, EPSRC NEXUS Service, Newcastle University). This study revealed there to be at least two resonances in the Cr 2p region at 577 eV ($2p$, $2p_{3/2}$) and 586 eV ($2p_{1/2}$), which are consistent with a species related to “ $\text{Cr}(\text{OH})_3$ ” present in the sample (Figure 7). These data agree well with those from an authentic sample of $\text{Cr}(\text{OH})_3$ formed *via* precipitation from a 1 M solution of $\text{CrCl}_3 \cdot 6\text{H}_2\text{O}$ and 0.1 M $\text{NH}_3(\text{aq})$.⁴⁹

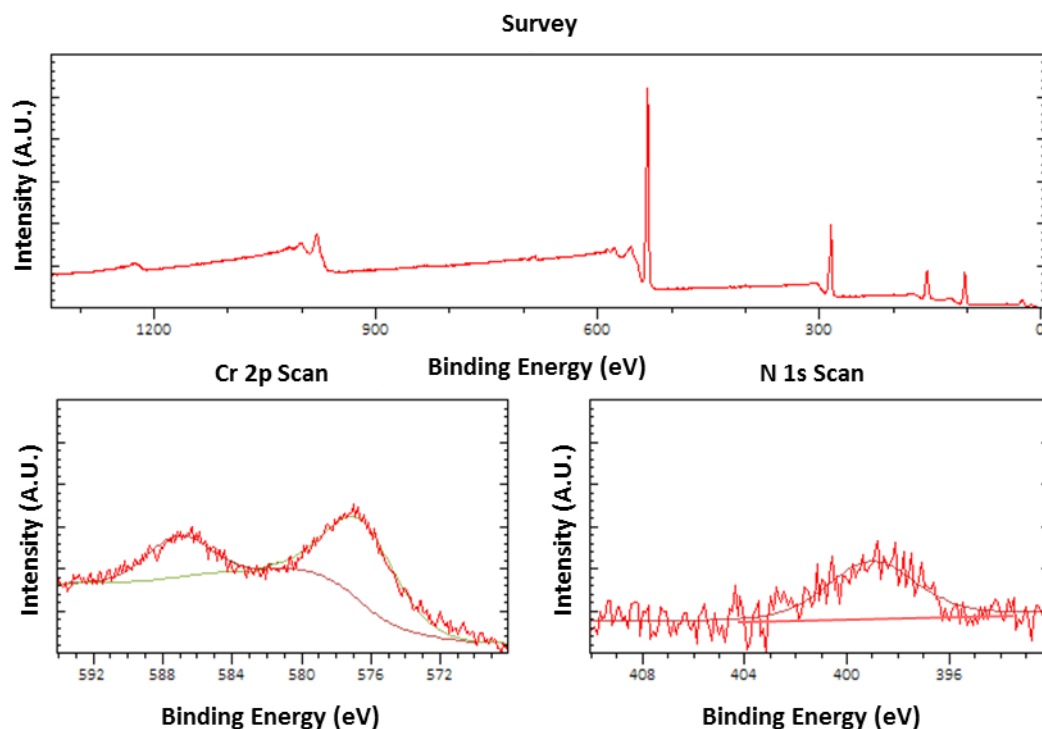
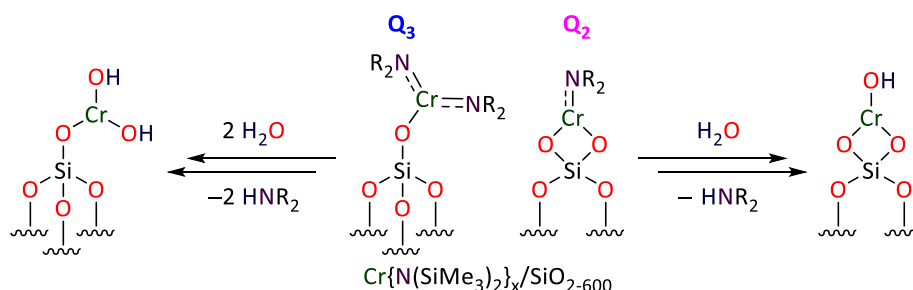


Figure 7: X-Ray spectroscopic analysis of the brown-coloured degraded material derived from $\text{Cr}\{\text{N}(\text{SiMe}_3)_2\}_x/\text{SiO}_{2-600}$ through exposure to the atmosphere, referenced to C 1s (284.8 eV)

The presence of a chromium hydroxide species in the XPS sample of the brown-coloured, degraded $\text{Cr}\{\text{N}(\text{SiMe}_3)_2\}_x/\text{SiO}_{2-600}$ pro-initiator is believed to result from hydrolysis of the supported chromium(III) amide species, as shown in Scheme 8. Unfortunately, the detection of such hydroxide-containing motifs offers no insight into the nature of the catalytically-relevant supported chromium(III) species. However, based on the surface-sensitivity of XPS ($\sim 30 \text{ \AA}$), this study does provide a potential indication that chromium is present at the surface of SiO_{2-600} .



Scheme 8: Proposed hydrolysis of $\text{Cr}\{\text{N}(\text{SiMe}_3)_2\}_x/\text{SiO}_{2-600}$ (charge-neutral H_2O ligands omitted for clarity)

2.2.4.4 Titration of SiO_{2-600} with $\text{Cr}\{\text{N}(\text{SiMe}_3)_2\}_3$

To further confirm the presence of two distinct supported chromium species at the surface of $\text{Cr}\{\text{N}(\text{SiMe}_3)_2\}_x/\text{SiO}_{2-600}$, a titration experiment was conducted in which a sample of SiO_{2-600} was treated with a heptane solution containing $\text{Cr}\{\text{N}(\text{SiMe}_3)_2\}_3$ to give a material with a chromium metal loading of 0.71 wt%. This resulted in the liberation of 1.03 molar equivalents of $\text{HN}(\text{SiMe}_3)_2$, which was isolated *via* vacuum transfer, and quantified by GC-FID against a known volume of an internal standard. For completeness, a sample of the ensuing $\text{Cr}\{\text{N}(\text{SiMe}_3)_2\}_x/\text{SiO}_{2-600}$ pro-initiator was exhaustively digested in HCl, and analysed by inductively coupled plasma-optical emission spectroscopy (ICP-OES), which verified that the chromium loading was indeed 0.71 wt%. Together with the fact that Q_3 silanols outnumber Q_2 sites in SiO_{2-600} by 29:1 (see Section 2.2.4.2.1), it is proposed that $\text{Cr}\{\text{N}(\text{SiMe}_3)_2\}_3$ reacts with Q_3 and Q_2 silanols resulting in the formation of one and two Cr–O–Si bonds respectively (see Scheme 7), as demonstrated by the elimination of 1.03 molar equivalents of the corresponding amine.

2.2.4.5 Rutherford Backscattering Spectrometric Analysis of $\text{Cr}\{\text{N}(\text{SiMe}_3)_2\}_x/\text{SiO}_{2-600}$

While inductively coupled plasma-optical emission spectroscopy (ICP-OES) provides an accurate measure of chromium concentration in solutions generated by exhaustive removal of chromium from the $\text{Cr}\{\text{N}(\text{SiMe}_3)_2\}_x/\text{SiO}_{2-600}$ pro-initiator using concentrated HCl, this protocol relies on all of the oxide-bound chromium being leached from the silica support during the acid washing process. Consequently, it was important to explore whether the chromium metal loading on the silica support could be obtained directly. In this regard, Rutherford backscattering spectrometry (RBS) is a technique ideally placed to achieve this quantification, being an analytical technique that is used to determine atomic composition by measuring the backscattering of a beam of high energy typically $^4\text{He}^+$ ions impacting upon a sample.⁵⁰ Indeed, RBS is particularly sensitive to the quantification of heavy elements in a light matrix.⁵¹ In brief, three main interactions are possible when a high energy incident ion beam hits the surface of a sample:⁵²

- Backscattering: an elastic collision that occurs when an incident $^4\text{He}^+$ ion strikes a target atom of greater atomic number.
- Recoiling: occurs when an incident $^4\text{He}^+$ ion strikes a target atom of smaller atomic number resulting in the expulsion of the target atom from the sample.
- Energy may also be dispersed through a series of low impact collisions with electrons within the sample.

For a given incident angle, nuclei of two different atomic numbers backscatter $^4\text{He}^+$ ions to different varying degrees and with different energies giving rise to separate peaks in a plot of measurement count against energy, which are characteristic of the elements present in the RBS sample. Relative concentration can be derived from peak height, whilst the width and shifted position of these peaks are indicative of sample depth.

Thus, in order to probe the chromium metal loading, a sample of the degraded (hydrolysed) brown solid derived from the air- and moisture-sensitive $\text{Cr}\{\text{N}(\text{SiMe}_3)_2\}_x/\text{SiO}_{2-600}$ pro-initiator upon exposure to the atmosphere was subject to RBS analysis by Dr R. Thompson (Durham University). The resulting spectrum was subsequently compared to that from its parent catalyst support (Figure 8 and Figure 9). In both cases, the atomic percentage (at%) was determined from the signals corresponding to chromium, silicon and oxygen before being converted to the weight percentage (wt%) of each element. According to this RBS analysis, the chromium loading was calculated to be 0.47 wt%, which is lower than that observed by ICP-OES (*i.e.* 0.71 wt% Cr). This difference in chromium concentration has been attributed to the heterogeneity of the supported chromium(III) species distributed throughout the amorphous silica support present in the RBS sample.⁵³

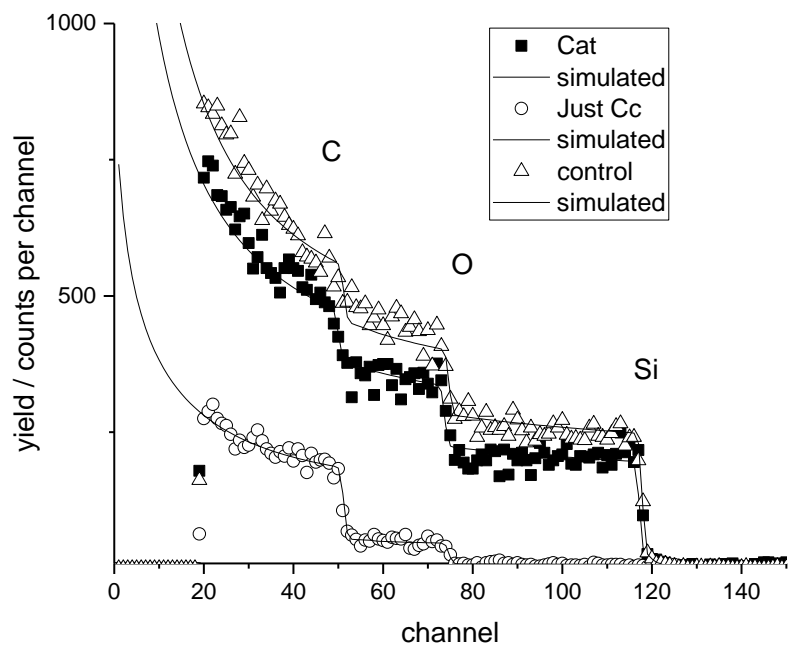


Figure 8: Linear plot showing contributions of major elements to the Rutherford backscattering spectra of the brown degraded solid material derived from the $\text{Cr}\{\text{N}(\text{SiMe}_3)_2\}_x/\text{SiO}_{2-600}$ pro-initiator, and the SiO_{2-600} catalyst support

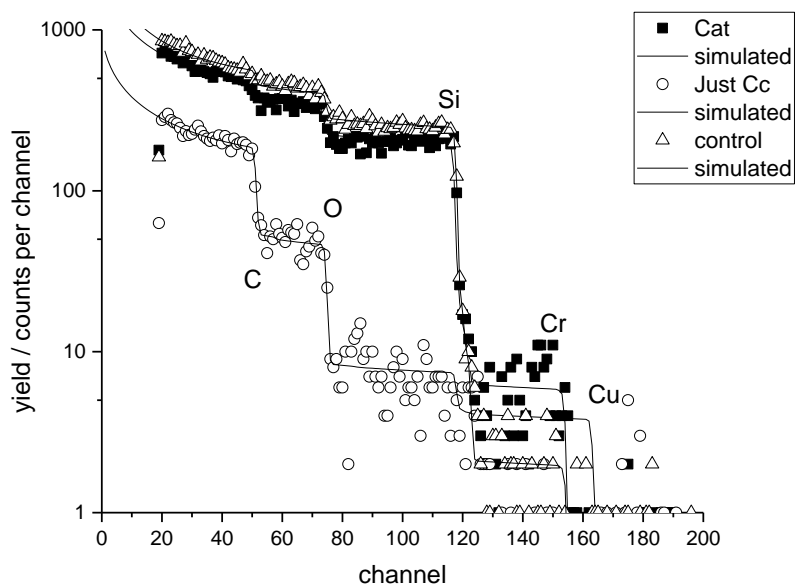
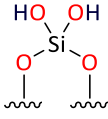
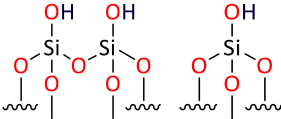
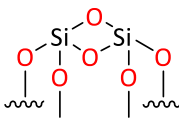


Figure 9: Log plot emphasizing contributions of higher mass trace elements to the Rutherford backscattering spectra of the brown degraded solid material derived from the $\text{Cr}\{\text{N}(\text{SiMe}_3)_2\}_x/\text{SiO}_{2-600}$ pro-initiator, and the SiO_{2-600} support. Note the significantly larger yield arising from chromium in the Cat sample from channels 125 – 145; Control = 0.05 atom% Cr (close to limit of detection), Cat = 0.18 atom% Cr.

2.2.5 Impact of Support Calcination Temperature on the Selectivity of the $\text{Cr}\{\text{N}(\text{SiMe}_3)_2\}_x/\text{SiO}_2/\text{MMAO-12}$ Initiator System

Since it has been established here in this thesis that there are at least two supported chromium(III) amide species at the surface of SiO_{2-600} , namely $\equiv\text{SiOCr}\{\text{N}(\text{SiMe}_3)_2\}_2$ and $=\text{SiO}_2\text{CrN}(\text{SiMe}_3)_2$, it is proposed that these two catalytically active species are responsible for the observed tri- and poly-merisation processes that occur following activation with MMAO-12. In order to further validate this hypothesis, a silica-supported chromium initiator system analogous to $\text{Cr}\{\text{N}(\text{SiMe}_3)_2\}_x/\text{SiO}_{2-600}/\text{MMAO-12}$ was prepared using Evonik Aeroperl 300/30 fumed silica thermally pre-treated at 200 rather than 600 °C for 24 hours under a flow of dry N_2 (*i.e.* SiO_{2-200}). This change was made in order to increase the relative population of Q_2 silanol functionalities with respect to Q_3 sites,^{39,40,41} something that was confirmed by solid-state ^{29}Si NMR spectroscopy (Table 6). It should, however, be highlighted that since vicinal silanols are known to fully condense at 400 °C,^{39,40,41} it is postulated that SiO_{2-200} retains some residual vicinal silanol sites as well as both Q_2 and Q_3 sites.

Table 6: Relative population of Q_2 , vicinal, Q_3 and Q_4 sites in Evonik Aeroperl 300/30 fumed silica (as received), SiO_{2-200} and SiO_{2-600} assigned based on a Gaussian distribution curve fit of the corresponding ^{29}Si DE MAS NMR spectra (79 MHz frequency, 6 kHz rotation); error associated with deconvolution <0.02%.

Sample	Q_2 Silanol (-91 ppm)	Vicinal and/or Q_3 Silanol (-99 ppm)	Q_4 Site (-110 ppm)
			
SiO_2	3%	20%	77%
SiO_{2-200}	3%	18%	79%
SiO_{2-600}	<1%	15%	85%

In order to further differentiate the nature of the reactive silanol functionalities remaining on the silica surface following calcination, a TGA study was undertaken. As expected from previous reports concerning the examination of a number of different silicas,^{39,41} the calcination of Evonik Aeroperl 300/30 fumed silica occurs over four distinct temperature regimes, as evidenced by TGA/DTG analysis (Figure 10; I – IV). Loss of physisorbed water occurs between 40 – 100 °C (I) and ~120 – 190 °C (II); condensation of vicinal, Q₂ and Q₃ silanols between ~190 – 450 °C (III); further dehydroxylation of Q₂ and Q₃ silanols >500 °C (IV). Consequently, SiO₂₋₂₀₀ may be regarded essentially as dehydrated silica, retaining a significant concentration of vicinal, Q₂ and Q₃ silanol functionalities, in accordance with the solid-state ²⁹Si NMR spectroscopic data (Table 6). In contrast, combining the TGA and ²⁹Si NMR spectroscopic studies, the surface of the SiO₂₋₆₀₀ support material is found to be both dehydrated and partially dehydroxylated, and thus comprises Q₂ and Q₃ silanol sites in a ratio of 1:29, respectively. These differences in the nature and hence reactivity of SiO₂₋₂₀₀ and SiO₂₋₆₀₀ will directly lead to the generation of different relative proportions of ≡SiOCr{N(SiMe₃)₂}₂ and =SiO₂CrN(SiMe₃)₂ species following the impregnation of these materials under anhydrous conditions with Cr{N(SiMe₃)₂}₃.

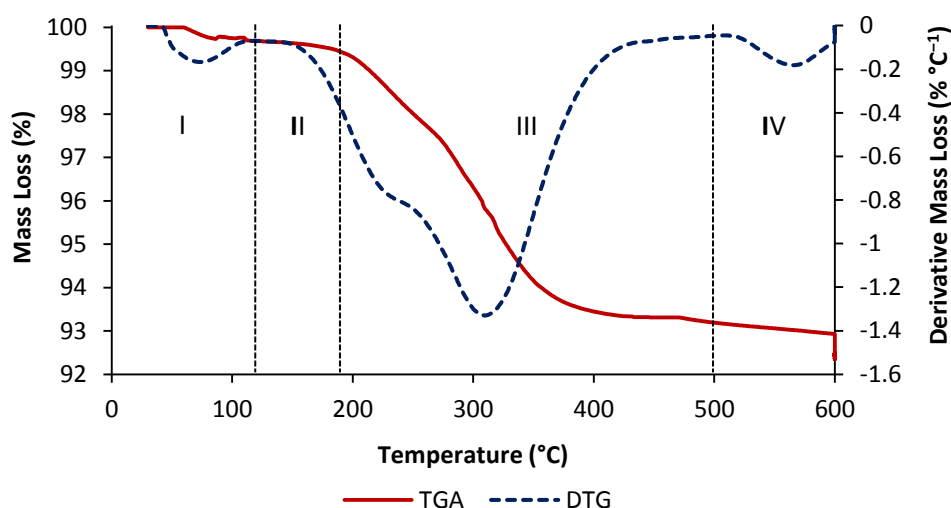
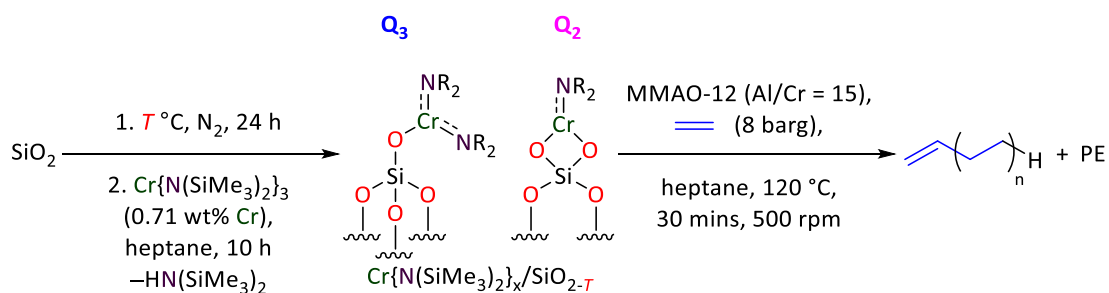


Figure 10: TGA/DTG profiles of Evonik Aeroperl 300/30 fumed silica; heating rate of 30 °C min⁻¹ to 600 °C; assignment of profile regions I – IV given in the text.

SiO₂₋₂₀₀ was treated with Cr{N(SiMe₃)₂}₃ using an analogous procedure to that used for the preparation of Cr{N(SiMe₃)₂}_x/SiO₂₋₆₀₀, and the catalytic performance of the resulting material evaluated in combination with MMAO-12 under standard test conditions (Scheme 9; Table 7). Not only is the Cr{N(SiMe₃)₂}_x/SiO₂₋₂₀₀/MMAO-12 system a much less active initiator (Entry 1), but it also shows a dramatic switch in product selectivity towards PE formation compared with the Cr{N(SiMe₃)₂}_x/SiO₂₋₆₀₀ system (Entry 2). This is consistent with previous observations made by Monoi and Sasaki (see Section 1.3.2.5), who demonstrated that the selectivity of the so-called “Cr{N(SiMe₃)₂}₂/SiO₂” ethylene trimerisation pro-initiator could be modified in favour of polymerisation by reducing the support calcination temperature from 600 to 300 °C.¹



Scheme 9: General reaction scheme used to probe the influence of support calcination temperature on the performance of the Cr{N(SiMe₃)₂}_x/SiO₂/MMAO-12 initiator system

Table 7: Comparison of ethylene oligomerisation tests initiated by Cr{N(SiMe₃)₂}_x/oxide (i.e. SiO₂₋₂₀₀ or SiO₂₋₆₀₀) with MMAO-12 as activator in heptane.

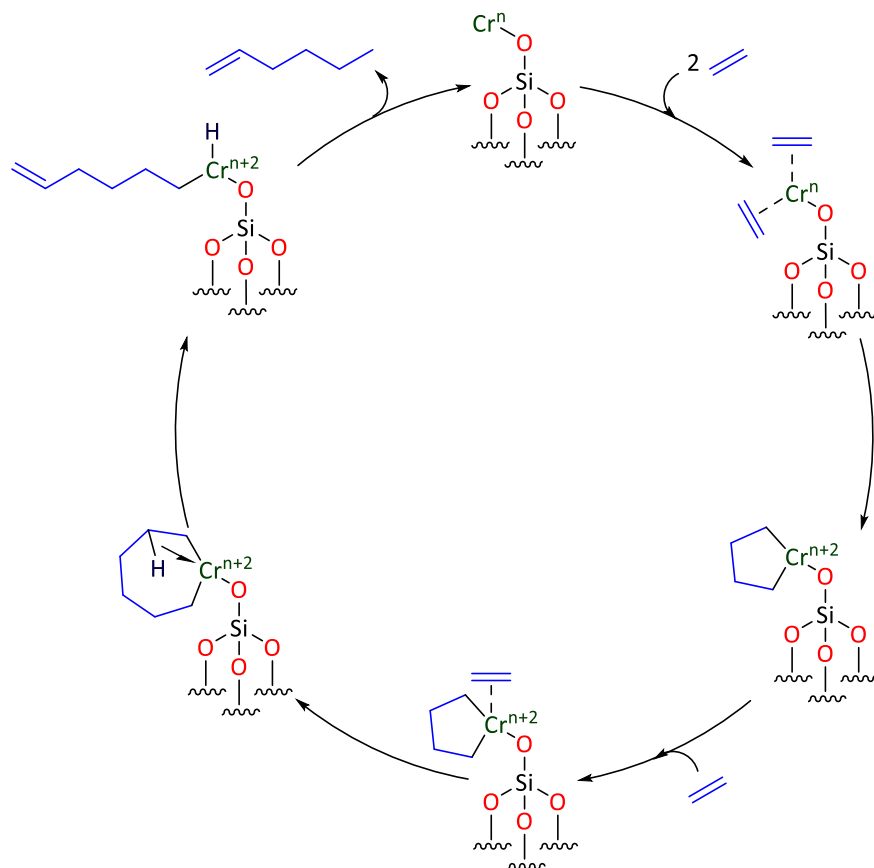
Entry	Catalyst Support	C ₄ = ^a {wt%}	C ₆ = ^a {wt%}	C ₈ = ^a {wt%}	C ₁₀ = ^a {wt%}	C ₁₂₊ = ^a {wt%}	PE ^b {wt%}	Total Activity {g g _{Cr} ⁻¹ h ⁻¹ }
1	SiO ₂₋₂₀₀	1	19 (93)	2	2	4	72	1363
2	SiO ₂₋₆₀₀	1	61 (79)	2	16	6	13	2403

Reaction conditions: 27 μmol Cr (mass of Cr{N(SiMe₃)₂}_x/oxide = 0.2 g); 410 μmol co-catalyst (Al:Cr = 15:1); 60 ml heptane; 120 °C; 500 rpm; 8 barg ethylene pressure; 0.5 h.

^a Determined by GC-FID relative to the internal standard (1 mL nonane).

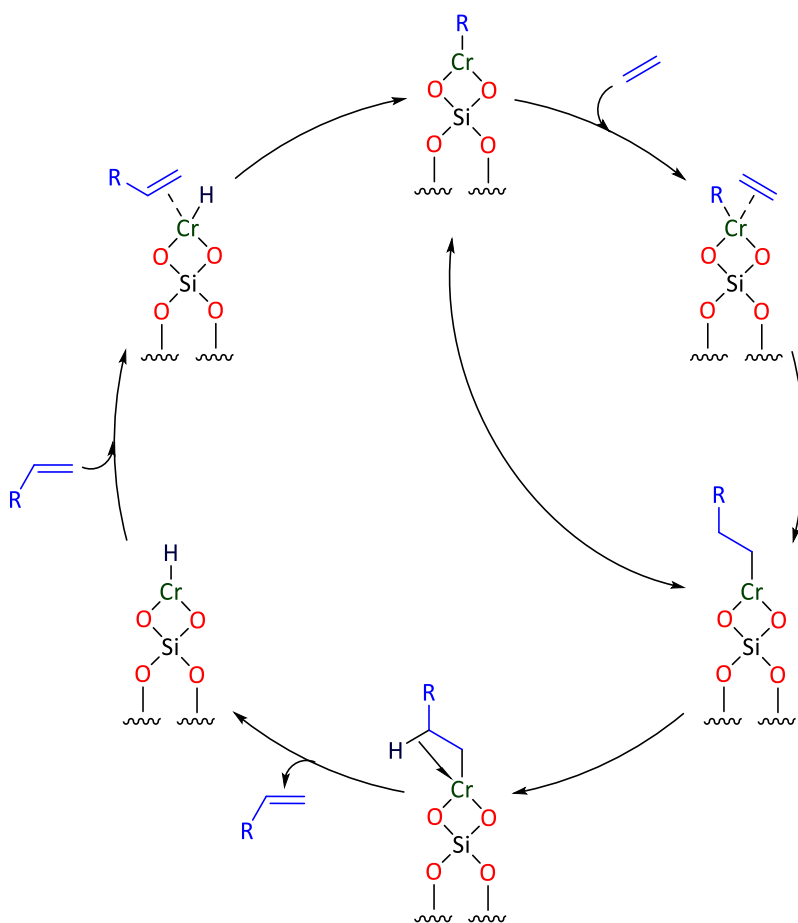
^b Polymer isolated by filtration, dried to constant mass and weighed.

Building on previous work,^{1,2} we have established a correlation between the relative population of Q_3 and Q_2 silanols at the surface of silica as a function of support calcination temperature using ^{29}Si DE MAS NMR spectroscopy, and the respective tri-/poly-merisation behaviour of the $\text{Cr}\{\text{N}(\text{SiMe}_3)_2\}_x/\text{SiO}_2$ -based initiator (Table 7). Since the ratio of $Q_2:Q_3$ silanols increases at higher support calcination temperatures, it is proposed that $\equiv\text{SiOCr}\{\text{N}(\text{SiMe}_3)_2\}_2$ activated with MMAO-12 facilitates ethylene trimerisation through an “oxide-supported” variant of the metallacycle mechanism (Scheme 10).^{4,5}



Scheme 10: Proposed oxide-supported variant of the metallacyclic trimerisation reaction manifold^{4,5}

Although it was previously envisaged that for chromium-based systems, the operation of a metallacyclic ethylene trimerisation reaction manifold precluded the formation of longer chain oligo-/poly-meric products,⁵⁴ more recent studies have since demonstrated that higher oligomers may also originate from a metallacycle-based reaction mechanism.^{6,55} In our work, however, the selective production of 1-hexene is not only accompanied by the formation of decenes, something that is likely to arise from secondary metallacycle-based ethylene/1-hexene co-trimerisation processes (see Section 1.3.1.5),^{6,7,8} but also by the formation of polyethylene (PE). It is therefore proposed that the $=\text{SiO}_2\text{CrN}(\text{SiMe}_3)_2$ functionality arising from the reaction between $\text{Cr}\{\text{N}(\text{SiMe}_3)_2\}_3$ and Q_2 silanols at the surface of $\text{SiO}_2\text{-600}$, upon activation with MMAO-12, mediates non-selective oligo-/poly-merisation *via* a classical Cossee-Arlman-type chain growth process (Scheme 11).^{9,10,11} Monoi and co-workers had previously suggested that $\text{Cr}\{\text{N}(\text{SiMe}_3)_2\}_3$ reacted either with vicinal silanols at the silica surface to generate an ethylene polymerisation catalyst precursor, or indeed residual Q_3 silanols to produce an ethylene trimerisation pro-initiator.^{1,2}



Scheme 11: Supported variant of the Cossee-Arlman chain growth mechanism^{9,10,11}

This page has been intentionally left blank.

2.2.5.1 *Electron Paramagnetic Resonance Spectroscopic Analyses of the SiO₂₋₂₀₀- and SiO₂₋₆₀₀-supported Chromium Pro-initiators*

Following the exploitation of the paramagnetic supported chromium(III) species as NMR shift reagents and relaxation agents to probe the nature of Cr{N(SiMe₃)₂}_x/SiO₂₋₆₀₀ (see Section 0), it was envisaged that electron paramagnetic resonance (EPR) spectroscopy may be used to observe =SiO₂CrN(SiMe₃)₂ and ≡SiOCr{N(SiMe₃)₂}₂ derived from Q₂ and Q₃ silanols, respectively. Distinctly different coordination spheres about the paramagnetic chromium(III) metal centre would lead to different g-values.^{56,57,58,59,60} For hyperfine interactions in EPR spectroscopy, the determination of the Fermi contact component can be measured by detection *via* the unpaired electron. If the anisotropy of the ²⁹Si hyperfine interaction is mapped onto the molecular frame as described by the g-tensor, then it may be possible to extract some structural information for the two supported chromium(III) amide species at the surface of silica. Since the ratio of =SiO₂CrN(SiMe₃)₂ and ≡SiOCr{N(SiMe₃)₂}₂ derived from Q₂ and Q₃ silanols at the surface of silica can be altered to an extent by lowering the support calcination temperature, as inferred from solid-state ²⁹Si NMR spectroscopic analyses (see Section 2.2.5), EPR spectroscopy may be able to distinguish between these two surface-bound chromium species.

To this end, samples of the SiO₂₋₂₀₀- and SiO₂₋₆₀₀-supported chromium pro-initiators were made up in quartz EPR tubes inside a nitrogen-filled glove box, before being carefully placed under dynamic vacuum (0.1 mbar), and flame-sealed prior to continuous-wave (CW) EPR spectroscopic analysis (Dr W. Myers, University of Oxford). Preliminary findings suggest that the EPR spectra of both samples display significant temperature dependence (Figure 11). By lowering the temperature at which the CW X-band EPR measurements were acquired from room temperature (RT; black) to 100 K (red), Cr{N(SiMe₃)₂}_x/SiO₂₋₆₀₀ was found to generate an orthorhombic g-tensor ($g_x = 2.013$; $g_y = 1.981$; $g_z = 1.931$), whilst Cr{N(SiMe₃)₂}_x/SiO₂₋₂₀₀ gives rise to an axial g-matrix ($g_{\perp} = 1.991$; $g_{\parallel} = 1.931$). Preliminary EPR spectroscopic analyses of the two SiO₂₋₂₀₀- and SiO₂₋₆₀₀ supported chromium pro-initiators provided further evidence to suggest that, by comparison, the former comprises a more diverse mixture of supported chromium(III) amide species. However, further EPR spectroscopic experiments must be conducted to quantify the relative proportion of chromium(III) *mono*- and *bis*-(hexamethyldisilazide) species at the surface of silica. Since the CW EPR spectra acquired here were not sufficiently resolved, hyperfine sublevel correlation spectroscopic (HYSCORE) analyses should be performed to determine the ligand hyperfine coupling between the supported chromium(III) metal centre and either one or two coordinated ¹⁴N nuclei.

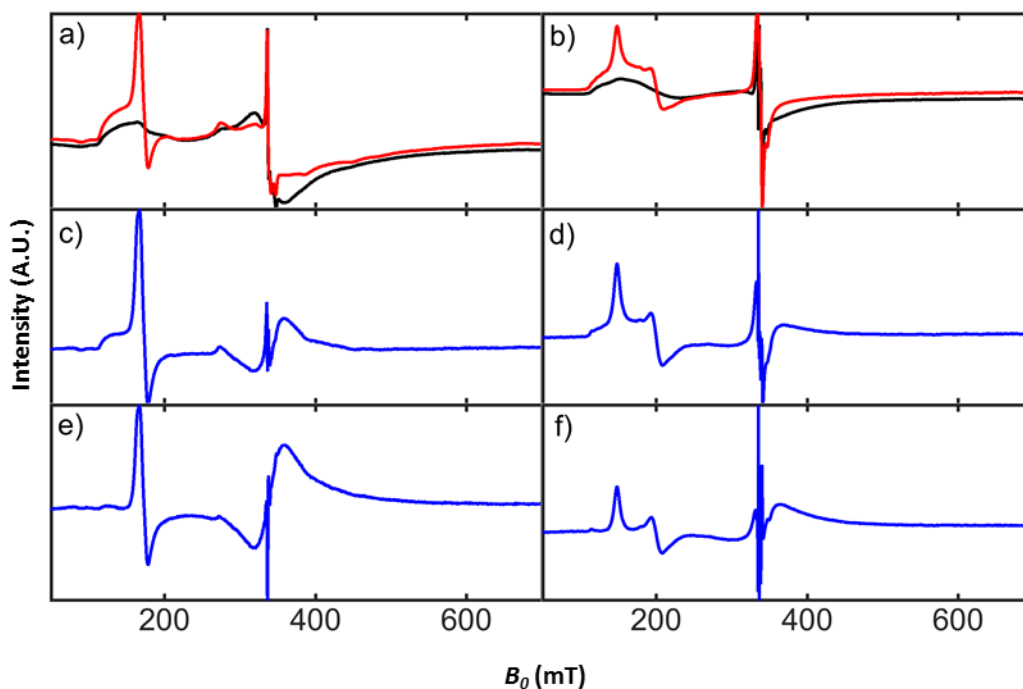


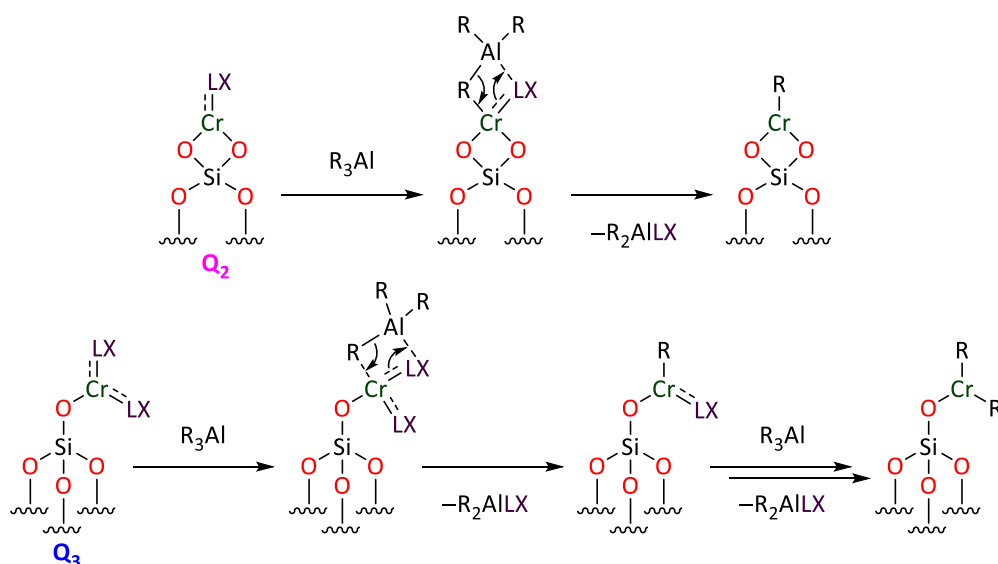
Figure 11: Solid-state continuous-wave X-band (9.4 GHz) electron paramagnetic resonance spectroscopic analyses of $\text{Cr}\{\text{N}(\text{SiMe}_3)_2\}_x/\text{SiO}_{2-200}$ in panels (a), (c) and (e); $\text{Cr}\{\text{N}(\text{SiMe}_3)_2\}_x/\text{SiO}_{2-600}$ in panels (b), (d) and (f); room temperature (black), 100 K (red) and subtractions (blue).

During the writing of this thesis a paper appeared in the literature from Delley, Copéret and co-workers, which describes their related investigation of various silica-supported metal amides and siloxides.⁶¹ In this work, $\text{Cr}\{\text{N}(\text{SiMe}_3)_2\}_3$ was reacted with isolated (Q_3) silanols at the surface of a siliceous catalyst support that had been pre-treated at 700 °C under ultra-high vacuum (10^{-5} mbar). The X-band (9.5 GHz) CW EPR spectrum of the resulting silica-supported chromium species in methylcyclohexane taken at 110 K was measured and compared to that of its molecular precursor.⁶¹ The EPR spectrum of $\text{Cr}\{\text{N}(\text{SiMe}_3)_2\}_3$ exhibited a hyperfine triplet corresponding to ^{14}N ($A_{\perp} = 145$ MHz) at an effective g-tensor $g_{\perp} = \sim 4$ and a negative signal at an effective g-matrix $g_{\parallel} = 1.995$, something that is considered to be consistent with a d^3 low spin transition metal with a principal axis of rotation (C_3).⁶¹ In contrast, hyperfine coupling with ^{14}N is not resolved in the EPR spectrum of $\text{Cr}\{\text{N}(\text{SiMe}_3)_2\}_2/\text{SiO}_2$ due to line broadening that arises from a broad distribution of zero-field splitting parameters, and no longer corresponds to axial symmetry ($g = 1.999$).⁶¹

Although Delley *et al.* weren't able to observe the ^{14}N hyperfine coupling in the CW EPR spectrum of $\text{Cr}\{\text{N}(\text{SiMe}_3)_2\}_2/\text{SiO}_2$, the authors were able to determine the hyperfine corresponding to ^{14}N for a silica-supported chromium species that had been prepared through the sequential calcination of $\text{Cr}\{\text{N}(\text{SiMe}_3)_2\}_2/\text{SiO}_2$ at 300 and 400 °C for 1 and 3 hours, respectively, by employing HYSORE EPR spectroscopy.⁶¹ This validates our assumption that HYSORE spectroscopic analyses should be able to resolve the ^{14}N hyperfine coupling present in the SiO_{2-200} - and SiO_{2-600} -supported chromium catalyst precursors described in this thesis.

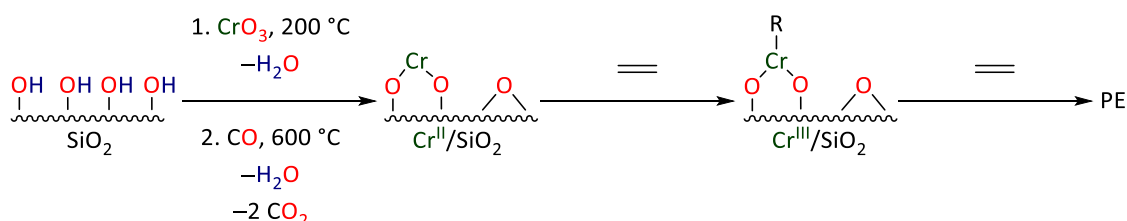
2.2.6 Activation of the Cr{N(SiMe₃)₂}_x/SiO₂₋₆₀₀ Pro-initiator

Having earlier in this chapter established that there are at least two supported chromium(III) species at the surface of Cr{N(SiMe₃)₂}_x/SiO₂₋₆₀₀, *i.e.* =SiO₂CrN(SiMe₃)₂ and ≡SiOCr{N(SiMe₃)₂}₂, one must consider their possible modes of activation by means of reaction with MMAO-12. In line with previous studies,¹⁸ it is postulated that MMAO-12 will alkylate the supported chromium(III) amide species *via* a metathesis-type pathway (Scheme 12). Since MMAO-12 contains a mixture of partially hydrolysed ^tBu₃Al (IBAO) and Me₃Al (MAO) as well as free/coordinated ^tBu₃Al and Me₃Al, the alkyl substituents have simply been referred to as R groups, for clarity.



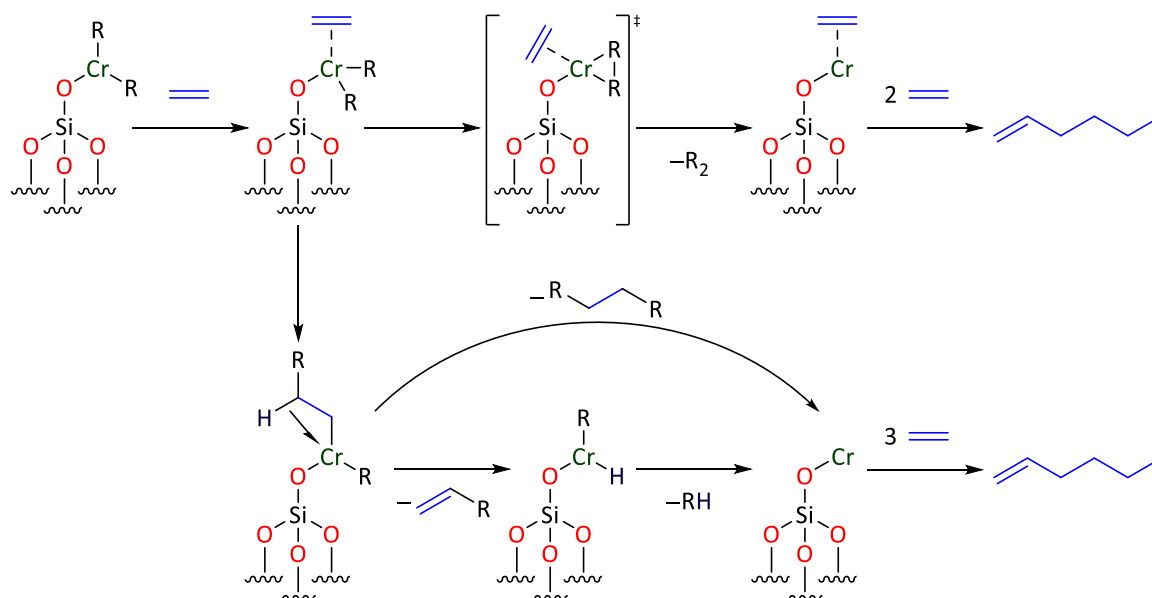
Scheme 12: Alkylation of supported chromium(III) amide species derived from **Q₂** and **Q₃** silanols at the surface of Cr{N(SiMe₃)₂}_x/SiO₂₋₆₀₀ upon reaction with MMAO-12; hexamethyldisilazide ligands denoted as LX in accordance with the covalent bonding classification method.

Most interestingly, the supported *mono*-alkylated chromium(III) species derived from =SiO₂CrN(SiMe₃)₂ is reminiscent of the Phillips heterogeneous Cr/SiO₂ ethylene polymerisation catalyst.⁶² As alluded to earlier in Section 1.3.2.1, Brown *et al.* employed *in situ* ultraviolet-visible (UV-Vis) spectroscopy to monitor the reduction of CrO₃/SiO₂ under an atmosphere of CO prior to its reaction with ethylene, which afforded an immobilised organometallic chromium(III) species that is considered to be catalytically significant (Scheme 13).⁵⁹ Parallels may therefore be drawn between the Cr{N(SiMe₃)₂}_x/SiO₂₋₆₀₀/MMAO-12 initiator system described herein and the Phillips heterogeneous Cr/SiO₂ ethylene polymerisation catalyst,^{62,63} as well as the more well-established *homogeneous* selective ethylene oligomerisation processes.^{64,65,66,67,68}



Scheme 13: Activation of Phillips CrO₃/SiO₂ ethylene polymerisation-active sites proposed by Brown *et al.*, 2015⁵⁹

Consequently, we postulate that the immobilised *bis*-(alkylated) chromium(III) species derived from $\equiv\text{SiOCr}\{\text{N}(\text{SiMe}_3)_2\}_2$ could potentially undergo reductive elimination, resulting in the formation of an active chromium(I) species responsible for 1-hexene production. Consequently, in line with previous work,^{20,69,70} we propose that $\equiv\text{SiOCrR}_2$ reacts with ethylene followed by migratory insertion and/or reductive elimination to generate a chromium(I)-based selective ethylene trimerisation catalyst (Scheme 14). Again, due to the complex nature of MMAO-12, the alkyl substituents have been referred to as R, for clarity.



Scheme 14: Proposed activation of silica-supported *bis*-(alkylated) chromium(III) ethylene trimerisation-active sites

As previously alluded to in Section 1.3.1.5.4, the exact structure of the active species for any known selective ethylene oligomerisation initiator system remains a matter of considerable debate.⁷¹ In the context of this thesis, elucidation of the active catalyst is complicated by both the paramagnetic nature of the silica-supported chromium species involved as well as the ill-defined nature of MMAO-12,¹⁸ and further complicated by the presence of multiple chromium species that each mediate separate reactions (*i.e.* trimerisation and polymerisation). In fact, it must be made clear in this thesis that the proposed activation pathways for the supported $=\text{SiO}_2\text{CrN}(\text{SiMe}_3)_2$ and $\equiv\text{SiOCr}\{\text{N}(\text{SiMe}_3)_2\}_2$ species described above are based on previous work that have studied somewhat related soluble (molecular) ethylene oligo-/poly-merisation systems.^{18,20,69,70}

2.3 Conclusions

Preliminary screening of $\text{Cr}\{\text{N}(\text{SiMe}_3)_2\}_x/\text{oxide}/\text{Al-activator}$ ethylene oligomerisation initiator systems has demonstrated that catalytic performance is intimately linked to the nature of the oxide support, aluminium activator, and organic diluent. In our hands, the best performing ethylene trimerisation initiator comprises $\text{Cr}\{\text{N}(\text{SiMe}_3)_2\}_x/\text{SiO}_{2-600}$ with MMAO-12 as activator operated as a slurry in heptane (61 wt% hexenes; 79% 1-hexene; $2403 \text{ g g}_{\text{Cr}}^{-1} \text{ h}^{-1}$). The observed product distribution is rationalised by two competing processes: trimerisation *via* a supported metallacyclic reaction manifold,^{4,5,6,7,8} and polymerisation through a Cossee-Arman chain growth pathway.^{9,10,11} Based on a combined TGA and solid-state ^{29}Si NMR spectroscopic study, two distinct silica-supported chromium species are present at the surface of $\text{Cr}\{\text{N}(\text{SiMe}_3)_2\}_x/\text{SiO}_{2-600}$. Upon activation with MMAO-12, $=\text{SiO}_2\text{CrN}(\text{SiMe}_3)_2$ arising from the reaction between $\text{Cr}\{\text{N}(\text{SiMe}_3)_2\}_3$ and geminal (**Q₂**) silanols are considered to be responsible for polyethylene (PE) formation, whilst $\equiv\text{SiOCr}\{\text{N}(\text{SiMe}_3)_2\}_2$ derived from isolated (**Q₃**) silanol sites may facilitate ethylene trimerisation and decene production *via* ethylene/1-hexene co-trimerisation. An activation pathway for the chromium(III) *mono*- and *bis*-(hexamethyldisilazide) species has been proposed whereby MMAO-12 alkylates the silica-supported chromium pro-initiator,¹⁸ resulting in the formation of a Phillips-type $=\text{SiO}_2\text{CrR}$ ethylene polymerisation catalyst^{62,63} as well as a $\equiv\text{SiOCrR}_2$ species. It is proposed that this latter moiety undergoes reductive elimination under an atmosphere of ethylene to afford a Cr^{I} -based initiator active for ethylene trimerisation.^{20,69,70}

2.4 References

- (1) T. Monoi, Y. Sasaki, *J. Mol. Catal. A: Chem.*, **2002**, *187*, 135-141.
- (2) T. Monoi, H. Ikeda, H. Ohira, Y. Sasaki, *Polym. J.*, **2002**, *34*, 461-465.
- (3) D. P. Debecker, M. Stoyanova, U. Rodemerck, A. Léonard, B. L. Su, E. M. Gaigneaux, *Catal. Today*, **2011**, *169*, 60-68.
- (4) R. M. Manyik, W. E. Walker, T. P. Wilson, *J. Catal.*, **1977**, *47*, 197-209.
- (5) J. R. Briggs, *J. Chem. Soc., Chem. Commun.*, **1989**, *11*, 674-675.
- (6) M. J. Overett, K. Blann, A. Bollmann, J. T. Dixon, D. Haasbroek, E. Killian, H. Maumela, D. S. McGuinness, D. H. Morgan, *J. Am. Chem. Soc.*, **2005**, *127*, 10723-10730.
- (7) L. H. Do, J. A. Labinger, J. E. Bercaw, *Organometallics*, **2012**, *31*, 5143-5149.
- (8) T. M. Zilbershtein, V. A. Kardash, V. V. Suvorova, A. K. Golovko, *Appl. Catal. A: Gen.*, **2014**, *475*, 371-378.
- (9) P. Cossee, *J. Catal.*, **1964**, *3*, 80-88.
- (10) E. J. Arlman, *J. Catal.*, **1964**, *3*, 89-98.
- (11) E. J. Arlman, P. Cossee, *J. Catal.*, **1964**, *3*, 99-104.
- (12) Y. Yang, H. Kim, J. Lee, H. Paik, H. G. Jang, *Appl. Catal. A: Gen.*, **2000**, *193*, 29-38.
- (13) I. Thapa, S. Gambarotta, I. Korobkov, R. Duchateau, S. V. Kulangara, R. Chevalier, *Organometallics*, **2010**, *29*, 4080-4089.
- (14) D. S. McGuinness, A. J. Rucklidge, R. P. Tooze, A. M. Z. Slawin, *Organometallics*, **2007**, *26*, 2561-2569.
- (15) A. J. Rucklidge, D. S. McGuinness, R. P. Tooze, A. M. Z. Slawin, J. D. A. Pelletier, M. J. Hanton, P. B. Webb, *Organometallics*, **2007**, *26*, 2782-2787.
- (16) S. Tang, Z. Liu, X. Yan, N. Li, R. Cheng, X. He, B. Liu, *Appl. Catal. A: Gen.*, **2014**, *481*, 39-48.
- (17) S. V. Kulangara, D. Haveman, B. Vidjayacoumar, I. Korobkov, S. Gambarotta, R. Duchateau, *Organometallics*, **2015**, *34*, 1203-1210.
- (18) E. Y.-X. Chen, T. J. Marks, *Chem. Rev.*, **2000**, *100*, 1391-1434.
- (19) K. Blann, A. Bollmann, H. de Bod, J. T. Dixon, E. Killian, P. Nongodlwana, M. C. Maumela, H. Maumela, A. E. McConnell, D. H. Morgan, M. J. Overett, M. Prétorius, S. Kuhlmann, P. Wasserscheid, *J. Catal.*, **2007**, *249*, 244-249.
- (20) A. Jabri, C. B. Mason, Y. Sim, S. Gambarotta, T. J. Burchell, R. Duchateau, *Angew. Chem. Int. Ed.*, **2008**, *47*, 9717-9721.
- (21) I. Vidyaratne, G. B. Nikiforov, S. I. Gorelsky, S. Gambarotta, R. Duchateau, I. Korobkov, *Angew. Chem. Int. Ed.*, **2009**, *48*, 6552-6556.
- (22) W. R. H. Wright, A. S. Batsanov, J. A. K. Howard, R. P. Tooze, M. J. Hanton, P. W. Dyer, *Dalton Trans.*, **2010**, *39*, 7038-7045.
- (23) P. D. Hustad, R. L. Kuhlman, D. J. Arriola, E. M. Carnahan, T. T. Wenzel, *Macromolecules*, **2007**, *40*, 7061-7064.
- (24) F. Rouholahnejad, D. Mathis, P. Chen, *Organometallics*, **2010**, *29*, 294-302.
- (25) J. M. Camara, R. A. Petros, J. R. Norton, *J. Am. Chem. Soc.*, **2011**, *133*, 5263-5273.
- (26) C. Ehm, R. Cipullo, P. H. M. Budzelaar, V. Busico, *Dalton Trans.*, **2016**, *45*, 6847-6855.
- (27) H. Hagimoto, T. Shiono, T. Ikeda, *Macromolecules*, **2002**, *35*, 5744-5745.
- (28) H. Hagimoto, T. Shiono, T. Ikeda, *Macromol. Chem. Phys.*, **2004**, *205*, 19-26.
- (29) R. Tanaka, T. Kawahara, Y. Shinto, Y. Nakayama, T. Shiono, *Macromolecules*, **2017**, *50*, 5989-5993.
- (30) C. Obuah, B. Omondi, K. Nozaki, J. Darkwa, *J. Mol. Catal. A: Chem.*, **2014**, *382*, 31-40.
- (31) E. Angelescu, C. Nicolau, Z. Simon, *J. Am. Chem. Soc.*, **1966**, *88*, 3910-3912.
- (32) L. McDyre, E. Carter, K. J. Cavell, D. M. Murphy, J. A. Platts, K. Sampford, B. D. Ward, W. F. Gabrielli, M. J. Hanton, D. M. Smith, *Organometallics*, **2011**, *30*, 4505-4508.
- (33) H. Guesmi, F. Tielens, *J. Phys. Chem. C*, **2012**, *116*, 994-1001.

- (34) C. Moisii, E. W. Deguns, A. Lita, S. D. Callahan, L. J. van de Burgt, D. Magana, A. E. Stiegman, *Chem. Mater.*, **2006**, *18*, 3965-3975.
- (35) A. Chakrabarti, M. Gierada, J. Handzlik, I. E. Wachs, *Top. Catal.*, **2016**, *59*, 725-739.
- (36) E. Groppo, A. Damin, F. Bonino, A. Zecchina, S. Bordiga, C. Lamberti, *Chem. Mater.*, **2005**, *17*, 2019-2027.
- (37) E. C. Alyea, D. C. Bradley, R. G. Copperthwaite, *J. Chem. Soc., Dalton Trans.*, **1972**, 1580-1584.
- (38) Anonymous, In *Studies in Surface Science and Catalysis*; E. F. Vansant, P. Van Der Voort, K. C. Vrancken, Eds.; Elsevier: 1995; Vol. 93, p 93-126.
- (39) Anonymous, In *Studies in Surface Science and Catalysis*; E. F. Vansant, P. Van Der Voort, K. C. Vrancken, Eds.; Elsevier: 1995; Vol. 93, p 59-77.
- (40) J. Amor Nait Ajjou, S. L. Scott, *Organometallics*, **1997**, *16*, 86-92.
- (41) L. T. Zhuravlev, *Colloids Surf. A*, **2000**, *173*, 1-38.
- (42) J. A. Chudek, G. Hunter, G. W. McQuire, C. H. Rochester, T. F. S. Smith, *J. Chem. Soc., Faraday Trans.*, **1996**, *92*, 453-460.
- (43) F. Devreux, J. P. Boilot, F. Chaput, B. Sapoval, *Phys. Rev. Lett.*, **1990**, *65*, 614-617.
- (44) E. R. Andrew, A. Bradbury, R. G. Eades, *Nature*, **1959**, *183*, 1802-1803.
- (45) I. J. Lowe, *Phys. Rev. Lett.*, **1959**, *2*, 285-287.
- (46) J. S. Hartman, B. L. Sherriff, *J. Phys. Chem.*, **1991**, *95*, 7575-7579.
- (47) I. Bertini, C. Luchinat, G. Parigi, E. Ravera, In *NMR of Paramagnetic Molecules (Second Edition)*; Elsevier: Boston, 2017, p 127-150.
- (48) G. Engelhardt, D. Michel, *High-Resolution Solid-State NMR of Silicates and Zeolites*; John Wiley & Sons Ltd., 1987.
- (49) M. C. Biesinger, B. P. Payne, A. P. Grosvenor, L. W. M. Lau, A. R. Gerson, R. S. C. Smart, *Appl. Surf. Sci.*, **2011**, *257*, 2717-2730.
- (50) J. H. Z. dos Santos, C. Krug, M. B. da Rosa, F. C. Stedile, J. Dupont, M. de Camargo Forte, *J. Mol. Catal. A: Chem.*, **1999**, *139*, 199-207.
- (51) R. L. Thompson, S. C. Gurusurthy, M. Pattabi, *J. Appl. Phys.*, **2011**, *110*, 043533.
- (52) R. J. Composto, R. M. Walters, J. Genzer, *Mater. Sci. Eng. R*, **2002**, *38*, 107-180.
- (53) J. Perrière, *Vacuum*, **1987**, *37*, 429-432.
- (54) W. J. van Rensburg, C. Grové, J. P. Steynberg, K. B. Stark, J. J. Huyser, P. J. Steynberg, *Organometallics*, **2004**, *23*, 1207-1222.
- (55) A. K. Tomov, J. J. Chirinos, D. J. Jones, R. J. Long, V. C. Gibson, *J. Am. Chem. Soc.*, **2005**, *127*, 10166-10167.
- (56) M. P. Conley, C. Copéret, C. Thieuleux, *ACS Catal.*, **2014**, *4*, 1458-1469.
- (57) M. P. Conley, M. F. Delley, G. Siddiqi, G. Lapadula, S. Norsic, V. Monteil, O. V. Safonova, C. Copéret, *Angew. Chem. Int. Ed.*, **2014**, *53*, 1872-1876.
- (58) M. F. Delley, F. Núñez-Zarur, M. P. Conley, A. Comas-Vives, G. Siddiqi, S. Norsic, V. Monteil, O. V. Safonova, C. Copéret, *Proc. Natl. Acad. Sci. U.S.A.*, **2014**, *111*, 11624-11629.
- (59) C. Brown, J. Krzystek, R. Achey, A. Lita, R. Fu, R. W. Meulenberg, M. Polinski, N. Peek, Y. Wang, L. J. van de Burgt, S. Profeta Jr., A. E. Stiegman, S. L. Scott, *ACS Catal.*, **2015**, *5*, 5574-5583.
- (60) B. Peters, S. L. Scott, A. Fong, Y. Wang, A. E. Stiegman, *Proc. Natl. Acad. Sci. U.S.A.*, **2015**, *112*, E4160-E4161.
- (61) M. F. Delley, G. Lapadula, F. Núñez-Zarur, A. Comas-Vives, V. Kalendra, G. Jeschke, D. Baabe, M. D. Walter, A. J. Rossini, A. Lesage, L. Emsley, O. Maury, C. Copéret, *J. Am. Chem. Soc.*, **2017**, *139*, 8855-8867.
- (62) J. P. Hogan, R. L. Banks, **1958**, *US22825721*, Phillips Petroleum Company.
- (63) M. P. McDaniel, *Adv. Catal.*, **2010**, *53*, 123-606.
- (64) J. R. Briggs, **1987**, *US4668838*, Union Carbide Corporation.
- (65) M. E. Lashier, J. W. Freeman, R. D. Knudsen, **1996**, *US5543375*, Phillips Petroleum Company.
- (66) Y. Araki, H. Nakamura, Y. Nanba, T. Okanu, **1999**, *US5856612*, Mitsubishi Chemical Corporation.

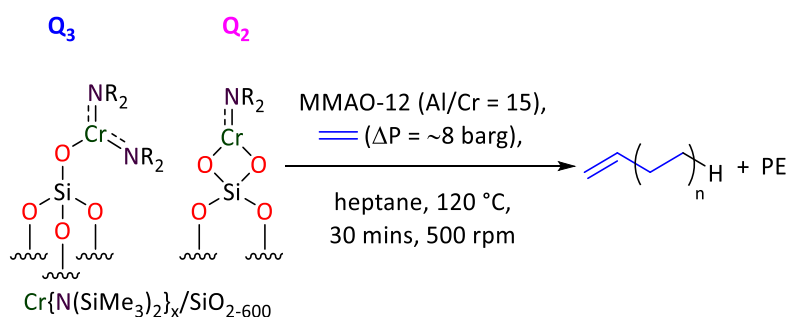
- (67) D. F. Wass, **2002**, *US6800702B2*, BP Chemicals Ltd.
- (68) K. Blann, A. Bollmann, J. T. Dixon, A. Neveling, D. H. Morgan, H. Maumela, E. Killian, F. M. Hess, S. Otto, M. J. Overett, **2004**, *WO2004056478A1*, Sasol Technology Ltd.
- (69) T. Agapie, J. A. Labinger, J. E. Bercaw, *J. Am. Chem. Soc.*, **2007**, 14281-14295.
- (70) Y. Chen, E. Callens, E. Abou-Hamad, N. Merle, A. J. P. White, M. Taoufik, C. Copéret, E. Le Roux, J.-M. Basset, *Angew. Chem. Int. Ed.*, **2012**, *51*, 11886-11889.
- (71) D. S. McGuinness, *Chem. Rev.*, **2011**, *111*, 2321-2341.

This page has been intentionally left blank.

Chapter 3:
Influence of Experimental Process Parameters on
Chromium-mediated Heterogeneous Ethylene
Trimerisation

3.1 Introduction

In Chapter 2 it has been shown that the performance of a silica-supported chromium ethylene trimerisation initiator, $\text{Cr}\{\text{N}(\text{SiMe}_3)_2\}_x/\text{SiO}_2/\text{Al}$ -activator, is dependent on the nature of the oxide support and its pre-treatment, the nature of the Lewis acidic alkyl aluminium-based co-catalyst, and the reaction diluent. Here the $\text{Cr}\{\text{N}(\text{SiMe}_3)_2\}_x/\text{SiO}_{2-600}$ variant activated with modified methyl aluminoxane (MMAO-12) in heptane gave rise to the most effective heterogeneous ethylene trimerisation system (Scheme 1), which generated a mixture of hexenes (61 wt%; 79% 1-hexene), decenes (16 wt%) and polyethylene (PE; 13 wt%) at a rate of $2403 \text{ g g}_{\text{Cr}}^{-1} \text{ h}^{-1}$. This organic product distribution was rationalised by the operation of two competing processes: i) trimerisation *via* an “oxide-supported” variant of the metallacycle mechanism,^{1,2} and ii) polymerisation through a Cossee-Arlman-type chain growth pathway.^{3,4,5} This proposal is based on there being two distinct chromium species at the surface of $\text{Cr}\{\text{N}(\text{SiMe}_3)_2\}_x/\text{SiO}_{2-600}$ by way of reaction between $\text{Cr}\{\text{N}(\text{SiMe}_3)_2\}_3$ with both isolated (Q_3) and geminal (Q_2) silanol sites, as inferred from solid-state ^{29}Si direct excitation (DE) magic-angle spinning (MAS) nuclear magnetic resonance (NMR) spectroscopy (see Section 2.2.4.2).



Scheme 1: Optimised heterogeneous $\text{Cr}\{\text{N}(\text{SiMe}_3)_2\}_x/\text{SiO}_{2-600}$ /MMAO-12 ethylene trimerisation system: 0.2 g $\text{Cr}\{\text{N}(\text{SiMe}_3)_2\}_x/\text{SiO}_{2-600}$, 27 μmol Cr, 0.71 wt% Cr to SiO_{2-600} .

This current chapter aims to determine the reproducibility of the heterogeneous $\text{Cr}\{\text{N}(\text{SiMe}_3)_2\}_x/\text{SiO}_{2-600}$ /MMAO-12 ethylene trimerisation initiator package at a constant ethylene concentration. The effect of experimental processing parameters including chromium concentration, Al/Cr mole ratio, reaction temperature, ethylene pressure, stirrer speed, reaction time, diluent volume, and the impact of potential promoters upon the silica-supported chromium initiator are investigated as part of a fundamental study into the field of heterogeneous selective ethylene oligomerisation. Detailed analyses of the liquid-phase oligomers and the PE by-product of the $\text{Cr}\{\text{N}(\text{SiMe}_3)_2\}_x/\text{SiO}_{2-600}$ /MMAO-12 ethylene trimerisation batch reaction will be compiled using gas chromatographic-flame ionisation detection (GC-FID), solution-phase NMR spectroscopy and differential scanning calorimetry (DSC). Based on these analyses, we will aim to elucidate plausible reaction mechanism(s) that are facilitated by the heterogeneous ethylene trimerisation catalyst.

3.2 Results

3.2.1 Catalyst Test Reproducibility

In the preceding chapter it was highlighted that the ethylene oligo-/poly-merisation activities reported for $\text{Cr}\{\text{N}(\text{SiMe}_3)_2\}_x/\text{oxide}/\text{Al-activator}$ were limited by the concentration of the monomer feedstock, since these preliminary tests were carried out by pressurising the autoclave to 8 barg before sealing it for the duration of the ethylene trimerisation run. These reactions are denoted hereon as “closed” runs. Under such conditions, reincorporation of 1-hexene into the metallacycle-based trimerisation manifold that is operative can lead to the formation of several decene isomers as a result of the increased mole fraction of 1-hexene in solution, coupled with the depleted concentration of ethylene at almost quantitative conversion (*i.e.* $\Delta P = \sim 8$ barg across the test period).^{6,7,8} Additionally, the preliminary tests described in Chapter 2 do not take into account the pressure dependency of ethylene solubility in the heptane diluent. Consequently, with both these factors in mind, it was imperative to conduct analogous chromium-mediated ethylene trimerisation reactions at a constant ethylene concentration – reactions hereon denoted as “open” runs – in order to establish a reproducible baseline activity.

To this end, the best-performing heterogeneous ethylene trimerisation catalyst precursor, $\text{Cr}\{\text{N}(\text{SiMe}_3)_2\}_x/\text{SiO}_{2-600}$ (as established in Chapter 2) was evaluated in combination with MMAO-12 in the slurry-phase using heptane as a diluent at a fixed ethylene pressure (*i.e.* 8 barg), over the course of three independent trials (Table 1). After 30 minutes, the reaction was terminated by isolating the autoclave from the ethylene supply, turning off the overhead mechanical stirrer, and cooling the reactor in an ice-water bath to 4 °C, before the system was carefully depressurised. An aliquot of the resulting liquid fraction was sampled and quenched in a 1:1 mixture of toluene and dilute aqueous HCl. The liquid organic phase was then extracted and filtered, prior to its analysis by GC-FID. The polymer by-product was isolated by filtration, dried overnight (10 h) at room temperature (RT), and analysed using DSC.

Table 1: Determination of the reproducibility of ethylene oligomerisation tests mediated by Cr{N(SiMe₃)₂}_x/SiO₂₋₆₀₀ with MMAO-12 as activator, heptane as diluent, undertaken at a fixed ethylene pressure (*i.e.* 8 barg) for 30 minutes; catalytic performance data averaged over three individual runs.

Run	C ₄ = ^a {wt%}	C ₆ = ^a {wt%}	C ₈ = ^a {wt%}	C ₁₀ = ^a {wt%}	C ₁₂₊ = ^a {wt%}	PE ^b {wt%}	Total Activity {g g _{Cr} ⁻¹ h ⁻¹ }
		(%1-C ₆ =)					
1	0.3	53.4 (88.9)	2.3	24.2	9.3	10.6	14004
2	0.3	55.5 (88.5)	2.5	22.4	8.7	10.6	13569
3	0.2	54.8 (91.3)	2.7	23.0	9.6	9.6	12966
Average of Runs 1 – 3	0.3	54.6 (89.6)	2.5	23.2	9.2	10	13513
Sample Standard Deviation	0.04	1.09 (1.51)	0.22	0.91	0.75	0.58	521

Reaction conditions: 27 μmol Cr (mass of Cr{N(SiMe₃)₂}_x/SiO₂₋₆₀₀ = 0.2 g); 410 μmol MMAO-12 (Al:Cr = 15:1); 60 mL heptane; 120 °C; 500 rpm; 8 barg constant ethylene pressure; 0.5 h.

^a Determined by GC-FID relative to the internal standard (1 mL nonane).

^b Polymer isolated by filtration, dried to constant mass and weighed.

The product selectivity exhibited by the “open” Cr{N(SiMe₃)₂}_x/SiO₂₋₆₀₀/MMAO-12 ethylene trimerisation batch process (at a constant ethylene concentration) outlined in Table 1 is consistent with that achieved in the analogous “closed” system described in the previous chapter. These data demonstrate that the productivity and selectivity displayed by the silica-supported chromium initiator at a fixed ethylene pressure of 8 barg for 30 minutes are reproducible. The experimental error associated with the total activity (*i.e.* g g_{Cr}⁻¹ h⁻¹ for all products combined) during these three independent trials is <4%. Consequently, hereinafter unless stated otherwise, the error associated with the total activities reported in this thesis will be ± 4%.

3.2.2 Influence of Catalyst Support Dehydroxylation upon the Selectivity of the Cr{N(SiMe₃)₂}_x/SiO₂/MMAO-12 Initiator

Building on preliminary work described in Chapter 2, it was necessary to validate the hypothesis that, upon activation with MMAO-12, supported =SiO₂CrN(SiMe₃)₂ species derived from Q₂ silanol functionalities at the surface of silica mediate ethylene polymerisation, and ≡SiOCr{N(SiMe₃)₂}₂ derived from Q₃ sites facilitate 1-hexene production at a constant ethylene concentration. To this end, the Cr{N(SiMe₃)₂}_x/SiO₂₋₂₀₀ variant was activated with MMAO-12 and then screened for its expected ethylene polymerisation behaviour at a fixed ethylene pressure (Table 2).

Table 2: Comparison of ethylene oligomerisation reactions catalysed by Cr{N(SiMe₃)₂}_x/support (i.e. SiO₂₋₂₀₀, SiO₂₋₄₀₀ or SiO₂₋₆₀₀) with MMAO-12 as activator, heptane as diluent, 8 barg ethylene pressure, for 30 minutes.

Entry	Catalyst Support	C ₄ ^a {wt%}	C ₆ ^a {wt%}	C ₈ ^a {wt%}	C ₁₀ ^a {wt%}	C ₁₂₊ ^a {wt%}	PE ^b {wt%}	Total Activity {g g _{Cr} ⁻¹ h ⁻¹ }
			(%1-C ₆ =)					
1	SiO ₂₋₂₀₀	0	13 (97)	1	1	1	83	3914 ± 157
2	SiO ₂₋₄₀₀	0	50 (94)	2	10	3	34	5690 ± 228
3	SiO ₂₋₆₀₀	0	55 (90)	3	23	9	10	13513 ± 521

Reaction conditions: 27 μmol Cr (mass of Cr{N(SiMe₃)₂}_x/support = 0.2 g); 410 μmol MMAO-12 (Al:Cr = 15:1); 60 mL heptane; 120 °C; 500 rpm; 8 barg fixed ethylene pressure; 0.5 h.

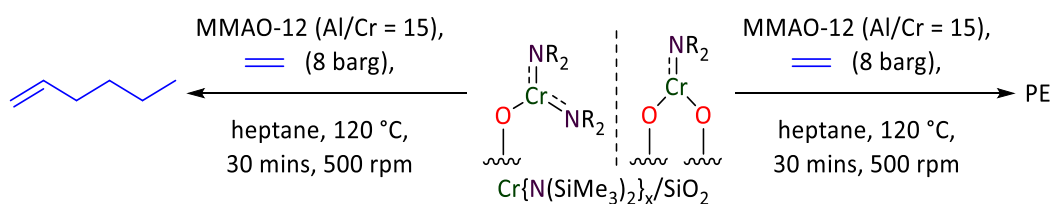
^a Determined by GC-FID relative to the internal standard (1 mL nonane).

^b Polymer isolated by filtration, dried to constant mass and weighed.

In line with our previous work (see Section 2.2.5), lowering the temperature at which silica was pre-treated from 600 to 200 °C altered the selectivity of the resulting initiator in favour of polymerisation (Entry 1). This is rationalised by the relative population of Q₂ and Q₃ silanols at the surface of silica (as determined by deconvolution of solid-state ²⁹Si DE MAS NMR spectra using a Gaussian distribution function). Solid-state ²⁹Si NMR spectroscopic analysis of SiO₂₋₆₀₀ revealed that it had a greater relative population of surface-based Q₃ silanol functionalities compared with that of SiO₂₋₂₀₀. As a result, reaction of SiO₂₋₆₀₀ with Cr{N(SiMe₃)₂}₃ leads to a greater proportion of a ≡SiOCr{N(SiMe₃)₂}₂ species than is the case for the system prepared from SiO₂₋₂₀₀. Consequently, based on this observation coupled with the catalytic test data, it is proposed that ≡SiOCr{N(SiMe₃)₂}₂ is the surface-bound species responsible for ethylene trimerisation (Entry 3). Conversely, the increased relative population of Q₂ sites at the surface of SiO₂₋₂₀₀, with respect to SiO₂₋₆₀₀, results in an increased proportion of the =SiO₂CrN(SiMe₃)₂ ethylene polymerisation catalytic precursor at the surface of Cr{N(SiMe₃)₂}_x/SiO₂₋₂₀₀ (Entry 1).

As previously discussed in Section 2.2.5, while it is necessary to highlight that solid-state ^{29}Si NMR spectroscopy alone cannot distinguish between Q_3 and vicinal silanols,⁹ because their respective resonant frequencies overlap at -99 ppm, it is well-established that vicinal silanols fully condense between $190 - 400$ °C.^{10,11} Hence, the silica sample calcined at 200 °C (*i.e.* SiO_{2-200}) may be considered to be dehydrated silica, retaining a significant population of vicinal silanol functionalities as well as both Q_2 and Q_3 silanols. Indeed the reaction between $\text{Cr}\{\text{N}(\text{SiMe}_3)_2\}_3$ and these residual vicinal silanols (liberating two molar equivalents of the corresponding amine) may lead to the formation of a third supported chromium(III) species that, upon activation with MMAO-12, may also be catalytically significant (*i.e.* $=\text{SiO}_2\text{CrN}(\text{SiMe}_3)_2$).¹²

Given that vicinal silanols are known to fully condense at 400 °C,^{10,11} a SiO_{2-400} -supported chromium initiator analogous to $\text{Cr}\{\text{N}(\text{SiMe}_3)_2\}_x/\text{SiO}_{2-600}/\text{MMAO-12}$ was prepared, and then tested for its ethylene tri-/poly-merisation behaviour under identical test conditions (Table 2; Entry 2). It was found that increasing the support calcination temperature from 200 to 400 °C led to an improved selectivity of the resulting $\text{Cr}\{\text{N}(\text{SiMe}_3)_2\}_x/\text{SiO}_{2-400}/\text{MMAO-12}$ initiator system at the expense of PE (Entries 1 and 2). These differences in catalytic performance cannot be explained by the proportion of $=\text{SiO}_2\text{CrN}(\text{SiMe}_3)_2$ and $\equiv\text{SiOCr}\{\text{N}(\text{SiMe}_3)_2\}_2$ derived from Q_2 and Q_3 silanols, respectively, since the relative population of Q_2 silanols at the surface of SiO_{2-400} was consistent with that of SiO_{2-200} ($\sim 3\%$), as inferred by solid-state ^{29}Si DE MAS NMR spectroscopy. Therefore, it is postulated that a secondary supported *mono*-(hexamethyldisilazide) chromium ethylene polymerisation catalyst precursor is formed by way of reaction between $\text{Cr}\{\text{N}(\text{SiMe}_3)_2\}_3$ and residual vicinal silanols at the surface of SiO_{2-200} , in addition to the tri- and poly-merisation-active sites derived from Q_2 and Q_3 sites (Scheme 2).



Scheme 2: The two silica-supported chromium pro-initiators proposed to be responsible for tri-/poly-merisation arising from the reaction between $\text{Cr}\{\text{N}(\text{SiMe}_3)_2\}_3$ with Q_3 and vicinal/ Q_2 silanol sites, respectively.

In order to increase the relative population of Q_3 silanols, and hence the proportion of the surface-bound trimerisation-active species derived from $\equiv\text{SiOCr}\{\text{N}(\text{SiMe}_3)_2\}_2$, a sample of the silica support was calcined at 700 °C for 24 hours *in vacuo* (*i.e.* 0.1 mbar) so as to dehydroxylate both vicinal and Q_2 silanol sites.^{13,14,15,16,17,18,19,20,21} The resulting oxide (denoted $\text{SiO}_{2-700\text{v}}$) was sequentially treated with solutions of $\text{Cr}\{\text{N}(\text{SiMe}_3)_2\}_3$ and MMAO-12 (15 molar equivalents), and subsequently evaluated for ethylene trimerisation behaviour (Table 3). To enable comparisons with both SiO_{2-600} - and $\text{SiO}_{2-700\text{v}}$ -supported systems, the $\text{Cr}\{\text{N}(\text{SiMe}_3)_2\}_x/\text{SiO}_{2-600\text{v}}$ /MMAO-12 variant was also screened under identical reaction conditions.

Table 3: Comparison of ethylene oligomerisation runs mediated by $\text{Cr}\{\text{N}(\text{SiMe}_3)_2\}_x/\text{support}$ (*i.e.* SiO_{2-600} , $\text{SiO}_{2-600\text{v}}$ or $\text{SiO}_{2-700\text{v}}$) with MMAO-12 as activator, heptane as diluent, at 8 barg ethylene pressure, for 30 minutes.

Entry	Catalyst Support	$\text{C}_4=^a$ {wt%}	$\text{C}_6=^a$ {wt%}	$\text{C}_8=^a$ {wt%}	$\text{C}_{10}=^a$ {wt%}	$\text{C}_{12+}=^a$ {wt%}	PE ^b {wt%}	Total Activity {g g _{Cr} ⁻¹ h ⁻¹ }
			(%1-C ₆ =)					
1	SiO_{2-600}	0	55 (90)	3	23	9	10	13513 ± 521
2	$\text{SiO}_{2-600\text{v}}$	0	52 (89)	2	24	11	11	14753 ± 590
3	$\text{SiO}_{2-700\text{v}}$	0	54 (89)	3	22	11	9	9772 ± 391

Reaction conditions: 27 μmol Cr (mass of $\text{Cr}\{\text{N}(\text{SiMe}_3)_2\}_x/\text{support}$ = 0.2 g); 410 μmol MMAO-12 (Al:Cr 15:1); 60 ml heptane; 120 °C; 500 rpm; 8 barg fixed ethylene pressure; 0.5 h.

^a Determined by GC-FID relative to the internal standard (1 mL nonane).

^b Polymer isolated by filtration, dried to constant mass and weighed.

Although the selectivity afforded by the $\text{Cr}\{\text{N}(\text{SiMe}_3)_2\}_x/\text{SiO}_{2-700\text{v}}$ /MMAO-12 initiator matched that achieved by both SiO_{2-600} - and $\text{SiO}_{2-600\text{v}}$ -supported systems (Table 3; Entries 1 and 2), increasing the temperature at which the catalyst support was calcined from 600 to 700 °C under dynamic vacuum led to a considerable drop in catalytic activity (Entry 3). This difference is rationalised by an increase in thermally-induced sintering of the oxide occurring at 700 °C, something consistent with the onset of sintering of silica being known to occur at around 600 °C.²² Sintering is a thermal process that involves inter-particle condensation; it typically results in a decreased specific surface area (SSA) and pore collapse.⁹ Unsurprisingly, therefore the Brunauer Emmett Teller (BET) SSA, Barrett Joyner Halenda (BJH) pore volume and size analyses of $\text{SiO}_{2-700\text{v}}$ (prepared by calcination at 700 °C for 24 hours *in vacuo*) was found to be significantly lower than that for SiO_{2-600} (Table 4). As a result, it was postulated that increasing the support calcination temperature beyond 700 °C would incur further reduction of its SSA and porosity, factors that will likely attenuate the performance of such silica-supported ethylene trimerisation initiators.

Table 4: BET specific surface area and BJH pore volume/size analyses of SiO₂₋₆₀₀, SiO_{2-600v} and SiO_{2-700v}

Catalyst Support	SSA (m ² g ⁻¹)	Pore Volume (cm ³ g ⁻¹)	Average Pore Diameter (Å)
SiO ₂₋₆₀₀	285 ± 5	1.86 ± 0.03	293 ± 5
SiO _{2-600v}	280 ± 5	1.80 ± 0.03	257 ± 5
SiO _{2-700v}	239 ± 5	1.56 ± 0.03	261 ± 5

3.2.3 Effect of Molecular Precursor on Catalytic Performance:

$\text{Cr}\{\text{N}(\text{SiMe}_3)_2\}_3$ vs. $\text{Cr}(\text{acac})_3$ vs. $\text{CrCl}_3(\text{thf})_3$

In Chapter 2, activation pathways for the respective $\equiv\text{SiOCr}\{\text{N}(\text{SiMe}_3)_2\}_2$ and $=\text{SiO}_2\text{CrN}(\text{SiMe}_3)_2$ tri- and poly-merisation-active surface species derived from Q_3 and Q_2 (and vicinal) silanols were proposed. It was postulated that the supported TM species were alkylated by MMAO-12, resulting in the cleavage of the $\text{Cr}-\text{N}(\text{SiMe}_3)_2$ linkages to yield a conventional Phillips-type ethylene polymerisation catalyst (*i.e.* $=\text{SiO}_2\text{CrR}$) and $\equiv\text{SiOCrR}_2$. The latter was proposed to undergo reductive elimination under an atmosphere of ethylene to generate a surface-bound Cr^I-based ethylene trimerisation-active site (see Section 2.2.6). Consequently, assuming that the amide ligands were cleaved from the supported chromium(III) species during the activation of the $\text{Cr}\{\text{N}(\text{SiMe}_3)_2\}_x/\text{SiO}_2$ pro-initiator, it was necessary to determine the role (if any) of the hexamethyldisilazide ligands in this class of heterogeneous ethylene trimerisation catalyst. This was achieved by substituting $\text{Cr}\{\text{N}(\text{SiMe}_3)_2\}_3$ with air-stable commercially-available derivatives chromium(III) *tris*-(2,4-pentanedionate) $\{\text{Cr}(\text{acac})_3\}$ and $\text{CrCl}_3(\text{thf})_3$.

To this end, the partially dehydroxylated SiO_{2-600} catalyst support was reacted with $\text{Cr}(\text{acac})_3$ and $\text{CrCl}_3(\text{thf})_3$ using an analogous procedure to that used for $\text{Cr}\{\text{N}(\text{SiMe}_3)_2\}_x/\text{SiO}_{2-600}$. The ensuing silica-bound chromium species were activated *in situ* with MMAO-12, and tested for ethylene oligo-/poly-merisation at a fixed run time of 30 minutes at a constant ethylene working pressure (Table 5).

Table 5: Comparison of ethylene oligomerisation tests using $\text{Cr}^{\text{III}}/\text{SiO}_{2-600}$, where $\text{Cr}^{\text{III}} = \text{Cr}\{\text{N}(\text{SiMe}_3)_2\}_x$, $\text{Cr}(\text{acac})_3$ and $\text{CrCl}_3(\text{thf})_3$, with MMAO-12 as activator, heptane as diluent, 8 barg ethylene pressure, for 30 minutes.

Entry	Molecular Precursor	$\text{C}_4=^a$ {wt%}	$\text{C}_6=^a$ {wt%}	$\text{C}_8=^a$ {wt%}	$\text{C}_{10}=^a$ {wt%}	$\text{C}_{12+}=^a$ {wt%}	PE ^b {wt%}	Total Activity {g Cr^{-1} h ⁻¹ }
		(%1-C ₆ =)						
1	$\text{Cr}\{\text{N}(\text{SiMe}_3)_2\}_3$	0	55 (90)	3	23	9	10	13513 ± 521
2	$\text{Cr}(\text{acac})_3$	1	5 (93)	2	1	2	89	1282 ± 51
3	$\text{CrCl}_3(\text{thf})_3$	0	1 (100)	1	1	3	94	1024 ± 41

Reaction conditions: 27 μmol Cr (mass of $\text{Cr}^{\text{III}}/\text{SiO}_{2-600} = 0.2$ g); 410 μmol MMAO-12 (Al:Cr = 15:1); 60 mL heptane; 120 °C; 500 rpm; 8 barg fixed ethylene pressure; 0.5 h.

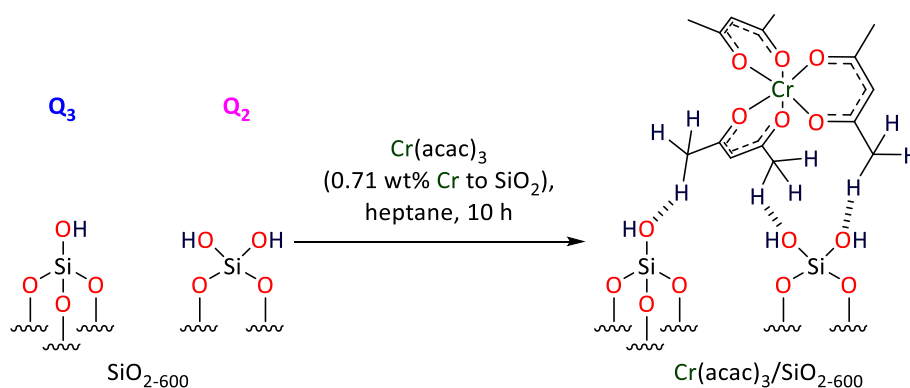
^a Determined by GC-FID relative to the internal standard (1 mL nonane).

^b Polymer isolated by filtration, dried to constant mass and weighed.

The best-performing ethylene trimerisation initiator package in terms of both productivity and selectivity was $\text{Cr}\{\text{N}(\text{SiMe}_3)_2\}_x/\text{SiO}_{2-600}/\text{MMAO-12}$ (Table 5; Entry 1). By comparison, the SiO_{2-600} -supported $\text{Cr}(\text{acac})_3$ - and $\text{CrCl}_3(\text{thf})_3$ -derived materials both fared poorly following activation with MMAO-12 predominantly generating PE (Entries 2 and 3). In line with our previous work (see Section 2.2.4.2), it was assumed that $\text{CrCl}_3(\text{thf})_3$ and $\text{Cr}(\text{acac})_3$ would react with residual

Q_2 and Q_3 silanol sites at the surface of SiO_{2-600} liberating one or two molar equivalents of either HCl or 2,4-pentanedione, respectively. However, one literature report has shown that instead $Cr(acac)_3$ can undergo physical adsorption to partially dehydroxylated silica support through hydrogen-bonding interactions between surface-based hydroxyls with one or more acac ligands.²³ Consequently, it is therefore postulated that the $Cr(acac)_3$ molecular precursor employed in our work was simply physisorbed to SiO_{2-600} rather than being covalently grafted through one or more Cr–O–Si bonds (Scheme 3). Therefore, considering that molecular (soluble) $Cr(acac)_3$ activated with an alkyl aluminium reagent has previously been employed as a *homogeneous* ethylene polymerisation initiator,²⁴ it is reasonable to propose that MMAO-12 reacts with the $Cr(acac)_3$ species physisorbed to the surface of SiO_{2-600} , and generates a molecular ethylene polymerisation catalyst *in situ* (Entry 2).

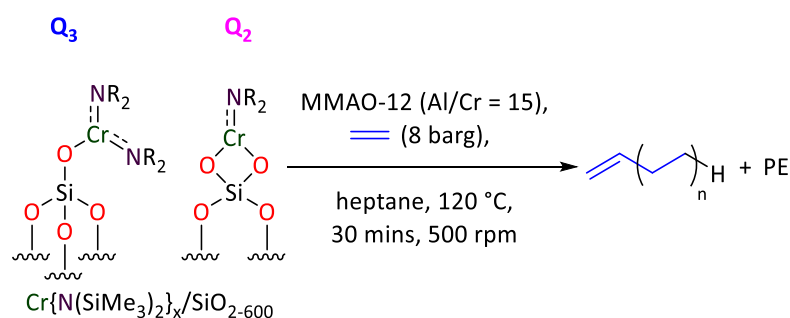
Further work must be undertaken to elucidate the role of hexamethyldisilazide ligands within such heterogeneous ethylene trimerisation systems. For example, screening $Cr(N^iPr_2)_3$ - and $Cr(NPh_2)_3$ -derivatives of the $Cr\{N(SiMe_3)_2\}_x/SiO_{2-600}$ pro-initiator would indicate whether the performance of the ethylene trimerisation catalyst is affected by either the steric bulk of the ligand sphere surrounding the chromium metal centre,²⁵ electronic effects,^{26,27} or indeed the potential variable coordination of the phenyl amide substituent.^{28,29} Although preliminary attempts were made to prepare both of these starting materials (see Chapter 4; Section 4.4.4), neither could be isolated with sufficient purity and hence their immobilisation on silica was not attempted.



Scheme 3: Proposed physical adsorption of $Cr(acac)_3$ to SiO_{2-600} through hydrogen-bonding interactions, adapted from Weckhuysen *et al.*, 2000²³

3.2.4 Impact of Process Parameters upon Chromium-mediated Heterogeneous Ethylene Trimerisation

Once the initial screening ethylene oligo-/poly-merisation experiments had been completed, and the reproducibility of the $\text{Cr}\{\text{N}(\text{SiMe}_3)_2\}_x/\text{SiO}_{2-600}/\text{MMAO-12}$ initiator determined at a constant ethylene concentration under a standard set of conditions (Scheme 4), it was important to investigate the effect of other important process parameters. In the subsequent sections, the effect of varying the following parameters will be explored: the influence of chromium concentration, Al/Cr loading, reaction temperature, ethylene pressure, stirrer speed, reaction time, diluent volume, and the impact of performance-enhancing additives upon the productivity and selectivity of the silica-supported chromium initiator.



Scheme 4: General reaction scheme for $\text{Cr}\{\text{N}(\text{SiMe}_3)_2\}_x/\text{SiO}_{2-600}/\text{MMAO-12}$ ethylene trimerisation batch process: 0.2 g $\text{Cr}\{\text{N}(\text{SiMe}_3)_2\}_x/\text{SiO}_{2-600}$, 27 μmol Cr, 0.71 wt% Cr to SiO_{2-600} .

The following investigations were carried out in batch mode using a 150 mL stainless steel autoclave. The contents of the reactor (*i.e.* $\text{Cr}\{\text{N}(\text{SiMe}_3)_2\}_x/\text{SiO}_{2-600}$, MMAO-12, heptane and nonane) were heated to the desired temperature T °C whilst being stirred at S rpm, before the system was pressurised with ethylene to P barg for t minutes. At time t , the reaction was terminated by isolating the autoclave from the ethylene feedstock, stopping the overhead stirrer and cooling the reactor to 4 °C in an ice-water bath, prior to the system being carefully and slowly depressurised. Catalytic performance was evaluated by quantifying the mass of the resulting organic liquid-phase oligomers using GC-FID against a known volume of an internal standard (nonane), and measuring the mass of any accompanying solid polymer that had previously been isolated by filtration and dried overnight (10 h) under ambient conditions.

3.2.4.1 Influence of Chromium Concentration upon the Heterogeneous $\text{Cr}\{\text{N}(\text{SiMe}_3)_2\}_x/\text{SiO}_{2-600}/\text{MMAO-12}$ Ethylene Trimerisation System

It was of interest to determine the dependence of the $\text{Cr}\{\text{N}(\text{SiMe}_3)_2\}_x/\text{SiO}_{2-600}/\text{MMAO-12}$ ethylene trimerisation initiator upon chromium metal loading at a constant ethylene concentration. This was achieved by reducing the chromium loading of the molecular precursor on the partially dehydroxylated siliceous catalyst support from 0.71 to 0.35 wt%.^{*} However, as a consequence, this also increases the number of unreacted silanols at the surface of the silica-supported chromium pro-initiator. By varying the mass of the 0.35 and 0.71 wt% $\text{Cr}\{\text{N}(\text{SiMe}_3)_2\}_x/\text{SiO}_{2-600}$ catalyst precursors, the impact of these unreacted silanols were explored whilst maintaining the number of moles of chromium in the system at either 14 or 27 μmol . For all chromium metal loadings, the silica-supported chromium pro-initiator was activated with 15 molar equivalents of MMAO-12, and evaluated for ethylene oligo-/poly-merisation at a fixed ethylene working pressure of 8 barg for 30 minutes (Table 6).

Table 6: Comparison of ethylene oligomerisation tests facilitated by $\text{Cr}\{\text{N}(\text{SiMe}_3)_2\}_x/\text{SiO}_{2-600}$ with MMAO-12 as activator, heptane as diluent, at 8 barg ethylene pressure, for 30 minutes.

Entry	Pro-initiator Mass (g)	Loading {wt%}	C ₄ = ^c {wt%}	C ₆ = ^c {wt%}	C ₈ = ^c {wt%}	C ₁₀ = ^c {wt%}	C ₁₂₊ = ^c {wt%}	PE ^d {wt%}	Total Activity {g Cr ⁻¹ h ⁻¹ }
1	0.2	0.35 ^a	0	58 (93)	3	16	9	14	13860 ± 554
2	0.2	0.71 ^b	0	55 (90)	3	23	9	10	13513 ± 521
3	0.4	0.35 ^b	0	47 (88)	2	25	13	12	14052 ± 562
4	0.1	0.71 ^a	0	65 (96)	4	15	4	12	13214 ± 529

Reaction conditions: 60 mL heptane; 120 °C; 500 rpm; 8 barg fixed ethylene pressure; 0.5 h.

^a 14 μmol Cr; 205 μmol MMAO-12 (Al:Cr = 15:1).

^b 27 μmol Cr; 410 μmol MMAO-12 (Al:Cr = 15:1).

^c Determined by GC-FID relative to the internal standard (1 mL nonane).

^d Polymer isolated by filtration, dried to constant mass and weighed.

* Chromium metal loadings on the silica support were experimentally determined by analysis of the chromium content of the solution generated by exhaustive extraction of $\text{Cr}\{\text{N}(\text{SiMe}_3)_2\}_x/\text{SiO}_{2-600}$ with concentrated HCl (1.5 mL (37% w/w, 10 h, 25 °C) by inductively coupled plasma-optical emission spectroscopy (ICP-OES).

3.2.4.2 Effect of Al/Cr Mole Ratio on Catalytic Performance

In the preceding chapter, it was shown that an alkyl aluminium-based co-catalyst (e.g. MMAO-12) is necessary to activate the heterogeneous $\text{Cr}\{\text{N}(\text{SiMe}_3)_2\}_x/\text{SiO}_{2-600}$ pro-initiator towards ethylene oligo-/poly-merisation (see Section 2.2.2). Consequently, it was of interest to probe the impact of varying the Al/Cr mole ratio upon the productivity and selectivity of the silica-supported chromium initiator system. To this end, the $\text{Cr}\{\text{N}(\text{SiMe}_3)_2\}_x/\text{SiO}_{2-600}$ catalyst precursor was activated with different Al/Cr loadings of MMAO-12, and subsequently screened for catalytic ethylene oligo-/poly-merisation behaviour at a constant ethylene concentration (Table 7).

Table 7: Comparison of ethylene oligomerisation tests mediated by $\text{Cr}\{\text{N}(\text{SiMe}_3)_2\}_x/\text{SiO}_{2-600}$ with 15, 24, 50 or 150 molar equivalents of MMAO-12 as activator, heptane as diluent, at 8 barg ethylene pressure, 30 minutes.

Entry	Al/Cr Mole Ratio	C ₄ = ^a {wt%}	C ₆ = ^a {wt%}	C ₈ = ^a {wt%}	C ₁₀ = ^a {wt%}	C ₁₂₊ = ^a {wt%}	PE ^b {wt%}	Total Activity {g g _{Cr} ⁻¹ h ⁻¹ }
		(%1-C ₆ =)						
1	15	0	55 (90)	3	23	9	10	13513 ± 521
2	24	0	53 (91)	2	25	9	11	17789 ± 712
3	50	1	50 (95)	3	5	3	38	7634 ± 305
4	150	1	17 (94)	4	3	6	68	2012 ± 80

Reaction conditions: 27 μmol Cr (mass of $\text{Cr}\{\text{N}(\text{SiMe}_3)_2\}_x/\text{SiO}_{2-600}$ = 0.2 g); 60 mL heptane; 120 °C; 500 rpm; 8 barg fixed ethylene pressure; 0.5 h.

^a Determined by GC-FID relative to the internal standard (1 mL nonane).

^b Polymer isolated by filtration, dried to constant mass and weighed.

3.2.4.3 Temperature Dependence of the Cr{N(SiMe₃)₂}_x/SiO₂₋₆₀₀/MMAO-12 Ethylene Trimerisation System

With a view to optimising the catalytic performance of the Cr{N(SiMe₃)₂}_x/SiO₂₋₆₀₀/MMAO-12 process, a series of batch ethylene trimerisation runs were conducted as a slurry in heptane at a constant ethylene concentration over a range of different reaction temperatures.[†] In this work, the silica-supported chromium pro-initiator was activated with MMAO-12 (15 molar equivalents), and tested for catalytic behaviour at a fixed ethylene pressure (*i.e.* 8 barg) for 30 minutes at varying reaction temperatures (Table 8). While these tests provide a crude measure of the temperature dependence of the Cr{N(SiMe₃)₂}_x/SiO₂₋₆₀₀/MMAO-12 system, they do not take into account the temperature dependence of ethylene solubility in the organic diluent phase.

Table 8: Comparison of ethylene oligomerisation runs catalysed by Cr{N(SiMe₃)₂}_x/SiO₂₋₆₀₀ with MMAO-12 as activator, heptane as diluent, at reaction temperature (*i.e.* 35, 80, 90, 100, 120 or 140 °C), at 8 barg ethylene pressure, for 30 minutes.

Entry	Reaction Temperature (°C)	C ₄ ^a {wt%}	C ₆ ^a {wt%}	C ₈ ^a {wt%}	C ₁₀ ^a {wt%}	C ₁₂₊ ^a {wt%}	PE ^b {wt%}	Total Activity {g g _{Cr} ⁻¹ h ⁻¹ }
			(%1-C ₆ =)					
1	35	1	3 (95)	2	1	1	92	5707 ± 228
2	80	0	6 (97)	1	1	2	89	7709 ± 308
3	90	1	43 (95)	4	14	7	32	11694 ± 191
4	100	0	53 (92)	4	16	7	20	11770 ± 86
5	120	0	55 (90)	3	23	9	10	13513 ± 521
6	140	1	40 (78)	1	32	17	9	18562 ± 34

Reaction conditions: 27 μmol Cr (mass of Cr{N(SiMe₃)₂}_x/SiO₂₋₆₀₀ = 0.2 g); 410 μmol MMAO-12 (Al:Cr = 15:1); 60 mL heptane; 500 rpm; 8 barg fixed ethylene pressure; 0.5 h.

^a Determined by GC-FID relative to the internal standard (1 mL nonane).

^b Polymer isolated by filtration, dried to constant mass and weighed.

[†] Reaction temperature monitored using an internal thermocouple, and maintained using an external electrical band heater fitted with a solid-state relay.

3.2.4.4 Effect of the Stirrer Speed Regime on the Catalytic Performance of $\text{Cr}\{\text{N}(\text{SiMe}_3)_2\}_x/\text{SiO}_{2-600}/\text{MMAO-12}$

In order to probe the influence of ethylene mass-transfer effects during heterogeneous ethylene trimerisation mediated by the $\text{Cr}\{\text{N}(\text{SiMe}_3)_2\}_x/\text{SiO}_{2-600}/\text{MMAO-12}$ initiator, the effect of stirrer speed was explored. Preliminary ethylene oligomerisation catalytic investigations were conducted in the slurry-phase in heptane at a constant temperature and pressure (*i.e.* 120 °C and 8 barg) whilst being stirred at either 500 or 1200 rpm using a customised magnetically-coupled overhead mechanical stirrer fitted with a turbine-type four-blade impeller (Table 9).[‡]

Table 9: Comparison of ethylene oligomerisation runs mediated by $\text{Cr}\{\text{N}(\text{SiMe}_3)_2\}_x/\text{SiO}_{2-600}$ with MMAO-12 as activator, heptane as diluent, at a fixed ethylene pressure of 8 barg, for 30 minutes against variation in stirring rate (*i.e.* 500 or 1200 rpm).

Entry	Stirrer Speed (rpm)	C ₄ ^a {wt%}	C ₆ ^a {wt%} (%1-C ₆ =)	C ₈ ^a {wt%}	C ₁₀ ^a {wt%}	C ₁₂₊ ^a {wt%}	PE ^b {wt%}	Total Activity {g Cr ⁻¹ h ⁻¹ }
1	500	0	55 (90)	3	23	9	10	13513 ± 521
2	1200	0	58 (92)	3	17	6	15	8738 ± 350

Reaction conditions: 27 μmol Cr (mass of $\text{Cr}\{\text{N}(\text{SiMe}_3)_2\}_x/\text{SiO}_{2-600}$ = 0.2 g); 410 μmol MMAO-12 (Al:Cr = 15:1); 60 mL heptane; 120 °C; 8 barg fixed ethylene pressure; 0.5 h.

^a Determined by GC-FID relative to the internal standard (1 mL nonane).

^b Polymer isolated by filtration, dried to constant mass and weighed.

[‡] Stirrer speed maintained using an IKA Yellow Line overhead mechanical homogeniser.

3.2.4.5 Pressure Dependency of the Cr{N(SiMe₃)₂}_x/SiO₂₋₆₀₀/MMAO-12 Initiator System

It was of interest to study the pressure dependency of the Cr{N(SiMe₃)₂}_x/SiO₂₋₆₀₀/MMAO-12 ethylene trimerisation process at a fixed ethylene concentration. To this end, the catalytic performance of this silica-supported chromium initiator was evaluated in heptane at 120 °C for ethylene oligo-/poly-merisation over a range of different ethylene working pressures (Table 10).[§] While these ethylene oligomerisation experiments were conducted at a fixed ethylene pressure, they do not make allowances for the pressure dependence of ethylene solubility in the heptane diluent.

Table 10: Comparison of ethylene oligomerisation tests initiated by Cr{N(SiMe₃)₂}_x/SiO₂₋₆₀₀ with MMAO-12 as activator, heptane as diluent, at a fixed ethylene working pressure (i.e. 2, 8, 14, 18, 24 or 30 barg) for 30 minutes.

Entry	Ethylene Pressure (barg)	C ₄ = ^a {wt%}	C ₆ = ^a {wt%}	C ₈ = ^a {wt%}	C ₁₀ = ^a {wt%}	C ₁₂₊ = ^a {wt%}	PE ^b {wt%}	Total Activity {g g _{Cr} ⁻¹ h ⁻¹ }
			(%1-C ₆ =)					
1	2	0	57 (82)	1	23	6	12	4732 ± 189
2	8	0	55 (90)	3	23	9	10	13513 ± 521
3	14	0	54 (88)	3	21	9	14	18662 ± 746
4	18	1	54 (91)	4	20	9	12	22435 ± 164
5	24	1	51 (91)	4	23	11	10	40541 ± 1622
6	30	1	49 (91)	3	26	12	9	68251 ± 1544

Reaction conditions: 27 μmol Cr (mass of Cr{N(SiMe₃)₂}_x/SiO₂₋₆₀₀ = 0.2 g); 410 μmol MMAO-12 (Al:Cr = 15:1); 60 mL heptane; 120 °C; 500 rpm; 0.5 h.

^a Determined by GC-FID relative to the internal standard (1 mL nonane).

^b Polymer isolated by filtration, dried to constant mass and weighed.

§ Ethylene working pressure controlled externally with an in-line Gas Arc GA600 0 – 41 bar fuel gas manifold regulator.

3.2.4.6 Influence of Reaction Time upon the Cr{N(SiMe₃)₂}_x/SiO₂₋₆₀₀/MMAO-12 Initiator System

An important parameter when assessing any new catalyst package is its operating lifetime. Hence, it was necessary to explore the period of time for which the Cr{N(SiMe₃)₂}_x/SiO₂₋₆₀₀/MMAO-12 ethylene trimerisation process maintained acceptable activity and selectivity towards 1-hexene at a constant ethylene pressure over different time intervals up to and including 3 hours (Table 11).

Table 11: Comparison of ethylene oligomerisation tests facilitated by Cr{N(SiMe₃)₂}_x/SiO₂₋₆₀₀ with MMAO-12 as activator, heptane as diluent, at 8 barg ethylene pressure for reaction time (*i.e.* 5, 30, 60, 120 or 180 minutes).

Entry	Reaction Time (minutes)	C ₄ = ^a {wt%}	C ₆ = ^a {wt%} (%1-C ₆ =)	C ₈ = ^a {wt%}	C ₁₀ = ^a {wt%}	C ₁₂₊ = ^a {wt%}	PE ^b {wt%}	Total Activity {g g _{Cr} ⁻¹ h ⁻¹ }
1	5	0	64 (94)	3	12	8	13	21554 ± 862
2	30	0	55 (90)	3	23	9	10	13513 ± 521
3	60	0	44 (88)	2	28	15	11	9590 ± 202
4	120	0	36 (84)	2	33	20	9	7997 ± 114
5	180	0	33 (86)	1	34	21	10	6343 ± 254

Reaction conditions: 27 μmol Cr (mass of Cr{N(SiMe₃)₂}_x/SiO₂₋₆₀₀ = 0.2 g); 410 μmol MMAO-12 (Al:Cr = 15:1); 60 mL heptane; 120 °C; 500 rpm; 8 barg fixed ethylene pressure.

^a Determined by GC-FID relative to the internal standard (1 mL nonane).

^b Polymer isolated by filtration, dried to constant mass and weighed.

3.2.4.7 Effect of Potential Promoters (1,2-DME or Et₂Zn) on the Catalytic Performance of Cr{N(SiMe₃)₂}_x/SiO₂₋₆₀₀/MMAO-12

The impact of known performance-enhancing additives 1,2-dimethoxyethane (1,2-DME) and Et₂Zn upon the heterogeneous Cr{N(SiMe₃)₂}_x/SiO₂₋₆₀₀/MMAO-12 initiator system were explored. The silica-supported chromium catalyst precursor was activated with MMAO-12 in a heptane solution containing the nonane standard and the promotor, and screened at a constant ethylene concentration for ethylene trimerisation behaviour (Table 12).

Table 12: Comparison of the effects of the additives 1,2-DME, Et₂Zn, and toluene on the ethylene oligomerisation catalytic performance of Cr{N(SiMe₃)₂}_x/SiO₂₋₆₀₀/MMAO-12; heptane diluent, 8 barg ethylene pressure, 30 minutes.

Entry	Additive	C ₄ ^a {wt%}	C ₆ ^a {wt%}	C ₈ ^a {wt%}	C ₁₀ ^a {wt%}	C ₁₂₊ ^a {wt%}	PE ^b {wt%}	Total Activity {g g _{Cr} ⁻¹ h ⁻¹ }
			(%1-C ₆ =)					
1	None	0	55 (90)	3	23	9	10	13513 ± 521
2	1,2-DME ^c	0	60 (94)	3	18	6	12	9195 ± 368
3	Diethyl Zinc ^d	26	22 (77)	7	4	10	31	1936 ± 77

Reaction conditions: 27 μmol Cr (mass of Cr{N(SiMe₃)₂}_x/SiO₂₋₆₀₀ = 0.2 g); 410 μmol MMAO-12 (Al:Cr = 15:1); 60 mL heptane; 120 °C; 500 rpm; 8 barg fixed ethylene pressure; 0.5 h.

^a Determined by GC-FID relative to the internal standard (1 mL nonane).

^b Polymer isolated by filtration, dried to constant mass and weighed.

^c 1,2-Dimethoxyethane (30 μL, 273 μmol; 10 molar equivalents).

^d Diethyl zinc (1.5 M solution in toluene; 1.8 mL, 2.7 mmol; 100 molar equivalents).

3.2.4.8 Influence of 1-Hexene Concentration on the Product Selectivity of the $\text{Cr}\{\text{N}(\text{SiMe}_3)_2\}_x/\text{SiO}_{2-600}/\text{MMAO-12}$ Ethylene Trimerisation Process

It was of interest to determine the impact of 1-hexene concentration on the selectivity exhibited by the heterogeneous $\text{Cr}\{\text{N}(\text{SiMe}_3)_2\}_x/\text{SiO}_{2-600}/\text{MMAO-12}$ ethylene trimerisation batch reaction at a constant ethylene concentration. To this end, chromium-mediated ethylene oligomerisation was conducted at a fixed ethylene working pressure in the presence of a known volume of 1-hexene that was added at the start of the test reaction (Table 13).

Table 13: Comparison of the effects of the additive 1-hexene on the ethylene oligomerisation catalytic performance of $\text{Cr}\{\text{N}(\text{SiMe}_3)_2\}_x/\text{SiO}_{2-600}$ with MMAO-12 as activator, heptane diluent, 8 barg ethylene pressure, 30 minutes.

Entry	Additive	$\text{C}_4=^a$ {wt%}	$\text{C}_6=^a$ {wt%}	$\text{C}_8=^a$ {wt%}	$\text{C}_{10}=^a$ {wt%}	$\text{C}_{12+}=^a$ {wt%}	PE ^b {wt%}	Total Activity {g g _{Cr} ⁻¹ h ⁻¹ }
			(%1-C ₆ =)					
1	None	0	55 (90)	3	23	9	10	13513 ± 521
2	1-Hexene ^c	0	37 (86)	2	34	16	11	14014 ± 561

Reaction conditions: 27 μmol Cr (mass of $\text{Cr}\{\text{N}(\text{SiMe}_3)_2\}_x/\text{SiO}_{2-600}$ = 0.2 g); 410 μmol MMAO-12 (Al:Cr = 15:1); 60 mL heptane; 120 °C; 500 rpm; 8 barg fixed ethylene pressure; 0.5 h.

^a Determined by GC-FID relative to the internal standard (1 mL nonane).

^b Polymer isolated by filtration, dried to constant mass and weighed.

^c 1-Hexene (3 mL, 24 mmol; 870 molar equivalents).

In addition to increasing the concentration of 1-hexene in solution through use of an “additive”, the mole fraction of 1-hexene afforded by the $\text{Cr}\{\text{N}(\text{SiMe}_3)_2\}_x/\text{SiO}_{2-600}/\text{MMAO-12}$ initiator can be systematically altered by varying the volume of the heptane diluent. To this end, the silica-supported chromium catalyst precursor was activated with MMAO-12 in different volumes of heptane before being tested for ethylene oligomerisation at a constant ethylene concentration (Table 14).

Table 14: Comparison of ethylene oligomerisation tests mediated by $\text{Cr}\{\text{N}(\text{SiMe}_3)_2\}_x/\text{SiO}_{2-600}$ with MMAO-12 as activator as a function of heptane diluent volume (*i.e.* 30, 60 or 90 mL), at 8 barg ethylene pressure, for 30 minutes.

Entry	Diluent Volume (mL)	$\text{C}_4=^a$ {wt%}	$\text{C}_6=^a$ {wt%}	$\text{C}_8=^a$ {wt%}	$\text{C}_{10}=^a$ {wt%}	$\text{C}_{12+}=^a$ {wt%}	PE ^b {wt%}	Total Activity {g g _{Cr} ⁻¹ h ⁻¹ }
			(%1-C ₆ =)					
1	30	0	39 (84)	2	33	17	10	14845 ± 594
2	60	0	55 (90)	3	23	9	10	13513 ± 521
3	90	0	61 (92)	3	20	7	9	11786 ± 471

Reaction conditions: 27 μmol Cr (mass of $\text{Cr}\{\text{N}(\text{SiMe}_3)_2\}_x/\text{SiO}_{2-600}$ = 0.2 g); 410 μmol MMAO-12 (Al:Cr = 15:1); 60 mL heptane; 120 °C; 500 rpm; 8 barg fixed ethylene pressure; 0.5 h.

^a Determined by GC-FID relative to the internal standard (1 mL nonane).

^b Polymer isolated by filtration, dried to constant mass and weighed.

This page has been intentionally left blank.

3.3 Discussion: Effects of Varying Reaction Test Parameters on the Performance of $\text{Cr}\{\text{N}(\text{SiMe}_3)_2\}_x/\text{SiO}_2\text{-600}/\text{MMAO-12}$

3.3.1 Effect of Chromium Metal Loading

From the results described in Section 3.2.4.1, there appears to be a linear correlation between chromium concentration and the total mass of all organic products afforded by the $\text{Cr}\{\text{N}(\text{SiMe}_3)_2\}_x/\text{SiO}_2\text{-600}/\text{MMAO-12}$ ethylene trimerisation initiator (Figure 1). This is in good agreement with homogeneous transition metal (TM)-mediated selective ethylene oligomerisation, which is widely accepted to be first order with respect to chromium concentration.^{30,31,32,33} Unlike in soluble (molecular) systems, the ethylene monomer feedstock must diffuse through the porous catalyst support material, and adsorb onto the surface of the silica-supported chromium initiator before undergoing catalysis. Therefore, mass-transfer and diffusion limitations cannot be ruled out, factors that will likely impact upon the performance of the $\text{Cr}\{\text{N}(\text{SiMe}_3)_2\}_x/\text{SiO}_2\text{-600}/\text{MMAO-12}$ ethylene trimerisation system. There may even be a critical concentration (*e.g.* $0.05 \text{ mmol}_{\text{Cr}} \text{ L}^{-1}$) under which silica-supported chromium-mediated ethylene trimerisation does not proceed.

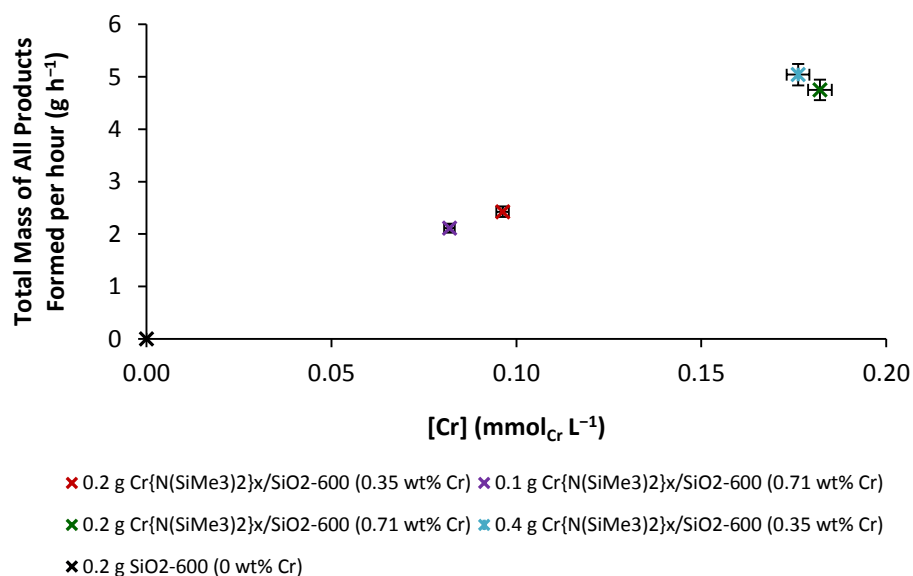
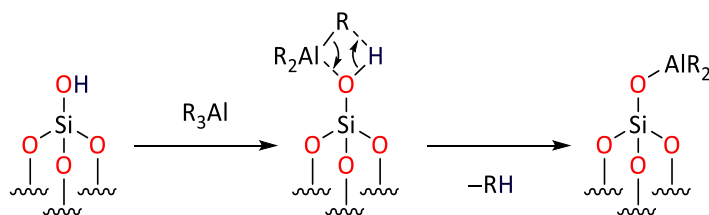


Figure 1: Scatter diagram showing the effect of chromium concentration upon the total mass of all products formed either by the $\text{Cr}\{\text{N}(\text{SiMe}_3)_2\}_x/\text{SiO}_2\text{-600}/\text{MMAO-12}$ initiator or the so-called “activated” catalyst support per hour. Reaction conditions: 205 or 410 μmol MMAO-12 (Al:Cr = 15:1); 60 mL heptane; 120 °C; 500 rpm; 8 barg constant ethylene pressure; 0.5 h. Error bars (Y-axis) represent one standard deviation; error bars (X-axis) represent relative standard deviation in chromium metal loading as determined by ICP-OES.

Furthermore, as previously alluded to in Section 3.2.4.1, the increased relative population of unreacted silanols at the surface of the $\text{Cr}\{\text{N}(\text{SiMe}_3)_2\}_x/\text{SiO}_{2-600}$ pro-initiator at lower chromium metal loadings (*i.e.* 0.35 wt%) may play a role during catalysis. Indeed, calcined oxides are established supports for R_3Al species in their own right (see Section 2.2.2).^{34,35,36} That said, the turnover frequency (TOF) achieved by the silica-supported chromium initiator remained constant at $\sim 13500 \text{ g g}_{\text{Cr}}^{-1} \text{ h}^{-1}$ under the reaction conditions employed in spite of the lower chromium loadings. This infers that an Al/Cr mole ratio of 15 is a sufficient excess to react with any accessible silanols (Scheme 5), and generate the ethylene tri-/poly-merisation-active catalyst.



Scheme 5: Reaction of an alkyl aluminium reagent with an isolated silanol, modified from Werghi *et al.*, 2015²⁰

3.3.2 Effect of Reaction Temperature

Following on from the experiments described in Section 3.2.4.3, the TOF achieved by the $\text{Cr}\{\text{N}(\text{SiMe}_3)_2\}_x/\text{SiO}_{2-600}/\text{MMAO-12}$ initiator system improves with increasing reaction temperature (Figure 2), in spite of the decreased mole fraction of ethylene dissolved in heptane typically observed at higher temperatures.^{37,38} Notably, the selectivity exhibited by this system switches from polymerisation to favouring ethylene trimerisation as the reaction temperature is increased from 80 to 90 °C. In line with previous reports in the literature that show that the rate at which soluble (molecular) selective ethylene oligomerisation-active species are generated is greater at elevated temperatures,^{30,31} it is anticipated that the activation of ethylene trimerisation sites at the surface of $\text{Cr}\{\text{N}(\text{SiMe}_3)_2\}_x/\text{SiO}_{2-600}$ is very likely to also be temperature-dependent. This is expected to play a crucial role in dictating the product selectivity of the ensuing silica-supported chromium initiator.

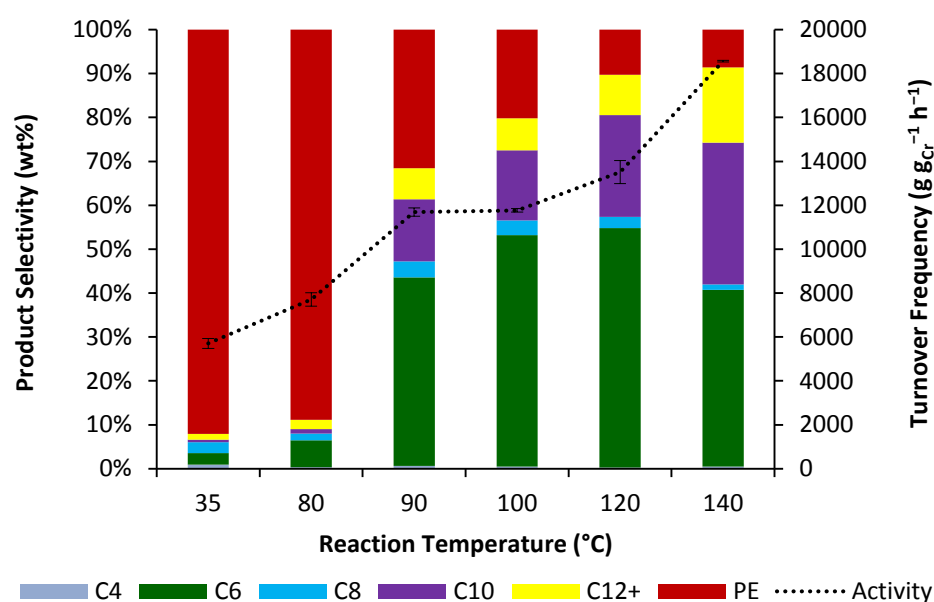


Figure 2: Selectivity and turnover frequency of the $\text{Cr}\{\text{N}(\text{SiMe}_3)_2\}_x/\text{SiO}_{2-600}/\text{MMAO-12}$ ethylene trimerisation system as a function of reaction temperature. Reaction conditions: 27 μmol Cr (mass of $\text{Cr}\{\text{N}(\text{SiMe}_3)_2\}_x/\text{SiO}_{2-600}$ = 0.2 g); 410 μmol MMAO-12 (Al:Cr = 15:1); 60 mL heptane; 500 rpm; 8 barg fixed ethylene pressure; 0.5 h.

Unfortunately, the complex interplay between tri- and poly-merisation catalysis precludes the accurate determination of individual values of activation energy (E_a) for 1-hexene production and for polymer formation. Although the natural logarithm of the TOF for all products afforded by $\text{Cr}\{\text{N}(\text{SiMe}_3)_2\}_x/\text{SiO}_{2-600}/\text{MMAO-12}$ may be plotted against the reciprocal of the reaction temperature, this Arrhenius plot would only provide an average E_a for a combination of all of the coincident processes, including ethylene trimerisation, olefin isomerisation, ethylene/1-hexene co-trimerisation and polymerisation. Therefore, in this case, the Arrhenius analysis has limited utility and has not been undertaken.

3.3.3 Effect of Stirrer Speed

In previous reports involving soluble (molecular) selective ethylene oligomerisation systems, catalytic activity has been plotted against the reciprocal of the stirring rate (at a constant temperature and ethylene concentration) in order to determine the point at which the reaction is free of any additional mass-transfer effects.³⁹ However, for the $\text{Cr}\{\text{N}(\text{SiMe}_3)_2\}_x/\text{SiO}_2\text{-600}/\text{MMAO-12}$ system of interest here, instead of reducing mass-transfer considerations, increasing the stirrer speed regime from 500 to 1200 rpm resulted in a reduced TOF (see Section 3.2.4.4). This observation has been attributed to the physical dispersion and accumulation of the solid catalyst on the surface of the reactor walls as opposed to being stirred as a suspension in the organic slurry-phase, thus removing it from the catalytically-relevant medium.

3.3.4 Effect of Ethylene Concentration

From the results described in Section 3.2.4.5, it is clear that the $\text{Cr}\{\text{N}(\text{SiMe}_3)_2\}_x/\text{SiO}_{2-600}/\text{MMAO-12}$ initiator system shows a pressure dependence. Although no true kinetic investigations of the performance of the silica-supported chromium initiator system have been undertaken, by plotting the individual TOFs for hexene and polyethylene (PE) formation as a function of ethylene pressure, it is postulated that there are two different reaction rates for these two processes as expected (Figure 3). The almost linear correlation between ethylene working pressure and the amount of solid PE afforded by the $\text{Cr}\{\text{N}(\text{SiMe}_3)_2\}_x/\text{SiO}_{2-600}/\text{MMAO-12}$ system (at a fixed ethylene pressure over 30 minutes) suggests that polymerisation is a first order reaction with respect to ethylene concentration. This is consistent with a typical Cossee-Arlman-type chain growth mechanism, in which the propagation of the alkyl chain is the rate-determining step (RDS).^{3,4,5}

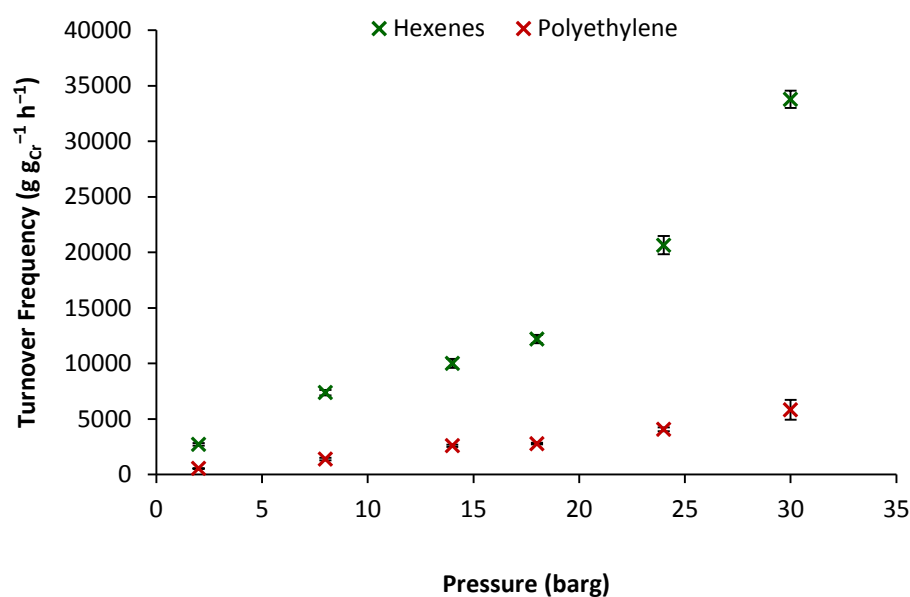


Figure 3: Scatter diagram correlating the turnover frequencies for hexene and polyethylene generated by the $\text{Cr}\{\text{N}(\text{SiMe}_3)_2\}_x/\text{SiO}_{2-600}/\text{MMAO-12}$ ethylene trimerisation initiator with ethylene working pressure. Reaction conditions: 27 μmol Cr (mass of $\text{Cr}\{\text{N}(\text{SiMe}_3)_2\}_x/\text{SiO}_{2-600}$ = 0.2 g); 410 μmol MMAO-12 (Al:Cr = 15:1); 60 mL heptane; 120 °C; 500 rpm; 0.5 h. Error bars represent one standard deviation.

For a rate equation in the form of $r = k[\text{Cr}][\text{C}_2\text{H}_4]^n$, a plot of the natural logarithm of the rate (or number of moles of product formed within a certain time) versus the natural logarithm of ethylene concentration or indeed ethylene pressure, a parameter that has been found to be a reliable approximation for concentration in solution, should provide a linear relationship in which the gradient of the slope equates to the reaction order in ethylene.³³ To this end, the natural logarithm of the number of moles of hexenes afforded by the $\text{Cr}\{\text{N}(\text{SiMe}_3)_2\}_x/\text{SiO}_{2-600}/\text{MMAO-12}$ initiator (at a constant ethylene concentration over 30 minutes) has been plotted as a function of the natural logarithm of absolute ethylene working pressure (Figure 4). Based on this evidence alone, the heterogeneous chromium-mediated ethylene trimerisation reaction described here can be approximated to be first order in ethylene. This is consistent with preliminary work carried out by Monoi and Sasaki who reported that ethylene trimerisation mediated by a silica-supported

chromium initiator derived from $\text{Cr}\{\text{N}(\text{SiMe}_3)_2\}_2/\text{SiO}_2$ activated with isobutyl aluminoxane (IBAO) is first order in ethylene.⁴⁰ Indeed observations made previously following examination of soluble (molecular), selective TM-catalysed ethylene oligomerisation systems have identified that the RDS for the proposed metallacyclic ethylene trimerisation manifold is the expansion of the chromacyclopentane intermediate to the chromacycloheptane species.^{28,31,33,39,41,42,43,44,45} Consequently, it is tentatively postulated that the RDS for the somewhat related supported variant described in this thesis, $\text{Cr}\{\text{N}(\text{SiMe}_3)_2\}_x/\text{SiO}_{2-600}/\text{MMAO-12}$, is the same.

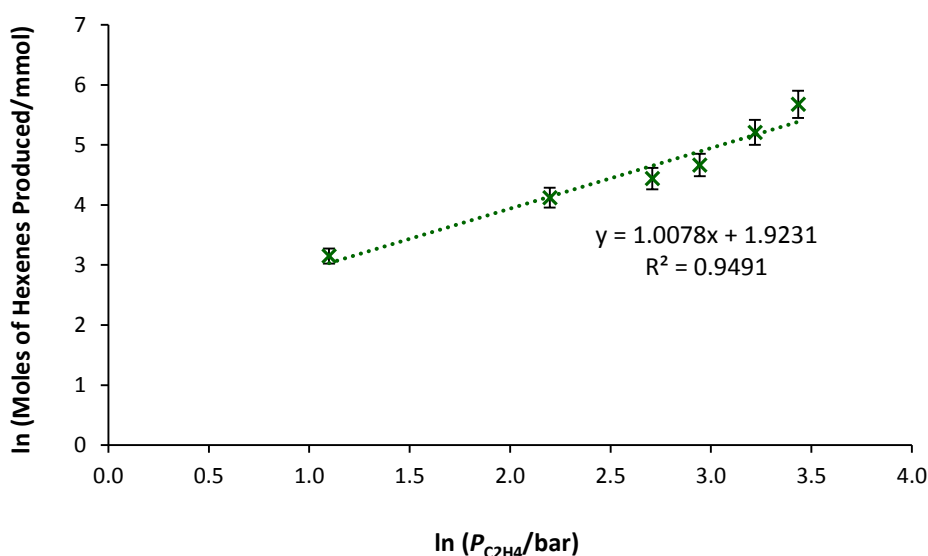


Figure 4: Scatter diagram correlating the natural logarithm of the number of moles of hexenes afforded by the $\text{Cr}\{\text{N}(\text{SiMe}_3)_2\}_x/\text{SiO}_{2-600}/\text{MMAO-12}$ initiator as a function of the natural logarithm of absolute ethylene pressure. Reaction conditions: 27 μmol Cr (mass of $\text{Cr}\{\text{N}(\text{SiMe}_3)_2\}_x/\text{SiO}_{2-600}$ = 0.2 g); 410 μmol MMAO-12 (Al:Cr = 15:1); 60 mL heptane; 120 °C; 500 rpm; 0.5 h. Error bars represent one standard deviation.

Since it has been reported that 1-hexene can be reincorporated into the metallacyclic trimerisation manifold *in situ* yielding several decene isomers,^{6,7,8} and co-polymerise with ethylene giving rise to butyl side chains within the PE backbone,^{12,46,47,48,49,50} the respective rates of ethylene trimerisation reported in this thesis are likely to be an underestimation of their true values. Moreover, by keeping the chromium concentration and the reaction temperature constant throughout the $\text{Cr}\{\text{N}(\text{SiMe}_3)_2\}_x/\text{SiO}_{2-600}/\text{MMAO-12}$ ethylene trimerisation run, increasing ethylene pressure not only increases the mole fraction of the monomer feedstock in solution, but also the mole ratio between chromium and ethylene as well, something that will influence the catalytic behaviour of the initiator. Although these crude heterogeneous ethylene trimerisation batch reactions provide a reasonable approximation that 1-hexene formation exhibits a first order dependence with respect to ethylene, these conclusions are tentative because of the complex interplay between tri-/poly-merisation catalysis. This is especially true when considering that there are several conflicting reports in the literature that suggest that 1-hexene formation is a second order reaction with respect to ethylene concentration, and that the RDS in the metallacycle mechanism is the formation of the metallacyclopentane intermediate.^{1,6,32,51,52}

3.3.5 Catalyst Lifetime

The lifetime of a catalyst can be considered a metric of how many turnovers a system can achieve before acceptable performance (activity and/or selectivity) is lost or, alternatively, as the length of time before the initiator undergoes deactivation. In the heterogeneous catalysis arena, catalyst deactivation (that results in a decrease in lifetime) is generally assumed to result from a combination of four broad deactivation pathways, namely: poisoning, fouling, coking, and mechanical damage.⁵³ Each of these pathways has a deleterious effect on catalyst performance. Consequently, it was important to explore how the TOF achieved by the heterogeneous $\text{Cr}\{\text{N}(\text{SiMe}_3)_2\}_x/\text{SiO}_2\text{-600}/\text{MMAO-12}$ initiator system varied as a function of reaction test duration at a fixed ethylene pressure (Figure 5). Due to the experimental difficulties associated with sampling from the autoclave, these data comprise a series of batch ethylene trimerisation runs rather than being from a continuous flow process. That said, the reproducibility of the batch testing regime (see Section 3.2) means that a reliable indication of catalyst performance as a function of time is achievable through comparison of several reactions of varying duration. Here, it was found that the observed TOF decreased considerably after approximately 5 minutes, before eventually reaching a plateau, a profile that is indicative of catalyst deactivation taking place. This may be rationalised by numerous factors:

- Reactor fouling arising from the accumulation of PE inside the autoclave.⁵⁴
- Blocking of the pores in the silica support.
- Thermal deactivation of the catalyst.
- Hydrolysis/deactivation of the MMAO-12 co-catalyst.
- Cleavage of the supported chromium species mediated by MMAO-12.⁵⁵

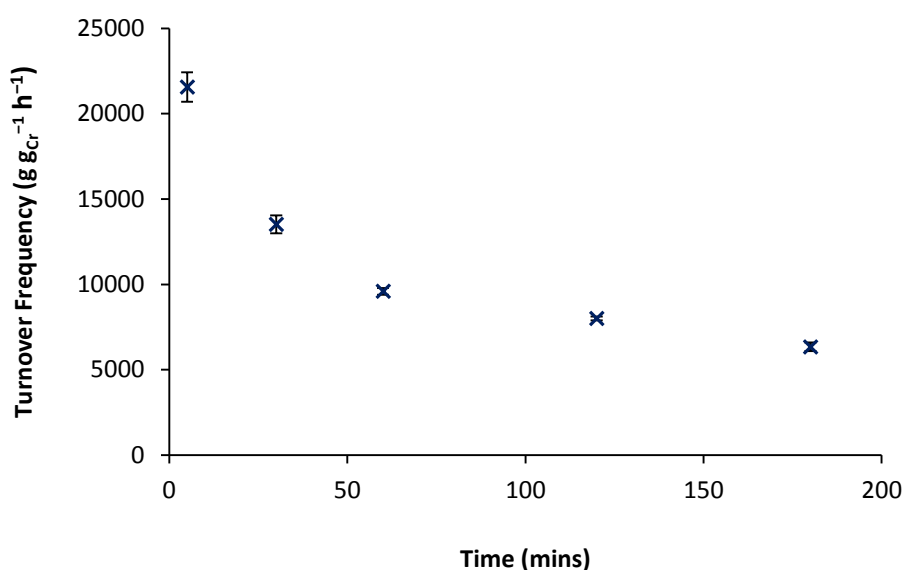


Figure 5: Turnover frequency achieved by the $\text{Cr}\{\text{N}(\text{SiMe}_3)_2\}_x/\text{SiO}_2\text{-600}/\text{MMAO-12}$ ethylene trimerisation system as a function of reaction time. Reaction conditions: 27 μmol Cr (mass of $\text{Cr}\{\text{N}(\text{SiMe}_3)_2\}_x/\text{SiO}_2\text{-600}$ = 0.2 g); 410 μmol MMAO-12 (Al:Cr = 15:1); 60 mL heptane; 120 °C; 500 rpm; 8 barg fixed ethylene pressure. Error bars represent one standard deviation.

This page has been intentionally left blank

3.3.6 Evaluation of Catalyst Poisoning Effects

As alluded to earlier in Section 1.3.1.1, the coordination of electron-donating additives such as 1,2-DME to ethylene trimerisation-active species has been shown to increase the E_a barrier for the expansion of the chromacycloheptane species, and thus favours the production of 1-hexene over higher oligomers.⁵⁶ In a similar context, Et_2Zn has previously been employed in the literature as a chain transfer agent in soluble (molecular) selective ethylene oligomerisation systems to reduce PE formation *via* transmetallation, giving rise to C_{10} - C_{22} olefins as well as a PE material with a comparatively low molecular weight.^{57,58,59} As discussed above (see Section 3.2.4.7), with a view to enhancing product selectivity in favour of 1-hexene, the $\text{Cr}\{\text{N}(\text{SiMe}_3)_2\}_x/\text{SiO}_{2-600}/\text{MMAO-12}$ initiator was treated with 1,2-DME and Et_2Zn as potential catalytic promoters. However, instead of a positive effect, the presence of either 1,2-DME or Et_2Zn resulted in the partial deactivation of the system (Figure 6).

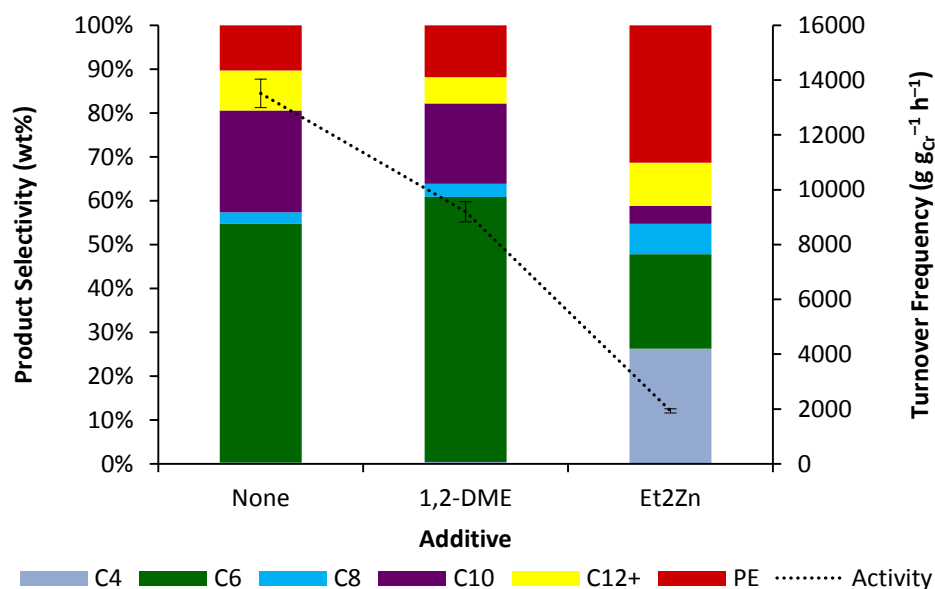


Figure 6: Effect of additives 1,2-dimethoxyethane (270 μmol) or Et_2Zn (2.7 mmol) upon catalytic performance of $\text{Cr}\{\text{N}(\text{SiMe}_3)_2\}_x/\text{SiO}_{2-600}/\text{MMAO-12}$ system. Reaction conditions: 27 μmol Cr (mass of $\text{Cr}\{\text{N}(\text{SiMe}_3)_2\}_x/\text{SiO}_{2-600}$ = 0.2 g); 410 μmol MMAO-12 (Al:Cr = 15:1); 60 mL heptane; 120 °C; 500 rpm; 0.5 h.

1,2-DME has been known to sequester alkyl aluminium reagents to yield adducts of the type $[\text{R}_x\text{AlCl}_{3-x}(1,2\text{-DME})]$.^{60,61} It is therefore postulated that residual R_3Al inherent in MMAO-12 may be abstracted, something that will likely lead to the inefficient activation of ethylene trimerisation sites, and thus lower the productivity of the silica-supported chromium initiator. While the origins of the inferior catalytic performance of $\text{Cr}\{\text{N}(\text{SiMe}_3)_2\}_x/\text{SiO}_{2-600}/\text{MMAO-12}$ in the presence of Et_2Zn remain obscure, it is tentatively proposed that the alkylating agent cleaves the active component from the catalyst support yielding an inactive molecular chromium species.

At this point, it should be highlighted that MMAO-12 and Et₂Zn were both commercially sourced as standard solutions in toluene and used as such. However, it has been shown previously that for some oligomerisation systems aromatic diluents such as toluene can act as a poison.^{62,63} With this in mind, given that the Cr{N(SiMe₃)₂}_x/SiO₂₋₆₀₀/MMAO-12 initiator fares poorly in aromatic diluents (see Section 2.2.3), it is proposed that the additional toluene from the respective MMAO-12 and Et₂Zn solutions lead to partial deactivation of the catalyst either at higher co-catalyst loadings (*i.e.* Al/Cr = 150), or indeed in the presence of Et₂Zn. To this end, the silica-supported chromium pro-initiator was activated with MMAO-12 (Al/Cr = 15) in the presence of a known volume of toluene, and screened for ethylene trimerisation (Figure 7). Although the additional toluene was found to reduce the TOF achieved by Cr{N(SiMe₃)₂}_x/SiO₂₋₆₀₀/MMAO-12, the so-called “promotor” Et₂Zn and the increased Al/Cr mole ratio of 150 both led to a much greater drop in catalytic activity, coupled with an associated switch in selectivity in favour of polymerisation. It is postulated that the increased concentration of MMAO-12 in the system at higher Al/Cr loadings may also lead to the alkylation of the Cr–O–Si linkage(s) generating an inactive molecular chromium species *in situ*, akin to the Et₂Zn additive. This is in good agreement with previous work by Varga *et al.*, who reported that an excess of methyl aluminoxane (MAO) mediated the methylation of a silica-supported titanium ethylene trimerisation-active catalyst (see Section 1.3.2.6.2)⁵⁵

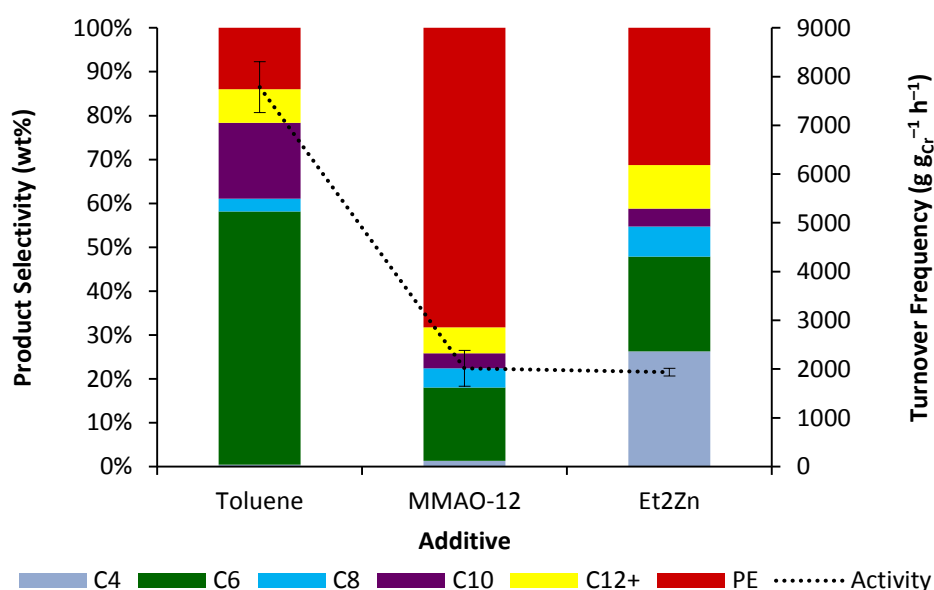


Figure 7: Effect of additives upon the catalytic performance of the Cr{N(SiMe₃)₂}_x/SiO₂₋₆₀₀/MMAO-12 initiator, where additives = toluene (1.8 mL), MMAO-12 (1.8 mL, 7 wt% toluene solution), Et₂Zn (1.8 mL, 1.5 M toluene solution). Reaction conditions: 27 μmol Cr (mass of Cr{N(SiMe₃)₂}_x/SiO₂₋₆₀₀ = 0.2 g); 410 μmol MMAO-12 (Al:Cr = 15:1); 60 mL heptane; 120 °C; 500 rpm; 0.5 h.

3.3.7 Exploring the Dependence of Decene Formation upon Hexene Concentration

It is generally accepted that 1-hexene can be reincorporated into the metallocycle mechanism mediated by soluble (molecular) selective ethylene oligomerisation systems to liberate several decene isomers.^{6,7,8} From the results described in the preceding sections of this chapter, it is clear that the production of decenes from ethylene mediated by the heterogeneous $\text{Cr}\{\text{N}(\text{SiMe}_3)_2\}_x/\text{SiO}_{2-600}/\text{MMAO-12}$ system is inherently linked to the mole ratio of 1-hexene in solution. Indeed the concentration of 1-hexene, and hence decene in the system can be manipulated using various experimental processing parameters such as chromium concentration, Al/Cr mole ratio, reaction temperature, ethylene pressure, reaction time and diluent volume. That said, this relationship is best illustrated by the concentration of hexenes and decenes afforded by the silica-supported chromium initiator at 120 °C, and at a fixed ethylene pressure (*i.e.* 8 barg) as a function of reaction time (Figure 8). This correlation provides strong evidence for the reincorporation of 1-hexene and decenes into a supported metallacyclic trimerisation manifold.

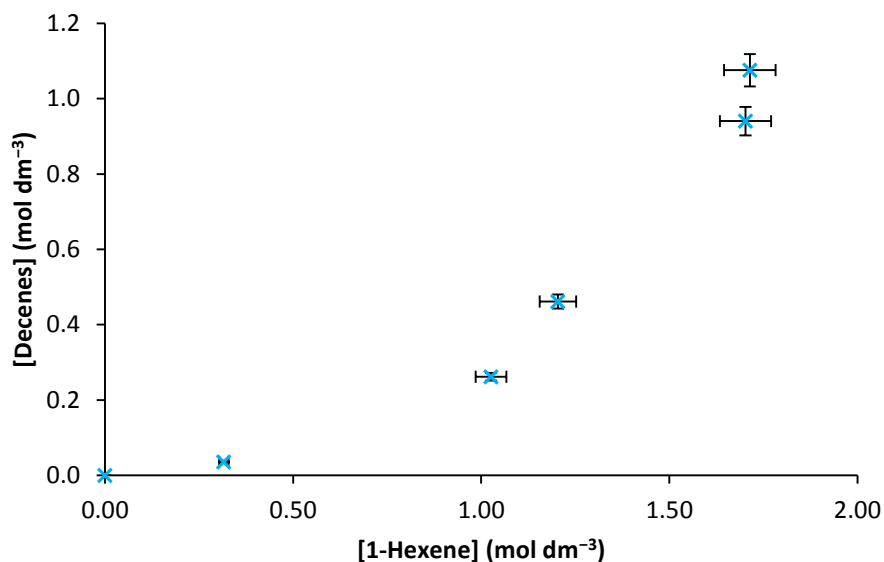


Figure 8: Concentration of hexenes and decenes in solution generated by the $\text{Cr}\{\text{N}(\text{SiMe}_3)_2\}_x/\text{SiO}_{2-600}/\text{MMAO-12}$ system as a function of time. Reaction conditions: 27 μmol Cr (mass of $\text{Cr}\{\text{N}(\text{SiMe}_3)_2\}_x/\text{SiO}_{2-600}$ = 0.2 g); 410 μmol MMAO-12 (Al:Cr = 15:1); 60 mL heptane; 120 °C; 500 rpm; 8 barg fixed ethylene pressure. Error bars represent one standard deviation.

3.4 Solution-phase NMR and DSC analyses of Organic Product Fractions Afforded by Cr{N(SiMe₃)₂}_x/SiO₂₋₆₀₀/MMAO-12

In order to more closely probe the composition of the liquid organic products (in particular the identification of isomeric products), a careful fractional distillation was attempted. To this end, the product stream obtained from an ethylene oligomerisation run mediated by Cr{N(SiMe₃)₂}_x/SiO₂₋₆₀₀/MMAO-12 (see Table 14; Entry 1) was separated, to an extent, into three fractions prior to GC-FID analysis. The first fraction (60 – 100 °C) was found to contain a mixture of hexene isomers as well as heptane, as evidenced by GC-FID. The second fraction (100 – 120 °C) consisted primarily of the heptane diluent. The final product fraction (156 – 157 °C) largely comprised C₁₀ oligomers as well as higher (C₁₂₊) olefins. Further analyses of the hexene- and decene-containing fractions were compiled using solution-phase ¹H and ¹³C NMR spectroscopy. This section will present our findings from these NMR spectroscopic analyses of the specific organic products generated during catalysis, which can be used to provide crucial mechanistic insight relevant to the silica-supported chromium initiator system.

3.4.1 Pureshift ^1H - ^{13}C HSQC NMR Spectroscopic Analysis of the Hexene-containing Distillate

Pureshift ^1H NMR spectroscopic experiments use a pulse sequence that suppresses homonuclear coupling, whilst maintaining heteronuclear coupling to simplify ^1H NMR spectra.⁶⁴ Heteronuclear single quantum correlation (HSQC) is a highly sensitive two-dimensional NMR spectroscopic technique that may be used to map heteronuclear ^1J couplings between ^1H and ^{13}C nuclei.⁶⁵ An insensitive nuclei enhanced by polarization transfer (INEPT) step may be used in combination with HSQC NMR spectroscopy to improve the signal resolution of ^{13}C nuclei.⁶⁵ By employing these Pureshift and HSQC spectroscopic techniques in tandem, vinyl resonances consistent with 1-hexene as well as internal isomers, including *cis*-2-hexene, *trans*-2-hexene and *trans*-3-hexene were all identified in the lowest-boiling distillate (60 – 100 °C) obtained from ethylene catalysed by $\text{Cr}\{\text{N}(\text{SiMe}_3)_2\}_x/\text{SiO}_2\text{-600}/\text{MMAO-12}$ (Figure 9, Table 15).^{66,67,68,69} These hexene isomers were identified based on their vinyl environments since the aliphatic region of the spectrum was dominated by resonances associated with heptane.

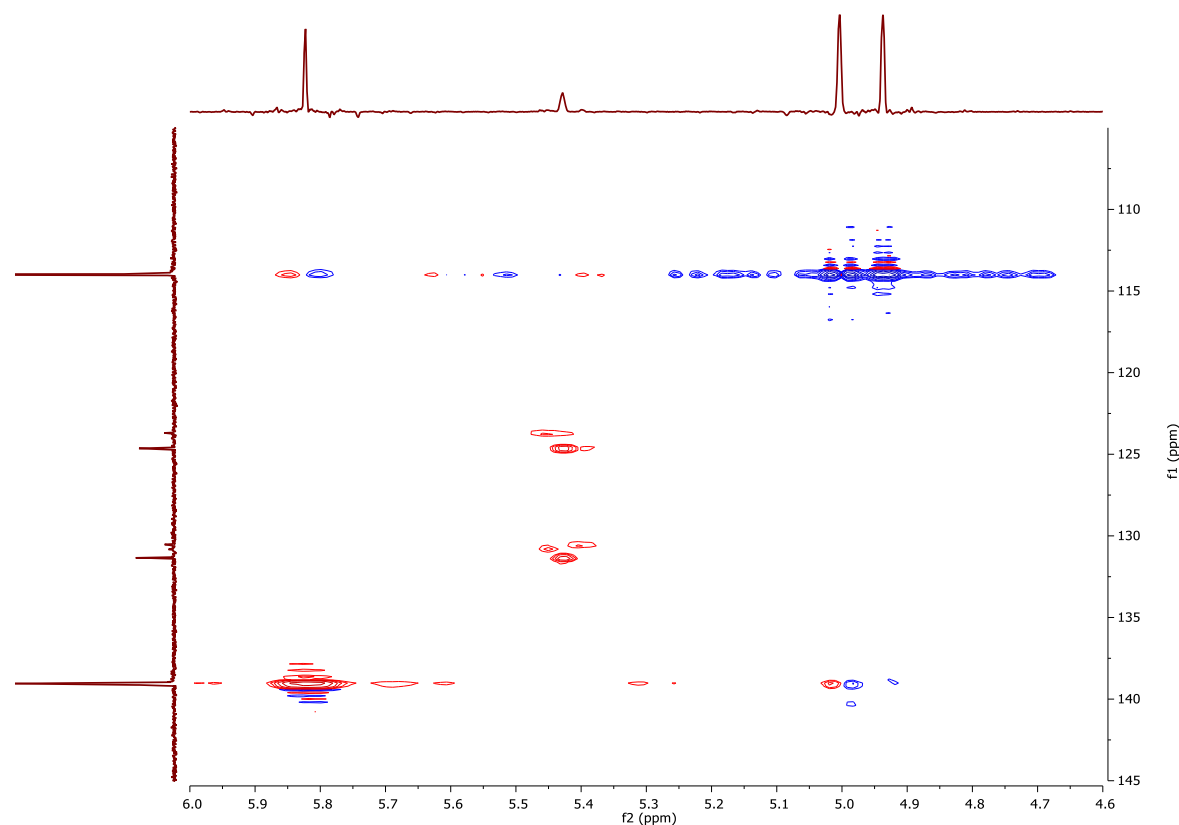
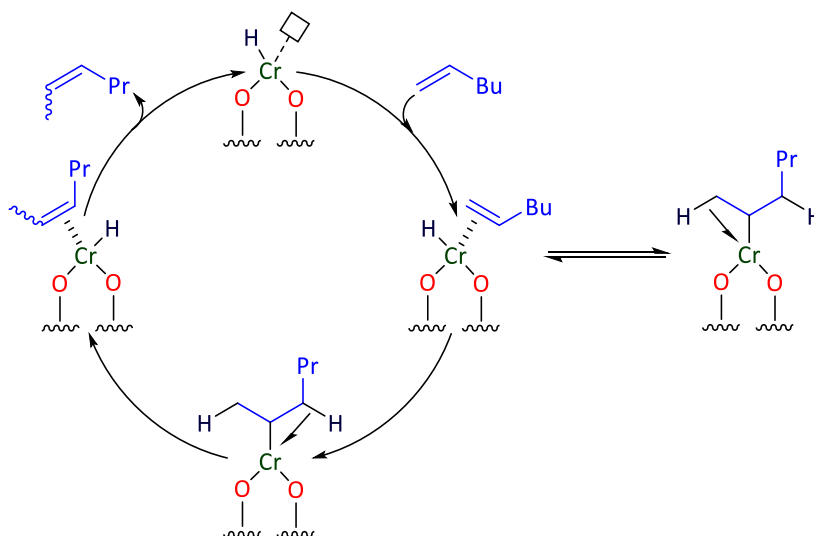


Figure 9: Pureshift ^1H - ^{13}C HSQC NMR spectrum of hexene-containing fraction (60 – 100 °C) distilled from the product stream afforded by $\text{Cr}\{\text{N}(\text{SiMe}_3)_2\}_x/\text{SiO}_2\text{-600}/\text{MMAO-12}$ ethylene oligomerisation system (see Table 14; Entry 1) over ranges 105 – 145 ppm (f1) and 4.6 – 6.0 ppm (f2); acquired at 600 (^1H) and 151 (^{13}C) MHz, referenced to CDCl_3 .
Reaction conditions: 27 μmol Cr (mass of $\text{Cr}\{\text{N}(\text{SiMe}_3)_2\}_x/\text{SiO}_2\text{-600}$ = 0.2 g); 410 μmol MMAO-12 (Al:Cr = 15:1); 30 mL heptane; 120 °C; 500 rpm; 8 barg fixed ethylene pressure; 0.5 h.

Table 15: Vinyl resonance assignments determined for various hexene isomers present in the distillate of the liquid fraction (see Table 14; Entry 1; 60 – 100 °C) experimentally-derived using Pureshift ^1H - ^{13}C HSQC NMR spectroscopy; acquired at 600 (^1H) and 151 (^{13}C) MHz, referenced to CDCl_3 .

Hexene Isomer	Environment	Integration	Chemical Shift (ppm)	
			^1H	^{13}C
1-Hexene	$\text{CHH}=\text{CH}$	1H	4.94	114.2
	$\text{CHH}=\text{CH}$	1H	5.00	114.2
	$\text{CHH}=\text{CH}$	1H	5.82	139.3
cis-2-Hexene	$\text{CH}_3\text{CH}=\text{CHCH}_2$	1H	5.40	124.0
	$\text{CH}_3\text{CH}=\text{CHCH}_2$	1H	5.45	130.8
trans-2-hexene	$\text{CH}_3\text{CH}=\text{CHCH}_2$	1H	5.43	124.9
	$\text{CH}_3\text{CH}=\text{CHCH}_2$	1H	5.43	131.6
trans-3-Hexene	$\text{CH}_2\text{CH}=\text{CHCH}_2$	2H	5.45	131.1

The assignment of vinyl resonances shown in Table 15 can be attributed to the step-wise “chain-walking” isomerisation of 1-hexene to the more thermodynamically stable *trans*-3-hexene isomer *via* a 2,1-insertion mechanism, presumably mediated by a supported chromium hydride species at the surface of $\text{Cr}\{\text{N}(\text{SiMe}_3)_2\}_x/\text{SiO}_{2-600}/\text{MMAO-12}$ (Scheme 6).⁷⁰ These findings are broadly in agreement with previous work involving the somewhat related Phillips heterogeneous Cr/SiO_2 ethylene polymerisation catalyst.^{48,50}



Scheme 6: 1-Hexene isomerisation *via* a “chain-walking” 2,1-insertion mechanism, adapted from Heck *et al.*, 1961⁷⁰

3.4.2 $^{13}\text{C}\{^1\text{H}\}$ NMR Spectroscopic Analysis of the Decene-containing Distillate

Vinyl resonances that are consistent with 1-decene, *cis*-4-decene, 5-decene, 5-methyl-1-nonene, 5-methylene-nonane, 4-ethyl-1-octene and 4-ethylene-octane were present in the solution-phase $^{13}\text{C}\{^1\text{H}\}$ NMR spectrum of the highest-boiling fraction (156 – 157 °C) distilled from the liquid product stream obtained from $\text{Cr}\{\text{N}(\text{SiMe}_3)_2\}_x/\text{SiO}_2\text{-600}/\text{MMAO-12}$ -mediated ethylene trimerisation (Figure 10; Table 16).^{6,7,8,52}

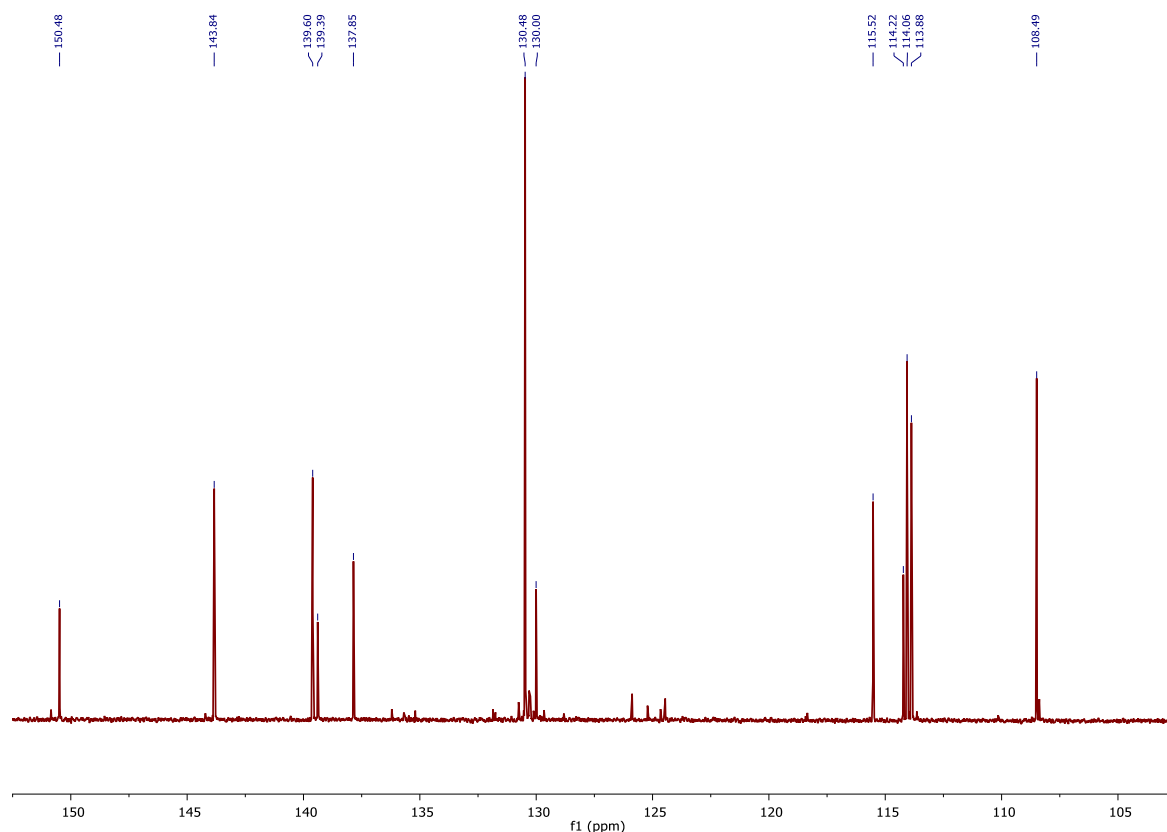
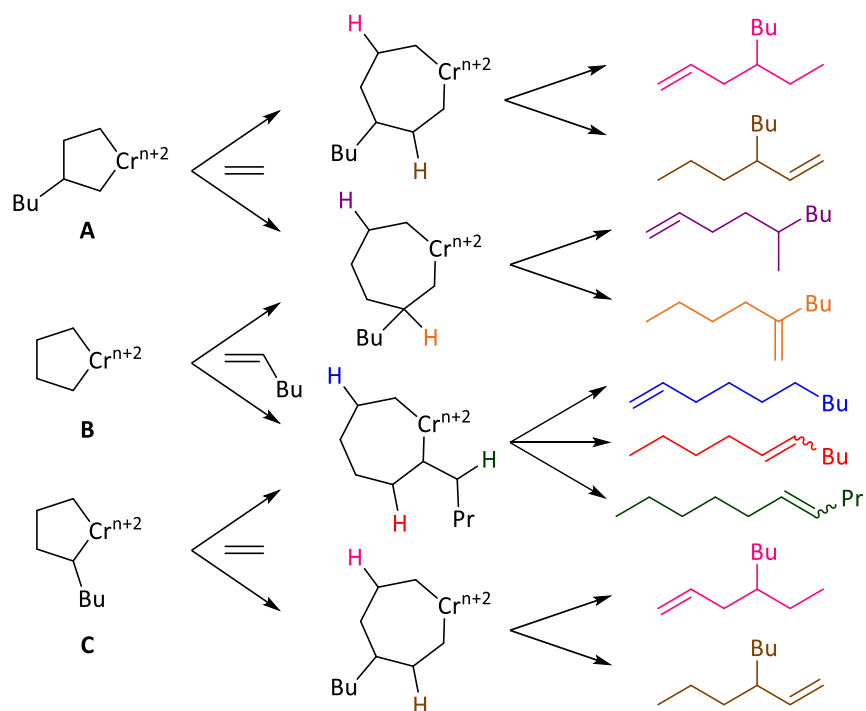


Figure 10: The 100 – 155 ppm region of the $^{13}\text{C}\{^1\text{H}\}$ NMR spectrum of the decene-containing fraction (156 – 157 °C) distilled from the product stream afforded by the $\text{Cr}\{\text{N}(\text{SiMe}_3)_2\}_x/\text{SiO}_2\text{-600}/\text{MMAO-12}$ system (see Table 14; Entry 1); acquired at 151 MHz, referenced to CDCl_3 . Reaction conditions: 27 μmol Cr (mass of $\text{Cr}\{\text{N}(\text{SiMe}_3)_2\}_x/\text{SiO}_2\text{-600}$ = 0.2 g); 410 μmol MMAO-12 (Al:Cr = 15:1); 30 mL heptane; 120 °C; 500 rpm; 8 barg fixed ethylene pressure; 0.5 h.

Table 16: Vinyl resonance assignments determined for various decene isomers present in the distillate of the liquid fraction (see Table 14; Entry 1; 156 – 157 °C) experimentally-derived from solution-phase $^{13}\text{C}\{^1\text{H}\}$ NMR spectroscopy; acquired at 151 MHz and referenced to CDCl_3 .

Decene Isomer	$^{13}\text{C}\{^1\text{H}\}$ NMR Chemical Shift(s) (ppm)	
1-Decene	114.2	139.4
<i>cis</i> -4-decene	130.0	130.5
5-Decene	130.5	-
5-Methyl-1-nonene	114.1	139.6
5-methylene-nonane	108.5	150.5
4-Ethyl-1-octene	115.5	137.9
4-Ethylene-octane	113.9	143.8

Notably, the $^{13}\text{C}\{^1\text{H}\}$ vinyl resonances associated with 1-decene, *cis*-4-decene, 5-decene, 5-methyl-1-nonene, 5-methylene-nonane, 4-ethyl-1-octene and 4-ethylene-octane outlined in Table 16 are in good agreement with prior work that studied soluble (molecular) selective ethylene oligomerisation systems.^{6,7,8} Consequently, it is proposed that the formation of these decene isomers also facilitated by the heterogeneous $\text{Cr}\{\text{N}(\text{SiMe}_3)_2\}_x/\text{SiO}_{2-600}/\text{MMAO-12}$ initiator described in this thesis can be attributed to a supported variant of the metallacycle mechanism (Scheme 7). While it may be true that all seven isomers of decene afforded by the silica-supported chromium initiator may originate from the 2- and 3-butyl chromacyclopentane intermediates shown below (**A** and **C**), the coordination and insertion of 1-hexene into a chromacyclopentane species (**B**) cannot be ruled out at this stage.



Scheme 7: Decene formation *via* metallacycle-based ethylene/1-hexene co-trimerisation^{6,7,8}

3.4.3 Analysis of Polyethylene By-product of Ethylene Oligomerisation Testing Mediated by Cr{N(SiMe₃)₂}_x/SiO₂₋₆₀₀/MMAO-12

The nature and composition of the polyethylene (PE) materials afforded by the heterogeneous Cr{N(SiMe₃)₂}_x/SiO₂₋₆₀₀/MMAO-12 ethylene trimerisation system was of interest in order to determine the relative degree of incorporation of 1-hexene into the polymer backbone. Polymers are routinely analysed using a combination of gel permeation chromatography (GPC) and ¹³C NMR spectroscopy to determine their mass- (M_w) and number-average (M_n) molar mass, dispersity index (Đ_M; M_w/M_n), and relative degree of branching.^{47,49} These solution-phase techniques, however, are limited by the solubility of the polymer sample. Since the solid by-products afforded by the Cr{N(SiMe₃)₂}_x/SiO₂₋₆₀₀/MMAO-12 initiator packages screened herein were not soluble in 1,2,4-trichlorobenzene, a solvent widely employed for the analysis of PE, both GPC and NMR spectroscopic analyses were not possible.⁷¹ Consequently, these solid PE by-products of heterogeneous ethylene trimerisation were analysed using differential scanning calorimetry (DSC).^{49,72,73,74} The melting point (T_m) and enthalpy of melting (ΔH_m) can be measured directly, with the latter being used to calculate the percentage crystallinity (χ_c) of the polymer sample. The ΔH_m is determined by integrating the area under the DSC heat curve, which may then be divided by the value of ΔH_m^o for a literature standard 100% crystalline PE material (*i.e.* 273 J g⁻¹),⁷⁵ and subsequently multiplied by 100 to calculate χ_c as a percentage (Equation 1).⁴⁹

Equation 1: Definition of sample percentage crystallinity (χ_c), as reported by Nenu *et al.*, 2007⁴⁹

$$\% \chi_c = \frac{\Delta H_m}{\Delta H_m^o} \times 100 = \frac{\Delta H_m}{273 \text{ J g}^{-1}} \times 100$$

The polymeric by-products of the heterogeneous Cr{N(SiMe₃)₂}_x/SiO₂₋₆₀₀/MMAO-12 ethylene trimerisation batch process all exhibited a T_m between 119.4 and 136.6 °C. According to the literature, values of T_m in this range are indicative of high molecular weight polyethylene (HMWPE).^{49,72,73} Attempts were then made to determine the ΔH_m and hence %χ_c of each polymer. Unfortunately, however, the values obtained exhibited large variations between samples, which despite undertaking repetitions could not be reduced. The semi-continuous line shape of the DSC heat cycle (Figure 11) meant that integrating the area under the curve relied overly on human judgement, and was therefore prone to error. This effect has been ascribed to account for the considerable variation in ΔH_m and χ_c values between samples. As an illustrated example, we have reported a comparative study of the DSC profiles of three HMWPE samples afforded by the heterogeneous Cr{N(SiMe₃)₂}_x/SiO₂₋₆₀₀/MMAO-12 ethylene trimerisation batch process under identical test conditions (Table 17).

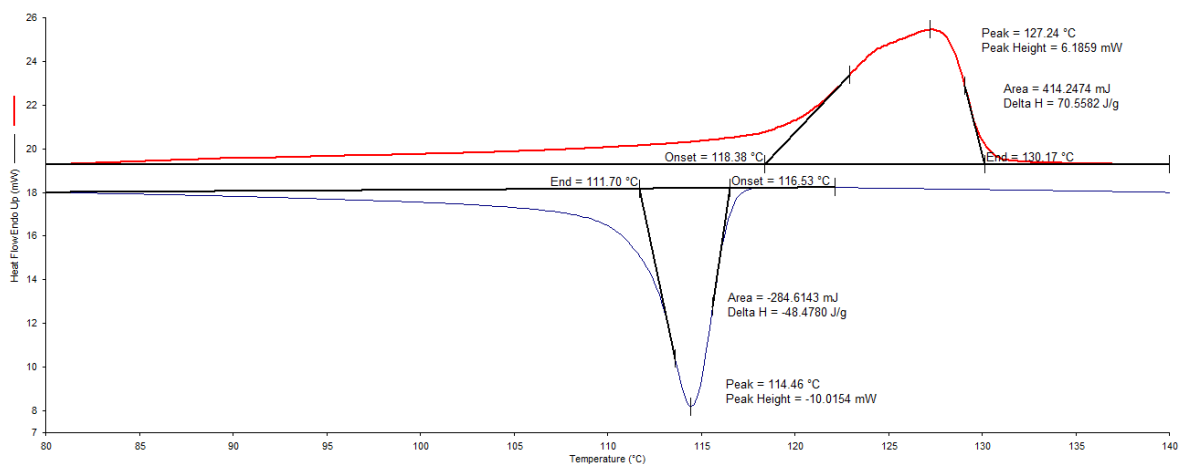


Figure 11: Representative DSC profile of high molecular weight polyethylene afforded by the heterogeneous $\text{Cr}\{\text{N}(\text{SiMe}_3)_2\}_x/\text{SiO}_{2-600}/\text{MMAO-12}$ ethylene trimerisation initiator system (see Section 3.2.1; Table 1; Run 1). Reaction Conditions: 27 μmol Cr (mass of $\text{Cr}\{\text{N}(\text{SiMe}_3)_2\}_x/\text{SiO}_{2-600}$ = 0.2 g), 410 μmol MMAO-12 (Al:Cr = 15:1), 60 mL heptane, 120 °C, 500 rpm, 8 barg fixed ethylene pressure, 0.5 h.

Table 17: Comparison of experimentally-derived T_m , ΔH_m and $\% \chi_c$ values of the high molecular weight polyethylene generated by the heterogeneous $\text{Cr}\{\text{N}(\text{SiMe}_3)_2\}_x/\text{SiO}_{2-600}/\text{MMAO-12}$ initiator (see Section 3.2.1; Table 1; Runs 1 – 3). Reaction Conditions: 27 μmol Cr (mass of $\text{Cr}\{\text{N}(\text{SiMe}_3)_2\}_x/\text{SiO}_{2-600}$ = 0.2 g), 410 μmol MMAO-12 (Al:Cr = 15:1), 60 mL heptane, 120 °C, 500 rpm, 8 barg fixed ethylene pressure; 0.5 h.

Run	T_m (°C)	ΔH_m (J/g)	$\% \chi_c$
1	127	71	26
2	127	126	46
3	124	156	57

While the ΔH_m and χ_c values (Table 17) do not offer any conclusive evidence as to the structure and composition of the polymer obtained, it is postulated that the solid afforded by $\text{Cr}\{\text{N}(\text{SiMe}_3)_2\}_x/\text{SiO}_{2-600}/\text{MMAO-12}$ (Runs 1 – 3) is an amorphous high molecular weight polyethylene (HMWPE) that contains butyl branches arising from ethylene/1-hexene co-polymerisation. This assignment is based on the similarity of the semi-continuous line shape of the DSC heat profile as reported by Nenu and co-workers,⁷⁶ as well as the T_m range exhibited by the polymer.^{49,72,73}

3.5 Conclusions

This chapter examined the influence of various experimental parameters including chromium concentration, Al/Cr mole ratio, reaction temperature, ethylene pressure, reaction time, diluent volume, and the effect of so-called “performance enhancing additives” on the productivity and selectivity of the $\text{Cr}\{\text{N}(\text{SiMe}_3)_2\}_x/\text{SiO}_{2-600}/\text{MMAO-12}$ ethylene trimerisation initiator. Employing a modified literature protocol,⁴⁰ $\text{Cr}\{\text{N}(\text{SiMe}_3)_2\}_x/\text{SiO}_{2-600}$ activated with MMAO-12 (Al:Cr = 15:1) at 120 °C in the slurry-phase in heptane, and at a constant ethylene working pressure of 30 barg for 30 minutes generated 49 ± 1 wt% hexenes with an overall activity of $68251 \pm 1544 \text{ g g}_{\text{Cr}}^{-1} \text{ h}^{-1}$. According to GC-FID analysis, the linear alpha olefin (LAO) purity of the hexene product fraction was determined to be 91 ± 1 wt%. Such high selectivity towards 1-hexene has been attributed to a supported variant of the metallacycle mechanism.^{1,2} This is consistent with an approximate first order dependence of the silica-supported chromium initiator with respect to ethylene concentration, where the RDS is the step in which expansion of the chromacyclopentane intermediate to the chromacycloheptane species takes place.^{28,31,33,39,41,42,43,44,45}

Based on Pureshift ^1H - ^{13}C HSQC NMR spectroscopic experiments, we have confirmed that the C_6 product fraction comprise 1-hexene as well as internal isomers, including *cis*-2-hexene, *trans*-2-hexene and *trans*-3-hexene. Consequently, to account for this partial product slate, it is proposed that 1-hexene is isomerised to the more thermodynamically favourable *trans*-3-hexene via a competing “chain-walking” 2,1-insertion mechanism *in situ*,⁷⁰ something that could be potentially mediated by a supported chromium hydride species.^{48,50}

Under batch reaction conditions, the most prominent side product of ethylene trimerisation mediated by $\text{Cr}\{\text{N}(\text{SiMe}_3)_2\}_x/\text{SiO}_{2-600}/\text{MMAO-12}$ is consistently a mixture of several decene isomers (23 ± 1 wt%). According to solution-phase $^{13}\text{C}\{^1\text{H}\}$ NMR spectroscopy, the C_{10} fraction consisted of 1-decene, *cis*-4-decene, 5-decene, 5-methyl-1-nonene, 5-methylene-nonane, 4-ethyl-1-octene and 4-ethylene-octane. These decene isomers are consistent with those afforded by operation of a secondary metallacycle-based ethylene/1-hexene co-trimerisation reaction mechanism.^{6,7,8} In all cases, the formation of liquid organic products through ethylene oligomerisation mediated by the $\text{Cr}\{\text{N}(\text{SiMe}_3)_2\}_x/\text{SiO}_{2-600}/\text{MMAO-12}$ system were accompanied by amorphous HMWPE materials that contain butyl side chains as a result of the *in situ* co-polymerisation of ethylene and 1-hexene.⁷⁶ The first order dependence of polymer formation with respect to ethylene is consistent with a classical Cossee-Arlman chain growth process being in competition with the aforementioned metallacyclic reaction manifold.^{3,4,5}

3.6 References

- (1) R. M. Manyik, W. E. Walker, T. P. Wilson, *J. Catal.*, **1977**, *47*, 197-209.
- (2) J. R. Briggs, *J. Chem. Soc., Chem. Commun.*, **1989**, *11*, 674-675.
- (3) P. Cossee, *J. Catal.*, **1964**, *3*, 80-88.
- (4) E. J. Arlman, *J. Catal.*, **1964**, *3*, 89-98.
- (5) E. J. Arlman, P. Cossee, *J. Catal.*, **1964**, *3*, 99-104.
- (6) M. J. Overett, K. Blann, A. Bollmann, J. T. Dixon, D. Haasbroek, E. Killian, H. Maumela, D. S. McGuinness, D. H. Morgan, *J. Am. Chem. Soc.*, **2005**, *127*, 10723-10730.
- (7) L. H. Do, J. A. Labinger, J. E. Bercaw, *Organometallics*, **2012**, *31*, 5143-5149.
- (8) T. M. Zilbershtein, V. A. Kardash, V. V. Suvorova, A. K. Golovko, *Appl. Catal. A: Gen.*, **2014**, *475*, 371-378.
- (9) Anonymous, In *Studies in Surface Science and Catalysis*; E. F. Vansant, P. Van Der Voort, K. C. Vrancken, Eds.; Elsevier: 1995; Vol. 93, p 93-126.
- (10) Anonymous, In *Studies in Surface Science and Catalysis*; E. F. Vansant, P. Van Der Voort, K. C. Vrancken, Eds.; Elsevier: 1995; Vol. 93, p 59-77.
- (11) L. T. Zhuravlev, *Colloids Surf. A*, **2000**, *173*, 1-38.
- (12) T. Monoi, H. Ikeda, H. Ohira, Y. Sasaki, *Polym. J.*, **2002**, *34*, 461-465.
- (13) D. Gajan, C. Copéret, *New J. Chem.*, **2011**, *35*, 2403-2409.
- (14) F. Rascon, R. Wischert, C. Copéret, *Chem. Sci.*, **2011**, *2*, 1449-1456.
- (15) Y. Chen, E. Callens, E. Abou-Hamad, N. Merle, A. J. P. White, M. Taoufik, C. Copéret, E. Le Roux, J.-M. Basset, *Angew. Chem. Int. Ed.*, **2012**, *51*, 11886-11889.
- (16) P. Laurent, L. Veyre, C. Thieuleux, S. Donet, C. Copéret, *Dalton Trans.*, **2013**, *42*, 238-248.
- (17) M. K. Samantaray, E. Callens, E. Abou-Hamad, A. J. Rossini, C. M. Widdifield, R. Dey, L. Emsley, J.-M. Basset, *J. Am. Chem. Soc.*, **2013**, *136*, 1054-1061.
- (18) M. P. Conley, C. Copéret, C. Thieuleux, *ACS Catal.*, **2014**, *4*, 1458-1469.
- (19) C. Copéret, V. Mougél, *Chem. Sci.*, **2014**, *5*, 2475-2481.
- (20) B. Werghi, A. Bendjeriou-Sedjerari, J. Sofack-Kreutzer, A. Jedidi, E. Abou-Hamad, L. Cavallo, J.-M. Basset, *Chem. Sci.*, **2015**, *6*, 5456-5465.
- (21) B. Hamzaoui, J. D. A. Pelletier, E. Abou-Hamad, J.-M. Basset, *Chem. Commun.*, **2016**, *52*, 4617-4620.
- (22) R. Saliger, T. Heinrich, T. Gleissner, J. Fricke, *J. Non-Cryst. Solids*, **1995**, *186*, 113-117.
- (23) B. M. Weckhuysen, R. Ramachandra Rao, J. Pelgrims, R. A. Schoonheydt, P. Bodart, G. Debras, O. Collart, P. Van Der Voort, E. F. Vansant, *Chem. Eur. J.*, **2000**, 2960-2970.
- (24) G. Henrici-Olivé, S. Olivé, *Angew. Chem. Int. Ed. Engl.*, **1971**, *10*, 776-786.
- (25) K. Blann, A. Bollmann, J. T. Dixon, F. M. Hess, E. Killian, H. Maumela, D. H. Morgan, A. Neveling, S. Otto, M. J. Overett, *Chem. Commun.*, **2005**, 620-621.
- (26) E. Killian, K. Blann, A. Bollmann, J. T. Dixon, S. Kuhlmann, M. C. Maumela, H. Maumela, D. H. Morgan, P. Nongodlwana, M. J. Overett, M. Pretorius, K. Höfener, P. Wasserscheid, *J. Mol. Catal. A: Chem.*, **2007**, *270*, 214-218.
- (27) M. J. Overett, K. Blann, A. Bollmann, R. de Villiers, J. T. Dixon, E. Killian, M. C. Maumela, H. Maumela, D. S. McGuinness, D. H. Morgan, A. Rucklidge, A. M. Z. Slawin, *J. Mol. Catal. A: Chem.*, **2008**, *283*, 114-119.
- (28) W. J. van Rensburg, C. Grové, J. P. Steynberg, K. B. Stark, J. J. Huyser, P. J. Steynberg, *Organometallics*, **2004**, *23*, 1207-1222.
- (29) S. J. Schofer, M. W. Day, L. M. Henling, J. A. Labinger, J. E. Bercaw, *Organometallics*, **2006**, *25*, 2743-2749.
- (30) R. Walsh, D. H. Morgan, A. Bollmann, J. T. Dixon, *Appl. Catal. A: Gen.*, **2006**, *306*, 184-191.

- (31) A. Wöhl, W. Müller, S. Peitz, N. Peulecke, B. R. Aluri, B. H. Müller, D. Heller, U. Rosenthal, M. H. Al-Hazmi, F. M. Mosa, *Chem. Eur. J.*, **2010**, *16*, 7833-7842.
- (32) S. Tang, Z. Liu, X. Yan, N. Li, R. Cheng, X. He, B. Liu, *Appl. Catal. A: Gen.*, **2014**, *481*, 39-48.
- (33) G. J. P. Britovsek, D. S. McGuinness, T. S. Wierenga, C. T. Young, *ACS Catal.*, **2015**, *5*, 4152-4166.
- (34) H. Hagimoto, T. Shiono, T. Ikeda, *Macromolecules*, **2002**, *35*, 5744-5745.
- (35) H. Hagimoto, T. Shiono, T. Ikeda, *Macromol. Chem. Phys.*, **2004**, *205*, 19-26.
- (36) R. Tanaka, T. Kawahara, Y. Shinto, Y. Nakayama, T. Shiono, *Macromolecules*, **2017**, *50*, 5989-5993.
- (37) A. Sahgal, H. M. La, W. Hayduk, *Can. J. Chem. Eng.*, **1978**, *56*, 354-357.
- (38) A. Dashti, S. H. Mazloumi, A. Akbari, H. R. Ahadiyan, A. R. Emami, *J. Chem. Eng. Data*, **2016**, *61*, 693-697.
- (39) S. Kuhlmann, C. Paetz, C. Hägele, K. Blann, R. Walsh, J. T. Dixon, J. Scholz, M. Haumann, P. Wasserscheid, *J. Catal.*, **2009**, *262*, 83-91.
- (40) T. Monoi, Y. Sasaki, *J. Mol. Catal. A: Chem.*, **2002**, *187*, 135-141.
- (41) R. D. Köhn, M. Haufe, G. Kociok-Köhn, S. Grimm, P. Wasserscheid, W. Keim, *Angew. Chem. Int. Ed.*, **2000**, *39*, 4337-4339.
- (42) P. J. W. Deckers, B. Hessen, J. H. Teuben, *Organometallics*, **2002**, *21*, 5122-5135.
- (43) H. Hagen, *Ind. Eng. Chem. Res.*, **2006**, *45*, 3544-3551.
- (44) P. H. M. Budzelaar, *Can. J. Chem.*, **2009**, *87*, 832-837.
- (45) G. J. Britovsek, D. S. McGuinness, *Chemistry*, **2016**, *22*, 16891-16896.
- (46) J. P. Hogan, R. L. Banks, **1958**, *US22825721*, Phillips Petroleum Company.
- (47) H. Ikeda, T. Monoi, Y. Sasaki, *J. Polym. Sci., Part A: Polym. Chem.*, **2003**, *41*, 413-419.
- (48) R. D. Köhn, D. Smith, D. Lilge, S. Mihan, F. Molnar, M. Prinz, In *Beyond Metallocenes*; ACS Symposium Series: Washington DC, 2003; Vol. 857, p 88-100.
- (49) C. N. Nenu, P. Bodart, B. M. Weckhuysen, *J. Mol. Catal. A: Chem.*, **2007**, *269*, 5-11.
- (50) M. P. McDaniel, *Adv. Catal.*, **2010**, *53*, 123-606.
- (51) A. Carter, S. A. Cohen, N. A. Cooley, A. Murphy, J. Scutt, D. F. Wass, *Chem. Commun.*, **2002**, 858-859.
- (52) Y. Suzuki, S. Kinoshita, A. Shibahara, S. Ishii, K. Kawamura, Y. Inoue, T. Fujita, *Organometallics*, **2010**, *29*, 2394-2396.
- (53) J. A. Moulijn, A. E. van Diepen, F. Kapteijn, *Appl. Catal. A: Gen.*, **2001**, *212*, 3-16.
- (54) N. Peulecke, B. H. Müller, S. E. Peitz, B. R. Aluri, U. Rosenthal, A. I. Wohl, W. Müller, M. H. Al-Hazmi, F. M. Mosa, *Chem. Cat. Chem.*, **2010**, *2*, 1079-1081.
- (55) V. Varga, T. Hodik, M. Lamac, M. Horacek, A. Zikal, N. Zilkova, W. O. Parker Jr., J. Pinkas, *J. Org. Chem.*, **2015**, *777*, 57-66.
- (56) Y. Qi, Q. Dong, L. Zhong, Z. Liu, P. Qiu, R. Cheng, X. He, J. Vanderbilt, B. Liu, *Organometallics*, **2010**, *29*, 1588-1602.
- (57) K.-s. Son, R. M. Waymouth, *Organometallics*, **2010**, *29*, 3515-3520.
- (58) M. J. Hanton, D. M. Smith, W. F. Gabrielli, M. W. Kelly, **2011**, *WO2011048527A1*, Sasol Technology Ltd.
- (59) J. E. Radcliffe, A. S. Batsanov, D. M. Smith, J. A. Scott, P. W. Dyer, M. J. Hanton, *ACS Catal.*, **2015**, *5*, 7095-7098.
- (60) N. C. Means, C. M. Means, S. G. Bott, J. L. Atwood, *Inorg. Chem.*, **1987**, *26*, 1466-1468.
- (61) W. R. H. Wright, A. S. Batsanov, J. A. K. Howard, R. P. Tooze, M. J. Hanton, P. W. Dyer, *Dalton Trans.*, **2010**, *39*, 7038-7045.
- (62) K. Blann, A. Bollmann, H. de Bod, J. T. Dixon, E. Killian, P. Nongodlwana, M. C. Maumela, H. Maumela, A. E. McConnell, D. H. Morgan, M. J. Overett, M. Prétorius, S. Kuhlmann, P. Wasserscheid, *J. Catal.*, **2007**, *249*, 244-249.
- (63) A. Jabri, C. B. Mason, Y. Sim, S. Gambarotta, T. J. Burchell, R. Duchateau, *Angew. Chem. Int. Ed.*, **2008**, *47*, 9717-9721.

- (64) J. A. Aguilar, G. A. Morris, A. M. Kenwright, *RSC Adv.*, **2014**, *4*, 8278-8282.
- (65) N. E. Jacobsen, *NMR Spectroscopy Explained: Simplified Theory, Applications and Examples for Organic Chemistry and Structural Biology*; Wiley-Blackwell, 2007.
- (66) T. Yamaji, T. Saito, K. Hayamizu, M. Yanagisawa, O. Yamamoto, "Spectral Database for Organic Compounds", <http://sdfs.db.aist.go.jp>, 18/10/17.
- (67) A. R. Katritzky, A. M. El-Mowafy, *J. Org. Chem.*, **1982**, *47*, 3506-3511.
- (68) M. Audit, P. Demerseman, N. Goasdoue, N. Platzer, *Org. Magn. Reson.*, **1983**, *21*, 698-705.
- (69) R. L. Pederson, I. M. Fellows, T. A. Ung, H. Ishihara, S. P. Hajela, *Adv. Synth. Catal.*, **2002**, *344*, 728 - 735.
- (70) R. F. Heck, D. S. Breslow, *J. Am. Chem. Soc.*, **1961**, *83*, 4023-4027.
- (71) A. Bivens, "Polymer-to-Solvent Reference Table for GPC/SEC", Agilent Technologies, Inc., 2016.
- (72) L. C. Thomas, "Characterization of Melting Phenomena in Linear Low Density Polyethylene by Modulated DSC", TA Instruments, Inc.
- (73) A. Prasad, *Polym. Eng. Sci.*, **1998**, *38*, 1716-1728.
- (74) Y. Chen, R. Credendino, E. Callens, M. Atiqullah, M. A. Al-Harhi, L. Cavallo, J.-M. Basset, *ACS Catal.*, **2013**, *3*, 1360-1364.
- (75) Y. M. Dong, *The Practical Analysis Technology of Polymer Materials*; Petrochemical Industry Press: Beijing, 1979.
- (76) C. N. Nenu, B. M. Weckhuysen, *J. Chem. Soc., Chem. Commun.*, **2005**, 1865-1867.

This page has been intentionally left blank

Chapter 4:
Experimental

4.1 General Experimental Considerations

Unless stated otherwise, all manipulations were carried out under an atmosphere of dry nitrogen using standard Schlenk line techniques, or in an Innovative Technologies nitrogen-filled glovebox. All glassware was oven-dried before use. Dry solvents were obtained from an Innovative Technologies Solvent Purification System and degassed prior to use by three freeze-pump-thaw cycles, unless otherwise stated. Pentane, 1-hexene, heptane, methylcyclohexane, nonane and 1,2-dimethoxyethane (1,2-DME) were dried over calcium hydride, distilled and degassed. Chlorobenzene was dried over phosphorus pentoxide, distilled and degassed. All other chemicals, unless stated otherwise, were obtained from Sigma Aldrich or Alfa Aesar, and were used without further purification.

Evonik Aeroperl 300/30 fumed silica obtained from Evonik Industries (described herein as SiO₂), Alfa Aesar γ -alumina (1/8" pellets ground and sieved to <250 μ m; described herein as γ -Al₂O₃), and Sigma Aldrich silica-alumina grade 135 catalyst support (13 wt% Al₂O₃;¹ described herein as SiO₂-Al₂O₃) were used as catalyst supports.

The complex Cr{N(SiMe₃)₂}₃ was synthesised according to the protocol reported previously by Bradley *et al.*,² and isolated as a dark green air-/moisture-sensitive solid, which was handled under an inert atmosphere.

Anal. Calc. for C₁₈H₅₄N₃CrSi₆: C, 40.55; H 10.21; N 7.88%. Found: C, 40.51; H, 10.30; N, 7.71%.

IR (KBr, Nujol ν_{\max} /cm⁻¹) 1263, 1254, 910, 860, 794, 760, 708, 678, 619 (lit.,³ 1260, 1250, 902, 865, 840, 820, 790, 758, 708, 676, 620).

Raman (solid, 532 nm, ν_{\max} /cm⁻¹) 2956, 2898, 1260, 1240, 904, 855, 805, 728, 707, 679, 636, 424, 382.

*i*Bu₃Al (25 wt% solution in toluene), isobutyl aluminoxane (IBAO; 0.9 M solution in toluene), Me₃Al (2M solution in toluene), methyl aluminoxane (MAO; 10 wt% solution in toluene), modified methyl aluminoxane {MMAO-12; 7 wt% solution in toluene; [(CH₃)_{0.95}(n-C₈H₁₇)_{0.05}AlO]_n}, and Et₂AlCl (25 wt% in toluene) were used as co-catalysts.

1,2-DME and Et₂Zn (1.5 M solution in toluene) were employed as potential "promoters".

Ethylene (BOC) was passed through a moisture scrubbing column containing molecular sieves (Sigma Aldrich; 3A, 4A and 13X) that had previously been activated at 400 °C for three hours under dynamic vacuum (0.05 mbar), before being cooled to room temperature (RT) and stored under ethylene.

Brunauer Emmett Teller (BET) specific surface area (SSA) and Barrett Joyner Halenda (BJH) pore size and volume analyses were compiled using a Micromeritics instrument either by S. Ridley and R. Fletcher of Johnson Matthey Process Technologies (Chilton), or Dr L. Li (Durham University).

Differential scanning calorimetric (DSC) analyses were completed by D. Carswell of Durham University using a TA Instruments Q1000 with a nitrogen purge gas. Samples were made up in a standard aluminium pan and run using a scan rate of 10 °C min⁻¹ between 30 and 300 °C.

Electron paramagnetic resonance (EPR) spectra were acquired by Dr W. Myers at the centre for advanced electron spin resonance (CAESR; University of Oxford). Continuous-wave (CW) EPR data collection involved use of a Bruker BioSpin EMXmicro spectrometer with a Premium bridge and a cylindrical TE₀₁₁ mode ER4122 SHQE-W resonator with a loaded Q-value of ~8300. Samples were loose powder and filled to the height of the resonator. Temperature was maintained by an Oxford Instruments ESR-900 cryostat with liquid helium transferred by a LLT-600 transfer line and the temperature was stabilized by an ITC-503S instrument temperature controller. Microwave power dependence was tested at each temperature to ensure non-saturating conditions. Pulsed EPR was collected on a Bruker BioSpin EleXsys II E580 spectrometer operating with an ER 4118X-MD5W1 sapphire dielectric resonator in the TE₀₁₆ mode. The continuous flow cryostat was an Oxford Instruments CF9350, with an additional Sogevac SV40B pump used on the back of the LLT-600 transfer to reach 2.5 K. Temperature was maintained with an Oxford Instruments Mercury temperature controller.

Elemental analysis (CHN) was carried out by S. Boyer (London Metropolitan University).

Gas chromatographic (GC) analyses were run using a Perkin Elmer Clarus 400 system equipped with a paraffins, olefins, naphthalenes and aromatics (PONA; 50 m × 0.20 mm × 0.50 μm) capillary column. Analytes were detected using a flame ionisation detector (FID). The oven temperature was maintained at 40 °C for 10 minutes, before the temperature was increased to 170 °C at a rate of 20 °C min⁻¹; this temperature was maintained for 5 minutes. Subsequently, the capillary column was heated further to 300 °C, again at a rate of 20 °C min⁻¹. The temperature was maintained at 300 °C for 12 minutes, prior to being allowed to cool to 40 °C. The total run time for GC-FID analyses was 40 minutes.

Inductively coupled plasma-optical emission spectroscopic (ICP-OES) analyses were measured either by D. Scott and R. Fleming (Johnson Matthey), or Dr E. Unsworth (Durham University).

Raman spectroscopy was conducted by Prof. A. Beeby (Durham University) using a Horiba LabRAM-HR spectrometer equipped with a 532 nm frequency-doubled Nd:YAG laser and an 1800 lines/mm grating. The solid-state Raman samples were loaded into a standard glass J. Young valve NMR tube inside a nitrogen-filled glove box, and sealed under an inert atmosphere.

Rutherford backscattering spectrometric (RBS) analyses were performed by Dr R. Thompson (Durham University) using a National Electrostatics Corporation 5SDH Pelletron Accelerator with RC43 endstation. RBS experiments were carried out using a 1.5 MeV ⁴He⁺ ion beam incident on the surface at 80° to the sample normal. The energy of the backscattered ⁴He⁺ ions was

determined using a Canberra passivated implanted planar silicon detector with a nominal energy resolution of 17 keV at 170° to the incident beam in a Cornell geometry.

Solid-state ^1H , ^{27}Al and ^{29}Si direct excitation (DE) magic-angle spinning (MAS) nuclear magnetic resonance (NMR) spectroscopic analyses (Varian VNMRS) were undertaken by Dr D. Apperley (Durham University). Samples were packed into an airtight rotor inside a nitrogen-filled glove box, and sealed under an inert atmosphere. Solid-state NMR samples were referenced to external $\text{Si}(\text{CH}_3)_4$ (^1H , ^{29}Si) or 1M $\text{Al}(\text{NO}_3)_{3(\text{aq})}$ (^{27}Al). The ^{29}Si NMR resonances attributed to geminal (Q_2) and isolated (Q_3) silanols, and the bulk silica (Q_4) were quantified using a Gaussian distribution curve fit using MestReNova (MestreLab). Longitudinal spin-lattice relaxation times (T_1) were measured using a saturation-recovery method. A five-parameter fit was used to model the result including a two-component exponential recovery plus baseline. Chemical shifts are reported in ppm.

Solution-phase ^1H and ^{13}C NMR spectroscopic experiments were carried out by Dr J. Aguilar of Durham University using either a Varian Mercury 200 or 400 MHz, Varian Inova 500 MHz, Varian VNMRS 600 or 700 MHz, or a Bruker Advance 400 MHz spectrometer at ambient probe temperatures (290 K). The resulting NMR spectra were interpreted using MestReNova and were referenced to either the residual *protio* impurity in the deuterated solvent, or the corresponding ^{13}C environment. Solvent ^1H shifts (ppm): CDCl_3 , 7.26 (s); C_6D_6 , 7.16 (s). Solvent ^{13}C shifts (ppm): CDCl_3 , 77.16 (t); C_6D_6 , 128.06 (t). Chemical shifts reported in ppm and coupling constants in Hz.

Thermogravimetric analyses (TGA) were conducted by D. Carswell (Durham University) using a Perkin Elmer Pyris 1 TGA, coupled to a Hiden HPR 20 MS unit purged with helium gas.

X-Ray photoelectron spectroscopic (XPS) analyses were conducted by Dr W. Murdoch of Newcastle University at the national EPSRC XPS users' service (NEXUS) using a Thermo Scientific K-Alpha X-ray photoelectron spectrometer. Each sample was mounted onto a borosilicate microscope slide (10 mm × 10 mm) using double-sided conductive carbon tape inside a nitrogen-filled glove box and transferred into a bespoke XPS cell and sealed under an inert atmosphere. Subsequently, the cell was placed under ultra-high vacuum (UHV), before being inserted into the XPS chamber. The C 1s, N 1s, Si 1s and Cr 2p XPS regions were measured using a micro-focussed monochromated Al $\text{K}\alpha$ X-ray source. The XPS spectra were interpreted using CasaXPS software on licence from Newcastle University and were referenced to the binding energy (eV): adventitious C 1s, 284.8 eV.

Laboratory coat, safety spectacles and gloves were worn at all times, and all experiments were conducted in an efficient fume-hood, following completion of appropriate COSHH and risk assessments. Solvents and solid residues were disposed of in the appropriate waste solvent receptacles (chlorinated/non-chlorinated), with aqueous heavy metal-containing residues being classified according to metal.

4.2 Characterisation of Oxide-based Catalyst Supports

4.2.1 ICP-OES Trace Elemental Analyses

ICP-OES was carried out to determine the concentration of trace elements (ppm) present in Evonik Aeroperl 300/30 fumed silica, Sigma Aldrich silica-alumina grade 135 catalyst support and Alfa Aesar γ -alumina (1/8" pellets). Each untreated oxide-based material was digested with HNO_3 and HF, before being neutralised with excess boric acid prior to analysis (Figure 1).

H																	He
Li	Be <10											B	C	N	O	F	Ne
Na	Mg <10											Al	Si	P	S	Cl	Ar
K	Ca	Sc <10	Ti	V	Cr	Mn <10	Fe	Co	Ni <10	Cu	Zn	Ga	Ge	As <10	Se <10	Br	Kr
Rb	Sr <10	Y	Zr	Nb	Mo	Tc	Ru	Rh	Pd	Ag	Cd <10	In	Sn	Sb	Te	I	Xe
Cs	Ba <10	Lu <10	Hf	Ta	W	Re	Os	Ir	Pt <10	Au	Hg	Tl	Pb <10	Bi	Po	At	Rn
Fr	Ra	Lr	Rf	Db	Sg	Bh	Hs	Mt	Ds	Rg	Cn	Nh	Fl	Mc	Lv	Ts	Og

La <10	Ce	Pr	Nd	Pm	Sm	Eu	Gd	Tb	Dy <10	Ho	Er	Tm	Yb
Ac	Th	Pa	U	Np	Pu	Am	Cm	Bk	Cf	Es	Fm	Md	No

Sample	Ca	Cr	Cu	Fe	Mn	Na	P	V	Zn
SiO_2	<10	22	<30	36	<10	85	<10	<10	15
$\text{SiO}_2\text{-Al}_2\text{O}_3$	56	<10	<30	10	<10	143	<10	<10	48
$\gamma\text{-Al}_2\text{O}_3$	<10	<10	403	63	<10	152	137	13	34

Figure 1: ICP-OES trace elemental analyses (ppm) of as received Evonik Aeroperl 300/30 fumed silica, Sigma Aldrich silica-alumina grade 135 catalyst support and Alfa Aesar γ -alumina (1/8" pellets; as received); relative standard deviation <2%.

4.2.2 BET Specific Surface Area and BJH Pore Volume/Size Analyses

The BET SSA and BJH pore volume/size distribution for as received Evonik Aeroperl 300/30 fumed silica, Sigma Aldrich silica-alumina grade 135 catalyst support, and Alfa Aesar γ -alumina (1/8" pellets ground and sieved to <250 μm) have been determined (Table 1). A sample of each untreated oxide was degassed at 140 °C with a nitrogen purge for one hour, prior to acquisition of BET SSA and isotherm measurements.

Table 1: Specific surface area and pore volume and diameter analyses of Evonik Aeroperl 300/30 fumed silica, Sigma Aldrich silica-alumina grade 135 catalyst support and Alfa Aesar γ -alumina using BET and BJH methods; Error associated with BET measurements \pm 2%; Isotherm shape indicates porosity extends beyond the upper limit of this technique – BJH pore volume and average pore diameter will be underestimates of true value.

Catalyst Support	SSA ($\text{m}^2 \text{g}^{-1}$)	Pore Volume ($\text{cm}^3 \text{g}^{-1}$)	Average Pore Diameter (\AA)
SiO_2	285	1.85	260
$\text{SiO}_2\text{-Al}_2\text{O}_3$	506	0.75	59
$\gamma\text{-Al}_2\text{O}_3$	244	0.76	124

4.1.1 Solid-state NMR Spectroscopy

Evonik Aeroperl 300/30 fumed silica, Sigma Aldrich silica-alumina grade 135 catalyst support and Alfa Aesar γ -alumina (1/8" pellets ground and sieved to <250 μm) were analysed using solid-state ^1H , ^{27}Al , ^{29}Si DE MAS NMR spectroscopy.

4.2.2.1 Evonik Aeroperl 300/30 Fumed Silica

^1H NMR (400 MHz, solid, 13 kHz rotation, 1 s recycle, 160 repetitions) $\delta = 3.7$.

^{29}Si NMR (79 MHz, solid, 6 kHz rotation, 120 s recycle, 547 repetitions) $\delta = -91$ (Q_2), -100 (Q_3), -110 (Q_4).

4.2.2.2 Sigma Aldrich Silica-alumina Grade 135 Catalyst Support

^1H NMR (400 MHz, solid, 13 kHz rotation, 1 s recycle, 160 repetitions) $\delta = 7.0, 5.0$.

^{27}Al NMR (104 MHz, solid, 13 kHz rotation, 0.2 s recycle, 750 repetitions) $\delta = 56$ (AlO_4), 4 (AlO_6).

^{29}Si NMR (79 MHz, solid, 6 kHz rotation, 30 s recycle, 1824 repetitions) $\delta = -91$ (Q_2), -102 (Q_3), -110 (Q_4).

4.2.2.3 Alfa Aesar γ -Alumina

^1H NMR (400 MHz, solid, 13 kHz rotation, 1 s recycle, 160 repetitions) $\delta = 4.9$.

^{27}Al NMR (104 MHz, solid, 13 kHz rotation, 0.2 s recycle, 3950 repetitions) $\delta = 64$ (AlO_4), 7 (AlO_6).

4.2.3 Thermogravimetric Analyses of Catalyst Supports

TGA was used to monitor the calcination of Evonik Aeroperl 300/30 fumed silica, Sigma Aldrich silica-alumina grade 135 catalyst support, and Alfa Aesar γ -alumina (1/8" pellets ground and sieved to <250 μm). A sample of each oxide-based support was transferred into a pre-weighed ceramic pan and heated from 30 to 600 $^{\circ}\text{C}$, at a rate of 30 $^{\circ}\text{C min}^{-1}$. The temperature was maintained at 600 $^{\circ}\text{C}$ for a further 24 hours (Figure 2).

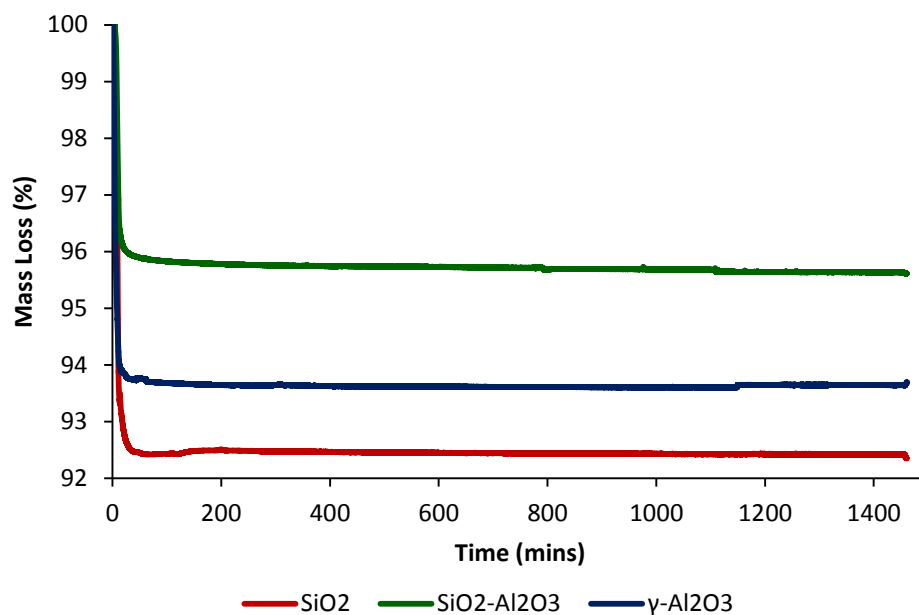
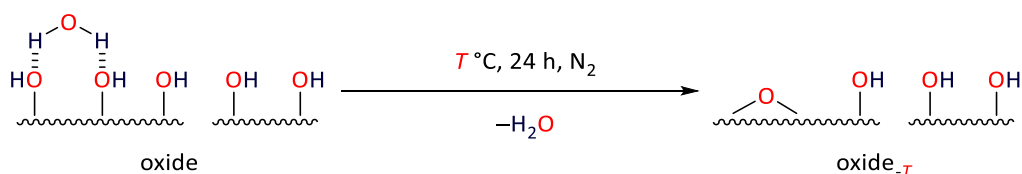


Figure 2: Thermogravimetric analysis profiles of Evonik Aeroperl 300/30 fumed silica, Sigma Aldrich silica-alumina grade 135 catalyst support and Alfa Aesar γ -alumina (1/8" pellets ground and sieved to <250 μm); heating rate of 30 $^{\circ}\text{C min}^{-1}$ to 600 $^{\circ}\text{C}$.

4.3 General Procedures for the Calcination of Oxide Supports

4.3.1 Thermal Pre-treatment of Oxide Supports under a Flow of N₂



Using a variation of an existing methodology,⁴ a quartz tube (20 mm I.D.) fitted with a porous quartz frit was sequentially charged with quartz wool (H. M. Baumbach) and an oxide support material (*e.g.* SiO₂, SiO₂-Al₂O₃ or γ -Al₂O₃; 5.0 g) to form a solid plug. The quartz tube was then placed vertically inside a tube furnace, such that the oxide was centred in the furnace; a thermocouple was attached to the outside of the quartz tube and located level with the centre of the oxide bed. Oxygen-free nitrogen gas, previously dried by passage through a drying column consisting of CaCl₂ and P₂O₅, was passed down through the oxide bed (1 mL s⁻¹) exiting the system *via* an empty liquid trap and a silicon oil bubbler. The oxide support material was heated either to 200, 400 or 600 °C at a rate of 10 °C min⁻¹, and then maintained for 24 hours under a flow of dry N₂ (1 mL s⁻¹). Subsequently, the calcined material was allowed to cool to RT under a flow of N₂ and then transferred under vacuum into a glovebox without exposure to the atmosphere. Supports are classified by the temperature at which they were calcined, *e.g.* SiO₂₋₆₀₀ denotes Aeroperl 300/30 fumed silica partially dehydroxylated at 600 °C for 24 hours under a flow of N₂.

4.3.1.1 NMR Spectroscopic Analysis of SiO₂₋₂₀₀

¹H DE MAS NMR (400 MHz, solid, 6 kHz rotation, 2 s recycle, 160 repetitions) $\delta = 1.9$.

²⁹Si DE MAS NMR (79 MHz, solid, 3.5 kHz rotation, 120 s recycle, 700 repetitions) $\delta = -91$ (Q₂), -100 (Q₃), -109 (Q₄).

4.3.1.2 NMR Spectroscopic Analysis of SiO₂₋₄₀₀

¹H DE MAS NMR (400 MHz, solid, 6 kHz rotation, 1 s recycle, 48 repetitions) $\delta = 1.9$.

²⁹Si DE MAS NMR (79 MHz, solid, 6 kHz rotation, 120 s recycle, 456 repetitions) $\delta = -91$ (Q₂), -99 (Q₃), -108 (Q₄).

4.3.1.3 Analysis of SiO₂₋₆₀₀

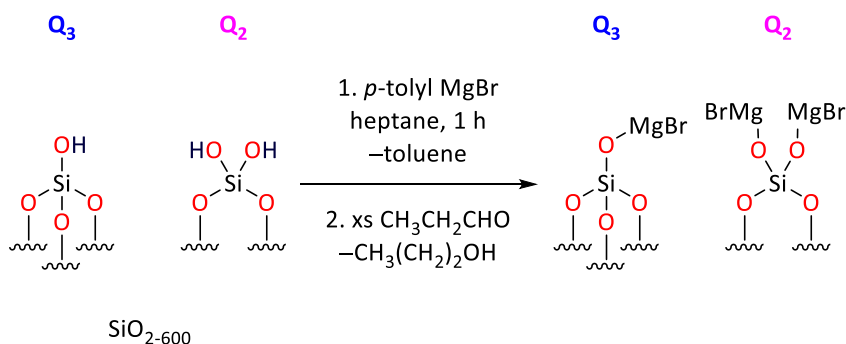
¹H DE MAS NMR (400 MHz, solid, 6 kHz rotation, 5 s recycle, 32 repetitions) $\delta = 1.9$.

²⁹Si DE MAS NMR (79 MHz, solid, 6 kHz rotation, 120 s recycle, 500 repetitions) $\delta = -91$ (Q₂),
-99 (Q₃), -109 (Q₄); T_1 (1) = 25 s (35%), T_1 (2) = 360 s (67%), $R^2 = 0.998$.

Raman (solid, 532 nm, $\nu_{\max}/\text{cm}^{-1}$) 455 cm^{-1} .

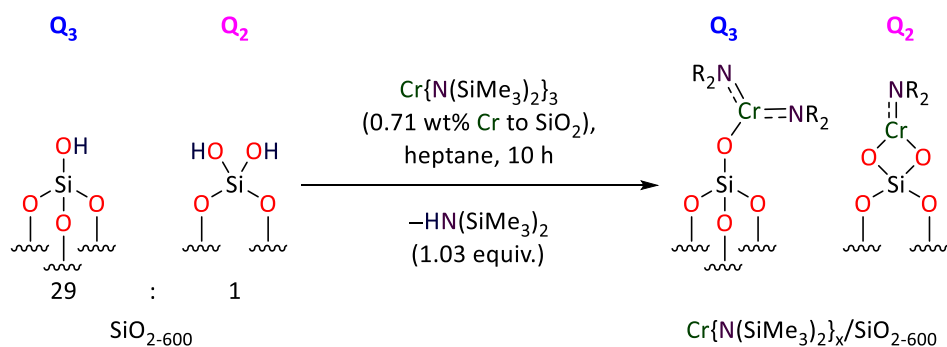
BET SSA $285 \pm 5 \text{ m}^2 \text{ g}^{-1}$; BJH pore volume $1.86 \pm 0.04 \text{ cm}^3 \text{ g}^{-1}$; average pore diameter $262 \pm 5 \text{ \AA}$.

4.3.1.3.1 Silanol Quantification: Titration of SiO₂₋₆₀₀ with *para*-Tolyl Magnesium Bromide



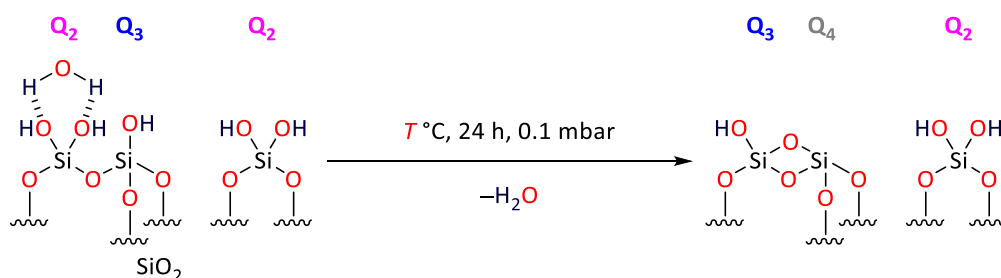
A Schlenk flask was charged with SiO₂₋₆₀₀ (0.2116 g) inside a glovebox and sealed under N₂. The calcined material was suspended in heptane (10 mL), stirred at 200 rpm *via* a Teflon-coated magnetic stirrer bar, and then cooled to 5 °C using an ice-water bath prior to being reacted with a diethyl ether solution of *para*-tolyl magnesium bromide (1.8 mL, 2M, 3.6 mmol), which was added slowly *via* a syringe. The stirred suspension was allowed to warm to RT. After 1 hour, the reaction was cooled to 0 °C using an ice-water bath and quenched with propanal (5 mL, 69.7 mmol), before nonane (1.0 mL, 5.6 mmol) was added as an internal standard. An aliquot of the organic phase was filtered through a plug of cotton wool/Celite®, and subsequently analysed by GC-FID. The concentration of residual silanols was determined, from the quantity of liberated toluene, to be 3.15 mmol_{OH} g⁻¹.

4.3.1.3.2 Titration of SiO₂₋₆₀₀ with Cr{N(SiMe₃)₂}₃



An ampoule was charged with freshly calcined SiO₂₋₆₀₀ (2.89 g) inside a glovebox, and sealed under N₂. The ampoule was connected to a Schlenk line *via* a vacuum transfer apparatus. A stock solution of Cr{N(SiMe₃)₂}₃ in heptane (50.5 mL, 0.0078 M, 0.39 mmol; Cr/SiO₂ = 0.71 wt%) was added portion-wise to the reaction vessel using a dry, degassed syringe. The resulting white solid, suspended in a green solution, was stirred for 10 hours at RT, by which time the solution had become colourless and the solid green. The combined reaction mixture was frozen at -196 °C and the reaction vessel evacuated prior to being sealed under vacuum (0.1 mbar). Upon thawing, all volatile components were isolated by vacuum transfer to afford a colourless organic solution. Subsequently nonane (1.0 mL, 5.6 mmol) was added to this solution before an aliquot of the resulting mixture was collected, passed through a solid plug of cotton wool/Celite®, and analysed by GC-FID to quantify the amount of HN(SiMe₃)₂ liberated on reaction of Cr{N(SiMe₃)₂}₃ with a known quantity of SiO₂₋₆₀₀. ICP-OES analysis confirmed that the chromium loading on silica was 0.71 wt%, and that no residual chromium was present in the organic phase (see Section 4.3.1). The mole ratio of the Cr : HN(SiMe₃)₂ was determined to be 1 : 1.03.

4.1.2 Thermal Pre-treatment of Silica *in vacuo*



A quartz tube (20 mm I.D.), which had been sealed at one end was successively charged with Evonik Aeroperl 300/30 fumed silica (5.0 g) and quartz wool (H. M. Baumbach) to form a solid plug. Subsequently, the quartz tube was connected to a Schlenk line, and carefully placed under dynamic vacuum (0.1 mbar). The quartz tube was then placed vertically inside a tube furnace, such that the oxide was centred in the furnace; a thermocouple was attached to the outside of the quartz tube and located level with the centre of the oxide bed. The oxide was heated to either 600 or 700 °C at a rate of 10 °C min⁻¹, and then maintained for 24 hours *in vacuo*. The partially dehydroxylated support was then allowed to cool to RT under dynamic vacuum (0.1 mbar), before being sealed and transferred into a nitrogen-filled glovebox without exposure to the atmosphere. Following calcination, catalyst supports are classified by the conditions under which they were calcined, *e.g.* SiO_{2-600v} denotes silica partially dehydroxylated at 600 °C for 24 hours *in vacuo*.

4.1.2.1 BET Specific Surface Area and BJH Pore Volume/Size Analyses

A sample of each partially dehydroxylated siliceous catalyst support was heated to 350 °C at a rate of 10 °C min⁻¹ *in vacuo*. The temperature was maintained for four hours, prior to BET SSA and isotherm measurements (Table 2).

Table 2: BET Specific surface area and BJH pore volume/size analyses of SiO_{2-600v} and SiO_{2-700v}

Catalyst Support	SSA (m ² g ⁻¹)	Pore Volume (cm ³ g ⁻¹)	Average Pore Diameter (Å)
SiO _{2-600v}	280 ± 5	1.80 ± 0.03	257 ± 5
SiO _{2-700v}	239 ± 5	1.56 ± 0.03	261 ± 5

4.2 Attempted Preparation of Cr(NPh₂)₃ and Cr(NⁱPr₂)₃

4.2.1 Lithium Diphenylamide

Employing a modified literature protocol,⁵ diphenylamine (1.603 g, 9.47 mmol), charged into a Schlenk flask inside a nitrogen-filled glove box, was dissolved in tetrahydrofuran (THF; 20 mL), cooled in a dry-ice acetone bath to $-78\text{ }^{\circ}\text{C}$, and stirred at 500 rpm *via* a Teflon-coated magnetic stirrer bar. The reaction vessel was then charged with *n*-butyl lithium (2.5 M solution in hexane; 3.8 mL, 9.47 mmol) and stirred for 1 hour at $-78\text{ }^{\circ}\text{C}$ before being allowed to warm to RT. Subsequently, the THF diluent was removed under dynamic vacuum (0.1 mbar) to yield a white solid. The resulting solid was dried at $60\text{ }^{\circ}\text{C}$ *in vacuo*, and then re-crystallised from a 2:1 mixture of hexane and diethyl ether at $-78\text{ }^{\circ}\text{C}$.

¹H NMR (400 MHz, C₆D₆) with 2-methylpyridine δ : 8.39 (C₆H₇N; ddd, $J = 4.9, 1.9, 1.0$ Hz, 1H), 7.37 – 7.29 (C₆H₇N; m, 1H), 7.29 – 7.19 (C₆H₇N; m, 1H), 6.93 (C₆H₇N; td, $J = 7.6, 1.9$ Hz, 1H), 6.76 (LiNPh₂; tt, $J = 7.2, 1.2$ Hz, 1H), 6.62 – 6.46 (LiNPh₂; m, 4H), 3.26 (Et₂O; q, $J = 7.0$ Hz, 2H), 2.33 (C₆H₇N; s, 3H), 1.11 (Et₂O; t, $J = 7.0$ Hz, 3H) (lit. with 4-methylpyridine,⁵ 7.95, 7.56, 7.32, 6.80, 6.34).

4.2.2 Chromium(III) Diphenylamide

Anhydrous (purple) CrCl₃ (0.456 g; 2.88 mmol) charged into a 250 mL round-bottomed flask (RBF) inside a nitrogen-filled glove box was suspended in THF (40 mL), cooled to $0\text{ }^{\circ}\text{C}$ in an ice-salt water bath, and stirred at 500 rpm *via* a Teflon-coated magnetic stirrer bar. The reaction vessel was then charged with a colourless solution of lithium diphenylamide (1.75 g, 8.59 mmol), which had been found to be 86 wt% pure by solution-phase ¹H NMR spectroscopy, dissolved in THF (20 mL) using a cannula under a flow of dry N₂ to yield a purple solution. The reaction mixture was stirred at $0\text{ }^{\circ}\text{C}$ for 2 hours prior to being allowed to warm to RT and stirred overnight (10 hours). Volatile components were then removed under dynamic vacuum (0.1 mbar). The resulting purple solid was dried *in vacuo* at $60\text{ }^{\circ}\text{C}$ over 4 hours. Subsequently, chromium(III) diphenylamide was extracted from LiCl in hexane seven times to maximise yield. Each washing consisted of the chromium(III) amide being dissolved in hexane (40 mL), heated to $50\text{ }^{\circ}\text{C}$ and stirred at 1200 rpm *via* a Teflon-coated magnetic stirrer bar for 20 minutes prior to its isolation *via* cannula filtration. Chromium(III) diphenylamide was re-crystallised from a hexane solution at $-18\text{ }^{\circ}\text{C}$.

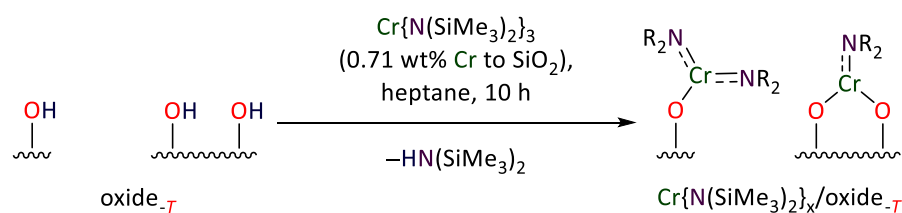
Anal. Calc. for C₃₆H₃₀N₃Cr: C, 77.68; H 5.43; N 7.55%. Found: C, 79.63; H, 5.91; N, 7.1%.

4.2.3 Chromium(III) Diisopropylamide

Anhydrous (purple) CrCl_3 (0.53 g; 3.35 mmol) charged into a 250 mL RBF inside a nitrogen-filled glove box was suspended in THF (35 mL), cooled in a dry-ice acetone bath to $-78\text{ }^\circ\text{C}$, and stirred at 500 rpm *via* a Teflon-coated magnetic stirrer bar. The reaction vessel was then charged with lithium diisopropylamide (2 M solution in THF; 5 mL, 10 mmol) obtained from Acros Organics using a dry, degassed syringe to yield a brown solution. The reaction mixture was stirred at $-78\text{ }^\circ\text{C}$ for 2 hours prior to being allowed to warm to RT and stirred overnight (10 hours). Volatile components were then removed under dynamic vacuum (0.1 mbar). The ensuing brown solid was dried *in vacuo* at $60\text{ }^\circ\text{C}$ over 4 hours. Chromium(III) diisopropylamide was extracted from LiCl in hexane seven times to maximise yield. Each washing consisted of the chromium(III) amide being dissolved in hexane (40 mL), heated to $50\text{ }^\circ\text{C}$ and stirred at 1200 rpm *via* a Teflon-coated magnetic stirrer bar for 20 minutes prior to its isolation *via* cannula filtration. Chromium(III) diisopropylamide was re-crystallised from a hexane solution at $-78\text{ }^\circ\text{C}$.

Anal. Calc. for $\text{C}_{18}\text{H}_{42}\text{N}_3\text{Cr}$: C, 61.32; H 12.01; N 11.92%. Found: C, 40.89; H, 6.91; N, 6.55%.

4.3 General Protocol for the Preparation of Oxide-supported Chromium Pro-initiators



A Schlenk flask was charged with the partially dehydroxylated oxide support (2.0 g) inside a nitrogen-filled glove box, and sealed under N_2 . The Schlenk flask was connected to a vacuum line, evacuated and re-filled with dry N_2 three times, and then charged with a stock solution of either $\text{Cr}\{\text{N}(\text{SiMe}_3)_2\}_3$, chromium(III) *tris*-(2,4-pentanedionate) $\{\text{Cr}(\text{acac})_3\}$ or $\text{CrCl}_3(\text{thf})_3$ in heptane (0.0078 M, 35 mL, 0.27 mmol; 0.71 wt% Cr). The reaction mixture was stirred at 500 rpm *via* a Teflon-coated magnetic stirrer bar for 10 hours at RT. At the end of this period, in each case, the coloured liquid phase had turned colourless, while the solid had changed colour from white to green [$\text{Cr}\{\text{N}(\text{SiMe}_3)_2\}_3$], purple $\{\text{Cr}(\text{acac})_3\}$ or pink $\{\text{CrCl}_3(\text{thf})_3\}$. All volatile components were then removed *in vacuo* and the resulting solid transferred into a nitrogen-filled glove box and stored at ambient temperature. The extent of the chromium metal uptake was assessed *via* ICP-OES analysis of the impregnated oxide materials (see Section 4.3.1). Pro-initiators are classified by the molecular precursor, the oxide catalyst support, and the conditions under which the oxide was calcined, *e.g.* $\text{Cr}\{\text{N}(\text{SiMe}_3)_2\}_x/\text{SiO}_2\text{-600}$ denotes a pro-initiator obtained by reaction of a chromium(III) amide complex with residual silanols at the surface of silica thermally pre-treated at 600 °C under a flow of N_2 , liberating either one or two equivalents of $\text{HN}(\text{SiMe}_3)_2$.

4.3.1 General Protocol for the Determination of Chromium Metal Loading in Oxide-supported Pro-initiators by ICP-OES

A known mass of each oxide-supported chromium-based pro-initiator was charged into a polypropylene vial under ambient conditions, and later suspended in an aqueous solution of HCl (1.5 mL; 37% w/w; 12.7 mmol). Following 10 hours standing at RT, the mixture was carefully diluted with deionised water (13.5 mL), prior to ICP-OES analysis. The ICP-OES instrument was calibrated using several different aqueous standard solutions of $\text{Cr}(\text{NO}_3)_3 \cdot 6\text{H}_2\text{O}$ (Figure 3).

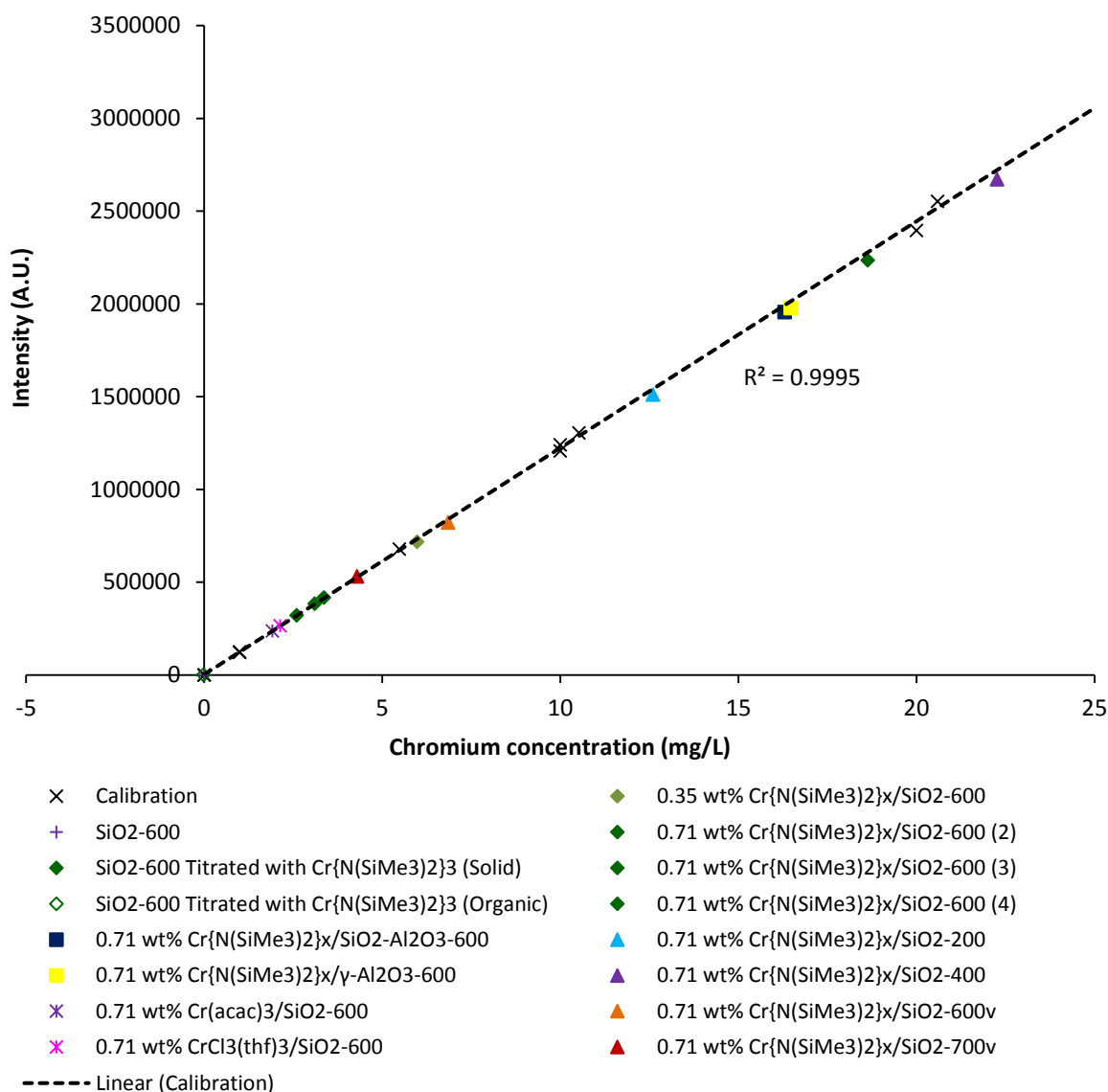


Figure 3: ICP-OES analyses of oxide-supported chromium pro-initiators measured at 357.9 nm for chromium concentration; relative standard deviation <1.75%

Table 3: Supplementary information for ICP-OES analyses of oxide-supported chromium pro-initiators measured at 357.9 nm for chromium concentration

Sample	Blank	Cr{N(SiMe ₃) ₂ } ₃ Titration	Titration (Organic Phase)	Cr{N(SiMe ₃) ₂ } ₃	Cr{N(SiMe ₃) ₂ } ₃	Cr(acac) ₃	CrCl ₃ (thf) ₃	Cr{N(SiMe ₃) ₂ } ₃
Expected Cr Loading (wt%)	-	0.71	0	0.71	0.71	0.71	0.71	0.35
Catalyst Support	N/A	SiO ₂₋₆₀₀	N/A	SiO ₂ -Al ₂ O ₃₋₆₀₀	γ-Al ₂ O ₃₋₆₀₀	SiO ₂₋₆₀₀	SiO ₂₋₆₀₀	SiO ₂₋₆₀₀
Mass of Pro-initiator (g)	-	0.0393 ± 1%	-	0.0344 ± 1%	0.0348 ± 1%	0.004 ± 1%	0.0045 ± 1%	0.0256 ± 1%
Volume (L)	0.015 ± 0.02%	0.015 ± 0.02%	0.015 ± 0.02%	0.015 ± 0.02%	0.015 ± 0.02%	0.015 ± 0.02%	0.015 ± 0.02%	0.015 ± 0.02%
Concentration (mg L ⁻¹)	0 ± 1.75%	18.65 ± 1.75%	0 ± 1.75%	16.28 ± 1.75%	16.47 ± 1.75%	1.89 ± 1.75%	2.13 ± 1.75%	5.97 ± 1.75%
Experimental Cr Loading (wt%)	-	0.712 ± 0.012	-	0.710 ± 0.012	0.710 ± 0.012	0.709 ± 0.012	0.710 ± 0.012	0.350 ± 0.006

Sample	Cr{N(SiMe ₃) ₂ } ₃ (2)	Cr{N(SiMe ₃) ₂ } ₃ (3)	Cr{N(SiMe ₃) ₂ } ₃ (4)	Cr{N(SiMe ₃) ₂ } ₃	Cr{N(SiMe ₃) ₂ } ₃	Cr{N(SiMe ₃) ₂ } ₃	Cr{N(SiMe ₃) ₂ } ₃
Expected Cr Loading (wt%)	0.71	0.71	0.71	0.71	0.71	0.71	0.71
Catalyst Support	SiO ₂₋₆₀₀	SiO ₂₋₆₀₀	SiO ₂₋₆₀₀	SiO ₂₋₂₀₀	SiO ₂₋₄₀₀	SiO _{2-600v}	SiO _{2-700v}
Mass of Pro-initiator (g)	0.0054 ± 1%	0.0071 ± 1%	0.0065 ± 1%	0.0266 ± 1%	0.047 ± 1%	0.0144 ± 1%	0.009 ± 1%
Volume (L)	0.015 ± 0.02%	0.015 ± 0.02%	0.015 ± 0.02%	0.015 ± 0.02%	0.015 ± 0.02%	0.015 ± 0.02%	0.015 ± 0.02%
Concentration (mg L ⁻¹)	2.60 ± 1.75%	3.36 ± 1.75%	3.08 ± 1.75%	12.59 ± 1.75%	22.25 ± 1.75%	6.82 ± 1.75%	4.26 ± 1.75%
Experimental Cr Loading (wt%)	0.722 ± 0.012	0.710 ± 0.012	0.711 ± 0.012	0.710 ± 0.012	0.710 ± 0.012	0.710 ± 0.012	0.710 ± 0.012

4.3.2 Analysis of Cr{N(SiMe₃)₂}_x/SiO₂-600

¹H DE MAS NMR (400 MHz, solid, 6 kHz rotation, 5 s recycle, 32 repetitions) $\delta = 0.18$.

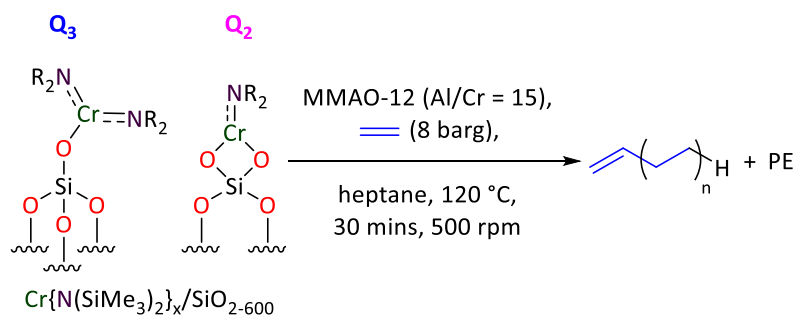
²⁹Si DE MAS NMR (79 MHz, solid, 8 kHz rotation, 1 s recycle, 56976 repetitions) $\delta = 10, -104$ (Q₃), -110 (Q₄); T_1 (1) = 14 s (47%), T_1 (2) = 24 s (31%), $R^2 = 0.998$.

Raman (solid, 532 nm, $\nu_{\max}/\text{cm}^{-1}$) 2960, 2899, 1252, 854, 726, 807, 726, 637, 423, 385.

4.4 Preparation of Isobutyl Aluminoxane

IBAO was prepared according to a modification of a previously disclosed protocol.⁶ Distilled, deionised water (20 mL) was degassed by purging with N₂ at a rate of 2 mL s⁻¹. An ampoule was charged with ⁱBu₃Al (25 wt% solution in toluene; 25 mL, 26.7 mmol), cooled in an ice-water bath to 4 °C, and stirred at 200 rpm *via* a Teflon-coated magnetic stirrer bar. An aliquot of distilled, deionised and degassed H₂O (0.41 mL, 22.8 mmol; 0.85 molar equivalents) was added, cautiously, drop-wise to the cool, stirring solution of ⁱBu₃Al. The reaction mixture was subsequently allowed to warm to RT, and stirred for a further 10 hours. The resulting colourless solution was stored at RT in an ampoule under N₂ and used, as prepared, without further analysis.

4.5 Typical “Closed” Ethylene Oligomerisation Test Procedure



Closed Run 1

A rigorously cleaned 150 mL stainless steel Parr 316SS autoclave (fitted with an internal thermocouple, a pressure gauge, a bursting disk and a dip stick) was taken into a nitrogen-filled glovebox under dynamic vacuum (~ 0.1 mbar) over 10 hours. The reaction vessel was charged with $Cr\{N(SiMe_3)_2\}_x/SiO_{2-600}$ (0.2 g, 0.71 wt% Cr, 27 μmol Cr), and sealed under a N_2 atmosphere. The reactor was then connected to a Schlenk line, and charged with a solution containing heptane (60 mL), nonane (1 mL) and MMAO-12 (7 wt% solution in toluene; 0.18 mL, 0.41 mmol) under a flow of N_2 *via* a cannula. Subsequently, the autoclave was sealed under N_2 , before being purged with ethylene (1 mL s^{-1}) for 10 seconds, and then sealed. The contents of the reactor were cautiously heated to 120 °C using an external solid-state electrical band heater, whilst being agitated at 500 rpm using a customised magnetically-coupled overhead stirrer fitted with a turbine-type four-blade impeller. On reaching 120 °C, the reactor was pressurised with ethylene to 8 barg, prior to being isolated from the gas supply – conditions denoted as a “Closed Run”. After 30 minutes, the reaction vessel was cooled in an ice-water bath to 4 °C (~ 30 mins), before being slowly vented inside a fume hood. An aliquot of the resulting liquid fraction was sampled, quenched with a 1:1 mixture of toluene and an aqueous solution of dilute HCl (10% w/w). A sample of this organic phase was taken, filtered through a solid plug of cotton wool/Celite® prior to being analysed by GC-FID against an internal standard (nonane). Any residual white solid polyethylene (PE) was isolated *via* filtration and combined with residual material collected from inside the autoclave, dried to constant weight at RT in air overnight (~ 10 h) and analysed using DSC. Catalytic performance data resulting from this closed ethylene oligomerisation run is presented in Chapter 2 of this thesis (see Table 1; Entry 2). This will be abbreviated hereinafter as follows:

Chapter 2; Table 1; Entry 2.

Closed Run 2

The procedure of **Closed Run 1** was followed, with the exception that a stock solution of $\text{Cr}\{\text{N}(\text{SiMe}_3)_2\}_3$ in heptane (0.0078 M, 3.5 mL, 27 μmol) was used in place of $\text{Cr}\{\text{N}(\text{SiMe}_3)_2\}_x/\text{SiO}_2\text{-600}$. In order to maintain the total volume of heptane in the system, 56.5 mL heptane was used instead of 60 mL.

Chapter 2; Table 1; Entry 1.

Closed Run 3

The procedure of **Closed Run 1** was followed, with the exception that $\text{Cr}\{\text{N}(\text{SiMe}_3)_2\}_x/\text{SiO}_2\text{-Al}_2\text{O}_3\text{-600}$ (0.2 g, 0.71 wt% Cr, 27 μmol Cr) was used in place of $\text{Cr}\{\text{N}(\text{SiMe}_3)_2\}_x/\text{SiO}_2\text{-600}$.

Chapter 2; Table 1; Entry 3.

Closed Run 4

The procedure of **Closed Run 1** was followed, with the exception that $\text{Cr}\{\text{N}(\text{SiMe}_3)_2\}_x/\gamma\text{-Al}_2\text{O}_3\text{-600}$ (0.2 g, 0.71 wt% Cr, 27 μmol Cr) was used in place of $\text{Cr}\{\text{N}(\text{SiMe}_3)_2\}_x/\text{SiO}_2\text{-600}$.

Chapter 2; Table 1; Entry 4.

Closed Run 5

The procedure of **Closed Run 1** was followed, with the exception that no co-catalyst was used.

Chapter 2; Table 2; Entry 1.

Closed Run 6

The procedure of **Closed Run 1** was followed, with the exception that 15 molar equivalents of $i\text{Bu}_3\text{Al}$ (25 wt% solution in toluene; 0.38 mL, 0.41 mmol) was used in place of MMAO-12.

Chapter 2; Table 2; Entry 2.

Closed Run 7

The procedure of **Closed Run 1** was followed, with the exception that 15 molar equivalents of IBAO (0.9 M solution in toluene; 0.46 mL, 0.41 mmol) was used in place of MMAO-12.

Chapter 2; Table 2; Entry 3.

Closed Run 8

The procedure of **Closed Run 1** was followed, with the exception that 15 molar equivalents of Me_3Al (2M solution in toluene; 0.20 mL, 0.41 mmol) was used in place of MMAO-12.

Chapter 2; Table 2; Entry 4.

Closed Run 9

The procedure of **Closed Run 1** was followed, with the exception that 15 molar equivalents of MAO (10 wt% solution in toluene; 0.27 mL, 0.41 mmol) was used in place of MMAO-12.

Chapter 2; Table 2; Entry 5.

Closed Run 10

The procedure of **Closed Run 1** was followed, with the exception that 15 molar equivalents of Et₂AlCl (25 wt% in toluene; 0.22 mL, 0.41 mmol) was used in place of MMAO-12.

Chapter 2; Table 2; Entry 7.

Closed Run 11

The procedure of **Closed Run 1** was followed, with the exception that methylcyclohexane (60 mL) was used in place of heptane.

Chapter 2; Table 3; Entry 2.

Closed Run 12

The procedure of **Closed Run 1** was followed, with the exception that toluene (60 mL) was used in place of heptane.

Chapter 2; Table 3; Entry 3.

Closed Run 13

The procedure of **Closed Run 1** was followed, with the exception that chlorobenzene (60 mL) was used in place of heptane.

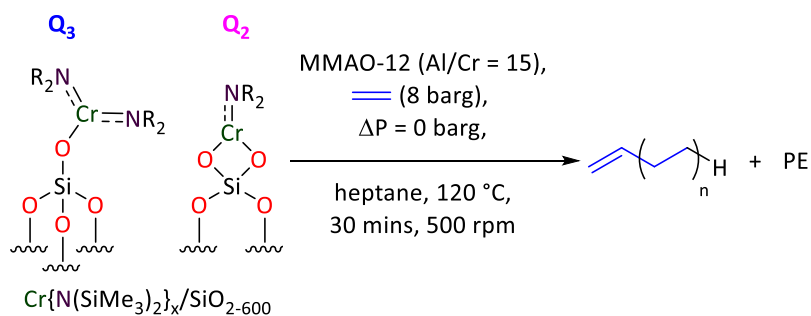
Chapter 2; Table 3; Entry 4.

Closed Run 14

The procedure of **Closed Run 1** was followed, with the exception that Cr{N(SiMe₃)₂}_x/SiO₂₋₂₀₀ (0.2 g, 0.71 wt% Cr, 27 μmol Cr) was used in place of Cr{N(SiMe₃)₂}_x/SiO₂₋₆₀₀.

Chapter 2; Table 7; Entry 1.

4.6 Typical “Open” Ethylene Oligomerisation Test Procedure



Open Run 1

A rigorously cleaned 150 mL stainless steel Parr 316SS autoclave (fitted with an internal thermocouple, a pressure gauge, a bursting disk and a dip stick) was taken into a nitrogen-filled glovebox under dynamic vacuum (~0.1 mbar) over 10 hours. The reaction vessel was charged with Cr{N(SiMe₃)₂}_x/SiO₂₋₆₀₀ (0.2 g, 0.71 wt% Cr, 27 μmol Cr), and sealed under a N₂ atmosphere. The reactor was then connected to a Schlenk line, and charged with a solution containing heptane (60 mL), nonane (1 mL) and MMAO-12 (7 wt% solution in toluene; 0.18 mL, 0.41 mmol) under a flow of N₂ *via* a cannula. Subsequently, the autoclave was sealed under N₂ before being purged with ethylene (1 mL s⁻¹) for 10 seconds, and then sealed once again. The contents of the reactor were cautiously heated to 120 °C using an external solid-state electrical band heater, whilst being agitated at 500 rpm using a customised magnetically-coupled overhead stirrer fitted with a turbine-type four-blade impeller. On reaching 120 °C, the reactor was pressurised with ethylene to 8 barg for 30 minutes – conditions denoted as an “Open Run”. At the end of the batch reaction, the autoclave was cooled in an ice-water bath to 4 °C (~30 mins), before being slowly vented inside a fume hood. An aliquot of the resulting liquid organic fraction was sampled, quenched with a 1:1 mixture of toluene and an aqueous solution of dilute HCl (10% w/w). A sample of this organic phase was taken, filtered through a solid plug of cotton wool/Celite® prior to being analysed by GC-FID against an internal standard (nonane). Any residual white solid PE was isolated *via* filtration and combined with residual material from inside the autoclave, dried to constant weight at RT in air overnight (~10 h) and analysed using DSC. Catalytic performance data for this ethylene oligomerisation run was averaged over three individual trials, and is presented in Chapter 3 of this thesis (Table 1; Runs 1 – 3). This will be abbreviated hereinafter as follows:

Chapter 3; Table 1; Runs 1 – 3.

Open Run 2

The procedure of **Open Run 1** was followed, with the exception that Cr{N(SiMe₃)₂}_x/SiO₂₋₂₀₀ (0.2 g, 0.71 wt% Cr, 27 μmol Cr) was used in place of Cr{N(SiMe₃)₂}_x/SiO₂₋₆₀₀.

Chapter 3; Table 2; Entry 1.

Open Run 3

The procedure of **Open Run 1** was followed, with the exception that $\text{Cr}\{\text{N}(\text{SiMe}_3)_2\}_x/\text{SiO}_{2-400}$ (0.2 g, 0.71 wt% Cr, 27 μmol Cr) was used in place of $\text{Cr}\{\text{N}(\text{SiMe}_3)_2\}_x/\text{SiO}_{2-600}$.

Chapter 3; Table 2; Entry 2.

Open Run 4

The procedure of **Open Run 1** was followed, with the exception that $\text{Cr}\{\text{N}(\text{SiMe}_3)_2\}_x/\text{SiO}_{2-600v}$ (0.2 g, 0.71 wt% Cr, 27 μmol Cr) was used in place of $\text{Cr}\{\text{N}(\text{SiMe}_3)_2\}_x/\text{SiO}_{2-600}$.

Chapter 3; Table 3; Entry 2.

Open Run 5

The procedure of **Open Run 1** was followed, with the exception that $\text{Cr}\{\text{N}(\text{SiMe}_3)_2\}_x/\text{SiO}_{2-700v}$ (0.2 g, 0.71 wt% Cr, 27 μmol Cr) was used in place of $\text{Cr}\{\text{N}(\text{SiMe}_3)_2\}_x/\text{SiO}_{2-600}$.

Chapter 3; Table 3; Entry 3.

Open Run 6

The procedure of **Open Run 1** was followed, with the exception that $\text{Cr}(\text{acac})_3/\text{SiO}_{2-600}$ (0.2 g, 0.71 wt% Cr, 27 μmol Cr) was used in place of $\text{Cr}\{\text{N}(\text{SiMe}_3)_2\}_x/\text{SiO}_{2-600}$.

Chapter 3; Table 5; Entry 2.

Open Run 7

The procedure of **Open Run 1** was followed, with the exception that $\text{CrCl}_3(\text{thf})_3/\text{SiO}_{2-600}$ (0.2 g, 0.71 wt% Cr, 27 μmol Cr) was used in place of $\text{Cr}\{\text{N}(\text{SiMe}_3)_2\}_x/\text{SiO}_{2-600}$.

Chapter 3; Table 5; Entry 3.

Open Run 8

The procedure of **Open Run 1** was were followed, with the exception that $\text{Cr}\{\text{N}(\text{SiMe}_3)_2\}_x/\text{SiO}_{2-600}$ (0.2 g, 0.35 wt% Cr, 14 μmol Cr) was used rather than 0.2 g $\text{Cr}\{\text{N}(\text{SiMe}_3)_2\}_x/\text{SiO}_{2-600}$ with a chromium metal loading of 0.71 wt%.

Chapter 3; Table 6; Entry 1.

Open Run 9

The procedure of **Open Run 1** was followed, with the exception that $\text{Cr}\{\text{N}(\text{SiMe}_3)_2\}_x/\text{SiO}_{2-600}$ (0.4 g, 0.35 wt% Cr, 27 μmol Cr) was used rather than 0.2 g $\text{Cr}\{\text{N}(\text{SiMe}_3)_2\}_x/\text{SiO}_{2-600}$ with a chromium metal loading of 0.71 wt%.

Chapter 3; Table 6; Entry 3.

Open Run 10

The procedure of **Open Run 1** was followed, with the exception that $\text{Cr}\{\text{N}(\text{SiMe}_3)_2\}_x/\text{SiO}_{2-600}$ (0.1 g, 0.71 wt% Cr, 14 μmol Cr) was used instead of 0.2 g $\text{Cr}\{\text{N}(\text{SiMe}_3)_2\}_x/\text{SiO}_{2-600}$.

Chapter 3; Table 6; Entry 4.

Open Run 11

The procedure of **Open Run 1** was followed, with the exception that 24 molar equivalents of MMAO-12 (7 wt% solution in toluene; 0.28 mL, 0.66 mmol) was used instead of 15 molar equivalents.

Chapter 3; Table 7; Entry 2.

Open Run 12

The procedure of **Open Run 1** was followed, with the exception that 50 molar equivalents of MMAO-12 (7 wt% solution in toluene; 0.59 mL, 1.37 mmol) was used instead of 15 molar equivalents.

Chapter 3; Table 7; Entry 3.

Open Run 13

The procedure of **Open Run 1** was followed, with the exception that 150 molar equivalents of MMAO-12 (7 wt% solution in toluene; 1.76 mL, 4.10 mmol) was used instead of 15 molar equivalents.

Chapter 3; Table 7; Entry 4.

Open Run 14

The procedure of **Open Run 1** was followed, with the exception that the reaction mixture was cautiously heated to 35 °C rather than 120 °C.

Chapter 3; Table 8; Entry 1.

Open Run 15

The procedure of **Open Run 1** was followed, with the exception that the reaction mixture was cautiously heated to 80 °C rather than 120 °C.

Chapter 3; Table 8; Entry 2.

Open Run 16

The procedure of **Open Run 1** was followed, with the exception that the reaction mixture was cautiously heated to 90 °C rather than 120 °C. Catalytic performance data averaged over two independent trials.

Chapter 3; Table 8; Entry 3.

Open Run 17

The procedure of **Open Run 1** was followed, with the exception that the reaction mixture was cautiously heated to 100 °C rather than 120 °C. Catalytic performance data averaged over two independent trials.

Chapter 3; Table 8; Entry 4.

Open Run 18

The procedure of **Open Run 1** was followed, with the exception that the reaction mixture was cautiously heated to 140 °C rather than 120 °C. Catalytic performance data averaged over two independent trials.

Chapter 3; Table 8; Entry 6.

Open Run 19

The procedure of **Open Run 1** was followed, with the exception that the reaction mixture was stirred at a rate of 1200 rpm rather than 500 rpm.

Chapter 3; Table 9; Entry 2.

Open Run 20

The procedure of **Open Run 1** was followed, with the exception that the autoclave was pressurised to 2 barg for 30 minutes rather than 8 barg.

Chapter 3; Table 10; Entry 1.

Open Run 21

The procedure of **Open Run 1** was followed, with the exception that the autoclave was pressurised to 14 barg for 30 minutes rather than 8 barg.

Chapter 3; Table 10; Entry 3.

Open Run 22

The procedure of **Open Run 1** was followed, with the exception that the autoclave was pressurised to 18 barg for 30 minutes rather than 8 barg. Catalytic performance data averaged over two independent trials.

Chapter 3; Table 10; Entry 4.

Open Run 23

The procedure of **Open Run 1** was followed, with the exception that the autoclave was pressurised to 24 barg for 30 minutes rather than 8 barg.

Chapter 3; Table 10; Entry 5.

Open Run 24

The procedure of **Open Run 1** was followed, with the exception that the autoclave was pressurised to 30 barg for 30 minutes rather than 8 barg. Catalytic performance data averaged over two independent trials.

Chapter 3; Table 10; Entry 6.

Open Run 25

The procedure of **Open Run 1** was followed, with the exception that the autoclave was pressurised to 8 barg for 5 minutes rather than 30 minutes.

Chapter 3; Table 11; Entry 1.

Open Run 26

The procedure of **Open Run 1** was followed, with the exception that the autoclave was pressurised to 8 barg for 60 minutes rather than 30 minutes. Catalytic performance data averaged over two independent trials.

Chapter 3; Table 11; Entry 3.

Open Run 27

The procedure of **Open Run 1** was followed, with the exception that the autoclave was pressurised to 8 barg for 120 minutes rather than 30 minutes. Catalytic performance data averaged over two independent trials.

Chapter 3; Table 11; Entry 4.

Open Run 28

The procedure of *Open Run 1* was followed, with the exception that the autoclave was pressurised to 8 barg for 180 minutes rather than 30 minutes.

Chapter 3; Table 11; Entry 5.

Open Run 29

The procedure of *Open Run 1* was followed, with the exception that 1,2-dimethoxyethane (30 μ L, 273 μ mol) was added to the solution containing MMAO-12, heptane and nonane.

Chapter 3; Table 12; Entry 2.

Open Run 30

The procedure of *Open Run 1* was followed, with the exception that diethyl zinc (1.5 M solution in toluene; 1.8 mL, 2.73 mmol) was added to the solution containing MMAO-12, heptane and nonane.

Chapter 3; Table 12; Entry 3.

Open Run 31

The procedure of *Open Run 1* was followed, with the exception that 1-hexene (3 mL; 24 mmol) was added to the solution containing MMAO-12, heptane and nonane.

Chapter 3; Table 13; Entry 2.

Open Run 32

The procedure of *Open Run 1* was followed, with the exception that 30 mL heptane was used instead of 60 mL.

Chapter 3; Table 14; Entry 1.

Open Run 33

The procedure of *Open Run 1* was followed, with the exception that 90 mL heptane was used instead of 60 mL.

Chapter 3; Table 14; Entry 3.

Open Run 34

The procedure of *Open Run 1* was followed, with the exception that toluene (1.8 mL, 17 mmol) was added to the solution containing MMAO-12, heptane and nonane.

Chapter 3; Figure 7.

4.6.1 Isolation/Separation of Hexene- and Decene-containing Product Fractions by Distillation

The liquid-phase organic products afforded by the $\text{Cr}\{\text{N}(\text{SiMe}_3)_2\}_x/\text{SiO}_{2-600}/\text{MMAO-12}$ ethylene trimerisation reaction (Open Run 32; Chapter 3, Table 14, Entry 1) was transferred into a 100 mL RBF containing a Teflon-coated magnetic stirrer bead, which was subsequently fitted with a Vigreux column (150 mm length, 15 mm I.D.), condenser and a single receiver flask. The colourless solution was gradually heated to 120 °C in a silicone oil bath using a hotplate stirrer attached to an external temperature probe. An aliquot of the distillate collected between 60 – 100 °C was analysed by GC-FID and solution-phase Pureshift ^1H - ^{13}C heteronuclear single quantum correlation (HSQC) NMR spectroscopy. Subsequently, the 100 mL RBF was heated to 120 °C to remove excess heptane from the C_{8+} product fraction *via* distillation at 100 °C. The second fraction was later analysed by GC-FID. The third product fraction was collected using a Kugelrohr distillation apparatus between 156 – 157 °C, and subsequently analysed by GC-FID and solution-phase $^{13}\text{C}\{^1\text{H}\}$ NMR spectroscopy. Below is a list of hexene and decene isomers that have been identified by their vinyl environments using solution-phase Pureshift ^1H and/or ^{13}C HSQC NMR spectroscopy.

1-Hexene

Boiling point 60 – 100 °C / 760 mm Hg

^1H NMR (600 MHz, CDCl_3) δ : 5.82, 5.00, 4.94 (lit.,⁷ 5.80, 4.96, 4.92).

$^{13}\text{C}\{^1\text{H}\}$ NMR (151 MHz, CDCl_3) δ : 139.3, 114.2 (lit.,⁸ 139.1, 114.1).

cis-2-Hexene

Boiling point 60 – 100 °C / 760 mm Hg

^1H NMR (600 MHz, CDCl_3) δ : 5.45, 5.40 (lit.,⁹ 5.43).

$^{13}\text{C}\{^1\text{H}\}$ NMR (151 MHz, CDCl_3) δ : 130.8, 124.0 (lit.,⁸ 130.4, 123.8).

trans-2-Hexene

Boiling point 60 – 100 °C / 760 mm Hg

^1H NMR (600 MHz, CDCl_3) δ : 5.43 (lit.,⁷ 5.45, 5.42).

$^{13}\text{C}\{^1\text{H}\}$ NMR (151 MHz, CDCl_3) δ : 131.6, 124.9 (lit.,⁸ 131.5, 124.8).

trans-3-Hexene

Boiling point 60 – 100 °C / 760 mm Hg

^1H NMR (600 MHz, CDCl_3) δ : 5.45 (lit.,¹⁰ 5.44).

$^{13}\text{C}\{^1\text{H}\}$ NMR (151 MHz, CDCl_3) δ : 131.1 (lit.,⁸ 131.0).

1-Decene

Boiling point 156 – 157 °C / 760 mm Hg

$^{13}\text{C}\{^1\text{H}\}$ NMR (151 MHz, CDCl_3) δ : 139.4, 114.2 (lit.,^{7,11} 139.3, 114.2).

***cis*-4-Decene**

Boiling point 156 – 157 °C / 760 mm Hg

$^{13}\text{C}\{^1\text{H}\}$ NMR (151 MHz, CDCl_3) δ : 130.5, 130.0 (lit.,¹² 130.4, 130.0).

5-Decene

Boiling point 156 – 157 °C / 760 mm Hg

$^{13}\text{C}\{^1\text{H}\}$ NMR (151 MHz, CDCl_3) δ : 130.5 (lit.,^{7,11} 130.4).

5-Methyl-1-nonene

Boiling point 156 – 157 °C / 760 mm Hg

$^{13}\text{C}\{^1\text{H}\}$ NMR (151 MHz, CDCl_3) δ : 139.6, 114.1 (lit.,¹¹ 139.5, 114.1).

5-Methylene-1-nonane

Boiling point 156 – 157 °C / 760 mm Hg

$^{13}\text{C}\{^1\text{H}\}$ NMR (151 MHz, CDCl_3) δ : 150.5, 108.5 (lit.,^{11,13} 150.2, 108.6).

4-Ethyl-1-octene

Boiling point 156 – 157 °C / 760 mm Hg

$^{13}\text{C}\{^1\text{H}\}$ NMR (151 MHz, CDCl_3) δ : 137.9, 115.5 (lit.,¹¹ 137.8, 115.6).

4-Ethylene-1-Octane

Boiling point 156 – 157 °C / 760 mm Hg

$^{13}\text{C}\{^1\text{H}\}$ NMR (151 MHz, CDCl_3) δ : 143.8, 113.9 (lit.,¹¹ 143.8, 114.0).

4.7 References

- (1) D. P. Debecker, M. Stoyanova, U. Rodemerck, A. Léonard, B. L. Su, E. M. Gaigneaux, *Catal. Today*, **2011**, *169*, 60-68.
- (2) D. C. Bradley, R. G. Copperthwaite, M. W. Extine, W. W. Reichert, M. H. Chisholm, In *Inorg. Synth.*; John Wiley & Sons, Inc.: 2007, p 112-120.
- (3) E. C. Alyea, D. C. Bradley, R. G. Copperthwaite, *J. Chem. Soc., Dalton Trans.*, **1972**, 1580-1584.
- (4) T. Monoi, Y. Sasaki, *J. Mol. Catal. A: Chem.*, **2002**, *187*, 135-141.
- (5) J. S. DePue, D. B. Collum, *J. Am. Chem. Soc.*, **1988**, *110*, 5518-5524.
- (6) D. N. Edwards, J. R. Briggs, A. E. Marcinkowsky, K. H. Lee, **1988**, US4772736, Union Carbide Corporation.
- (7) T. Yamaji, T. Saito, K. Hayamizu, M. Yanagisawa, O. Yamamoto, "Spectral Database for Organic Compounds", <http://sdb.sdb.aist.go.jp>, 18/10/17.
- (8) A. R. Katritzky, A. M. El-Mowafy, *J. Org. Chem.*, **1982**, *47*, 3506-3511.
- (9) M. Audit, P. Demerseman, N. Goasdoue, N. Platzer, *Org. Magn. Reson.*, **1983**, *21*, 698-705.
- (10) R. L. Pederson, I. M. Fellows, T. A. Ung, H. Ishihara, S. P. Hajela, *Adv. Synth. Catal.*, **2002**, *344*, 728 - 735.
- (11) T. M. Zilbershtein, V. A. Kardash, V. V. Suvorova, A. K. Golovko, *Appl. Catal. A: Gen.*, **2014**, *475*, 371-378.
- (12) L. H. Do, J. A. Labinger, J. E. Bercaw, *Organometallics*, **2012**, *31*, 5143-5149.
- (13) Y. Suzuki, S. Kinoshita, A. Shibahara, S. Ishii, K. Kawamura, Y. Inoue, T. Fujita, *Organometallics*, **2010**, *29*, 2394-2396.

Chapter 5:
Appendix

5.1 GC-FID Analysis of the Liquid Fraction Obtained from Chromium-mediated Ethylene Trimerisation

The liquid-phase organic products resulting from chromium-mediated ethylene oligomerisation experiments described earlier in this thesis were analysed primarily by gas chromatography (GC) using a flame ionisation detector (FID). Here, the analytical methodology for this technique is outlined. Additionally, owing to the somewhat controversial nature of the various expressions used to describe catalytic performance (*e.g.* productivity, activity, *etc.*),¹ the metrics employed in this thesis are hereby defined. The following abbreviations are used throughout:

- C_2 , C_4 , C_6 , 1- C_6 , C_8 , 1- C_8 , C_{10} , 1- C_{10} , C_{12+} , 1- C_{12} , 1- C_{14} , PE = **Ethylene, butenes, hexenes, 1-hexene, octenes, 1-octene, decenes, 1-decene, higher oligomers** in the liquid-phase, including **1-dodecene** and **1-tetradecene**, and **polyethylene**, respectively.
- m_{C_4} , m_{C_6} , m_{1-C_6} , m_{C_8} , $m_{C_{10}}$, $m_{C_{12+}}$, m_{PE} , m_{Cr} = **Mass of butenes, hexenes, 1-hexene, octenes, decenes, higher oligomers** in the liquid-phase, **polyethylene** and **chromium**.
- wt% = **Weight percentage**: the *mass of each product fraction* afforded by the initiator system with respect to the *total mass of all products combined*:

$$\text{➤ } C_4 \text{ (wt\%)} = \frac{m_{C_4}}{m_{C_4} + m_{C_6} + m_{C_8} + m_{10} + m_{C_{12+}} + m_{PE}} \times 100 \quad (\text{Equation A1})$$

$$\text{➤ } C_6 \text{ (wt\%)} = \frac{m_{C_6}}{m_{C_4} + m_{C_6} + m_{C_8} + m_{10} + m_{C_{12+}} + m_{PE}} \times 100 \quad (\text{Equation A2})$$

$$\text{➤ } C_8 \text{ (wt\%)} = \frac{m_{C_8}}{m_{C_4} + m_{C_6} + m_{C_8} + m_{10} + m_{C_{12+}} + m_{PE}} \times 100 \quad (\text{Equation A3})$$

$$\text{➤ } C_{10} \text{ (wt\%)} = \frac{m_{C_{10}}}{m_{C_4} + m_{C_6} + m_{C_8} + m_{10} + m_{C_{12+}} + m_{PE}} \times 100 \quad (\text{Equation A4})$$

$$\text{➤ } C_{12+} \text{ (wt\%)} = \frac{m_{C_{12+}}}{m_{C_4} + m_{C_6} + m_{C_8} + m_{10} + m_{C_{12+}} + m_{PE}} \times 100 \quad (\text{Equation A5})$$

$$\text{➤ } PE \text{ (wt\%)} = \frac{m_{PE}}{m_{C_4} + m_{C_6} + m_{C_8} + m_{10} + m_{C_{12+}} + m_{PE}} \times 100 \quad (\text{Equation A6})$$

- %1- C_6 = **1-Hexene purity**: the *percentage of the C_6 product fraction* corresponding to the *1-alkene* as opposed to branched and/or internal isomers: $\frac{m_{1-C_6}}{m_{C_6}} \times 100$ (Equation A7)
- TON = **Turnover number**: the *number of grams of all products formed per gram of chromium* (*i.e.* $g \text{ g}_{Cr}^{-1}$): $\frac{m_{C_4} + m_{C_6} + m_{C_8} + m_{10} + m_{C_{12+}} + m_{PE}}{m_{Cr}}$ (Equation A8)
- TOF = **Turnover frequency**: the *number of grams of all products formed per gram of chromium per unit time t* (*i.e.* $g \text{ g}_{Cr}^{-1} \text{ h}^{-1}$): $\frac{m_{C_4} + m_{C_6} + m_{C_8} + m_{10} + m_{C_{12+}} + m_{PE}}{m_{Cr} \times t}$ (Equation A9)

5.2 Quantifying the Mass of Analytes using GC-FID Analysis

In order to evaluate the catalytic performance parameters described in Section 5.1, the composition of the liquid fraction arising from ethylene oligomerisation experiments was determined by GC-FID analysis.^{2,3} During this project when preparing the samples for GC-FID analysis it is important to factor in the volatility of the various liquid-phase analytes generated during olefin oligomerisation catalysis. Consequently, samples of liquid-phase organic products were analysed by GC-FID according to the following method:

1. A 1:1 mixture of toluene and HCl (10% w/w) was made up in a polypropylene sample vial.
2. A cotton wool/Celite® filter plug was prepared in a Pasteur pipette and placed in an oven maintained at 110 °C.
3. At the end of a catalytic run, the autoclave was cooled in an ice-water bath to 4 °C.
4. The cotton wool/Celite® filter plug was allowed to cool to room temperature (RT).
5. An aliquot (~2 mL) of the reaction mixture was transferred into the polypropylene sample vial containing 3 mL of a 1:1 mixture of toluene and dilute HCl (10% w/w) to quench the catalyst.
6. The resulting organic layer was extracted and filtered through the cooled cotton wool/Celite® plug into a labelled sample vial, which was stored in a dry-ice bath until the sample was analysed by GC-FID.

Once the sample had been prepared, a 10 µL micro-syringe was successively purged several times with toluene, and then the analyte before a known volume (1 µL) of the analyte solution was collected and then injected into the GC-FID instrument (Perkin Elmer Clarus 400 GC). The sample was vaporised within the injector (250 °C) and allowed to pass through a paraffins, olefins, naphthalenes and aromatics (PONA) capillary column (50 m × 0.2 mm × 0.5 mm) under a constant flow of the carrier gas into the FID. The PONA column can provide ample separation of olefinic components within each sample,⁴ something exemplified by their respective retention times within the column (Figure 1). A known volume of an internal standard (*i.e.* 1 mL nonane) is used to quantify the conversion of the starting material and the selectivity towards various products.

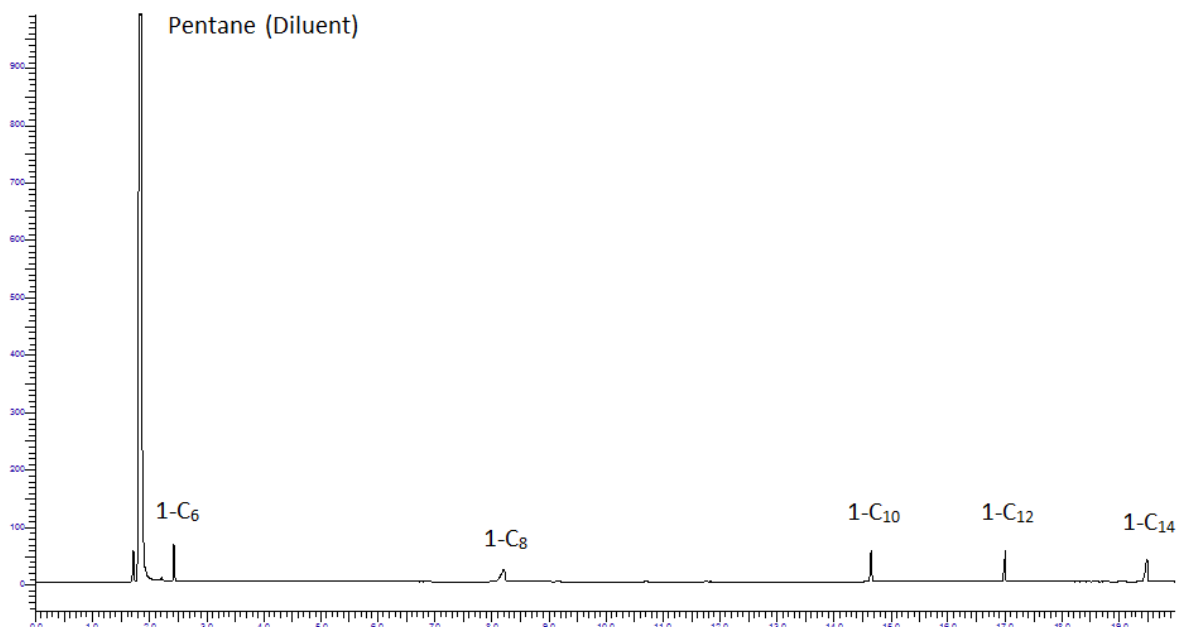


Figure 1: GC-FID trace of a standard pentane solution containing 1-hexene (2.43 mins), 1-octene (8.22 mins), 1-decene (14.65 mins), 1-dodecene (17.00 mins) and 1-tetradecene (19.49 mins) acquired using a Perkin Elmer Clarus 400 GC through a PONA column

The calculations involved in the quantification of the olefinic components present in each GC-FID trace have been defined along with an evaluation of the precision of the technique. The following abbreviations are used throughout this appendix:

i = **Component**.

st = **Internal Standard**.

A_i, A_{st} = **Peak Area** for component (i) and internal standard (st).

RF_i, RF_{st} = **Response Factor** of the FID for component (i) and internal standard (st).

$n_i, n_i^{inj}, n_i^{col}, n_i^{FID}$ = **Number of Moles** of component (i) in the reaction vessel, injected into the Perkin Elmer Clarus 400 GC instrument, inside the PONA column, and detected by the FID.

V, V^{inj} = **Volume** of the reaction mixture and of the sample injected into the Perkin Elmer Clarus 400 GC instrument.

n_{st} = **Number of Moles** of internal standard (st) in the reaction vessel.

m_i, m_{st} = **Mass** of component (i) and internal standard (st) in the reaction vessel.

FW_i, FW_{st} = **Formula Weight** of component (i) and internal standard (st).

m, \bar{m} = **General Mass** and **Average Mass**.

Each component (*i*) within the injected sample that reaches the FID is recorded electronically in a chromatogram at a specific retention time. The area of the peak in the chromatogram is directly proportional to the number of moles of that analyte. Hence:

$$A_i = RF_i \times n_i^{\text{FID}} \quad (\text{Equation A10})$$

Considering that:

$$n_i^{\text{FID}} \propto n_i^{\text{col}} \propto n_i^{\text{inj}} \quad (\text{Equation A11})$$

And:

$$n_i^{\text{inj}} = \frac{n_i \times V^{\text{inj}}}{V} \quad (\text{Equation A12})$$

Equation **A10** becomes:

$$A_i = \frac{RF_i \times n_i \times V^{\text{inj}}}{V} \quad (\text{Equation A13})$$

This is also true for the internal standard:

$$A_{st} = \frac{RF_{st} \times n_{st} \times V^{\text{inj}}}{V} \quad (\text{Equation A14})$$

Dividing Equation **A13** by Equation **A14** results in:

$$\frac{A_i}{A_{st}} = \frac{RF_i \times n_i}{RF_{st} \times n_{st}} \quad (\text{Equation A15})$$

Since:

$$n = \frac{m}{FW} \quad (\text{Equation A16})$$

Then:

$$\frac{A_i}{A_{st}} = \frac{RF_i \times m_i \times FW_{st}}{RF_{st} \times m_{st} \times FW_i} \quad (\text{Equation A17})$$

The mass of component (*i*) can therefore be calculated by re-arranging Equation **A17**:

$$m_i = \frac{A_i \times RF_{st} \times FW_i \times m_{st}}{A_{st} \times RF_i \times FW_{st}} \quad (\text{Equation A18})$$

The peak area (*A*) and formula weight (*FW*) of component (*i*) and the internal standard (*st*) are known. The volume, density and therefore the mass of the internal standard (*m_{st}*) is also known. However, the FID response factor (*RF*) and the mass of component (*m_i*) are unknown.

Numerous studies have been compiled to calculate the FID response factor (RF) of flame ionisation detectors (FIDs) for a variety of organic molecules and have concluded that the RF for any given hydrocarbon is proportional to the number of carbon atoms it contains.^{5,6,7,8} Moreover, it has been suggested that homolytic fission of a hydrocarbon occurs inside the FID to produce radicals that contain a single carbon atom, which is then chemically ionised to form CHO⁺.⁸ Therefore, the RF of the FID should be equal to the FW of the compound:

$$RF_i = FW_i \quad (\text{Equation A19})$$

5.2.1 Validating the Assumption that $RF_i = FW_i$

5.2.1.1 Using the Formula Weight of the Analyte as its Response Factor

To confirm the validity of Equation A19, a test mixture containing pentane, hexane, 1-hexene, heptane, octane and nonane (80 μ L of each using a 250 μ L micro-syringe) was analysed using a Perkin Elmer Clarus 400 GC-FID fitted with a PONA capillary column (Figure 2). Here, nonane was employed as the internal standard.

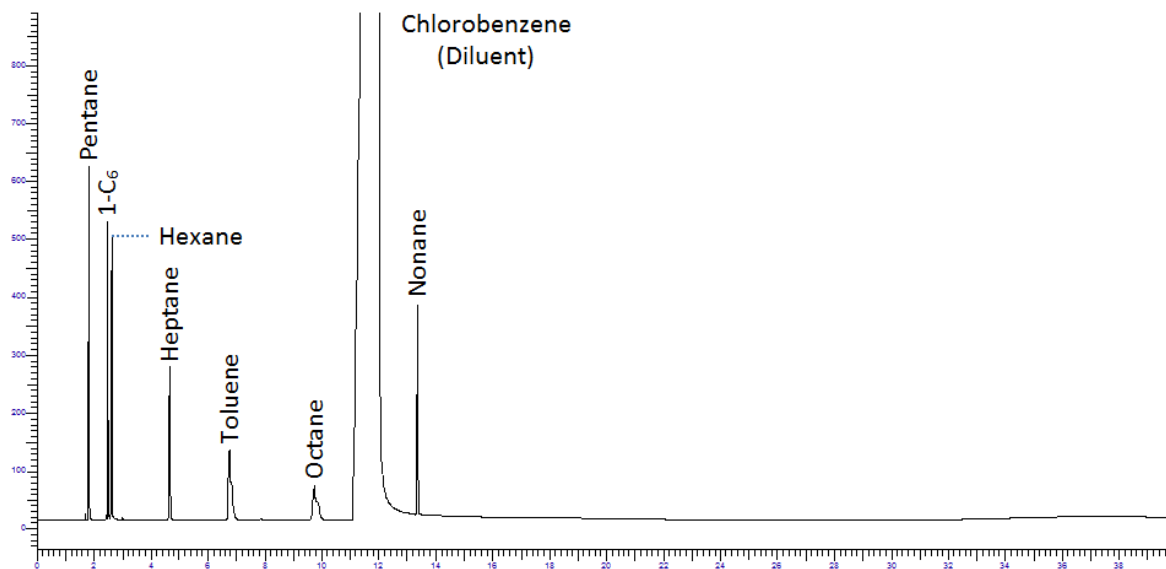


Figure 2: GC-FID of a test mixture containing known volumes of pentane, hexane, 1-hexene, heptane, octane and nonane obtained using a Perkin Elmer Clarus 400 GC instrument equipped with a PONA capillary column

Equation A18 was rearranged to calculate the relative response factor for each component in the solution (Table 1):

$$\frac{RF_{st}}{RF_i} = \frac{m_i \times FW_{st} \times A_{st}}{m_{st} \times FW_i \times A_i} \quad (\text{Equation A20})$$

Should $RF_i = FW_i$, then:

$$\frac{RF_{st}}{RF_i} = \frac{FW_{st}}{FW_i} \quad (\text{Equation A21})$$

Table 1: Determination of relative response factors for pentane, 1-hexene, hexane, heptane and octane; data averaged over four GC-FID analyses acquired with a Perkin Elmer Clarus 400 GC through a PONA column.

Analyte	Pentane	1-Hexene	Hexane	Heptane	Octane
m_i (mg)	50.1 \pm 1%	53.8 \pm 1%	52.4 \pm 1%	54.4 \pm 1%	56.2 \pm 1%
FW_i (g mol ⁻¹)	72.15	84.16	86.18	100.21	114.23
n_i (mmol)	0.694 \pm 1%	0.640 \pm 1%	0.608 \pm 1%	0.542 \pm 1%	0.492 \pm 1%
Area (μ V s)	677707 \pm 6%	721704 \pm 6%	695063 \pm 6%	722883 \pm 6%	709285 \pm 6%
A_{st} / A_i	1.09 \pm 1.3%	1.02 \pm 0.3%	1.06 \pm 0.3%	1.02 \pm 0.4%	1.04 \pm 0.6%
m_i / m_{st}	0.87 \pm 1%	0.94 \pm 1%	0.91 \pm 1%	0.95 \pm 1%	0.98 \pm 1%
FW_{st} / FW_i	1.78	1.52	1.49	1.28	1.12
RF_{st} / RF_i	1.69 \pm 0.05	1.46 \pm 0.04	1.44 \pm 0.03	1.24 \pm 0.03	1.15 \pm 0.02

As predicted, $\frac{RF_{st}}{RF_i} \approx \frac{FW_{st}}{FW_i}$ and therefore may now be considered to be a constant, namely a_{st}^i . As a result, Equations **A18** and **A19** can now be combined and simplified in order to calculate the mass of the analyte:

$$m_i = \frac{A_i \times m_{st}}{A_{st}} \quad (\text{Equation A22})$$

The same GC-FID trace used to confirm the validity of Equation **A19** was also used to verify whether Equation **A22** can accurately determine the mass of analytes in solution (m_i ; Table 2), and therefore be applied to the GC-FID analysis of the liquid fraction obtained from olefin oligomerisation catalysis. Here again, nonane is used as the internal standard.

Table 2: Quantitative analysis of a chlorobenzene solution containing known volumes of pentane, 1-hexene, hexane, heptane and octane; data averaged over four GC-FIDs obtained using a Perkin Elmer Clarus 400 GC equipped with a PONA column.

Analyte	m_i	m_i	m_i	m_i	\bar{m}	m	Error (%)
	Run 1	Run 2	Run 3	Run 4	(mg)	(mg)	
	(mg)	(mg)	(mg)	(mg)			
Pentane	53.2	52.8	51.7	53.0	52.7 ± 0.65	50.1 ± 1%	5.2
1-Hexene	56.2	55.8	56.1	56.2	56.1 ± 0.18	53.8 ± 1%	4.2
Hexane	54.2	53.8	54.0	54.1	54.0 ± 0.17	52.4 ± 1%	3.1
Heptane	56.2	55.9	56.3	56.2	56.2 ± 0.2	54.4 ± 1%	3.3
Octane	55.3	54.7	55.1	55.4	55.1 ± 0.31	56.2 ± 1%	2

From the experimentally-derived values of m_i (Table 2), it is clear that Equation **A22** is a reasonable approximation, compared with the known masses (m) of pentane, 1-hexene, hexane, heptane and octane, respectively, with a percentage error of less than 5.2%. It should be highlighted that this percentage error also encompasses the error incurred by measuring 80 μL of each component using a 250 μL micro-syringe (*i.e.* $\pm 1\%$). The error associated with injecting 1 μL of the test mixture into the GC-FID with a 10 μL micro-syringe, however, is discounted because the analytes are quantified against an internal standard.

5.2.1.2 Determination of the Relative Response Factor with a Calibration Curve

The relationship between the relative response factor and the relative formula weight of the analyte and the internal standard may be treated as a constant, a_{st}^i .

Equation **A17** can now be simplified:

$$\frac{A_i}{A_{st}} = \frac{a_{st}^i \times m_i}{m_{st}} \quad (\text{Equation A23})$$

Equation **A23** may be used to plot a calibration curve in order to determine a_{st}^i . In this work, three test solutions containing different, but known volumes of 1-hexene, nonane and 1-dodecene were probed by GC-FID (Table 3). Based on these data, a calibration plot was derived (Figure 3):

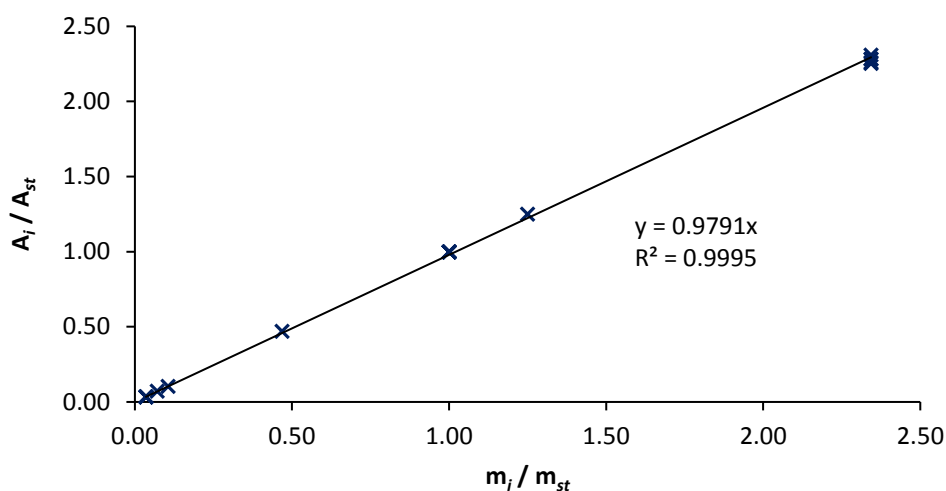


Figure 3: GC-FID calibration plot for 1-hexene, nonane and 1-dodecene acquired with a Perkin Elmer Clarus 400 GC fitted with a PONA capillary column

Linear regression analysis of the resulting calibration plot reveals a strong linear correlation between $\frac{A_i}{A_{st}}$ and $\frac{m_i}{m_{st}}$ with R^2 values exceeding 0.999. The gradient of the linear trend line, which is equal to a_{st}^i , was calculated to be 0.98. Hence, the percentage error in the quantification of analytes by GC-FID was considered to be $\pm 2.1\%$.

It is clear that the calibration curve Equation **A23** is more accurate in determining the mass of analytes (m_i) present in the GC-FID trace than using the assumption that $RF_i = FW_i$. In order to maintain the accuracy of the GC-FID analyses, however, the calibration curve requires verification on a regular basis, which can often be laborious. Hence, the liquid-phase oligomers obtained as a part of this project by the ethylene oligomerisation systems described previously in this thesis were quantified based on the reasonable approximation that $RF_i = FW_i$. The GC-FID trace of a standard solution containing a known volume of 1-hexene (1.5 mL), nonane (0.6 mL) and 1-dodecene (0.02 mL) in toluene was measured using a Perkin Elmer Clarus 400 GC equipped with a PONA capillary column at the start of every week of initiator testing to ensure valid comparisons were made between catalytic runs.

Table 3: Experimentally-derived relative peak areas and masses of 1-hexene, nonane and 1-dodecene analytes in a series of test mixtures for the calibration of the Perkin Elmer Clarus 400 GC instrument

Solution	1			2			3		
Analyte / Standard	<i>i</i>	<i>st</i>	<i>i</i>	<i>i</i>	<i>st</i>	<i>i</i>	<i>i</i>	<i>st</i>	<i>i</i>
Compound	1-Hexene	Nonane	1-Dodecene	1-Hexene	Nonane	1-Dodecene	1-Hexene	Nonane	1-Dodecene
V (mL)	1.5 ± 3%	0.6 ± 2%	0.02 ± 1%	0.4 ± 1%	0.3 ± 1%	0.02 ± 1%	0.2 ± 1%	0.4 ± 1%	0.04 ± 1%
Density (g mL⁻¹)	0.673	0.72	0.76	0.673	0.72	0.76	0.673	0.72	0.76
m (g)	1.01 ± 3%	0.431 ± 2%	0.015 ± 1%	0.269 ± 1%	0.215 ± 1%	0.015 ± 1%	0.135 ± 1%	0.287 ± 1%	0.0303 ± 1%
FW (g mol⁻¹)	84.16	128.26	168.32	84.16	128.26	168.32	84.16	128.26	168.32
n (mmol)	12 ± 3%	3.36 ± 2%	0.09 ± 1%	3 ± 1%	1.68 ± 1%	0.09 ± 1%	2 ± 1%	2.24 ± 1%	0.18 ± 1%
Area	1350550 ± 2%	589191 ± 3%	20739 ± 3%	838558 ± 2%	670143 ± 3%	49149 ± 3%	302301 ± 2%	640626 ± 3%	67113 ± 3%
A_{st} / A_i	0.44 ± 0.7%	1 ± 0%	28.41 ± 0.7%	0.8 ± 0.7%	1 ± 0%	13.64 ± 0.7%	2.12 ± 0.7%	1 ± 0%	9.55 ± 0.7%
m_i / m_{st}	2.34 ± 3%	1 ± 2%	0.04 ± 1%	1.25 ± 1%	1 ± 1%	0.07 ± 1%	0.47 ± 1%	1 ± 1%	0.11 ± 1%
FW_{st} / FW_i	1.52	1	0.76	1.52	1	0.76	1.52	1	0.76
RF_{st} / RF_i	1.56 ± 0.02	1 ± 0	0.76 ± 0	1.52 ± 0.001	1 ± 0	0.73 ± 0.04	1.51 ± 0.007	1 ± 0	0.77 ± 0.01
aⁱ_{st}	0.98 ± 0.02	1 ± 0	1 ± 0	1 ± 0.001	1 ± 0	1.04 ± 0.04	1.01 ± 0.007	1 ± 0	0.99 ± 0.01
m_i (g)	0.988 ± 0.02	0.431 ± 0	0.015 ± 0	0.270 ± 0.001	0.215 ± 0	0.016 ± 0.04	0.136 ± 0.007	0.287 ± 0	0.0301 ± 0.01

5.2.2 Quantifying the Mass of Liquid-phase Oligomers afforded from Chromium-mediated Ethylene Oligomerisation using GC-FID Analysis

It was important to demonstrate the validity of this technique in the quantification of liquid-phase oligomers generated by the chromium-mediated ethylene trimerisation systems described herein using a known volume (1 mL) of the internal standard (nonane). Below is the GC-FID trace of the liquid fraction arising from an ethylene oligomerisation run (Figure 4). Since the mass of the nonane standard (m_{st}) is known to be 0.718 g, Equation **A22** can be applied accordingly:

$$m_i = \frac{A_i \times 0.718 \text{ g}}{A_{st}} \quad (\text{Equation A22})$$

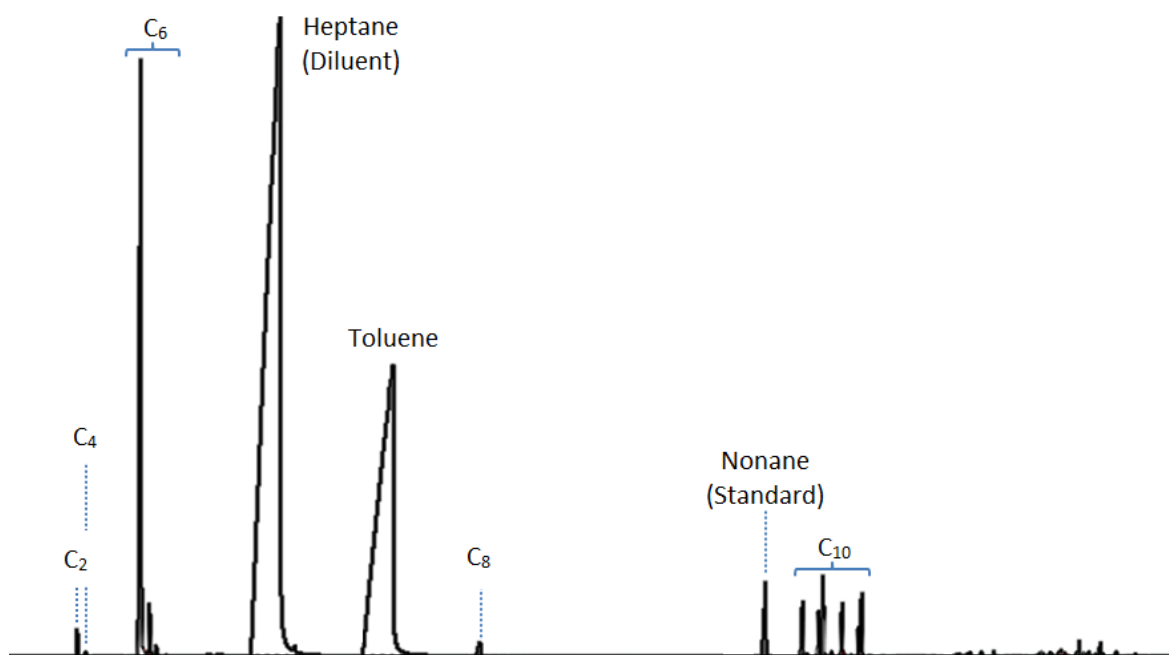


Figure 4: GC-FID of the liquid fraction afforded by the heterogeneous $\text{Cr}\{\text{N}(\text{SiMe}_3)_2\}_x/\text{SiO}_{2-600}/\text{MMAO-12}$ ethylene trimerisation system (see Chapter 3; Table 1; Run 1) obtained using a Perkin Elmer Clarus 400 GC fitted a PONA column. Reaction Conditions: 27 μmol Cr (mass of $\text{Cr}\{\text{N}(\text{SiMe}_3)_2\}_x/\text{SiO}_{2-600} = 0.2 \text{ g}$); 410 μmol MMAO-12 (Al:Cr = 15:1); 60 mL heptane; 120 $^\circ\text{C}$; 500 rpm; 8 barg fixed ethylene pressure; 1 mL nonane; 0.5 h.

Table 4: Quantification of liquid-phase oligomers produced by silica-supported chromium-mediated heterogeneous ethylene trimerisation using a Perkin Elmer Clarus 400 GC equipped with a PONA capillary column

Analyte	Area ($\mu\text{V s}$)	A_i / A_{st}	m_{st} (g)	m_i (g)
C ₄	4941	0.04	0.718 \pm 5%	0.029 \pm 5%
C ₆	937142	7.60	0.718 \pm 5%	5.453 \pm 5%
1-C ₆	832788	6.75	0.718 \pm 5%	4.846 \pm 5%
C ₈	40504	0.33	0.718 \pm 5%	0.236 \pm 5%
C ₁₀	424094	3.44	0.718 \pm 5%	2.468 \pm 5%
C ₁₂₊	162910	1.32	0.718 \pm 5%	0.948 \pm 5%

Partial loss of volatile components (such as ethylene and butenes) whilst carefully depressurising the reactor at the end of the ethylene trimerisation run is inevitable. Catalytic performance was therefore measured in this thesis by the total mass of all liquid-phase oligomers formed during catalysis derived from the GC-FID using an internal standard (nonane), as well as the mass of the polyethylene (PE) by-product rather than by ethylene consumption.

Process Selectivity:

$$\text{➤ } C_4 = \frac{0.029}{0.029+5.453+0.236+2.468+0.948+1.083} \times 100 \approx 0 \text{ wt\%} \quad (\text{Equation A1})$$

$$\text{➤ } C_6 = \frac{5.453}{0.029+5.453+0.236+2.468+0.948+1.083} \times 100 = 53 \text{ wt\%} \quad (\text{Equation A2})$$

$$\text{➤ } C_8 = \frac{0.236}{0.029+5.453+0.236+2.468+0.948+1.083} \times 100 = 2 \text{ wt\%} \quad (\text{Equation A3})$$

$$\text{➤ } C_{10} = \frac{2.468}{0.029+5.453+0.236+2.468+0.948+1.083} \times 100 = 24 \text{ wt\%} \quad (\text{Equation A4})$$

$$\text{➤ } C_{12+} = \frac{0.948}{0.029+5.453+0.236+2.468+0.948+1.083} \times 100 = 9 \text{ wt\%} \quad (\text{Equation A5})$$

$$\text{➤ } PE = \frac{1.083}{0.029+5.453+0.236+2.468+0.948+1.083} \times 100 = 11 \text{ wt\%} \quad (\text{Equation A6})$$

$$\text{➤ } \%1-C_6 = \frac{4.846}{5.453} \times 100 = 89\% \quad (\text{Equation A7})$$

Catalytic Activity:

$$\text{➤ } TON = \frac{0.029+5.453+0.236+2.468+0.948+1.083}{0.001459} = 7002 \text{ g g}_{Cr}^{-1} \quad (\text{Equation A8})$$

$$\text{➤ } TOF = \frac{0.029+5.453+0.236+2.468+0.948+1.083}{0.001459 \times 0.5} = 14004 \text{ g g}_{Cr}^{-1} \text{ h}^{-1} \quad (\text{Equation A9})$$

5.3 References

- (1) S. Kozuch, J. M. L. Martin, *ACS Catal.*, **2012**, *2*, 2787-2794.
- (2) F. Bressolle, M. Bromet-Petit, M. Audran, *J. Chromatogr. B, Biomed. Appl.*, **1996**, *686*, 3-10.
- (3) D. Harvey, *Modern Analytical Chemistry*; McGraw-Hill New York, 2000; Vol. 381, 563-578.
- (4) M. J. Hanton, L. Daubney, T. Lebl, S. Polas, D. M. Smith, A. Willemse, *Dalton Trans.*, **2010**, *39*, 7025-7037.
- (5) A. E. Messner, D. M. Rosie, P. A. Argabright, *Anal. Chem.*, **1959**, *31*, 230-233.
- (6) W. A. Dietz, *J. Chromatogr. Sci.*, **1967**, *5*, 68-71.
- (7) H. Y. Tong, F. W. Karasek, *Anal. Chem.*, **1984**, *56*, 2124-2128.
- (8) Y. Huang, Q. Ou, W. Yu, *Anal. Chem.*, **1990**, *62*, 2063-2064.

Chapter 6:
Thesis Summary, Outlook and Future Work

6.1 Summary

In this PhD thesis, the development of a solid-phase ethylene trimerisation process has been described as part of a fundamental study into the field of heterogeneous selective olefin oligomerisation. Initial work was based on a system previously reported by Monoi and Sasaki, which led to the detailed investigation presented here around an initiator derived from the $\text{Cr}\{\text{N}(\text{SiMe}_3)_2\}_3$ molecular precursor, partially dehydroxylated silica, and isobutyl aluminoxane (IBAO; see Section 1.3.2.5).¹ Following preliminary screening investigations, it has been shown in this thesis that the observed catalytic oligo- and poly-merisation behaviour of the $\text{Cr}\{\text{N}(\text{SiMe}_3)_2\}_x/\text{oxide}/\text{Al-activator}$ initiator is dependent on the nature of the oxide support and its thermal pre-treatment, the alkyl aluminium-based co-catalyst, and reaction diluent. In our hands, the best performing system comprised $\text{Cr}\{\text{N}(\text{SiMe}_3)_2\}_3$ grafted onto silica that had previously been thermally treated at 600 °C for 24 hours under a flow of N_2 (denoted SiO_{2-600}), and then activated with modified methyl aluminoxane (MMAO-12; $\text{Al}/\text{Cr} = 15$). The application of the resulting initiator as a slurry in heptane at 120 °C, and at a constant ethylene pressure of 30 barg for 30 minutes gave rise to a mixture of hexenes (49 wt%; 91% 1-hexene), decenes (26 wt%) and polyethylene (PE; 9 wt%) at a rate of $68251 \text{ g g}_{\text{Cr}}^{-1} \text{ h}^{-1}$ (see Section 3.2.4.5). Subsequent investigations described in this manuscript have identified that this organic product distribution can be accredited to the operation of two competing processes: i) trimerisation *via* a supported variant of the metallacycle mechanism,^{2,3} and ii) polymerisation through a Cossee-Arlman-type chain growth pathway.^{4,5,6}

Using a combination of solid-state Raman and ^{29}Si nuclear magnetic resonance (NMR) spectroscopic analyses, it has been shown that $\text{Cr}\{\text{N}(\text{SiMe}_3)_2\}_3$ reacts with both isolated (Q_3) and geminal (Q_2) silanols at the surface of SiO_{2-600} liberating one and two equivalents of the corresponding amine to form two distinct supported chromium(III) amide species, respectively (see Section 2.2.4). The formation of these two distinct active sites at the surface of SiO_{2-600} is considered to be the origin of the simultaneous catalytic tri- and poly-merisation processes observed. Notably, increasing the relative population of Q_2 and/or vicinal silanols at the silica surface with respect to Q_3 sites, something that can be achieved by lowering the support calcination temperature, results in a switch in the selectivity exhibited by the ensuing $\text{Cr}\{\text{N}(\text{SiMe}_3)_2\}_x/\text{SiO}_2/\text{MMAO-12}$ -based initiator from 1-hexene to PE formation (see Section 2.2.5).

An alkyl aluminium-based co-catalyst is required to generate the active species responsible for ethylene tri-/poly-merisation. MMAO-12 is believed to alkylate the supported $=\text{SiO}_2\text{CrN}(\text{SiMe}_3)_2$ and $\equiv\text{SiOCr}\{\text{N}(\text{SiMe}_3)_2\}_2$ species, derived from Q_2 /vicinal and Q_3 silanols respectively,⁷ yielding a Phillips-type $=\text{SiO}_2\text{CrR}$ ethylene polymerisation catalyst^{8,9} as well as $\equiv\text{SiOCrR}_2$. The latter may then undergo reductive elimination to generate a silica-supported Cr^{I} -based trimerisation-active initiator that is responsible for 1-hexene and decene production (see Section 2.2.6).^{10,11,12}

Further work described in this thesis has probed the influence of several processing parameters including chromium concentration, Al/Cr mole ratio, reaction temperature, ethylene pressure, reaction time, diluent volume, and the effect of so-called “promoters” upon the productivity and selectivity of the $\text{Cr}\{\text{N}(\text{SiMe}_3)_2\}_x/\text{SiO}_{2-600}/\text{MMAO-12}$ initiator system have been explored. It has been found that:

- Ethylene tri- and poly-merisation were both determined to be first order processes with respect to chromium and ethylene concentration:
 - The rate-determining step (RDS) in the “oxide-supported” variant of the metallacyclic trimerisation manifold is the insertion of one molecule of ethylene into the metallacyclopentane intermediate.
 - The RDS in the Cossee-Arlman-type chain growth mechanism is migratory insertion of ethylene into the propagating alkyl chain.
- Decene formation is dependent upon 1-hexene concentration:
 - Reincorporation of 1-hexene into the metallacyclic trimerisation reaction manifold leads to the formation of seven decene isomers, as inferred from solution-phase $^{13}\text{C}\{^1\text{H}\}$ NMR spectroscopic analysis.
- 1-Hexene and ethylene co-polymerise to yield high molecular weight polyethylene (HMWPE) with butyl side chains incorporated into the polymer backbone, according to differential scanning calorimetry (DSC).
- The catalytic performance of the $\text{Cr}\{\text{N}(\text{SiMe}_3)_2\}_x/\text{SiO}_{2-600}/\text{MMAO-12}$ ethylene trimerisation initiator improves with increasing reaction temperature:
 - Below a certain temperature threshold (*i.e.* 90 °C), ethylene trimerisation does not occur.
 - The rate at which MMAO-12 generates active sites at the surface of $\text{Cr}\{\text{N}(\text{SiMe}_3)_2\}_x/\text{SiO}_{2-600}$ increases with higher reaction temperatures.
- An Al/Cr mole ratio of 50 and above, aromatic diluents such as toluene and chlorobenzene, and potential catalytic “promoters” 1,2-dimethoxyethane (1,2-DME) and Et_2Zn diminish catalyst performance:
 - Aromatic compounds may coordinate to the catalytically-relevant chromium species, and effectively poison the catalyst.
 - 1,2-DME is thought to sequester residual R_3Al species inherently present in aluminoxanes such as MMAO-12, which are necessary to generate the active catalyst responsible for 1-hexene production.
 - Large molar excesses of MMAO-12 ($\text{Al}/\text{Cr} \geq 50$) and Et_2Zn ($\text{Zn}/\text{Cr} = 100$) may cleave the catalytically-relevant chromium species from the silica support *via* alkylation affording an inactive molecular species.

6.2 Outlook

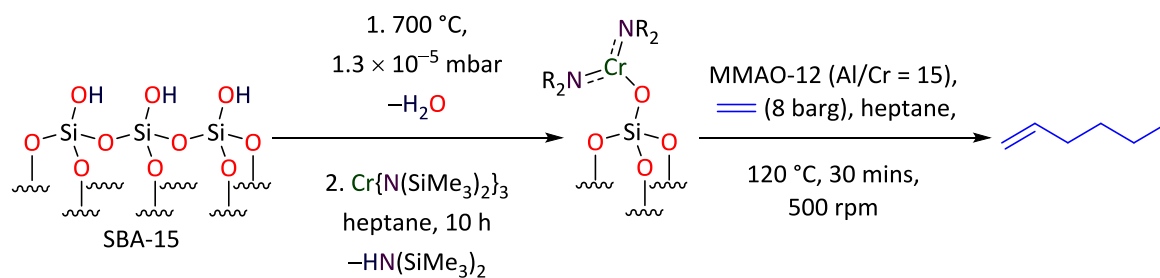
The primary purpose of this PhD project was to undertake a fundamental study into the field of heterogeneous selective ethylene oligomerisation catalysis, and to develop underpinning knowledge and mechanistic insight, which can be used in the advancement of future systems. Thus far, parallels have been drawn between the solid-phase $\text{Cr}\{\text{N}(\text{SiMe}_3)_2\}_x/\text{SiO}_{2-600}/\text{MMAO-12}$ initiator described herein, the closely-related Phillips heterogeneous “Cr/SiO₂” ethylene polymerisation catalyst, and molecular (*homogeneous*) selective ethylene oligomerisation systems. However, it is clear that the productivity and selectivity afforded by the $\text{Cr}\{\text{N}(\text{SiMe}_3)_2\}_x/\text{oxide}/\text{Al-activator}$ initiator systems described in this thesis are significantly lower than those achieved by the homogeneous selective ethylene oligomerisation systems commercialised by the Chevron-Phillips Chemical Company and Sasol Technology. This said, there remains significant scope for the development and optimisation of potentially more industrially applicable heterogeneous systems. Solid-phase catalysts offer numerous advantages over their soluble (molecular) counterparts in the field of selective olefin oligomerisation, including more efficient product separation, improved catalyst stability and recyclability as well as the potential for solvent-free processing.

6.3 Future Work

Further electron paramagnetic resonance (EPR) spectroscopic analyses of the highly air- and moisture-sensitive $\text{Cr}\{\text{N}(\text{SiMe}_3)_2\}_x/\text{SiO}_{2-200}$ and $\text{Cr}\{\text{N}(\text{SiMe}_3)_2\}_x/\text{SiO}_{2-600}$ pro-initiators must be carried out under an inert atmosphere to quantify the relative proportion of chromium(III) *mono*- and *bis*-(hexamethyldisilazide) species at the surface of silica. Since the preliminary continuous-wave (CW) EPR spectra acquired were not sufficiently resolved (see Section 2.2.5.1), hyperfine sublevel correlation spectroscopic (HYSCORE) analyses should be carried out to determine the ligand hyperfine coupling between the supported chromium(III) metal centre and either one or two coordinated ^{14}N nuclei. In addition to these EPR spectroscopic experiments, X-ray photoelectron spectroscopy (XPS) should also enable quantification of the ratio of Cr : N as a function of support calcination temperature, as well as the oxidation state of the chromium metal centre.

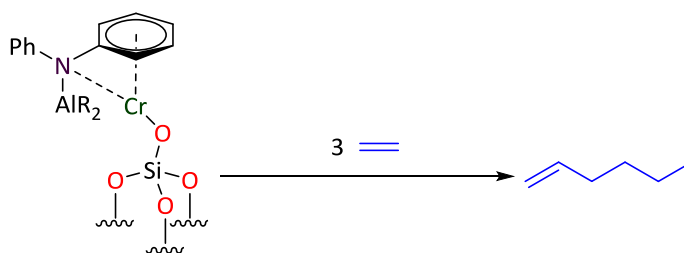
Following on from the results described in Chapter 3, in which a series of experimental processing parameters were investigated including the effect of the stirrer speed regime upon catalytic performance, the productivity exhibited by the $\text{Cr}\{\text{N}(\text{SiMe}_3)_2\}_x/\text{SiO}_{2-600}/\text{MMAO-12}$ initiator may be enhanced by using a gas-entrainment stirrer rather than a classical turbine-type four-blade impeller. This would maximise ethylene gas dispersion into the heptane diluent by continuously recirculating gases from the reactor head space (above the liquid) through the impeller into the liquid-phase. This said, work will also need to be undertaken to very significantly lower the rate of polymer formation, which is still dramatically too high for industrial applications (levels of 1 wt% PE are deemed too great from an industrial perspective). This means that the potential risk of reactor fouling is significant as well as giving rise to an unwanted side product, and thus reduces the overall efficiency of the process.

In order to improve the selectivity of the $\text{Cr}\{\text{N}(\text{SiMe}_3)_2\}_x/\text{SiO}_{2-600}/\text{MMAO-12}$ system towards 1-hexene (at the expense of PE), it is necessary to dehydroxylate both Q_2 and vicinal silanol functionalities at the surface of silica so to prepare a so-called “single-site” pro-initiator by way of reaction between $\text{Cr}\{\text{N}(\text{SiMe}_3)_2\}_3$ and Q_3 silanols. Copéret, Basset *et al.* have previously demonstrated that SBA-15, a *meso*-porous silica, calcined overnight at 700 °C under ultra-high vacuum (*i.e.* 10^{-5} mbar) comprises Q_3 silanols.^{12,13,14,15,16,17,18,19,20} Thus, sequential treatment of this partially dehydroxylated oxide support with solutions of $\text{Cr}\{\text{N}(\text{SiMe}_3)_2\}_3$ and MMAO-12 (Al/Cr = 15) could potentially yield a highly selective heterogeneous ethylene trimerisation-active initiator (Scheme 1).



Scheme 1: Preparation of a so-called "single-site" $\text{Cr}\{\text{N}(\text{SiMe}_3)_2\}_2/\text{SBA-15-700v}/\text{MMAO-12}$ heterogeneous ethylene trimerisation catalyst, modified from Chen *et al.*, 2012¹²

As alluded to earlier in Section 3.2.3, the influence of the hexamethyldisilazide ligand in the heterogeneous $\text{Cr}\{\text{N}(\text{SiMe}_3)_2\}_x/\text{SiO}_2\text{-600}/\text{MMAO-12}$ ethylene trimerisation initiator can be explored by varying the electronic and steric effects of the amide ligand. A series of well-defined molecular precursors, $\text{M}(\text{NR}_2)_n$ {M = Cr, W; R = alkyl, aryl, pyrrolyl; n = 2, 3, 5}, could be grafted onto a partially dehydroxylated siliceous catalyst support *via* a single M–O–Si linkage, and subsequently activated with MMAO-12 to yield initiators active for ethylene oligomerisation and/or polymerisation. The precise nature of the ligands is crucial in determining activity and product selectivity. In this context, Deckers and co-workers have previously reported that the variable coordination of a hemilabile phenyl substituent switched the product selectivity of a soluble (molecular) titanium-based ethylene polymerisation catalyst in favour of 1-hexene production.²¹ By employing a $\text{Cr}(\text{NPh}_2)_3$ -derivative of the silica-supported chromium initiator, the potential coordination of the phenyl substituent may stabilise coordinatively unsaturated intermediates in the metallacyclic trimerisation manifold during ethylene trimerisation catalysis (Scheme 2), akin to the 2,5-dimethylpyrrolide (2,5-DMP) and diphosphinoamine ($\text{PNP}^{\text{OCH}_3}$) ligands utilised in the Chevron-Phillips and BP systems, respectively.^{22,23}



Scheme 2: Potential η^6 -coordination of the $[\text{R}_2\text{Al}][\text{NPh}_2]$ adduct to the trimerisation-active chromium(II) metal centre

6.4 References

- (1) T. Monoi, Y. Sasaki, *J. Mol. Catal. A: Chem.*, **2002**, *187*, 135-141.
- (2) R. M. Manyik, W. E. Walker, T. P. Wilson, *J. Catal.*, **1977**, *47*, 197-209.
- (3) J. R. Briggs, *J. Chem. Soc., Chem. Commun.*, **1989**, *11*, 674-675.
- (4) P. Cossee, *J. Catal.*, **1964**, *3*, 80-88.
- (5) E. J. Arlman, *J. Catal.*, **1964**, *3*, 89-98.
- (6) E. J. Arlman, P. Cossee, *J. Catal.*, **1964**, *3*, 99-104.
- (7) E. Y.-X. Chen, T. J. Marks, *Chem. Rev.*, **2000**, *100*, 1391-1434.
- (8) J. P. Hogan, R. L. Banks, **1958**, *US22825721*, Phillips Petroleum Company.
- (9) M. P. McDaniel, *Adv. Catal.*, **2010**, *53*, 123-606.
- (10) T. Agapie, J. A. Labinger, J. E. Bercaw, *J. Am. Chem. Soc.*, **2007**, 14281-14295.
- (11) A. Jabri, C. B. Mason, Y. Sim, S. Gambarotta, T. J. Burchell, R. Duchateau, *Angew. Chem. Int. Ed.*, **2008**, *47*, 9717-9721.
- (12) Y. Chen, E. Callens, E. Abou-Hamad, N. Merle, A. J. P. White, M. Taoufik, C. Copéret, E. Le Roux, J.-M. Basset, *Angew. Chem. Int. Ed.*, **2012**, *51*, 11886-11889.
- (13) D. Gajan, C. Copéret, *New J. Chem.*, **2011**, *35*, 2403-2409.
- (14) F. Rascon, R. Wischert, C. Copéret, *Chem. Sci.*, **2011**, *2*, 1449-1456.
- (15) P. Laurent, L. Veyre, C. Thieuleux, S. Donet, C. Copéret, *Dalton Trans.*, **2013**, *42*, 238-248.
- (16) M. K. Samantaray, E. Callens, E. Abou-Hamad, A. J. Rossini, C. M. Widdifield, R. Dey, L. Emsley, J.-M. Basset, *J. Am. Chem. Soc.*, **2013**, *136*, 1054-1061.
- (17) M. P. Conley, C. Copéret, C. Thieuleux, *ACS Catal.*, **2014**, *4*, 1458-1469.
- (18) C. Copéret, V. Mougel, *Chem. Sci.*, **2014**, *5*, 2475-2481.
- (19) B. Werghi, A. Bendjeriou-Sedjerari, J. Sofack-Kreutzer, A. Jedidi, E. Abou-Hamad, L. Cavallo, J.-M. Basset, *Chem. Sci.*, **2015**, *6*, 5456-5465.
- (20) B. Hamzaoui, J. D. A. Pelletier, E. Abou-Hamad, J.-M. Basset, *Chem. Commun.*, **2016**, *52*, 4617-4620.
- (21) P. J. W. Deckers, B. Hessen, J. H. Teuben, *Angew. Chem. Int. Ed.*, **2001**, *40*, 2516-2519.
- (22) W. J. van Rensburg, C. Grové, J. P. Steynberg, K. B. Stark, J. J. Huyser, P. J. Steynberg, *Organometallics*, **2004**, *23*, 1207-1222.
- (23) S. J. Schofer, M. W. Day, L. M. Henling, J. A. Labinger, J. E. Bercaw, *Organometallics*, **2006**, *25*, 2743-2749.